An Investigation of Regulatory T Cell Therapy in Advanced Human Skin Experimental Transplantation Models

George Adigbli

Keble College
Nuffield Department of Surgical Sciences
University of Oxford

Supervisors: Dr Joanna Hester and Professor Fadi Issa
Thesis submitted for DPhil in Surgical Sciences in Trinity Term 2021

Abstract

Regulatory T cells (Tregs) are powerful suppressors of immune responses and help preserve immune homeostasis and self-tolerance. Specific Treg subsets—including those expressing the chemokine receptors CCR4 and CCR8—demonstrate high suppressive potency in certain clinical contexts. Several studies have revealed the promise of Treg cellular therapies in counteracting immune-mediated pathologies including transplant rejection. Clinical translation of Treg therapies must be supported by ongoing pre-clinical and clinical research to both evidence and enhance its safety and efficacy.

Humanised experimental mice provide a cost-effective and practical approach to create *in vivo* models for pre-clinical transplant research. However, issues including high technical demand and variable capacities to represent human biology can limit their use.

The two aims of this study were to develop an advanced humanised mouse model that could support multilineage human haematopoeisis and accurately represent human allotransplantation, and to investigate whether specific skin-homing human Treg subsets can provide effective anti-rejection therapy for skin allografts.

In the first part of this study, HSPC-NBSGW mice—non-irradiated NOD,B6.SCID IL-2r$\gamma^{-/-}$ Kit$^{W41/W41}$ (NBSGW) mice engrafted with human CD133^{+} hematopoietic stem and progenitor cells (HSPCs)—were assessed for function capability in the context of allotransplantation. In depth characterisation of durable human haematopoeitic cell engraftment was followed by quantitative transcriptomic and immunophenotypic analyses of complete skin allograft rejection, which this model can effect through functional human innate and adaptive immune cells.

In the second part, the suppressive capabilities of chemokine receptor-expressing Tregs were evaluated phenotypically and functionally. In addition to potent immune suppression mediated by CCR4-expressing Tregs, subcutaneous CCL22 administration in the presence of Treg therapy prevented skin allograft rejection.

As the potential of Treg therapy has become clearer, pre-clinical research is becoming an increasingly essential tool for uncovering features of Treg behaviour and function that may help optimise safety and efficacy. The findings presented in this thesis advance the *in vivo* research toolkit and describe an additional method by which Tregs may be manipulated to enhance their therapeutic application.

Table Of Contents

Acknowledgements

First and foremost, my sincerest thanks to Dr Joanna Hester and Professor Fadi Issa for taking a chance on me. Their influence has shaped the course of my career and their offer of an opportunity to undertake a DPhil under such incredible supervision has been a pivotal point in my life. I am grateful for their endless guidance, which repeatedly enabled me to overcome hurdles I never thought I could. Witnessing their infectious enthusiasm for science, observing their brilliant minds process solutions to problems, and experiencing their unwavering dedication to high quality research of integrity has been a true privilege.

I continuously reflect on the patience they afforded me as I (slowly) re-learned the philosophy of research in the purist method that symbolises the Transplantation Research and Immunology Group (TRIG). Finally, I thank them for the support and encouragement they gave me when writing an article of personal significance to me, addressing inequities in science and medicine. The positive comments I have since received reflect the ethos of balanced writing that they painstakingly drummed into me.

I would also like to thank the wonderful colleagues and friends I made at Oxford. Within TRIG I was fortunate to have presented to and learned from Professor Kathryn Wood, who's legacy is our incredible lab. Thanks to Monica Dolton, for her exceptional efficiency, knowledge of all things and joyful demeanour, which brightened our socials. Also to Dr Kate Milward, Dr Rebeca Arroyo Hornero, Dr Hisashi Hashimoto, Dr Amy Cross, Ms Alaa Alzhrani and the many visiting scientists with whom I shared countless red-eye shifts, to our clinician scientists— Dr Matt Brook, Dr Sushma Shankar, Dr Matt Bottomley, Dr Helen Stark, Dr Masateru Uchiyama, Dr Prateek Katti, Dr Liz Wallin and Dr Oliver McCallion who are such a

credit to our profession, to the formidable Peng Hua and our collaborators in the humanised mouse project, and the ever helpful staff in the Nuffield Department of Surgical Sciences and the animal house staff at BMS JR. Thanks also to the kind surgeons in the department of Plastic and Reconstructive Surgery at the John Radcliffe Hospital for procuring human tissue samples used in several experiments.

A special thank you to my co-lab rat Dr Kento Kawai, who was by my side from the start and became a brother to me. I look forward to seeing you flourish.

My experience was made all the more fruitful thanks to the generous scholarship awarded by the Clarendon fund and the DeBreyne fund. In addition to fantastic experiences as a Clarendon scholar, this support allowed me to concentrate on research and achieve outputs that I hope will honour their kindness. Thanks also to the Wellcome Trust and Kidney Research UK for their financial support of this project.

Thank you to the wonderful team at Keble College – Sir Jonathan Phillips, Dr Ali Rodgers, Dr Simon Butt and the wonderful deanship and welfare teams I am proud to have been part of.

Last, and certainly not least my family and friends—my rock. The past few years have presented my greatest challenges but as ever you have been there, with an ear, a smile, a hug or a nod, letting me know together, we will get there.

To you

Abbreviations

7-Aminoactinomycin D	7-AAD
A Proliferation-Inducing Ligand	APRIL
Activation-Induced Cytidine Deaminase	AID
Activator Protein 1	AP-1
Adoptive Cellular Therapies	ACT
Alternative Pathway	AP
Analysis Of Variance	ANOVA
Antibody Mediated Rejection	ABMR
Antibody-Dependent Cellular Cytotoxicity	ADCC
Antigen Presenting Cells	APC
B Cell Maturation Protein	BCMA
B Cell Receptor	BCR
B Cell-Activating Factor	BAFF
B Cell-Activating Factor Receptor	BAFFR
B Lymphocyte Stimulator	BlyS
Bromodomain And Extra-Terminal Motif	BET
C-Jun N-Terminal Kinase	JNK
Carboxyfluorescein Succinimidyl Ester	CFSE
Cba/Ca	CBA
Central Memory T Cell	Tcm
Chimeric Antigen Receptor T Cells	CAR-T
Class Switch Recombination	CSR
Classical Pathway	CP
Clodronate Liposome	CloLip
Complementary DNA	cDNA
Conventional Dendritic Cell	cDC
Coronavirus Disease 2019	COVID
Cutaneous T Cell Lymphoma	CTCL
Cytotoxic T Lymphocyte	CTL
Cytotoxic T Lymphocyte-Associated Protein 4	CTLA-4
Damage-Associated Molecular Pattern	DAMP
Delayed-Type Hypersensitivity	DTH
Dendritic Cell	DC
Donor-Specific Allo-Antibodies	DSA
Double-Positive	DP
Effector Memory T Cell	Tem

Electron Coupled Dye	ECD
Epstein-Barr Virus	EBV
Ethylenediaminetetraacetic Acid	EDTA
Extracellular Signal-Regulated Kinase	ERK
Factor B	FB
Factor D	FD
False Discovery Rate	FDR
Fluorescence-Activated Cell Sorting	FACS
Foetal Calf Serum	FCS
For Long-Term Haematopoietic Stem Cell	LT-HSC
Forehead Box P3	FoxP3
Glucose Transporter Type 1	GLUT1
Graft Versus Host	GvH
Graft Versus Host Disease	GvHD
Granulocyte Macrophage Colony-Stimulating Factor	GM-CSF
Granzyme Exocytosis	GE
Growth Factor Receptor-Bound Protein 2	GRB2
Haematopoeitic Stem And Progenitor Cell-Humanised NOD,B6.SCID IL-2r^{-}/$^{-}$Kit$^{w41/W41}$	HSPC-NBSGW
Haematopoietic Stem And Progenitor Cell	HSPC
Haematopoietic Stem Cell	HSC
Haematoxylin And Eosin	H&E
Heat Shock Protein	HSP
Histone Deacetylase	HDAC
Human	h
Human Erythropoeitin	hEPO
Human Leukocyte Antigen	HLA
Human Serum Albumin	HSA
Human Umbilical Cord Blood	hUCB
Humanised Immune System	HIS
Immunoglobulin	Ig
Immunoglobulin Superfamily	IgSF
Indoleamine 2,3-Dioxygenase	IDO
Intercellular Adhesion Molecule 1	ICAM-1
Interferon	IFN
Interferon Gamma-Induced Protein 10	IP-10
Interleukin	IL
Irradiated	ir

Ischaemia-Reperfusion Injury	IRI
Iscove's Modified Dulbecco's Medium	IMDM
Knockout	KO
Lectin Pathway	LP
Lymph Node	LN
Lymphocyte Function-Associated Antigen 1	LFA-1
Lymphocyte Separation Medium	LSM
Magnetic Cell Separater	MACS
Major Histocompatibility Complex	MHC
Mammalian Target Of Rapamycin	mTOR
Mannose-Associated Serine Protease	MASP
Median Survival Time	MST
Membrane Attack Complex	MAC
Messenger RNA	mRNA
Minor Histocompatibility	miH
Monoclonal Antibody	mAb
Monokine Induced By Gamma Interferon	MIG
Mononuclear Cell	MNC
Mouse	m
Mycophenolate Mofetil	MMF
Myeloid-Derived Suppressor Cells	MDSC
National Health Service	NHS
Natural Killer	NK
NOD,B6.SCID IL-2r^{-}/$^{-}$Kit$^{w41/W41}$	NBSGW
NOD/SCID/IL-2 Receptor Gamma Chain Null (IL2r^{-}/$^{-}$) Mouse	NSG
NOD/Shi-*Scid*/IL-2Rγ^{null}	NOG
Non-Obese Diabetic	NOD
Nuclear Factor Kappa-Light-Chain-Enhancer Of Activated B Cells	NFkB
Nuclear Factor Of Activated T-Cells	NFAT
Optimal Cutting Temperature	OCT
Paraformaldehyde	PFA
Pattern Recognition Receptor	PRR
Peripheral Blood Leucocyte	PBL
Peripheral Blood Mononuclear Cell	PBMC
Phosphate Buffered Saline	PBS
Phycoerythrin	PE

Polymorphonuclear Neutrophil	PMN
Reactive Oxygen Species	ROS
Recombinant Human	rh
Recombinant Mouse	rm
Recombination Activating Gene	RAG
Red Blood Cell	RBC
Red Blood Cell-Derived Nanovesicle	RDNV
Regulated Upon Activation, Normal T-Cell Expressed And Secreted	RANTES
Regulatory T Cell	Treg
Roswell Park Memorial Institute	RPMI
Severe Combined Immunodeficiency	SCID
Severe Combined Immunodeficiency Disease	*Scid*
Solid Organ Transplantation	SOT
Stem Cell Factor	SCF
T Cell Receptor	TCR
T Cell Receptor Excision Circle	TREC
T Cell-Mediated Rejection	TCMR
T Follicular Helper	Tfh
T Helper	Th
Thrombospondin-1	TSP-1
Tissue Resident Memory T Cell	Trm
Toll-Like Receptor	TLR
Transforming Growth Factor	TGF
Transmembrane Activator And CAML Interactor	TACI
Tumour Necrosis Factor (TNF)	TNF
Tumour Necrosis Factor Receptor Superfamily	TNFRSF
Vascularised Composite Allograft	VCA
Very Late Antigen-4	VLA-4
Violet Proliferation Dye	VPD
Visceral Adipose Tissue Macrophage	VATM
Xenograft Versus Host Disease	XvHD
α-chemokine	CXCR
β-chemokine	CCR

Chapter 1: Introduction

1.1. Allogeneic solid organ and vascularised composite transplantation– a brief history

Treatment of end-stage organ failure or unsalvageable tissue loss may include artificial replacement of tissue function, repair or regeneration of functional units or replacement with functional tissues transplanted from donor humans or animals. Transplantation currently remains the most appropriate and the most commonly used solution, as research into tissue engineered and bionic constructs continues to develop.

Poor outcomes following transplantation predominantly result from transplant rejection. This classically follows attacks on transplanted donor tissues by the recipients' immune system, which before the development of immunosuppressive treatments in the late 1950s, effectively rendered successful transplantation obsolete.

The first clinical description of allogeneic transplantation published in a scientific journal was a case of skin transplantation in 1869[1]. However, between then and the early 20th century it was rarely described and almost invariably unsuccessful in the long-term. The tissue destruction observed was typically ascribed to operative failure or impaired viability of the transplanted tissue.

The first instance of successful human allotransplantation was of a corneal transplant in 1906[2,3]. We now know that the inherent immune privilege and mechanisms of tolerance in the anterior segment of the eye[4] make this event unsurprising.

Appreciation for the immunological basis of allograft destruction evolved with developments in reconstructive surgery brought about by Sir Harold Gillies and Sir Archibald McIndoe, who utilised autologous tissues including skin grafts to replace tissues lost to burn and explosion injuries in soldiers[5]. Attempts to replicate these procedures in genetically disparate individuals however could only support temporary graft survival[6]. Pioneering investigations into this by Sir Peter Medawar and colleagues provided the first evidence of the immunological basis of allograft rejection[7-9], marking the advent of the field of transplant immunology.

Stemming from Alexis Carrel's transplant experiments in dogs—for which he won the Nobel Prize in 1912[10]—exploration of solid organ transplantation (SOT) as a means of restoring organ function gained traction. As surgical techniques to achieve successful transplantation in humans improved, so did research seeking to overcome immune-mediated rejection. In 1941, Frank Macfarlane Burnet proposed a theory of immune tolerance based on the notion that molecular distinctions between "self" and "non-self" dictate antibody formation[11]. At the same time the concept of acquired immunological tolerance—identified in dizygotic twin calves which developed mixed chimerism following mixing of venous blood *in utero*—influenced Sir Peter Medawar's seminal 1953 paper, which demonstrated the generation of tolerance to allogeneic murine skin grafts following *in utero* transplantation of cells from the same donor mouse strain[12].

Joseph Murray provided corroborating human results after performing the first successful human kidney transplant in 1954—an isograft between the identical Herrick twins[13]—then the first successful kidney transplant in non-identical twins[14], for which he used total body irradiation to overcome the immunological barrier evidenced by the rejection of skin

transplanted between the same brothers. Owing to multiple deaths from irradiation however, interest in alternative anti-rejection therapies cultivated interest in immunosuppressants. Azathioprine—developed by Elion, Lange and Hitchings and tested by Sir Roy Calne in 1957[15]—supported the first successful unrelated deceased donor transplant, which was performed by Murray in 1962[16] and opened the door to modern transplantation. In the same hospital that same year, the first successful upper limb replant was performed by Robert Malt, paving the way for the first vascularised composite allograft (VCA)—a hand transplant performed in Ecuador in 1964[17]. In this case, despite chemical immunosuppression, the allograft succumbed to rejection within 3 weeks[18]. Further complete failures in experimental animals[19] quelled the appetite for attempting VCA over the next three decades. The strong belief that skins antigenicity was insurmountable by immunosuppressants underlay this change and may have been reinforced by successful allotransplantation of liver, heart, lung, pancreas, and small bowel, which were supported by expanding options for immunosuppression. Development of mycophenolate mofetil (MMF) and tacrolimus, which enabled the survival of skin-bearing allografts in animal studies, restored belief in VCAs and led to the first successful human hand transplant in 1998[20], and partial face transplant in 2005[21,22], led by Jean-Michel Dubernard.

Building on this success, there have been over 150 upper extremity and 40 face transplants in addition to allografts of the abdominal wall, lower extremity, scalp, ear, larynx, uterus, and penis[23]. Encouragingly, the majority of recipients have regained function and the ability to work and complete activities of daily living.

1.2. The immunology of transplant rejection – an overview

1.2.1 Distinguishing self from non-self

The immune system is an elaborate network of cells and messengers capable of clearing foreign organisms and mutated host cells to protect hosts against infections and malignancies. To prevent immune system attacks against our own tissues (autoimmunity), mechanisms of differentiating between healthy self and foreign 'non-self' cells have been genetically encoded.

As such, where foreign antigens are identified within our bodies, immune responses are triggered and stimulate production of antibodies that mark infected cells for destruction and help to amplify broad immune system responses. Two molecules of the Human Leukocyte Antigen (HLA) system—a group of proteins unique to individuals and encoded by the major histocompatibility complex (MHC)—are present on a) all nucleated cells (MHC class I) and b) B cells, APCs and activated T cells[24]. These molecules present foreign antigen to the immune system, targeting them for destruction.

Immune responses to allo-transplantation are complex sequences of events that follow coordinated interactions between innate and adaptive immune cells. By virtue of their effectiveness in protecting us from foreign foes, manipulating these immune responses to tolerate foreign friends makes for a formidable task.

1.2.1. Processes in allo-rejection

Transplant rejection is the terminal result of destructive attacks effected by a recipient's immune system on tissues transplanted from an allogeneic donor. Allo-rejection is usually triggered by identification of donor HLA proteins.

Histocompatibility describes the degree of similarity between donor and recipient HLA genes and determines how tolerant of a transplant a recipient's immune system is likely to be. Nonetheless, even with substantial similarities, unless transplanted tissues are isografts (i.e., between genetically identical twins) allo-transplantation always results in a degree of rejection. Additionally, even following isografting other donor antigens can be identified as non-self and trigger immune responses.

Less commonly, 'graft versus host' (GvH) reactions occur, in which mature donor immune cells from within transplanted tissues attack non-self recipient cells. This typically occurs after stem cell transplantation and less frequently after blood transfusions.

1.3. Mechanisms of allograft rejection in skin and solid organs

Seminal studies led by Medawar evidenced the immunological basis of transplant rejection[7-9]. Employing a rabbit skin transplant model, he demonstrated long term survival of syngeneic grafts, contrasting with macroscopic rejection and microscopic immune infiltrates in allografts. Additionally, he unearthed the concept of donor-specific memory by demonstrating that after initial allograft rejection, subsequent transplants from the same donor reject more quickly. Together with evidence suggesting that innate immune cells alone may be insufficient to effect rejection[25], these discoveries concentrated interest in the role of adaptive immunity as the main drivers of rejection. More recently however, greater understanding of innate immunity in allo-rejection is emerging[26], from effector and regulatory functions to recent descriptions of innate cell memory to non-self antigens following transplantation[27].

1.3.1. Innate immune responses

1.3.1.1. The early tissue injury response

Antigen-independent injuries to both donor and recipient tissues (e.g. during surgery) can provoke pro-inflammatory stress responses by the innate immune system[28]. In transplanted tissues surgical trauma, oxidative stress from ischaemia-reperfusion injury (IRI)[29-32] and inflammatory cytokine release after brainstem or cardiac death can activate and recruit immune cells[33,34]. This typically involves recognition of damage-associated molecular patterns (DAMPs) by pattern recognition receptors (PRRs)—particularly toll-like receptors (TLRs)—which recognise allograft cellular molecules damaged by heat shock proteins (HSP), reactive oxygen species (ROS), high-mobility group box 1 proteins, heparan sulphate or donor brainstem death[35]. TLR ligation activates immune cells, which leads to danger signalling—including chemokine release and mobilisation of adhesion molecules such as P-selectin—stimulating recruitment of host leucocytes toward the transplant[36,37]. Within tissues, macrophages secrete inflammatory cytokines including interleukin (IL)-1, IL-6 and tumour necrosis factor (TNF)α, activating donor and host antigen presenting cells (APCs) and triggering migration to draining lymphoid tissues. Here, donor antigens are presented to host T cells, initiating the adaptive immune response[38-43].

1.3.1.2. Innate cell-mediated graft rejection

Activated infiltrating innate effector cells can damage allografts through several proinflammatory and cytotoxic mechanisms[26].

In the first 24h post-transplantation, macrophages comprise 40-60% of infiltrating cells[44]. Through phagocytosis and the production of reactive nitrogen and oxygen species,

macrophages damage vascular epithelium and parenchyma within allografts[45]. Additionally, by secreting proinflammatory cytokines, macrophages accelerate rejection directly and through activation of the adaptive immune system[46,47].

Polymorphonuclear neutrophils (PMNs) also infiltrate allografts within hours of surgery and cause tissue injury through similar mechanisms. Accordingly, interruption of neutrophil trafficking by depletion[48] or CXCL1/CXCL2 blockade[49,50] has been shown to prolong allograft survival.

Natural Killer (NK) cells are innate immune lymphocytes capable of clearing transformed and virus-infected cells without prior antigen priming. Their effector mechanisms include rapid cytokine release (e.g. interferon (IFN)-γ and TNF) and contact-mediated cytotoxicity through perforin, granzymes and Fas ligand[51]. Following transplantation, NK cells recognise non-self antigens through the "missing-self" system of activating and inhibitory receptors—including NKG2A/CD94—which activate NK cells upon detection of cells not expressing self-MHC class I.

Early experiments which showed inability of NK cells to reject heart and skin allografts in mice lacking adaptive immunity—recombination activating gene (RAG) 1 knockout (*Rag1*$^{-/-}$) or severe combined immunodeficiency disease (*Scid*) models—, suggested these cells were insignificant in rejection[51,52]. More recently however, the ability of fully activated NK cells (e.g., following IL-15 stimulation) to effect direct skin allograft rejection in RAG knockout mice has altered this notion[53]. In addition, allograft endothelial cells unable to deliver HLA I-mediated inhibitory signals to recipient NK cells have been shown to trigger microvascular inflammation and endothelial damage that results in rejection[54].

Dichotomous roles of NK cells in rejection have been indicated by tolerogenic activities identified following transplantation. Among other studies, Beilke *et al* demonstrated NK cells to be essential for tolerance induction via costimulatory blockade of CD154 or CD11a blockade[55], and Yu *et al* showed NK cells to regulate T cell alloreactivity by reducing passenger APC populations in recipients[56]. In both effector and regulatory roles, NK cells form an integral part of the host response to allo-transplantation.

The complement system represents a programme of over 30 proteins, which get exchanged between allograft and host tissues upon reperfusion[57]. These proteins modulate adaptive immunity and independently effect acute rejection through interactions with TLRs, the inflammasome and the clotting cascade[58]. Three complement activation pathways—classical (CP), lectin (LP), and alternative (AP)—are engaged by specific pathological stimuli and generate common downstream effectors. The CP becomes activated by antibodies bound to their target ligands, including donor-specific antibodies (DSAs) reactive to HLAs on allograft endothelial cells. The LP is activated following binding of ligands expressed on injured cells and pattern recognition molecules (e.g., mannose-binding lectin), which stimulate cleavage events through mannose-associated serine proteases (MASPs). The non-specific AP is continuously activated in plasma and amplifies downstream complement fragment generation.

Activation of complement through all three pathways results in C3 cleavage into C3a and C3b, the latter of which binds covalently to nearby surfaces, opsonising the target cells (Figure 1. Grafals, 2019[57]). Full activation results in cleavage of C5 into C5a and C5b, the latter of which recruits C5b-C9—the membrane attack complex (MAC)—which inserts pores into target cells,

leading to lysis or activation[59]. Additionally, certain complement proteins (e.g. C5a) are chemotactic and activate macrophages, neutrophils, T and B cells[57].

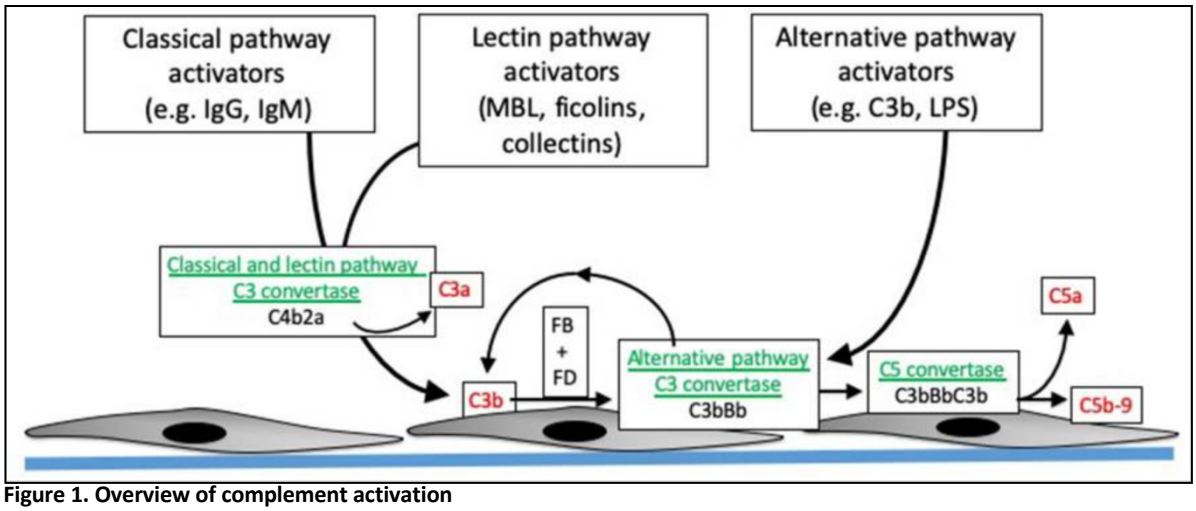

Figure 1. Overview of complement activation

Specific activating molecules engage the classical, lectin and alternative pathways. Cleavage of C4 and C2 generates C4b2a, the classical and lectin pathway C3 convertases (enzymes that cleave C3). C3 generated by the classical and lectin pathways can combine with factor B (FB), which is then cleaved by factor D (FD), to form C3bBb. C3bBb is the alternative pathway C3 convertase and can also be generated by spontaneous formation of C3b. The C3 convertases combine with another C3b to form the C5 convertase, which then cleaves C5 into C5b and C5a. C5b combines with C6, C7, C8 and C9 to form C5b-9- the membrane attack complex. Convertases are depicted in green and pro-inflammatory molecules generated during complement activation in red.

(The Role of Complement in Organ Transplantation by Grafals and Thurman[57] is licensed under CC BY 4.0).

In addition to its roles in effecting tolerance, immediate and acute rejection, increasing recognition for the role of the innate immune system in chronic rejection is emerging. Animal experiments and clinical studies demonstrating NK cell and macrophage populations dominating infiltrates in chronic rejection[60], together with evidence of poor graft outcomes following early macrophage infiltration[61], cause several authors to argue that innate mechanisms are as important as adaptive mechanisms in direct effector cell-mediated allograft rejection[62]. As an example, allograft damage that follows DSA production involves complement activation and/or NK cell recruitment in addition to intense B and T follicular helper (Tfh) cell interactions that occur in germinal centers[63]. Additionally, recent discoveries of heterogeneity, plasticity and memory functions suggest that understanding innate immune responses in transplantation may unearth valuable insights for therapy[62].

It is now worth exploring the long-perceived principal function of the innate system in transplantation – induction of the adaptive immune response.

1.3.2. Responses of the adaptive immune system

Owing in part to Medawar's discoveries of donor-specific immune responses and immunological memory, transplant research has concentrated for decades on the adaptive immune response and has yielded insights into three key lymphocyte processes – allo-recognition, signalling and responses.

1.3.2.1. Allo-antigen recognition by the adaptive immune system

Allo-recognition is a process by which genetically encoded polymorphisms between different organisms of the same species are detected by the immune system[64]. Following transplantation, APCs deliver donor tissue antigens to secondary lymphoid organs for presentation to recipient T cells in the context of MHC molecules. Recognition of specific donor peptide/MHC complexes initiates the adaptive immune response, leading ultimately to allograft rejection.

The primary effectors of allo-recognition are host T cell receptors (TCR), and donor HLA and minor histocompatibility (miH) antigens. Recognition of mismatched donor HLA antigens by TCRs triggers vigorous host rejection responses. Donor miH antigens (peptides typically derived from housekeeping proteins, and displaying some polymorphism[65]) are presented to host T cells in the context of host HLA molecules. In the absence of HLA mismatch (e.g. siblings with identical HLA antigens), miH mismatches lead to slow rejection[66].

The potency of T cell effector responses creates a requirement for mechanisms of protection against excessive T cell activation. Such protection comes in the form of three essential signals, all of which must be delivered to T cells to support full activation. The first signal follows binding of peptide-MHC complexes (where either peptide, MHC or both are derived from the donor) to TCRs of specific alloreactive T cells, initiating intracellular signalling cascades through the TCR-CD3 complex. The second signal is delivered when co-stimulatory ligands on the surface of APCs engage co-stimulatory receptors on T cells[67]. The third signal derives from cytokines typically produced by macrophages or dendritic cells (DCs) (IL12 and IFNα/β for $CD8^+$ T cells and IL-1 for $CD4^+$ T cells)[68]. After this, signalling and adhesion molecules are recruited into immunological synapses, initiating expression of genes that permit full T cell activation and clonal expansion.

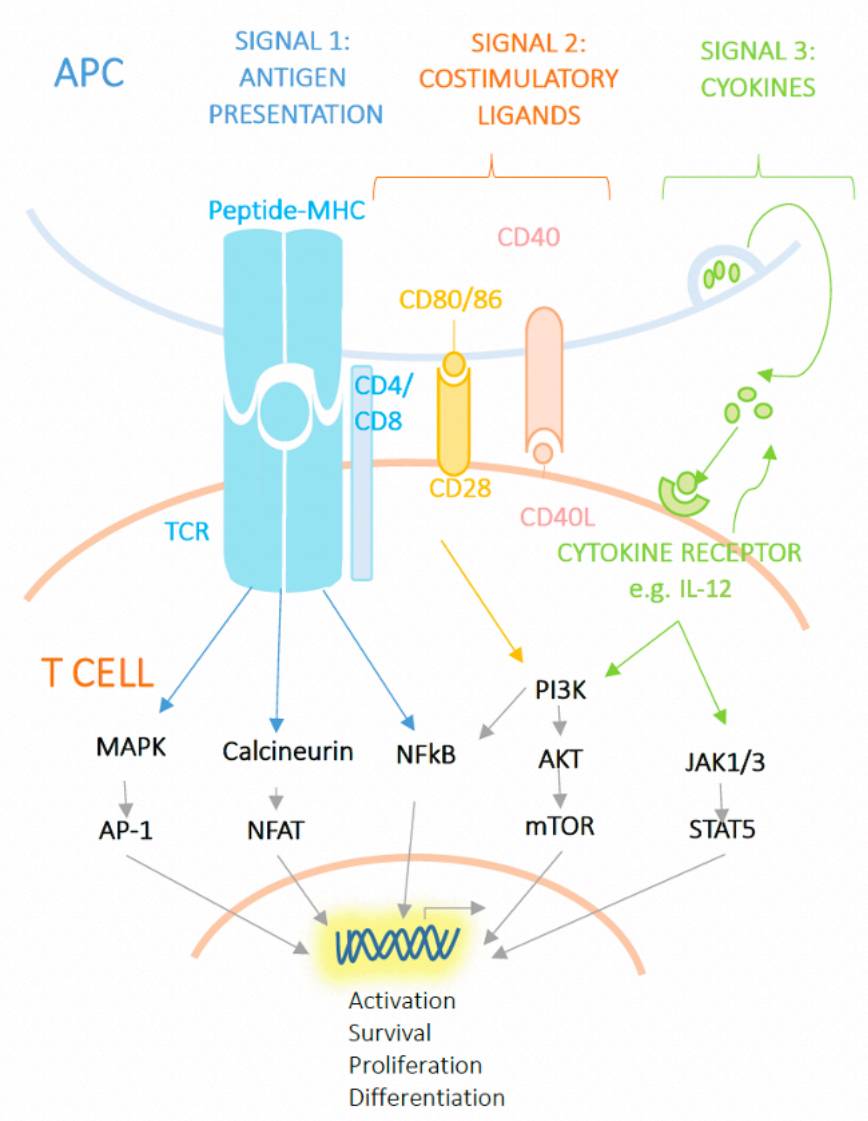

Figure 2 - Three-Signal Model of T Cell Activation
Antigen-dependent T Cell activation requires three biochemical signals. The first event in T cell activation is engagement of the TCR by its cognate peptide-MHC complex. The stability of the TCR:MHC interaction and the intracellular signalling events propagated by TCR stimulation are also dependent upon the interaction of a co-receptor (CD4 or CD8) with the MHC. These interactions initiate signalling pathway that ultimately activate the transcription factors, Nuclear Factor kappa-light-chain-enhancer of activated B cells (NFkB), Activator protein 1 (AP-1) and Nuclear factor of activated T-cells *(*NFAT*)*, responsible for orchestrating the transcriptional programs necessary for T cell activation. Further intracellular signalling, to stimulate T cell activation and survival, is induced downstream of costimulatory receptors or ligands on the surface of the T cell when these molecules engage with their binding partners expressed on the surface of the APC. One of the consequences of these signalling events is elevated secretion of mitogenic cytokines, especially IL-2, which stimulate proliferation in an autocrine and a paracrine manner.
(Adapted from Investigation of the cell biology of human regulatory T cells in the context of transplantation by K Milward (2016) with permission).

There are three known pathways through which recipient T cells can recognise donor allo-antigens—direct, indirect, and semi-direct[64].

Direct allo-recognition occurs early after transplantation, when donor DCs (passenger leucocytes) migrate through lymphatics and into recipient regional lymph nodes (LNs)[69,70], where recognition of allogeneic MHC molecules activate donor-reactive naïve T cells[71]. The direct T cell allo-response differs from conventional responses of T cells primarily in its polyclonality. It is estimated that less than 0.1% of the total T cell repertoire typically reacts to nominal protein antigens, whereas direct allorecognition involves up to 10% of T cells[72-75]. Two models proposed to explain this unique allo-response are:

1) the 'high determinant density' model, which proposes that TCRs recognise donor MHC polymorphisms independently of the peptide within the MHC groove[76]. As such, all polymorphic MHC molecules presented by donor cells (i.e., any of the molecules on any of the cells) effectively serve as ligands for the allo-reactive T cells TCRs, creating a high ligand density. By virtue of this, the affinity threshold required to generate an optimal allo-response may be substantially lower than that required by self-MHC-peptide complexes[77].

2) The 'multiple binary complex' model, which by contrast is based on the principle that individual allo-reactive T cell clones interact with allogeneic MHC molecules that are occupied by a defined peptide. As MHC molecules present a multitude of different peptides, several allo-MHC-peptide complexes can act as ligands for different T cell clones.

Indirect allo-recognition occurs when allogeneic MHC peptides are presented to recipient allo-specific T cells by self- MHC molecules on recipient APCs, triggering activation. Where and how recipient APCs take up and process donor antigens remains unclear. It is possible that acquisition occurs either within the graft, in host lymphoid organs via pinocytosis of shed

donor proteins, following donor antigen transfer by cell-cell contact or by phagocytosis of donor-secreted extracellular vesicles, dead donor cells or apoptotic bodies[64].

Determinant mapping and studies of TCR repertoire have demonstrated that indirect allo-recognition is initially oligoclonal, mediated by a small set of T cell clones specific for a few dominant allogeneic MHC peptide determinants[78]. Over time, it expands to include allo-MHC peptides that were 'cryptic' (i.e. not processed or presented with sufficient efficiency to trigger T cell responses)[79] but become detectable as systems such as "MHC-guided processing" increase the chances of successful recognition[80]. Antigen spreading in this manner may also promote sustained responses involved in chronic rejection[81].

Indirect allo-recognition is also perceived to be the main driver of miH allo-recognition.

Semi-direct allo-recognition occurs when MHC molecules are transferred between donor and host APCs, leading to 'cross-dressed' allo-presentation, which triggers allo-specific T cell stimulation. In this regard, both professional APCs and endothelial cells have been shown to exchange MHC molecules, which can occur via cell-cell contact[82] and through secretion of donor exosomes[83]. MHC acquisition activates recipient APCs, which can trigger full activation of T cells. Depletion of recipient DCs has been shown to drastically reduce donor MHC presentation and prolong graft survival[84], leading some to question the significance of direct allo-recognition[83], particularly within allografts.

The prevailing notion has long been that early acute rejection is mediated by the potent inflammatory responses of directly activated T cells, and that as donor APC numbers progressively reduce, this mechanism subsides and is superseded by indirect activation, which is the predominant driver of chronic rejection. Recent appreciation for the extent and potency of cross-dressed activation—described recently as "a major antigen presentation pathway

driving effector T cell responses within allografts"[85]—opens new perspectives for therapeutic research.

1.3.2.2. Adaptive immune cell activation

1.3.2.2.1. T cells

Successful T cell activation requires three extracellular stimulatory signals—delivered through TCRs, co-stimulatory receptors and cytokines. Without these, T cells would undergo cell death or anergy (Figure 2).

Firstly, TCRs and their respective CD4 or CD8 co-receptors must recognise their specific cognate antigens presented within MHC molecules[86].

Secondly, co-stimulatory receptors colocalising with TCR molecules at immunological synapses should simultaneously deliver non-antigen-specific stimulatory signals. Such synergistic signalling promotes T cell activation and determines effector function, subset differentiation and survival[87].

Most co-stimulatory molecules in T cell activation are members of either the immunoglobulin superfamily (IgSF) or the tumour necrosis factor receptor superfamily (TNFRSF). An array of receptors from both groups influence T-, B- and NK-cell signalling (Figure 2). T cell activation predominantly follows signalling through CD28, B7 (IgSF) and TNFSRs (e.g. 4-1BB, OX40, CD27, CD30, DR3, GITR and HVEM). Interactions between CD28 (constitutively expressed on T cells) and CD80/CD86 (B7 proteins induced on activated APCs) stimulate signalling cascades including the PI3K-AKT pathway, which activates Nuclear Factor kappa-light-chain-enhancer of activated B cells (NF-κB), nuclear factor of activated T cells (NFAT), BCL-XL, mammalian target of rapamycin (mTOR), glucose transporter type 1 (GLUT1) and other downstream

targets, promoting cell proliferation and survival[88]. This is due in large part to upregulated expression of the T cell growth factor IL-2 and its high affinity receptor IL-2 (IL-2R) α-chain. CD28 signalling upregulates expression of additional co-stimulatory molecules including CD154 (CD40 ligand), which binds CD40 and activates APCs. These activated APCs increase B7 expression, enhancing their capacity to activate further T cells.

CD28 co-stimulation also promotes IL-2 production through recruitment and activation of factors such as the adaptor protein growth factor receptor-bound protein 2 (GRB2) to its intracellular motifs[89], and induces expression of other cytokines, leading to autocrine/paracrine activation.

To counteract co-stimulatory signalling, co-inhibitory receptors regulate T cell function through mechanisms including inhibiting cytokine production and cell cycle progression, and by rendering T cells unresponsive or anergic. Most notably, Cytotoxic T Lymphocyte-Associated protein 4 (CTLA-4) exerts co-inhibitory function by:

1) Preventing B7-mediated CD28 co-stimulation through
    a. competitive inhibition (higher avidity binding)[90]
    b. trans-endocytosis (physical removal) of APC surface CD80 and CD86[91]
2) Inducing expression of indoleamine 2,3-dioxygenase (IDO), which inhibits T cell function through tryptophan deprivation[92]
3) Modulating distal signalling events by inhibiting phosphorylation c-Jun N-terminal kinases (JNKs) and extracellular signal-regulated kinases (ERKs)[93].

The third essential signal for T cell activation is received from cytokines released by lymphocytes, innate cells and epithelial cells. These chemical messengers—detected in autocrine, paracrine or endocrine fashion—direct T cells to become specific effector subtypes[87]. For T helper cells, exposure to IL-12 directs differentiation into Th1 subtype cells, IL-4 into Th2 cells, and IL-6/IL-23 into Th17 cells (discussed below). Cytokine stimulation also amplifies clonal expansion of T cells and activation of other immune cells.

The balance of stimulatory and inhibitory signals to T cells determines whether activated or anergic phenotypes are expressed.

1.3.2.2.2. B cells

B cell activation follows binding of the IgM/IgD B cell receptor (BCR) on resting cells, to soluble or membrane bound antigen. Upon activation, BCRs form microclusters capable of triggering downstream signalling pathways. BCR microclusters subsequently enter a contraction phase and form immunological synapses, which permit stable interactions to form with T cells and support delivery of bi-directional co-stimulatory activation signals. Activated B cells may undergo class switch recombination, in which unwanted Immunoglobulin (Ig) genes (e.g., IgM/IgD) are excised so that desired genes (either IgA, IgE or IgG) can be expressed.

Co-stimulation is received following interactions between three TNFRS receptors—'transmembrane activator and CAML interactor (TACI)', 'B cell-activating factor receptor' (BAFFR) and 'B cell maturation protein' (BCMA)—and their ligands—'a proliferation-inducing

ligand' (APRIL) and 'B cell-activating factor' (BAFF)[87]. Co-stimulation delivered through these receptors promotes survival and class-switch recombination in activated B cells.

1.3.2.3. Adaptive immune system effector responses to allogeneic tissue

Activation of alloantigen-reactive lymphocytes initiates a multifaceted process in which the adaptive immune system can target allogeneic tissue in a manner that can be rapidly escalated upon repeated exposure. Following allo-recognition and activation, donor tissues are rejected by cytotoxic T cells and NK cells (cell-mediated rejection) or by B-and plasma cell-derived antibodies (humoral rejection)[94].

1.3.2.3.1. B cells

Following transplantation, B cells present allo-antigens to T cells and contribute to acute rejection through allo-antibody induction. During this process, allo-antigen recognition by BCRs initiates signalling cascades that lead to B cell maturation and secretion of donor-reactive antibodies. Following binding of antibodies to cognate allo-antigens on donor cells, complement becomes fixed on donor cell surfaces, innate cells are recruited via their Fc- and complement receptors, and donor cells are killed by complement-mediated cytolysis, phagocytosis or antibody-mediated cellular cytotoxicity (by macrophages and NK cells). Antibody-mediated rejection following generation of *de novo* donor-specific antibodies also participates in chronic as well as acute allograft dysfunction[95]. Identification of B cell infiltrates and deposits of antibody and complement protein c4d in biopsies of rejecting allografts supports this theory[94]. A causal link between antibodies and graft rejection has been demonstrated in a murine heart transplant model in which allo-reactive antibodies

transferred into lymphocyte-deficient mice induced chronic allograft vasculopathy, whereas B cell-deficient mice did not develop arterial lesions[96].

Contrasting studies have demonstrated B cells to be dispensable for allograft rejection and there is mounting evidence indicating the presence of intragraft B cells which are neutral or even protective against allograft rejection[97].

Hyperacute rejection of vascularised allografts is a well-characterised phenomenon triggered upon allograft re-perfusion, in which pre-formed anti-donor antibodies activate complement and stimulate endothelial cell release of Von Willebrand procoagulant factor, causing rapid vessel thrombosis and graft necrosis[98].

1.3.2.3.2. T cells

In allograft recipients who do not possess pre-formed anti-donor antibodies, cell-mediated rejection (principally by T cells) is widely regarded as the dominant allo-response.

Following activation by DCs, naive alloreactive $CD4^+$ T cells can differentiate into T helper cells (e.g., Th1, Th17, Th2), or regulatory T cells (Tregs). In pro-inflammatory environments such as allograft sites, naive $CD4^+$ T cells predominantly differentiate into pro-inflammatory Th1 and Th17 cells.

Th1 cell differentiation is induced by IL-12 and Th1 responses correlate with acute rejection episodes. Th1 cells secrete IFN-γ and IL-2, which assist in CTL priming, stimulation of humoral immunity, and activation of both macrophage-dependent delayed-type hypersensitivity and NK cell effector function. CTLs effect graft rejection by secreting cytolytic enzymes (granzyme

A, B and perforin), and by triggering apoptosis on target cells expressing allogeneic MHC class I molecules, through the Fas/FasL pathway.

Th17 cells are potent pro-inflammatory lymphocytes associated with several autoimmune and inflammatory diseases[99]. They have been identified as early migrators into cardiac allografts[100] and Th1/Th17 cells (a subset of the Th17 response) as critical participants in late acute and chronic rejection[101]. Th17 cells are induced in inflammatory environments by transforming growth factor (TGF) β, IL-6, and IL-1β and matured by IL-23. They secrete IL-17, IL-21 and IL-22, and reduce T cell IL-10 production[102]. IL-17 stimulates production of inflammatory cytokines and chemokines, which recruit neutrophils and macrophages. IL-21 potentiates cytotoxicity of $CD8^+$ T cells and NK cells[103] and promotes development of antibody-producing plasma cells. In kidney transplant recipients, frequencies of IL-21 producing cells has been shown to predict risk of early and late rejection[104]. IL-22 has multiple functions and is critical for DTH responses[101].

Th2 cells are induced by IL-4, produce IL-4, IL-5, IL-9, IL-10 and IL-13, and are strongly correlated with chronic rejection. Mechanisms of Th2-mediated rejection include B cell activation via cell-cell contact, proliferation and antibody class-switching via IL-2, IL-4 and IL-5 release, and eosinophil recruitment.

Memory T cells induce quicker and more effective immune responses than naïve T cells and require less antigen stimulation to do so. In transplantation, studies have demonstrated high memory T cell frequencies to correlate with higher risk of acute rejection[105,106], reduced allograft survival[107] and impaired tolerance[108]. Memory T cells are $CD45RO^+CD45RA^-$ and exist

as central (Tcm) or effector (Tem) type depending on their expression of the lymph-node homing molecules CCR7/CD62L and differ functionally by homing potential and effector function.

Owing in part to absent CCR7 and low CD62L, together with high expression of CCR1, CCR3, CCR5 and β1 and β2 integrins, Tem cells are frequently peripheral, migrating to inflamed non-lymphoid tissues where they immediately demonstrate effector functions (e.g., IFN-γ production). In contrast, high CD62L and CCR7 expression and intermediate CCR4 and CCR6 expression localises Tcm cells predominantly to lymphoid tissues. Tcm cells do not demonstrate immediate effector function, however they produce IL-2 and proliferate more extensively upon re-stimulation than Tem[109,110].

Skin-homing T cells follow anatomically demarcated migration patterns, with $CD4^+$ cells predominantly accessing the dermis and $CD8^+$ cells accessing the epidermis[111,112]. This may be associated with expression of the chemokine receptors CCR4 and CCR10, for which the cognate ligands CCL17 and CCL27 are expressed in the dermis and epidermis, respectively[113].

1.3.2.4. Regulatory T cells in transplantation

Regulatory T cells (Tregs)—$CD4^+CD25^+$T cells expressing the transcription factor FoxP3—are important mediators in preventing immunity against self-antigens and non-harmful foreign antigens. They also participate in suppressing anti-tumour immunity and responses against chronic infections[114]. Within animal models, augmenting Treg function has been shown to be effective in prevention and treatment of immune-mediated diseases. As such, approaches to boost Treg activity are being translated to humans. Recent clinical trials of regulatory immune

cell therapies indicate that they are achievable, safe and potentially useful in kidney transplantation, minimising the burden of general immunosuppression[115].

Mechanisms of Treg-mediated suppression include:

1) Immunosuppressive cytokine production (e.g., IL-10, TGF-β, IL-35)
2) Coinhibitory molecule expression, dampening APC function (e.g., CTLA-4, PD-1, LAG-3)
3) Metabolic environment disruption, through sequestering of IL-2 and pericellular adenosine production
4) Cytotoxicity

In vitro studies showing cell-contact–dependent suppressive effects and *in vivo* demonstrations of physical interactions between Tregs, effector T cells and APCs indicate that these mechanisms require cells to be in close proximity[116-118].

1.3.2.5. Chemokines

Chemokines are a family of chemoattractant cytokines with critical roles in inflammatory processes, including transplant rejection. Initially characterised by their ability to induce leucocyte migration, chemokines and their receptors also participate in leucocyte activation, promotion of effector function, modulation of hematopoiesis and angiogenesis, homeostatic trafficking of leucocytes through tissues and lymphatics[119] and modulation of the adaptive immune response through positioning of cells in lymph nodes[120]. As such, chemokines expressed in allografts are potential therapeutic targets for the prevention of allograft rejection.

Chemokines are broadly divided into 2 categories:

1) Constitutive chemokines, which regulate lymphocyte and DC trafficking through peripheral tissues in homeostatic (non-inflammatory) immune surveillance

2) Inducible chemokines, which are typically expressed at sites of inflammation and control recruitment of effector leucocytes and orchestrate innate and adaptive immune responses.

There are approximately 50 low–molecular-weight chemokines (8-14 kd), which bind and signal through 7 transmembrane-spanning G-protein–coupled receptors expressed on leucocyte and other cell surfaces[121,122]. Homologous sequences are shared between chemokines and these are classified into 4 main families (CXC, CC, C, and CX3C) based on a cysteine motif in the amino-terminal portion of the protein. These families recruit different leucocyte types (e.g., CC chemokines predominantly recruit monocytes-macrophages and lymphocytes and CXC chemokines principally recruit neutrophils).

Chemokines also induce expression of integrins on leucocyte surfaces and facilitate bidirectional leucocyte-endothelial cell interactions, which augment adherence to and transmigration through vessel walls and into tissues[123,124]. Chemokines involved in alloreactive T cell recruitment include RANTES (regulated upon activation, normal T-cell expressed and secreted), MIG and IP-10, which bind the chemokine receptors CCR1, CCR3, CCR5 (RANTES), and CXCR3 (MIG and IP-10)[125-133]. Thus, interactions between chemokine- and chemokine receptor–expressing lymphocytes in tissues have implications for locally directed recruitment of leucocytes into allografts.

1.3.2.5.1. Chemokines in allograft rejection

1.3.2.5.1.1. The role of chemokines in inflammation

Following transplantation, chemokines influence four key immune processes[134]:

1) Mononuclear cell recruitment to inflammatory sites

2) APC migration to draining lymph nodes (LNs)

3) Naive T cell-APC interactions within LNs

4) Trafficking of primed alloreactive T cells to allografts

Early leucocyte recruitment is often initiated by local inflammatory responses to surgery and ischemia-reperfusion injury (IRI), which develops following restoration of blood flow to vascularised allografts. Cytokines (including IL-1, IL-2, TNF and IL-4)[135,136]; chemokines (RANTES, MCP-1, CCL3, CXCL10, CCL7, CCL11, CCL2, CCL22, CXCL1, CXCL8 and CX3CL1[137]); and adhesion molecules (P- and E selectin and intercellular adhesion molecule 1 (ICAM-1)) promote leucocyte recruitment and activation of innate and cell mediated immune responses[135,138].

Chemokines participate in all stages of the allo-immune response during acute and chronic rejection—antigen presentation, activation of the host immune system, effector responses and regulation. Notable receptor-ligand pairs are shown in Table 1[139]. The roles each play in transplantation have been investigated directly—through expression profiling—and functionally—using knockout (KO) mice, receptor agonists/antagonists and blocking antibodies.

Receptor	Chemokine	Cell types
CXCR1	CXCL8 (IL-8), CXCL6 (GCP2)	Neutrophils, monocytes
CXCR2	CXCL8 (IL-8), CXCL1 (GROα), CXCL2 (GROβ)	Neutrophils, monocytes, endothelial cells
CXCR3	CXCL9 (MIG), CXCL10 (IP-10), CXCL11 (I-TAC)	T cells, Th1 T cells
CCR2	CCL2 (MCP-1), CLL8 (MCP-2)	T cells, memory T cells, monocytes, DCs,
CCR4	CCL17 (TARC), CCL22 (MDC)	T cells (regulatory?), DCs
CCR5	CCL3 (MIP-1α), CCL4 (MIP-1β), CCL5 (RANTES)	T cells, monocytes
CCR7	CCL19 (ELC), CCL21 (SLC)	T cells, DCs
CCR8	CCL1 (I309)	T cells (regulatory?)

Table 1. Chemokines & their receptors in transplantation
(Reprinted from Transplantation Reviews, Vol 21, issue 2, Schadde & Knechtle, Review: chemokines in transplantation[139], Pages 107-118, Copyright (2007), with permission from Elsevier (License no. 5182161288611)

Three important inflammatory chemokine/receptor pairs involved in allo-immune responses are CXCL10 (IP-10)/CXCR3, RANTES/CCR5 and MCP-1/CCR2.

1.3.2.5.1.2. IP-10/CXCR3

CXCR3 is expressed on T cells and has been shown to influence T- and mononuclear cell recruitment to allografts. IP-10 expression was first described in human heart transplant rejection[129]. In kidney transplant rejection elevated urinary IP-10 and CXCL9 (MIG) (another CXCR3 ligand) have been identified[140]. Additional experimental evidence of CXCR3 knockout and blockade prolonging allograft survival[139] suggests IP10/MIG-CXCR3 signalling participates in accelerating acute rejection and these molecules may therefore serve as markers of rejection.

1.3.2.5.1.3. RANTES/CCR5

RNA and protein expression of CCR5 (on T cells and monocytes) and its ligands—RANTES, Macrophage inflammatory protein (MIP)-1α, and MIP-1β—is commonly described in acute and chronic human allograft rejection[141]. In these investigations alloimmune rejection was demonstrated to involve chemokine production, and expression of CXCR3 and CCR5 on intragraft leucocytes identified as infiltrating effector cells. An important observational study identified improved transplant survival in patients with a naturally occurring human CCR5 mutation (*CCR5Δ32*), which results in defective CCR5 expression[142]. There was no corresponding decrease in acute rejection episodes, however this study and others stimulated research which has broadened our understanding of CCR5 biology, pharmacology and non-chemotactic properties[143] including modulation of immune cell behaviour, survival and retention in tissues[144]. The CCR5 antagonist Maraviroc effectively prevents CCR5 internalisation and blocks T cell chemotaxis in high-risk GvHD patients[145]. However, concerns regarding hepatotoxicity have limited trials investigating its efficacy as a prophylactic treatment[146].

1.3.2.5.1.4. MCP-1/CCR2

CCL2 (MCP-1) is expressed in acutely rejecting human transplants. Its receptor—CCR2—is expressed on monocytes and a small percentage of T cells. Similarly to CCR5, mutants of the CCR2 receptor influence intragraft leucocyte populations[147], allograft rejection and survival[148,149].

Interestingly, the influence of some chemokine receptors on rejection appears to be organ-dependent. For example, in a murine major mismatch model Abdi *et al* showed CCR2

deficiency to double islet allograft survival time, whereas major mismatched heart transplant survival was not prolonged[150]. This phenomenon may relate to lower involvement of CCR2 in inflammatory trafficking of T cells than APCs or to varying effects on certain receptor-bearing immune cells under different conditions[139]. Importantly, it suggests that chemokine pathway-targeting therapies may have organ-specific efficacies.

1.3.2.5.2. Chemokines in memory cell trafficking

Owing to their high frequency, low co-stimulatory requirements, low activation thresholds, and relative resistance to apoptosis, allo-reactive memory cells are formidable proponents of allo-immunity, and render many tolerance induction therapies ineffective[139]. Donor-reactive memory T cells can arise from:

1) Pre-transplant sensitisation (e.g., following blood transfusion)

2) Residual effector T cells, which do not undergo post-transplant apoptosis in response to the immunosuppressive treatment

3) Heterologous immunity, in which T cells primed by environmental antigens or infections cross-react with allogeneic MHC molecules.

Classification systems used to distinguish memory T cell subsets are frequently based on chemokine-influenced cellular distributions. A common functional classification describes

1) T_{CM} cells—which survey lymph nodes and return to the blood after infection[151],

2) T_{EM} cells—which survey non-lymphoid peripheral tissues and egress into the blood via lymphatics

3) Tissue resident memory T (T_{RM}) cells—which provide rapid and long-lasting immunological protection in skin and other peripheral tissues, and do not recirculate the blood[152].

T_{RM} cells play vital roles in the recurrence of chronic inflammatory skin disorders such as psoriasis and vitiligo and are thought to be associated with vascular and epithelial injury following facial transplantation[153,154]. T_{RM} cells can differentiate from other T cells in response to signals received within allografts and can persist long-term[155]. Given that intragraft allo-reactive memory T cells proliferate and can mediate significant injury; inhibiting trafficking into allografts is an attractive strategy—one which has been used to prolong allograft survival[156]. The sphingosine-1 phosphate receptor agonist FTY720—used to treat multiple sclerosis—sequesters T cells in the thymus and lymph nodes by preventing migration. In transplantation, this can inhibit trafficking to peripheral graft sites, as seen in murine heart allograft models in which delayed rejection was associated with sequestration of $CD4^+$ memory T cells[157]. Disruption of adhesion molecules, notably leucocyte integrins including LFA-1 and VLA-4 has been shown to inhibit infiltration of memory T cells into grafts and prolong allograft survival. However, in human renal transplantation efalizumab (anti-LFA-1) was associated with a higher rate of EBV-associated malignancy[158]. Despite this undesirable effect, the findings of animal studies suggest that targeting other trafficking molecules on memory T cells could be efficacious. Further investigations into this are ongoing.

1.3.2.5.3. Chemokines in immune regulation

Tregs prudently prevent systemic autoimmunity[159] and possess the capacity to regulate more localised inflammation in tissues such as rejecting allografts[160]. This capacity owes in part to their ability to both migrate and direct migration of other immune cells.

The essential roles chemokine receptors play in Treg trafficking and immune regulation are well described[161-164]. Treg homing is also essential in suppressing graft-versus-host disease[165] and for accessing paracrine IL-2, which is required to maintain certain Treg populations[166].

Harnessing the chemotactic capacities of Treg-attracting chemokine receptors could provide an enticing approach for eliciting beneficial anti-rejection responses. Two candidate receptors, which are associated with Treg migration both to sites of inflammation and to skin are CCR4 and CCR8.

1.3.2.5.3.1. CCR4 on lymphocytes

The chemokine receptor CCR4 is expressed by Tregs, effector T cells and certain T cell lymphomas, however not by naïve, cytotoxic or Th1 cells[167,168]. Its ligands CCL22 and CCL17 are mainly produced by DCs and macrophages and are highly expressed in skin and lymphoid tissues. The CCR4–CCL17/22 axis plays a major role in Treg migration. Enhanced CCR4 expression is seen on activated effector Tregs residing in non-lymphoid tissues (e.g., skin and lung) or in the periphery[169], suggesting that CCR4 both directs activated effector T cells and recruits Tregs to sites of inflammation to maintain immune homeostasis. Indeed, CCR4-deficient Tregs have been unable to infiltrate areas of localised tissue inflammation and failed to control immune responses in a number of inflammatory disease models[169,170].

CCR4-expressing Tregs migrate to tumour microenvironments in response to CCL22 secreted by tumour cells[171] and clinical studies have identified an abundance of $CCR4^+$ Tregs in tumour microenvironments in adult T cell lymphoma/leukaemia[172], breast cancer[173], non-Hodgkin's lymphoma[174], head and neck cancer [175] and melanoma[167,176]. In all, the preponderance of $CCR4^+$ Tregs is thought to provide immunoregulatory activity, which hinders induction of effective anti-tumour immunity. Mice with $CCR4^{-/-}$ Tregs develop severe skin inflammation[169], and in an adoptive transfer model CCR4 expression was necessary for Treg-mediated suppression of the effector phases of allergic responses[177]. Following skin transplantation, recruitment of greater numbers of immunosuppressive Tregs may prevent or delay allo-rejection. In support of this view, anti-CCL22 mAbs significantly reduced Treg migration into tumours in an ovarian cancer model[178]. In addition, *in silico* analyses identified small molecule CCR4 antagonists, which significantly reduce CCL22 and CCL17-mediated human Treg migration *in vitro* and in murine Tregs *in vivo*. These CCR4 antagonists enhance immune responses by inducing antigen-specific effector CTLs when combined with vaccines, consistent with the concept that blocking CCR4 alleviates immune suppression[168,179]. Mogamulizumab, an anti-CCR4 monoclonal antibody has been shown to selectively deplete activated Tregs and increase production of IFN-γ and TNFα by $CD8^+$ T cells[167]. It has successfully completed phase I&II clinical trials and demonstrated clinically meaningful antitumor activity in relapsed patients with adult peripheral T cell lymphoma and cutaneous T-cell lymphoma[180].

1.3.2.5.3.2. CCR8 on Tregs

CCR8 is expressed on several types of immune cells including lymphocytes. In Tregs, CCL1 is the cognate ligand and induces Treg migration *in vitro*[181]. CCR8-deficient Tregs demonstrate greater susceptibility to cell death after allogeneic adoptive transfer and have been shown to be unable to prevent T cell-induced GVHD in the colon and lungs[182], indicating that CCR8 plays an essential role in Treg preservation, long-term fitness and functionality in non-lymphoid organs. It has recently been shown that when compared with peripheral Tregs and other T-cell subsets, intra-tumour Tregs or Tregs in adjacent tissues selectively up-regulate CCR8 expression[183], which is proposed to correlate with enhanced suppressive capability. Intra-tumour Tregs in breast cancer demonstrate markedly high CCR8 expression compared with normal breast and peripheral blood Tregs[183]. High CCR8/FOXP3 mRNA ratios in intra-tumour Tregs have been associated with lower disease free and overall survival in breast cancer patients, purportedly due to enhanced suppressive activity of $CCR8^+$ Tregs, abrogating the anti-tumour immune response. CCR8 blockade has recently been shown to destabilise intra-tumour Tregs and coincide with increased antitumour immunity[184] in invasive bladder cancer, and depletion of CCR8+ Tregs by means of an FcyR engaging anti-CCR8 antibody, to produce dose-dependent, effective, long-lasting anti-tumour immunity[185,186].

Other recent investigations have identified a key role for $CCR8^+FOXP3^+$ Tregs as master drivers of immune regulation, capable of suppressing experimental autoimmune encephalitis in response to administration of a CCL1 activating antibody[187]. As part of this, $CCR8^+$ Tregs employ a 'self-feeding' mechanism producing CCL1, which upregulates CCR8 expression and potentiates *in vivo* proliferation and suppressive activity[187]. These findings suggest that high levels of $CCR8^+$ Tregs are associated with an increased immunosuppressive requirement. Abrogation of CCL1-CCR8 signalling in a murine atherosclerosis model has also been shown

to reduce Treg migration and IL-10 expression and increase Th1/Th2 ratio and vessel atherosclerosis[188].

In addition to expressing chemokine receptors, Tregs also produce chemokines, which direct immune cell trafficking. Human Tregs have been shown to produce the neutrophil attractant CXCL8[189], and the T- and NK-cell attractant XCL1[190]—both of which contribute to their suppressive capability—and the T-cell attractants CCL3 and CCL4, which are expressed less by Tregs in patients with type 1 diabetes[191]. The notion of human Tregs producing chemokines was somewhat surprising, as chemokines were traditionally thought of as promoters of inflammation[192].

1.4. Humanised mouse models in transplantation research

The ability to conduct experiments on human cells and tissues in small animal models holds great value for immunological research. Humanised immune system (HIS) mice are produced by successful transfer and engraftment of human haematopoietic cells into immunodeficient mice. These *in vivo* models provide a powerful tool for the study of long-term human haematopoiesis and for the preclinical investigation of transplant rejection, cancer, autoimmunity and infection. Humanisation can be achieved through adoptive transfer of haematopoietic stem and progenitor cells (HSPCs) or peripheral blood mononuclear cells (PBMCs) or mononuclear cells (MNCs) into different immunodeficient mouse strains, depending on experimental settings.

Immunodeficient strains such as the non-obese diabetic (NOD)/severe combined immunodeficiency (SCID)/IL-2 receptor gamma chain null (IL2r$\gamma^{-/-}$) mouse (NSG) [193] have

profound deficiencies of innate and adaptive immunity and impaired capacity to repopulate the murine bone marrow, both of which enhance engraftment of human haematopoietic stem cells (HSCs)[194]. Limitations in HSC humanisation include (i) the requirement for myeloablative pre-conditioning of host mice in order to create a bone marrow niche in which human HSCs can engraft and (ii) the challenges that remain in reconstituting entire the spectrum of immune cells[195,196]. To overcome these, microenvironmental alterations to favour human haematopoiesis have been described (Figure 3 – Adigbli *et al*, 2020[197]). Methods include (i) mutation of critical murine growth factor receptors, such as the c-kit receptor (NSGW41, NSGWv/+, NSGWv, NBSGW, SRG-W41 and BRgWv mice)[198,199], (ii) inhibition of growth factor receptor function (e.g. anti-c-kit receptor antibody)[200] (iii) exogenous human cytokine administration (e.g. BlyS for mature human B cell reconstitution[201] and IL-7 analogues for T cell reconstitution[202]) and (iv) knock-in of human cytokine genes such as in SGM3[203], MISTRG[204], SRG-15[205] and hIL-6 Tg NSG[206] strains, which include knock-ins of IL-3, IL-15, GM-CSF, M-CSF or IL-6 to support engraftment of the wider human hematopoietic repertoire, including innate cells and regulatory T cells[203].

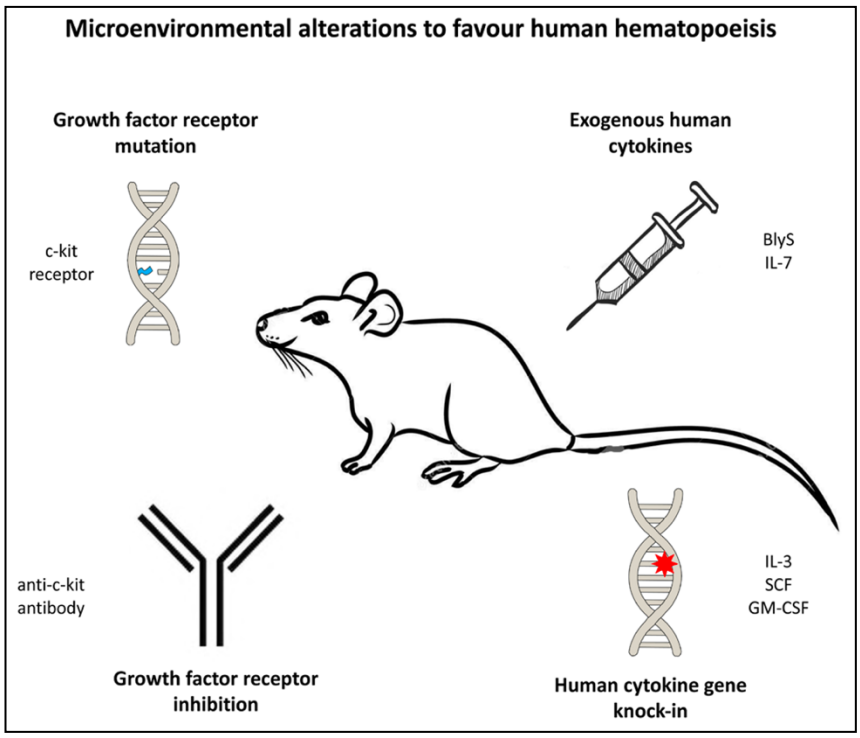

Figure 3. Microenvironment alterations to enhance human haematopoiesis.
BlyS, B lymphocyte stimulator; GM-CSF, granulocyte macrophage colony-stimulating factor; IL, interleukin; SCF, stem cell factor
(Reprinted from Transplantation, Vol 104, issue 11, Adigbli et al, Humanization of Immunodeficient Animals for the Modeling of Transplantation, Graft Versus Host Disease, and Regenerative Medicine, Pages 2290-2306, Copyright (2018), with permission from Wolters Kluwer Health (License no. 5182170630287)

To address the requirement for preconditioning and adoptive transfer of large numbers of HSCs to attain high levels of human leucocyte chimaerism[195,207], the NOD,B6.SCID IL-2rγ$^{-/-}$ Kit$^{W41/W41}$ (NBSGW) immunodeficient mouse strain was developed by adding *Kit$^{W41/W41}$* alleles to the NSG[208]. This allele affords a competitive advantage to transplanted HSCs through a loss-of-function mutation of the tyrosine kinase motif of the stem cell factor receptor, c-Kit. A recent study demonstrated successful humanisation of NBSGW mice using HSCs sourced from human umbilical cord blood (hUCB), bone marrow and mobilised peripheral blood [209]. The majority of HSC-based HIS models in current use utilise human umbilical cord blood (hUCB)-derived cells, with HSC isolation based on expression of CD34. However, because HSC yields from individual hUCB units are both highly variable and expensive to procure and isolate [210], there is a need for mouse models that can support immune reconstitution following

transplantation of low numbers of primitive HSCs. In NBSGW mice, successful humanisation with high levels of chimerism is achievable following transplantation of $0.25x10^6$–$1x10^6$ $CD34^+$ HSCs [211]. In contrast to CD34, CD133, a pentaspan transmembrane protein on human HSCs, is a key biomarker, expressed on the surface of human HSCs before and then with CD34 [212], and used in place of CD34 for the isolation and characterisation of human HSCs [213,214]. In UCB, the $CD133^+$ subpopulation has been shown to be particularly enriched for long-term (LT)-HSCs and the $CD133^{neg}$ fraction to lack LT-HSCs [215,216]. Additionally, the $CD133^+$ population includes a small fraction of $CD34^{neg}$ LT-HSCs which have the capacity for self-renewal [216], are increasingly appreciated as the determinants of successful transplantation [217], and are likely discarded where transplantation is based only on CD34 selection. In NOG mice, isolation based on CD133 positivity has been shown to improve engraftment of UCB HSCs compared with $CD133^-$ HSCs [218].

For immunological research, combined reconstitution of functional human adaptive and innate immune cells is desirable to enable more accurate experimental representation of human immunity to be achieved *in vivo*. Currently available models demonstrate cellular tropism, with biased reconstitution of particular populations of cells (Table 2). Peripheral blood leucocyte (PBL) HIS models are commonly used examples, which are typically T cell-biased [219]. HSC-based HIS models tend to support myeloid cell engraftment but are typically skewed toward reconstitution of immature B cells [220] which fail to mature into functional mature B cells.

T cells that develop within the thymi of HIS mice include $CD4^+$ and $CD8^+$ cells with broad $V\beta$ distribution together with regulatory T cells (Tregs) and $\gamma\delta$ T cells [221]. To date, successful intra-

thymic *de novo* T cell development following human HSC transplantation has required the use of irradiated new-born mice [222-224]. When this has also been demonstrated in adult mice, its achievement requires irradiation and weekly injections of human Fc-IL7 fusion protein, which conferred the additional effect of diminishing the human B cell population [207].

Name	Strain	Phenotype	Reference
SCID	B6.CB17-*Prkdc*^{scid}/SzJ	T & B cell deficiency	[225]
NOD-*scid*	NOD.CB17-*Prkdc*^{scid}/J	T & B cell deficiency Phagocytic tolerance	[226]
NSG	NOD.Cg-*Prkdc*^{scid} *Il2rg*^{tm1Wjl}/SzJ	T, B & NK cell deficiency Phagocytic tolerance	[227]
NSG B2M, β2m KO NSG	NOD *scid Il2ry*^{null} *B2m*^{null}	T, B & NK cell deficiency Xeno-GvHD-resistance	[228]
NSG HLA-A2/HDD	NOD.Cg-*Prkdc*^{scid}*Il2rg*^{tm1Wjl}Tg (HLA-A2/H2-D/B2M)1Dvs/Sz(NSG-HLA-A2/HHD)	T, B & NK cell deficiency Human HLA-A2 expression	[229]
NSG HLA-DR	NOG/HLA-DR4/I-Ab$^{-/-}$	T, B & NK cell deficiency Human HLA-DR expression	[230]
NSG-SGM3	NOD.Cg-*Prkdc*^{scid}*Il2rg*^{tm1Wjl} Tg(CMV-IL3,CSF2,KITLG)1Eav/MloySzJ	T, B & NK cell deficiency Human IL-3, GM-CSF & SCF expression	[203]
hIL-6 Tg NSG	NOD.Cg-*Prkdc*^{scid}*Il2rg*^{tm1Wjl} Tg(BAC1/2-IL6)	T, B & NK cell deficiency Human IL-6 expression	[206]
NSGW41	NOD.Cg-*Kit*$^{W-41J}$*Prkdc*^{scid} *Il2rg*^{tm1Wjl}/WaskJ	T, B & NK cell deficiency, Impaired HSC development	[231]
NSGWv/+	NOD/SCID*Il2rg*$^{-/-}$*Kit*$^{Wv/+}$	T, B & NK cell deficiency, Impaired HSC development	[198]
NSGWv	NOD/SCID*Il2rg*$^{-/-}$ *Kit*$^{Wv/Wv}$	T, B & NK cell deficiency, Impaired HSC development	[198]
NBSGW	NOD,B6.SCID *Il2rγ*$^{-/-}$ *Kit*$^{W41/W41}$	T, B & NK cell deficiency, Impaired HSC development	[208]
NOG	NOD.Cg-*Prkdc*^{scid} *Il2rg*^{tm1Sug}/JicTac	T, B & NK cell deficiency Phagocytic tolerance	[227]
IL-15-NOG Tg	NOD.Cg-*Prkdc*^{scid} *IL-2Rrgc*^{m1Sug} Tg (CMV-IL2/IL15)1-1Jic/JicTac	T, B & NK cell deficiency Phagocytic tolerance, human IL-15 expression	[232]
NOG-EXL	NOD.Cg-*Prkdc*^{scid} *Il2rg*^{tm1Sug} Tg(SV40/HTLV-IL3,CSF2)10-7Jic/JicTac	T, B & NK cell deficiency Phagocytic tolerance, human GM-CSF & IL-3 expression	[233]
NOG-IL2 Tg	NOD.Cg-*Prkdc*^{scid} *IL-2rgc*^{m1Sug} Tg(CMV-IL2)4-2Jic/JicTac	T, B & NK cell deficiency Phagocytic tolerance, human IL-2 expression	[234]
DRAG	NOD.Cg-*Rag1*^{tm1Mom} *Il2rg*^{tm1Wjl} Tg(HLA-DRA,HLA-DRB1*0401)39-2Kito/ ScasJ	T, B & NK cell deficiency Phagocytic tolerance, human HLA class II expression	[235]
NRG	*NOD.Cg-Rag1*^{tm1Mom} *Il2rg*^{tm1Wjl}	T, B & NK cell deficiency Phagocytic tolerance	[236]

SRG	Tg(hSIRPA)*Rag2*$^{-/-}$*Il2rg* $^{-/-}$	T, B & NK cell deficiency Phagocytic tolerance	[237]
SRG-W41	NOD,*Rag2*$^{-/-}$*Il2rg*$^{-/-}$*Kit*$^{Wv/Wv}$	T, B & NK cell deficiency Phagocytic tolerance, Impaired HSC development	[238]
BALB *scid*	CBySmn.CB17-*Prkdc*^{scid}		[239]
BRG	BALB/c *Rag2*$^{-/-}$ *Il2rg*^{tm1Sug}/JicTac	T, B & NK cell deficiency	[240 241]
BRG hIL-3 hGM-CSF	BALB/c *Rag2*$^{-/-}$ *IL-2Rgc*$^{-/-}$ IL3^{h} CSF2^{h}	T, B & NK cell deficiency Human IL-3 & GM-CSF expression	[242]
BRGS	BALB/c *Rag2*$^{-/-}$ *IL-2Rgc*$^{-/-}$ NOD.*sirpa*	T, B & NK cell deficiency, NOD SIRPα expression	[240,243]
BRGSF	BALB/c *Rag2*$^{-/-}$ *IL-2Rgc*$^{-/-}$Flt3$^{-/-}$	T, B & NK cell deficiency, NOD SIRPα expression, impaired HSC development	[244]
BRgWv	BALB/c*Rag2*$^{-/-}$*Il2rg*$^{-/-}$*Kit*$^{Wv/Wv}$	T, B & NK cell deficiency, Impaired HSC development	[198]
MISTRG	M-CSF,IL-3,Sirpa, TPO, *Rag2*$^{-/-}$ *IL-2Rgc*$^{-/-}$	T, B & NK cell deficiency, human M-CSF, IL-3, GM-CSF, SIRPα & TPO expression	[204]
HUMAMICE	C57BL/6 *HLAA2*$^{+/+}$*/DR1*$^{+/+}$*/H2b2m* $^{-/-}$ */IAb* $^{-/-}$*/Rag2* $^{-/-}$*/IL2Rg* $^{-/-}$*/perf* $^{-/-}$	T, B & NK cell deficiency, No mouse MHC expression human HLA expression	[245]
Nude mouse, athymic nude	*Foxn1*^{nu}	T & NK cell deficiency	[246]

Table 2. Immunodeficient mouse models in humanised mouse research
(Reprinted from Transplantation, Vol 104, issue 11, Adigbli et al, Humanization of Immunodeficient Animals for the Modeling of Transplantation, Graft Versus Host Disease, and Regenerative Medicine, Pages 2290-2306, Copyright (2018), with permission from Wolters Kluwer Health (License no. 5182170630287)

Human erythropoiesis is not well supported in humanised mouse models. Within the NBSGW mouse, bone marrow-based erythropoiesis occurs with complete maturation, enucleation and globin gene expression [211]. However, survival of mature human erythrocytes in the peripheral blood does not occur, likely as a result of murine macrophage-mediated erythrocyte phagocytosis.

In this study we harness stemness properties of CD133^{+} hUCB LT-HSCs to achieve successful irradiation-independent human haematopoietic reconstitution in NBSGW mice using low doses of HSCs. The model is technically easy to use and achieves robust multilineage

reconstitution of lymphoid and myeloid human cells which persist long-term. For decades, achieving this has challenged several of the available HIS mouse models, which are unable to support both engraftment of all lymphocytes and myeloid cells and maturation and survival into the long-term [247]. Human thymocytes develop in a humanised thymic microenvironment and both naïve and memory $CD4^+$ and $CD8^+$ T cells repopulate in the periphery. Both immature and mature B cells are present, which are antibody class-switching and functional. Finally, we identify human erythropoiesis within the bone marrow.

1.5. Conclusion

The risk of rejection and consequent requirement for life-long immunosuppression following SOT and VCA presents an important challenge. In burn/wound reconstruction, reducing the high risk of skin allo-rejection could widen clinical application of skin and VCA transplantation. Regulatory cell therapies indicate the potential to reduce immunosuppressant requirements, and this may be reduced further by localising delivery of anti-rejection therapies.

Considering the superior functional and cosmetic outcomes of VCAs, the induction of allograft tolerance could provide advantageous alternatives to free flap reconstructions. As the demand for tissue reconstruction is far greater than the requirement for SOT, successful tolerance induction for VCAs could make this the predominant modality of transplantation.

Although attaining complete tolerance is the ideal aim, it is widely agreed that therapies capable of reducing the requirement for immunosuppression without detriment to graft function or survival are worth pursuing, as these are likely to substantially impact on patient morbidity and mortality.

Anti-rejection cellular therapies using human Tregs are proving to be efficacious in both experimental models and clinical trials in transplantation. Localising Tregs to desired sites of action following skin transplantation may serve to concentrate their immunoregulatory function, increase local potency and limit the potential for off-target effects. Employing the chemoattractant properties of Treg-reactive skin-homing chemokines represents a feasible opportunity to achieve this.

Humanised experimental models provide the ability to investigate human immune processes in the murine in vivo setting. In skin transplantation, commonly used humanised mice have demonstrated the capacity to model the rejection process, however their inability to re-create human haematopoietic systems replete with both innate and adaptive immune cells introduces potentially important investigative limitations.

There is therefore a need to develop a more haematologically representative experimental model of human skin transplant rejection, in which innate and adaptive allogeneic responses may be assessed without direct patient risk. In this context, assessments of cellular responses to allografts and the effects of experimental therapies will become more robust.

1.6. Thesis aims & objectives

- Develop a multilineage hematopoietic humanised mouse model of human skin allotransplantation through which human skin rejection may be examined and characterised (Chapters 3 and 4), and;

- Develop a translational therapeutic strategy based on cellular Treg therapy to prevent human skin allograft rejection (Chapter 5)

Chapter 2: Materials & Methods

2.1. Reagents

Monoclonal antibodies

Antigen and fluorochrome	Supplier (cat number)	Clone
Anti-human CD45RA FITC	Biolegend (304106)	HI100
Anti-human CD27 FITC	BD (555440)	M-T271
Anti-human Lineage FITC (anti-CD3, CD14, CD16, CD19, CD20, CD56)	BD (340546)	SK7 (CD3), 3G8 (CD16), SJ25C1 (CD19), L27 (CD20), MϕP9 (CD14), NCAM16.2 (CD56)
Anti-human CD11b FITC	eBioscience (11-0118-42)	ICRF44
Anti-human CD3 FITC	Biolegend (300406)	UCHT1
Anti-human CD14 FITC	Biolegend (325604)	HCD14
Anti-human CD19 FITC	Biolegend (302206)	HIB19
Anti-human FoxP3 FITC	eBioscience (11-4776-42)	PCH101
Anti-human CD8 PE	BD (555635)	HIT8a
Anti-human CD19 PE	Biolegend (302208)	HIB19
Anti-human CD34 PE	eBioscience (12-0349-42)	4H11
Anti-human CD61 PE	Biolegend (336406)	VI-PL2
Anti-human CD14 PE	eBioscience (12-0149-42)	61D3
Anti-human CD47 PE	Biolegend (323108)	CC2C6
Anti-human TACI PE	Biolegend (311906)	1A1
Anti-human CD127 PE	BD Biosciences (557938)	hIL-7R-M21
Anti-human FoxP3 PE	eBioscience (12-4776-42)	PCH101
Anti-human CCR8 PE	Biolegend (360603)	L263G8
Anti-human Lag3 PE	BD Biosciences (565617)	T47-530
Anti-human IL1R2 PE	Invitrogen (MA5-23543)	34141
Anti-human HLA-DR ECD	Beckman Coulter (IM3636)	Immu-357
Anti-human CD4 PE-efluor 610	eBioscience (61-0049-42)	RPA-T4

Anti-human CD3 PE-Cy7	**BD (557851)**	**SK7**
Anti-human IgD PE-Cy7	**BD (561314)**	**IA6-2**
Anti-human CD33 PE-Cy7	**eBioscience (25-0338-42)**	**WM-53**
Anti-human CD71 PE-Cy7	**Biolegend (334112)**	**CY1G4**
Anti-human HLA-ABC PE-Cy7	**Biolegend (311429)**	**W6/32**
Anti-human CD25 PE-Cy7	**BD (560920)**	**M-A251**
Anti-human CCR4 PE-CY7	**Biolegend (359409)**	**L291H4**
Anti-human CD27	**BD Biosciences (560609)**	**M-T271**
Anti-human CCR7 APC	**Biolegend (353213)**	**G043H7**
Anti-human CD10 APC	**Biolegend (312210)**	**HI10a**
Anti-human CD38 APC	**eBioscience (17-0389-41)**	**HIT2**
Anti-human CD45 APC	**Invitrogen (MHCD4505)**	**HI30**
Anti-human CD56 APC	**Invitrogen (17-0566-42)**	**TULY56**
Anti-humanCD235a (Gly A) APC	**eBioscience (17-9987-42)**	**HIR2 (GA-R2)**
Anti-human CD11c APC	**BD (559877)**	**B-ly6**
Anti-human BCMA APC	**Biolegend (357505)**	**19F2**
Anti-human CD4 APC	**BD (353213)**	**RPA-T4**
Anti-human HLA-DP/DQ/DR APC	**Miltenyi Biotec (130-104-870)**	**REA332**
Anti-human BAFF APC	**Invitrogen (17-9017-42)**	**1D6**
Anti-human CD45 APC/Fire 750	**Biolegend (368518)**	**2D1**
Anti-human CD3 APC-eFluor780	**eBioscience (47-0038-42)**	**UCHT1**
Anti-human BAFF-R APC-Cy7	**Biolegend (316912)**	**11C1**
Anti-human CD25 APC-Cy7	**Biolegend (302611)**	**BC96**
Anti-human FoxP3 eFluor450	**Invitrogen (48-4776-41)**	**PCH101**
Anti-human CCR4 V450	**BD Biosciences (561123)**	**1G1**
Anti-human CCR8 V421	**BD Biosciences (566379)**	**433H**
Anti-mouse Ter119 FITC	**eBioscience (11-5921-82)**	**TER-119**
Anti-mouse CD45 PE-TR	**BD biosciences (562420)**	**30-F11**

Anti-mouse CD41 PerCP/Cy5.5	Biolegend (133918)	MWReg30
Anti-mouse CD11b PE-Cy7	eBioscience (25-0112)	M1/70
Anti-mouse CD45 eFluor450	eBioscience (48-0451-82)	30-F11
Anti-mouse Gr-1 APC	eBioscience (17-5931)	RB6-8C5

Cytokines & Chemokines

Cytokine	Supplier
Human IFN-γ	Peprotech
Human IL2 (Proleukin)	Novartis Pharmaceuticals, UK
Mouse IFN-γ	Peprotech
Chemokine	**Supplier**
Human CCL17	Peprotech
Human CCL22	Peprotech
Human CCL1	Peprotech
Mouse CCL22	Peprotech
Mouse CCL1	Peprotech
Mouse MCP1	Peprotech

Other reagents

Reagent	Function	Supplier
7-aminoactinomycin D (7AAD)	Cell viability analysis	Biolegend
Violet Proliferation Dye (VPD)	Cell proliferation analysis	BD

2.2. Cell isolation, culture & expansion

2.2.1. Human umbilical cord blood (hUCB) HSPC and MNC isolation

Human UCB (provided by Dr Peng Hua) was collected from the John Radcliffe Hospital, (Oxford) or provided via the NHS Cord Blood Bank (London) and used with informed, written pre-consent and ethical approval from the South Central Oxford C and Berkshire Ethical Committees (# 15/SC/0027) and the Oxfordshire Research Ethics Committee B (#07/H0605/130).

hMNCs (density <1.077g/ml) were isolated by density gradient centrifugation less than 24h after hUCB collection. $hCD133^+$/$hCD34^+$ HSPCs were enriched by magnetic bead selection using hCD133/hCD34 direct microbead kits (MACS, Miltenyi Biotec GmbH) and cryopreserved until use. Purity was assessed by flow cytometry. Cell isolates with >90% $hCD133^+$ or $hCD34^+$ cell purity were used for experiments.

2.2.2. PBMC isolation

Human PBMCs were isolated from healthy donor blood (provided by the National Health Service Blood and Transplant, Oxford, U.K and used with ethics approval from the Oxfordshire Research Ethics Committee B (#07/H0605/130)) using LSM 1077 (GE Healthcare, USA) for density gradient centrifugation at 2200rpm for 30mins at room temperature. Buffy coats were collected, washed with PBS and erythrocytes lysed with PharmLyse lysing buffer (BD biosciences, Franklin Lakes, NJ, USA) for 5mins. Isolated PBMCs were used fresh or cryopreserved and stored in liquid nitrogen until needed.

2.2.3. Human Treg isolation

To isolate $CD25^+$ cells, PBMCs were incubated with CD25 microbeads (MACS, Miltenyi Biotec GmbH) for 15mins (4°C), washed, resuspended and enriched by magnetic bead positive selection (MACS LS columns) according to the manufacturer's protocol.

CD25-enriched PBMCs were stained with αCD4-ECD (Beckmann Coulter, USA), αCD25-PE-Cy7 (BD Biosciences), αCD127–PE (BD Biosciences) antibodies and $CD4^{+}CD25^{+}CD127^{lo}$ cells sorted by flow cytometry (BD FACSAriaII flow cytometer).

For all *in vitro* cell culture and assays, human Tregs were cultured in complete medium: RPMI medium supplemented with L-glutamine (Sigma-Aldrich, USA), 100U/mL penicillin, 10mg/mL streptomycin (Sigma-Aldrich) and heat-inactivated (20mins, 55˚C) 10% FCS (general complete medium) or 10% human AB serum (Seralab, U.K; complete Treg medium).

2.2.4. *In vitro* human Treg expansion

After isolation, Tregs were cultured for 16days in complete Treg medium (RPMI medium supplemented with L-glutamine (Sigma-Aldrich, USA), 100U/mL penicillin, 10mg/mL streptomycin (Sigma-Aldrich) and heat-inactivated (20mins, 55˚C) 10% human AB serum (Seralab, U.K)). During the first 14days culture medium was supplemented with 1000U/mL recombinant human IL-2 (Novartis Pharmaceuticals, UK). Tregs were stimulated with αCD3αCD28 T cell activator beads (ThermoFisher Scientific) on day 0 of culture (3 beads/cell) and restimulated on day 7 (1 bead/cell). Cultures were split and medium replaced as required. For the final 2days, Tregs were rested without beads, in the presence of 200U/mL rhIL-2.

2.3. Animal procedures

2.3.1. Animals

BALB/c $Rag2^{-/-}$ $c\gamma^{-/-}$ (BRG), NOD,B6.SCID $Il2r\gamma^{-/-}$ $Kit^{W41/W41}$ (NBSGW), and CBA/Ca (CBA) mice (The Jackson Laboratory, USA) were housed under specific pathogen-free conditions at the John Radcliffe Hospital Biomedical Services Unit. Mice were housed in individually ventilated cages and handled with gloves. All experiments performed utilised protocols approved by

Oxford University's Committee on Animal Care and Ethical Review and in accordance with the UK Animals (Scientific Procedures) Act 1986, under the PPL P8869535A.

Mice between the ages of 6 and 12wks at the time of the first experimental procedure were used. Any mice developing signs of xenograft versus host disease (XvHD) or weight loss of >20% (compared with starting weight) were euthanised in accordance with local animal welfare regulations.

2.3.2. Adoptive transfer of human HSPCs

Cells were quantified for injection using Countbright absolute counting beads (Molecular Probes) by flow cytometry[248]. 1,000-250,000 $CD133^+$ HSPCs suspended in 200µl IMDM/1%HSA (human serum albumin) were injected intravenously (lateral tail vein) into non-irradiated adult (5-16week old) male or female mice. Mice were regularly bled for human leucocyte reconstitution assessment. 20-22wks after HSPC injection peripheral blood, spleen, thymus and bone marrow were harvested. Engraftment was defined as >0.1% $hCD45^+$ cell chimaerism in bone marrow at final harvest[227].

For HSPC-MNC-NBSGW skin transplant experiments, 13wks after humanisation HSPC-NBSGW mice were injected intravenously with $5x10^6$ hUCB $CD34^-$ MNCs (from the same cord blood unit as initial humanisation), suspended in 200µl IMDM/1%HSA.

A separate group of 8–10week-old male or female mice were injected intravenously with $5x10^6$ human PBMCs suspended in 200µl RPMI 1650. 4-6wks after humanisation, peripheral blood, spleen and thymus were harvested.

2.3.2.1. Secondary transplantation

For secondary transplant experiments, bone marrow cells from primary recipient mice in unexpanded, vehicle/cytokine-expanded or CPI203/cytokine-expanded groups (from mice in cell doses of 500, 1000 and 10000 cells) were pooled respectively and $5x10^6$ cells injected into each secondary recipient mouse. hCD45 cell engraftment was analysed 22 weeks post-transplantation.

2.3.3. Phagocyte depletion

For phagocyte depletion assays, mice were injected with 50,000 $CD34^+$ hUCB HSPCs. 10wks later, human leucocyte reconstitution was assessed by flow cytometry and mice allocated to clodronate or PBS groups with comparable reconstitution levels. Mice received intraperitoneal injections of either 200µl clodronate liposomes (5mg clodronate/ml; Liposoma B.V.) or 200µl PBS. 5 days later, peripheral blood mouse macrophage and human RBC levels were analysed by flow cytometry[249]. The next day mice were euthanised and blood, bone marrow and spleens harvested, processed (as in section 2.3.4.5.) and analysed by flow cytometry for expression of erythroid and megakaryocyte lineage markers and CD47.

2.3.4. Humanised mouse model of human skin allograft rejection

2.3.4.1. Pre- and post-surgical care

Skin transplantation and Matrigel injection procedures were conducted with mice under general anaesthetic (inhaled Sevofluorane). Post-operatively, mice were recovered in warmed recovery cabinets with their litter mates.

2.3.4.2. Human skin procurement

Human skin was obtained from unused excess abdominal tissue, with the informed consent of plastic surgery patients undergoing reconstructive breast surgery at the John Radcliffe Hospital, Oxford. Ethical approval was issued by the Oxfordshire Research Ethics Committee, study number 07/H0605/130. 0.010in split-thickness skin grafts were taken using a dermatome (Zeiss, Jena, Germany). Full-thickness grafts were excised with a number 15 blade and subcutaneous fat removed.

Exclusion criteria included patients with inflammatory skin conditions or those taking immunosuppressive medications. Skin was stored at 4°C in RPMI medium for up to 12hrs prior to transplantation.

2.3.4.3. Skin transplant procedure

Under anaesthesia, $1cm^2$ skin was excised from pre-shaven left flanks of un-humanised BRG mice (age 8-12wks), or NBSGW mice (age 21-25wks) humanised 13wks earlier. $1cm^2$ human skin grafts were inset microscopically, using 8-0 polypropylene sutures (Ethicon, USA). Mini fenestrations were made in the centre of each graft to prevent haematoma accumulation. Skin grafts were dressed with Inadine (Scapa, U.K.), gauze (Scapa, U.K.), and secured for 10days (or 3wks for full-thickness grafts) with a band-aid and autoclave tape, wrapped circumferentially around the abdomen for light compression. Grafts on HSPC-NBSGW and HSPC-MNC-NBSGW mice were monitored bi-daily for macroscopic features of rejection. Mice were sacrificed when late features of rejection appeared, or 100 days post-skin transplantation (whichever occurred sooner).

2.3.4.4. Adoptive transfer of PBMC and Tregs

5wks post-skin transplantation, BRG mice received intra-peritoneal injections of $5x10^6$ cryopreserved allogeneic human PBMCs resuspended in 200µl RPMI, with or without $1x10^6$ *ex vivo*-expanded Tregs (from the same PBMC donor). Control mice (not adoptively transferred) received 200µl RPMI alone. Grafts were monitored bi-daily for macroscopic features of rejection. Mice were sacrificed when late features of rejection appeared, or 100 days post-adoptive transfer (whichever occurred sooner).

Mice demonstrating human leucocyte chimerism <1% in the spleen or <0.1% in blood at the time of sacrifice were excluded from survival analysis.

2.3.4.5. Organ & tissue harvest and processing

Under anaesthesia, peripheral blood was harvested from the inferior vena cava prior to euthanasia. Spleens, thymi and femurs (+ pelvic bones and vertebrae for secondary transplantation experiments) were then harvested, placed in Eppendorf tubes containing PBS and stored on ice prior to processing. Internal surfaces of skin allografts were photographed. Skins were then excised, placed longitudinally in Eppendorf tubes containing OCT and snap-frozen by dropping into safety flasks containing liquid nitrogen, prior to long-term storage.

In filtered biosafety cabinets, bones were crushed using the back end of a syringe plunger to release marrow. Bone marrow, spleens and thymi were macerated separately, using the soft ends of syringe plungers, washed through 70µm nylon mesh and centrifuged. For erythroid-megakaryocyte analysis bone marrow, spleen, and blood cells were resuspended and lysed in 10mL PharmLyse buffer (BD) for 8mins, before washing in FACS buffer. Otherwise, bone marrow, spleen, thymus and blood cells were resuspended in FACS buffer and analysed by flow cytometry following viability and fluorophore-conjugated antibody staining for cell surface marker expression.

2.3.4.6. Histology - Haematoxylin and Eosin (H&E) staining

Snap frozen skin samples were cross sectioned into 6μm thick slices using a Bright*® 5040 cryostat. Slices were air-dried at room temperature for 1 hour and stored at -80°C. Frozen sections were thawed at room temperature for 20mins before staining with Haematoxylin (20s) and Eosin (10s) (Raymond Lamb, UK).

2.3.5. *In vivo* mouse model of localised chemotaxis

2.3.5.1. Preparation of chemokine-impregnated Matrigel

Matrigel (Corning, USA) was thawed slowly according to the manufacturer's instructions. In filtered biosafety cabinets, on ice, Matrigel (200μl/injection) was resuspended in a solution containing 200ng thawed rmCCL1, rmCCL22 and rmCXCL12, with or without 4μg rmIFNγ (non-humanised mouse experiments) or 200ng rhCCL22±rhCCL1, with or without 80U rhIL-2 (humanised mouse experiments) and made up to 400μl with RPMI. Solutions were vortexed and inserted into pre-frozen 0.3ml syringes and kept on ice prior to injection.

2.3.5.2. Injection of chemokine-impregnated Matrigel

2.3.5.2.1. Non-skin transplant experiments

CBA or BRG mice were anaesthetised and flanks shaved prior to subcutaneous injection of 400μl Matrigel solutions (chemokine-impregnated - left flank / control Matrigel - right flank). Gauze (Scapa, U.K.) dressings were applied and band-aid and autoclave tape wrapped circumferentially around the abdomen for 24hrs to prevent mouse fighting.

2.3.5.2.2. Skin transplant experiments

BRG mice receiving 1cm^2 human full-thickness skin transplants 5wks earlier and adoptively transferred allogeneic human PBMCs and Tregs 3-4wks earlier were anaesthetised and shaven around injection site prior to subcutaneous injection of 400µl Matrigel solution beneath skin allografts. Skins were managed as in section 2.3.4.4

2.3.5.3. Matrigel harvest and leucocyte isolation

3 days after injection (non-skin-transplant experiments) or at the time of skin allograft rejection/after 100days (skin transplant experiments), mice were euthanised and organs harvested (as in section 2.3.4.5.). Matrigels were harvested following excision of overlying skin, from which they were separated and stored in PBS on ice prior to processing. Matrigels were incubated in cell recovery solution (Corning, USA) for 30mins (4°C), vortexed for 30s, macerated over 70µm nylon mesh using the soft ends of syringe plungers, then washed through with MACS buffer (PBS, 0.5% FCS, 2mM EDTA) and centrifuged at 1500rpm for 5mins (4°C) prior to analysis by flow cytometry.

2.4. Flow cytometry

2.4.1. Cell surface marker staining

Single cell suspensions were stained with fluorophore-conjugated antibodies (listed in Table 2.1) in 96-well plates according to manufacturers specified concentrations and incubated in the dark for 30mins (4°C). Cells were then washed with FACS buffer (PBS + 5% FCS + 0.2% sodium azide), centrifuged at 1500rpm for 5mins (4°C), resuspended in 200µL 1% paraformaldehyde (PFA) and analysed on the BD FACSCanto II.

2.4.2. Intracellular immunostaining

Staining for intracellular markers was conducted using the Foxp3/Transcription factor staining buffer set (eBioscience, Invitrogen) according to the manufacturer's instructions. After washing, surface-stained cells were incubated in 50µL fixation-permeabilisation buffer in the dark, for 45mins (15°C) or overnight (4°C) then washed twice with 200µL permeabilisation buffer. Following this, cells were incubated in 3µL/well rat and/or mouse serum (eBioscience) in the dark for 15mins (15°C), stained with fluorophore-conjugated antibody in the dark for 45mins (15°C). Cells were washed with FACS buffer, resuspended in 100µL 2% v/v formaldehyde (Sigma, USA) and by flow cytometry the same day or after overnight storage (4°C).

2.4.3. Cytometric bead array

For cytokine assessment, supernatants from cell cultures were collected after 72-96hrs stimulation and stored (-80°C) until use. For immunoglobulin assessment, plasma was isolated from 0.5ml peripheral blood by centrifugation at 1300rcf for 10 mins (room temperature), then stored (-80°C) until use. Thawed supernatants and plasma were probed using the LEGENDplex™ Human Th Cytokine Panel (BioLegend) and LEGENDplex™ Human Immunoglobulin Isotyping Panel (BioLegend) Flow cytometric bead array kits respectively, according to manufacturers instructions.

2.4.4. Cell viability assessment

Cells being prepared for flow cytometry were incubated for 30mins at 4°C in the dark with 0.3µl/sample of 7-aminoactinomycin D (7AAD) (eBioscience), in addition to staining antibodies. Cells were washed with FACS buffer and fixed in 1% PFA prior to acquisition on the flow cytometer.

2.4.5. Cell proliferation dye staining

Cells to be assayed for proliferation were washed twice in PBS, and $30x10^6$ cells/ml incubated in a total concentration of 1μM VPD (BD, USA) for 10mins (37°C). Following this, cells were washed twice in PBS and resuspended in culture media prior to counting and use. Cells to be stained with carboxyfluorescein succinimidyl ester (CFSE) were incubated in 1ml RPMI with 10μm CFSE for 10 mins (37°C), then washed with RPMI+10% FCS.

2.4.6. Analysis of flow cytometry data

Analysis of all flow cytometry data was performed using FlowJo v. 10 (Tree Star, USA).

2.5. *In vitro* cell culture assays

2.5.1. HSPC-NBSGW leucocyte assessment of function

2.5.1.1. Flow cytometric analysis of *in vitro* T cell proliferation

T cells from spleens of HSPC-NBSGW mice demonstrating *in vivo* skin allograft rejection were isolated using human CD3 microbeads (MACS, Miltenyi Biotec GmbH) (as in section 2.2.3.) and labelled with violet proliferation dye (VPD) (section 2.4.5.) prior to culture ($1x10^5$ cells/well) for 72-96h with either αCD3/αCD28 beads ($2x10^5$ per well) or irradiated allogeneic $CD3^-$ PBMCs (derived from the skin donor), pooled allogeneic 3rd party $CD3^-$ PBMCs, NBSGW mouse bone marrow cells or human bone marrow cells ($5x10^5$ cells/well). Cells were then harvested and dye dilution determined by flow cytometry. Assays were performed in triplicate.

2.5.1.2. Flow cytometric analysis of *in vitro* myeloid cell stimulation and antigen presenting capacity

Human $CD45^+$ leucocytes were isolated from HSPC-NBSGW mouse bone marrow using human CD45 microbeads (MACS, Miltenyi Biotec GmbH) (as in section 2.2.3.). Human $CD45^+$ cells were similarly isolated from bone marrow and PBMCs. Cells were irradiated prior to culture ($5x10^5$ cells/well) with VPD-stained allogeneic human $CD3^+$ T cells ($1x10^5$ cells/well). Assays were performed in triplicate. After the first 18hrs CD80, CD86, CD1a and HLA-DR expression on $CD33^+$ cells was analysed by FACS. After 5 days of culture, cells were harvested and dye dilution in T cells determined by flow cytometry.

2.5.1.3. Flow cytometric analysis of hBAFF production

$1x10^6$ thawed HSPC-NBSGW bone marrow cells were cultured in 24 well plates in the presence of 1μg/ml IFN-ɣ for 36 hours, then analysed by FACS for intracellular expression of hBAFF.

2.5.2. *In vitro* Treg stimulation (polyclonal, low-dose): CCR4 & CCR8 expression & time-course

Freshly isolated human Tregs were sorted by FACS into $CCR4^+$, $CCR4^-$, $CCR8^+$ and $CCR8^-$ fractions and cultured in 96 well V-bottom plates in the presence of αCD3αCD28 T cell activator beads (1:5 bead:cell ratio) and rhIL-2 (200U/mL) for 14 days. Cells were analysed by flow cytometry bi-daily for analysis of αCCR4 and αCCR8 expression.

2.5.3. *in vitro* bead-stimulated Treg suppression assay

PBMC responders were stained with 1μM VPD (BD) (Section 2.4.5) and cultured (1x10^5/well) for 72hrs either alone (negative control), with αCD3αCD28 beads (positive control) or with Tregs, at ratios ranging from 1:1 to 1/64:1 (Treg:responder). In triplicate wells, T cells were stimulated with αCD3αCD28 T cell activator beads (Invitrogen) at a 1:5 (bead:responder) ratio. To quantify responder proliferation from VPD dilution was analysed by flow cytometry and division indices calculated using the following formula[250]:

$$\text{Div. Index} = \frac{\text{\# cell divisions}}{\text{\# precursor cells}} = \frac{\frac{(\text{\# cell divisions}_1)}{2^1} + \frac{(\text{\# cell divisions}_2)}{2^2} + \cdots + n\frac{(\text{\# cell divisions}_n)}{2^n}}{\frac{(\text{\# cell divisions}_0)}{2^0} + \frac{(\text{\# cell divisions}_1)}{2^1} + \cdots + n\frac{(\text{\# cell divisions}_n)}{2^n}}$$

n= # of the division peak

2.6. Cryopreservation and thawing of human leucocytes

Human leucocytes were resuspended in freezing medium (45% RPMI, 45% Foetal Calf Serum (FCS), 10% DMSO) at 5-200x10^6 cells/ml in 1.5ml cryovials and placed in freezing boxes at -80°C prior to long-term storage (-160°C).

Frozen vials were transferred to -80°C for 1h, prior to thawing at 37°C. Thawed cell suspensions were washed immediately in 10ml RPMI, added dropwise.

2.7. Gene expression analysis

2.7.1. Cell and RNA isolation

For transcriptomic analysis of splenocytes and skins from skin-allografted HSPC-NBSGW mice and skins of xenografted NBSGW mice, 1x10^6 whole splenocytes and 5x6μm thawed human skin slices from each mouse were taken for isolation of RNA using the RNeasy Mini or Microkit (Qiagen, Venlo, Netherlands) depending on cell number, as per manufacturer's instructions.

2.7.2. RNA assessment and data analysis

Gene expression was analysed using the nCounter® Sprint Profiler (NanoString Technologies, USA) and the PanCancer Immune Profiling Panel. 25ng RNA was taken for analysis. Data quality control and analysis was performed on the nSolver™ Software (v4.0, Nanostring) according to the manufacturer's instructions. The Advanced Analysis platform (v. 2.0) was used to compare data sets. Adjusted p values were calculated with control of Benjamini-Yekutieli or Benjamini-Hochberg False Discovery Rate (FDR) (Adjusted p value > 0.05 considered significant).

2.8. Statistical analysis

GraphPad Prism software was used for all statistical analyses, except transcriptomic data (section 2.7.2). Nonparametric Mann-Whitney U tests, Student's t tests, one- or two-way ANOVA tests were applied as appropriate. Log-rank tests were used to analyse survival data. p values below 0.05 were taken to be significant.

Chapter 3: Development And Characterisation Of A Humanised Mouse Model Capable Of Multilineage Haematopoetic Reconstitution Without Irradiation

3.0. Introduction

For decades, immunological studies have benefited from the ability to learn from experiments in small animal models. However, it is increasingly clear that the mechanistic gap between human and murine immune responses is significant, which can lead to challenges in the translation of findings from to human. This can, on occasion, have devastating results[251-253]. Humanised laboratory animals have been developed to bridge this gap and provide a powerful method for the preclinical assessment of human immune responses in the context of transplantation and regenerative medicine. The vast majority of these models are created using immunodeficient mice engrafted with human cells and tissues. A challenge faced by most models used in this way has been long-term engraftment and reconstitution of cells representing all haematopoietic lineages. Mice engineered with essential immune deficiencies support engraftment of human lymphocytes (predominantly T lymphocytes) without the need for irradiative preconditioning and have been used with great success in studies of allograft rejection and GvHD. However, to enable more accurate recapitulation of the human immune response to disease and its treatment, models supporting the engraftment of the complete range of innate and adaptive immune cells is desirable. Additionally, for studies with an interest in human diseases of erythrocytes and platelets, support for the long-term engraftment of human non-leucocyte myeloid lineage cells is important and has been the focus of intense research. Injection of stem cells has enabled humanised immune system (HIS) models to achieve multilineage humanisation however

many of these currently in use are limited by undesirable and technically demanding processes such as irradiative preconditioning, procurement of human fetal tissues or challenging injection techniques. In NBSGW mice, successful humanisation with high levels of chimaerism is achievable following transplantation of $0.25x10^6$–$1x10^6$ $CD34^+$ HSPCs [211]. In UCB, $CD133^+$ HSCs have been shown to be particularly enriched for long-term (LT)-HSCs and the $CD133^{neg}$ fraction to lack LT-HSCs [215,216]. $CD133^+$ HSCs include a small fraction of $CD34^{neg}$ LT-HSCs with the capacity for self-renewal [216], are increasingly appreciated as the determinants of successful transplantation [217], and are likely discarded where transplantation is based only on CD34 selection. In NOG mice, isolation based on CD133 positivity has been shown to improve engraftment of UCB HSCs compared with $CD133^-$ HSCs[218].

In this chapter, we sought to develop a HIS mouse model capable of supporting robust long-term multilineage haematopoietic reconstitution using $CD133^+$ UCB HSPCs, without the requirement for irradiative preconditioning. Building upon a similar model published by McIntosh *et al*[208], we produce a model capable of reliable reconstitution using low numbers of unexpanded HSPCs. Additionally, as proof of concept for assessment of therapeutics, we demonstrate the ability to expand HSPCs with a novel small molecule epigenetic modifier to significantly increase the number of HSPCs useable from a single unit of UCB.

3.0.1. Chapter aim

The aim of this chapter is to develop a robust humanised immune system mouse model capable of long term multilineage haematopoietic reconstitution from $CD133^+$ UCB HSPCs, without the requirement for irradiative myeloablation.

3.1. Results

3.1.1. Human leucocytes successfully engraft in primary and secondary lymphoid organs following CD133$^+$ HSPC injection

Intravenous injections of between 1x10^3 and 2.5x10^5 CD34$^+$ UCB-derived human HSPCs have frequently been used to achieve xenogeneic haemato-lymphopoeitic reconstitution in immunodeficient mice[223,254]. In many such studies HSPCs were isolated and cryopreserved for later use once mice were at the desired age for the adoptive cell transfer. This method has not been found to be of detriment to HSPC reconstitution efficiency. For these reasons, in this study cryopreservation of HSPCs was used before all instances of adoptive cell transfer unless indicated otherwise. Successful engraftment has been described as the attainment of >0.1% human CD45$^+$ leucocytes in the bone marrow by flow cytometry[227]. High chimaerism has been described as >50% circulating human leucocytes[223]. Human chimerism levels here are calculated as the proportion of live human 7AAD$^-$CD45$^+$ cells as a percentage of total live 7AAD$^-$CD45$^+$ (mouse + human) cells.

To achieve adequate statistical power, we aimed to include at least 4 mice per experimental group for reconstitution experiments. Using groups in which lower numbers of HSPCs were injected per mouse, we were able to reconstitute a greater number of mice per HSPC donor. This is particularly important when aiming to keep the HSC donors consistent between groups within individual experiments. The lowest dose of UCB CD34$^+$ HSPCs consistently used with success within the literature is 2x10^4 HSCs per mouse, injected intravenously[223].

We therefore asked whether 1) $CD133^+$ HSPCs can effectively reconstitute each NBSGW mouse and 2) whether doses as low as $1x10^3$ can produce successful engraftment and reconstitution.

We first examined human hematopoietic chimaerism in the peripheral blood following transplantation of hUCB $CD133^+$ HSPCs (≥$1x10^3$ $CD133^+$ cells injected) into non-irradiated NBSGW mice (referred to herein as HSPC-NBSGW mice). Following isolation, >96% of $CD133^+$ cells were strongly positive for CD34, and included a small number of the rare but highly potent $CD133^+CD34^-$ LT-HSCs (***Figure 3.1.1 (a)***). Tail vein intravenous injections of $1x10^3$, $5x10^3$, $5x10^4$ or $2.5x10^5$ $CD133^+$ HSPCs, were followed by measurement of human leucocyte chimerism levels in mouse peripheral blood at intervals beginning two weeks post-adoptive transfer. Successful humanisation was demonstrated by a dose-dependent increase in human $CD45^+$ cell chimaerism in the bone marrow, spleen and peripheral blood by 20-22 weeks (***Figure 3.1.1 (b-f)***). Engraftment was greatest in the bone marrow (mean±SD from 35.0±36.2 to 97.4±1.9%) and spleen (from 32.0±39.4 to 98.5±0.9%) (***Figure 3.1.1 (d)***). Robust engraftment was also present in the peripheral blood (from 12.1±24.7 to 80.0±14.2%), with higher chimaerism than described in comparable irradiated HSPC mice similarly humanised intravenously with hUCB HSCs[254]. At all doses administered, reconstitution in the blood demonstrated no signs of declining at 20-22 weeks (***Figure 3.1.1 (c)***). Recipient sex did not significantly affect chimaerism in the bone marrow, spleen or peripheral blood (***Figure 3.1.1 (g-l)***), however we identified a trend consistent with other immunodeficient strains including NSG mice in which lower levels of human $CD45^+$ cell engraftment are seen in the bone marrow of male recipients. From this evidence we concluded that $CD133^+$ UCB HSPC doses as low as $1x10^3$ can successfully attain human leucocyte reconstitution levels as high as those seen in other established and newer HSC HIS mouse models at 20 weeks[198]. Furthermore, whereas in

other models, human $CD45^+$ proportions appear to trend downward around this time point, leucocyte chimerism levels in HSPC-NBSGW mice continued to increase to the point of harvest. Considering the robust engraftment achieved with HPSC doses $\geq 5x10^4$, functional experiments conducted later in this thesis, investigating the effects of high chimerism in this model will be conducted in mice humanised with HSPC doses $\geq 5x10^4$.

3.1.2. Multilineage reconstitution of human leucocytes following $CD133^+$ HSPC injection

To investigate the range of human haematopoeitic cells reconstituting the bone marrow of recipient HSPC-NBSGW mice following $CD133^+$HSPC transplantation, we assessed for the presence of human lymphoid, myeloid and erythroid cells between 12 and 20 weeks post-adoptive transfer. As has been described in pre-irradiated HSC engrafted HIS mouse models, there was multilineage human leucocyte engraftment in the bone marrow, spleen and peripheral blood (***Figure 3.1.2***). B cells engrafted with the greatest frequency[220,255-258] (***Figure 3.1.2 (a-d)***), followed by myeloid and T cells (***Figure 3.1.1 (d-e)***). In mice receiving $1x10^3$ hUCB HSPCs, $hCD19^+$ B cell engraftment was higher in females (***Figure 3.1.2 (e)***). No other sex-specific differences in leucocyte subset engraftment were observed (***Figure 3.1.2 (e-g)***). $CD19^+$ B cells reconstituted the blood earliest (***Figure 3.1.2 (h)***), followed by $CD33^+$ myeloid and $CD3^+$ T cells appearing after 12-14 weeks in a dose-dependent manner (***Figure 3.1.2 (i-j)***). We also identified human NK cells, which were most populous in the peripheral blood. (***Figure 3.1.2 (k-l)***).

3.1.3. Human lymphoid subset engraftment I: B cells

B cell hematopoiesis was assessed by examining the developmental stages of B cells in the bone marrow, spleen and peripheral blood 20-22 weeks after humanisation (***Figure 3.1.3 (a)***). Within the bone marrow, immature B cells expressing CD10 were most populous[259] (***Figure 3.1.3 (b-c)***), contrasting with increasing frequencies of larger $CD10^-$ mature B cells in the spleen and blood (***Figure 3.1.3 (c-d)***), supporting early observations of the memory phenotype being associated with greater-sized B cells[260]. This is similar to bone marrow in healthy humans, which has an abundance of high density CD10-expressing cells[259]. Next, we analysed mature B cell phenotypes. As expected, only a small proportion of $CD10^-$ B cells populated the bone marrow and the majority were naïve, lacking CD27 expression (***Figure 3.1.3 (e-f)***). Of these, almost half were $CD27^-IgD^-$ double-negative B cells (***Figure 3.1.3 (f)***), a heterogenous population described as early-stage bone marrow cells[261], and more recently as memory precursor, extracellular antibody secreting cell precursor, and atypical/tissue based memory cells, with activated phenotypes in inflammatory diseases[262]. As in humans, antigen-inexperienced $CD27^-IgD^+$ B cells formed the other major mature B cell population in the bone marrow[263] (***Figure 3.1.3 (f)***). Within the spleen a greater proportion of mature B cells was observed and among them both unswitched ($CD27^+IgD^+$) and class-switched memory B cells ($CD27^+IgD^-$) (***Figure 3.1.3 (e-f)***). This reflected the notion that class switch recombination (CSR) occurs predominantly (although not exclusively) in germinal centre (secondary lymphoid organ) B cells, initiated by activation-induced cytidine deaminase[264]. To assess the capacity for isotype switching to be stimulated *in vivo*, we introduced an antigen challenge by transplanting allogeneic human skin onto HSPC-NBSGW mice 11-13 weeks after humanisation. At the point of skin allograft rejection (or after 100 days), we analysed splenic B cells and their surface immunoglobulin subtypes (***Figure 3.1.3 (g-h)***). We found significantly higher frequencies of splenic $CD27^+IgD^-$ memory B cells (***Figure 3.1.3 (h)***) in mice exposed to

allogeneic skin transplants compared with mice not exposed, indicating the potential for specific human B cell responses to be mounted in response to antigen challenge within this model.

Altogether, these findings demonstrate that following transplantation of hUCB CD133$^+$ HSPCs a continuous process of human B cell development and functional maturation occurs within the primary and secondary lymphoid organs of HSPC-NBSGW mice.

The robust level of B cell development in HSPC-NBSGW mice may be explained in part by the ability of engrafted human cells to produce human BAFF in a similar fashion to adult human peripheral blood cells (***Figure 3.1.3 (i)***) and by the expression of receptors for BAFF on HSPC-NBSGW B cells (***Figure 3.1.3 (j)***). In keeping with human findings, in which transitional B cells express less BAFF-R than mature B cells (and are more susceptible to apoptosis)[265], HSPC-NBSGW B cells show increasing BAFF-R expression on mature B cells (***Figure 3.1.3 (k)***). Similarly, as recognised in the literature[266], TACI expression on HSPC-NBSGW B cells is greater in the mature B cell pool (***Figure 3.1.3 (l)***).

Altogether, these findings demonstrate that following transplantation of hUCB CD133$^+$ HSPCs a continuous process of human B cell development and functional maturation occurs within the primary and secondary lymphoid organs of HSPC-NBSGW mice.

3.1.4. Human lymphoid subset engraftment II: T cells

Having identified long-term engraftment of T cells (***Figure 3.1.2 (a); Figure 3.1.1 (d)***), we sought to evaluate HSPC-NBSGW T cell development by assessing subset profiles within the bone marrow, spleen and blood (***Figure 3.1.4***). Transplantation of high doses (≥50x10^3) of HSPCs produced robust engraftment of both CD8$^+$ and CD4$^+$ T cells, predominantly in the spleen and peripheral blood (***Figure 3.1.4 (a-b)***). At these doses we identified the major T cell

subtypes within both $CD8^+$ and $CD4^+$ T cell populations: 1) central memory (Tcm), 2) effector memory (Tem), 3) T effector memory re-expressing CD45RA (TemRA) and 4) naïve (Tn) (***Figure 3.1.4 (c-e)***). Tem and Tcm cells were the most populous subtypes, however a significant proportion of CD45RA-expressing cells also persisted long-term (***Figure 3.1.4 (c-g, h-blue symbols)***). We found T cell reconstitution in HSPC-NBSGW mice to reproduce the average human peripheral blood profiles more accurately than in NBSGW mice humanized with PBMCs, which fail to reconstitute CD45RA-expressing T cells and are instead composed entirely of Tem and Tcm (***Figure 3.1.4 (h-k)***).

To assess the potential of $CD8^+$ T cells to exert cytotoxic effector function, we evaluated expression of cytolytic molecules (***Figure 3.1.4 (l-m)***). Granzyme A, Granzyme B and Perforin expression in unstimulated $CD8^+$ T cells was at comparable levels to those found in healthy adult subjects (***Figure 3.1.4 (l-n)***). Additionally, on analysis of expression within unstimulated $CD8^+$ T cell subsets, Granzyme A expression was highest in Tem cells (***Figure 3.1.4 (m)***), and significantly greater in $CD8^+$ than $CD4^+$ Tem cells.

Altogether, these findings demonstrate that following transplantation of hUCB $CD133^+$ HSPCs a continuous process of human T cell development and functional maturation occurs in HSPC-NBSGW mice.

3.1.5. Human lymphoid subset engraftment III: T cell thymic development

To identify whether *de novo* T cell development from transplanted HSPCs occurs in this model, we analysed human and mouse leucocyte populations in the thymi of recipient mice humanised with HSPCs or PBMCs (***Figure 3.1.5***). The majority of thymic cells were human $CD45^+$ leucocytes (***Figure 3.1.5 (a-b)***) expressing CD3, together with a small population of

$CD19^+$ cells (***Figure 3.1.5 (c)***). The majority of $CD3^+$ cells were $CD4^+CD8^+$ double-positive (DP) thymocytes (***Figure 3.1.5 (d-e)***) with an average frequency equivalent to those seen in thymus biopsies from human infants[198] in a dose-dependent manner (***Figure 3.1.5 (d-f)***). In contrast, following humanization with mature PBMCs, no double-positive T cells were identified within the thymus (***Figure 3.1.5 (g-h)***). Interestingly, robust engraftment of $CD19^+$ cells was found (***Figure 3.1.5 (h)***).

Substantial populations of HLA class I and class II-expressing $hCD3^-$ cells engrafted the thymi of HSPC-NBSGW mice (***Figure 3.1.5 (i-l)***), suggesting potential for the re-creation of human antigen presentation. For comparison with adoptively transferred human cells replete with HLA class I & II molecules, thymi harvested from PBMC-humanised NBSGW mice were similarly assessed, and demonstrated high thymic expression on $hCD3^-$ cells (***Figure 3.1.5 (m-n)***).

Altogether these findings suggest that within HSPC-NBSGW mice *de novo* T cell development within a humanised thymic environment may support continuous human T cell development and long term reconstitution.

3.1.6. Successful engraftment and reconstitution of phenotypically distinct subsets of innate myeloid cells

Developing humanized mouse models capable of reconstituting cells of the innate and adaptive immune systems and long-term survival is difficult to achieve, especially in the absence of irradiation and engineered or exogenous cytokine expression. Within both the established BRG humanised mouse model frequently used in transplantation studies and the NBSGW model, humanisation with human PBMCs leads to lymphocyte-biased engraftment

of predominantly T cells (together with low frequencies of B cells within the spleen and bone marrow), but no engraftment of myeloid cells (***Figure 3.1.6 (a & b)***). Having identified engraftment of human $CD33^+$ myeloid cells in the HSPC-NBSGW model (***Figure 3.1.2 (a, b); Figure 3.1.1 (d)***), we assessed reconstitution of myeloid subsets. At all doses of HSPCs transplanted, myeloid cells engrafted with the greatest frequency in the bone marrow (***Figure 3.1.6 (c); Figure 3.1.2 (b)***). Within the bone marrow and spleen we identified populations of HLA-DR^{hi}, HLA-DR^{int} and HLA-DR^- cells ***(Figure 3.1.6 (d-g)).*** The CD33+HLA-DRhi subset, which includes CD11c+ conventional dendritic cells (cDCs), formed the most common subtype in the bone marrow ***(Figure 3.1.6 (d-k); Figure 3.1.6 (m-n))***. As similarly described in human bone marrow, these cDCs expressed CD33, high levels of CD11c and HLA-DR, and were $CD14^-$ [267] and $CD11b^{lo/-}$ aiding the distinction from monocyte/macrophage lineage cells ***(Figure 3.1.6 (h-j))***. The HLA-DR^{int} fraction, which includes CD14-expressing mature monocytes/macrophages is found predominantly in the blood where it forms approximately half of all myeloid cells ***(Figure 3.1.6 (d-j & l))***. A less mature $CD14^+$HLA-DR^- population, which may include myeloid-derived suppressor cells is also present, especially in the spleen ***(Figure 3.1.6 (g))***. Among the $CD33^+$HLA-DR^- cells, a sizeable proportion express CD11b, suggesting a population of myeloid-derived suppressor cells (MDSCs)[268] (***Figure 3.1.6 (o)***), a cellular group of increasing interest in transplant research owing to their immunoregulatory activity[269,270]. Altogether, these data demonstrate successful engraftment and reconstitution of phenotypically distinct subsets of innate myeloid cells, which express molecules involved in antigen presentation.

3.1.7. Phagocytosis-dependent impairment in peripheral engraftment of human erythrocytes

Having established successful human cell leucopoiesis in the HSPC-NBSGW mouse model, we next investigated engraftment of erythrocytes. In normal physiology, erythrocytes derive from HSCs in the bone marrow before migrating into the blood following nuclear extrusion[271]. In HSPC-NBSGW mice, Glycophorin A analysis (CD235a) demonstrated the dose-dependent engraftment of erythroid cells within the bone marrow (***Figure 3.1.7 (a-b)***), however only a small, transient population of RBCs was found in the peripheral blood (***Figure 3.1.7 (c-d)***). To determine whether absence from the periphery results from defective erythroid lineage differentiation, we assessed erythroid cell maturity in the bone marrow (***Figure 3.1.7 (e-h)***). In addition to a small population of mature erythrocytes (***Figure 3.1.7 (b, e-f)***), dose-dependent frequencies of erythroid precursors at various stages of development were identified, with no significant discrepancies noted between male and female mice (***Figure 3.1.7 (g-h & i-k)***). To identify whether the lack of peripheral reconstitution results instead from phagocytosis of human erythroid cells by mouse phagocytes, we assessed survival following phagocyte depletion (***Figure 3.1.7 (l-s)***). Using a previously reported technique[249], clodronate liposomes (CloLip) were injected intravenously 11 weeks after HSPC injection, successfully reducing the frequencies of monocytes in the peripheral blood ($p=0.0315$), but not in the bone marrow ($p=0.2222$) or spleens, which interestingly showed an increased frequency of monocytes after CloLip injection ($p=0.0236$) (***Figure 3.1.7 (l)***). CloLip treatment was associated with increased numbers of mature erythrocytes predominantly in the blood (168-fold compared with control; 335 ± 237 vs 2 ± 1.6 per µl of blood) and spleen (***Figure 3.1.7 (m-p)***), suggesting that phagocytosis contributes at least in part to the impaired reconstitution of human erythroid cells in this model. While there was no significant difference in the frequencies of early erythroid precursors in the bone marrow following phagocyte clearance, as expected, an increase in reticulocytes and mature erythrocytes was seen (19% (16-27.7%)

vs 31.5% (5.2-36.9%) as median (with range), p<0.05) (***Figure 3.1.7 (q-s)***). The protective effect of macrophage clearance appeared to be greater outside the bone marrow as within, a more modest increase in numbers of erythroid precursors or mature erythrocytes were observed following CloLip (***Figure 3.1.7 (p-s)***).

The CD47-SIRPα interaction is known to deliver a 'don't eat me' signal from a CD47-expressing cell to a SIRPα-expressing phagocyte. To investigate a potential survival effect of CD47 expression on HSPC-NBSGW human haematopoeitic cells, we compared surface expression on leucocytes and erythrocytes (***Figure 3.1.7 (t-w)***). CD47 expression was greater on HSPC-NBSGW leucocytes than erythrocytes within the bone marrow, spleen and blood. To assess whether phagocyte clearance may influence leucocyte and erythrocyte CD47 expression differently, we compared expression following CloLip treatment (as above) (***Figure 3.1.7 (x-y)***). CD47 expression was more significantly increased on erythrocytes following CloLip treatment, (71.2% vs 26.6% ; fold change 1.7 vs 1.26). Of note, CD47 expression was higher on bone marrow-derived leucocytes and erythrocytes than spleen-derived. CloLip treatment had no effect on CD47-expression on cells within the bone marrow (***Figure 3.1.7 (x)***).

3.1.8. Human thrombocyte engraftment

We also investigated HSPC-NBSGW platelet engraftment, which was greatest in the bone marrow and spleen and minimally detectable in peripheral blood at the highest HSPC dose (***Figure 3.1.8 a-b***). Clearance of mouse phagocytes with CloLip (as in 3.1.7) led to a modest increase in numbers of platelets in the peripheral blood (***Figure 3.1.8 c***).

3.1.9. Self-renewing human HSPCs successfully engraft in NBSGW mouse bone marrow following CD133$^+$ HSPC injection

To investigate whether the bone marrow microenvironment of HSPC-NBSGW mice supports self-renewal of human HSPCs, we analysed engraftment and phenotype. A sizeable proportion of engrafted Lin^-CD34^+ and $Lin^-CD34^+CD38^{lo/-}$ cells was seen in the bone marrow and suggests a pool of stable, self-renewing HSPCs is maintained for at least 20 weeks (***Figure 3.1.9 (a-d)***), with comparable numbers to both irradiated and non-irradiated HSC HIS mouse models[198]. Relative engraftment of HSPCs was greater in the bone marrow of female as compared to male recipients when 5-10x10^3 HSPCs were transplanted (***Figure 3.1.9 (c-d)***).

3.1.10. Expansion of $CD133^+$ HSPCs using a small molecule epigenetic modifier does not negatively affect HSPC engraftment or pluripotency

The challenges of obtaining HSCs from UCB for clinical use and research are widely understood. Primary issues of difficulty include 1) high variability and often low yields per UCB unit and 2) high cost of procurement and HSC isolation[210]. These often result in low or insufficient numbers of HSCs available for clinical or experimental use. Cytokine-mediated HSC expansion can produce high yields of haematopoeitic progenitors, however typically at the expense of bone marrow HSC repopulating ability. To identify whether *ex-vivo* expansion of UCB $CD133^+$ HSPCs using a novel bromodomain and extra-terminal motif (BET) domain inhibitor "CPI203" (sourced from Prof Angela Russell) can proliferate and generate functional HSPCs capable of long-term self-renewal and pluripotency, we adoptively transferred HSPCs expanded *ex vivo* with CPI203 into tail veins of NBSGW mice and analysed human leucocyte chimaerism. Comparing chimaerism against transplanted unexpanded $CD133^+$ HSPCs and $CD133^+$ HSPCs cultured with 0.1% DMSO as the vehicle control, despite a five-fold increase in HSPCs following expansion[272], no deficiencies in leucocyte engraftment or multilineage

leucopoeisis were identified (***Figure 3.1.10 (a-d)***). The capacity to expand the content of UCB units may help researchers overcome experimental biases that result from having low numbers of donor replicates where only few animals can be engrafted with HSPCs from individual units of cord blood. The potential to use larger experimental group sizes without compromising cell functionality may help make the results from stem cell-based experiments more robust.

3.1.11. Engrafted HSPC-NBSGW HSPCs are capable of long term haematopoeitic reconstitution

To identify whether engrafted HSPCs identified in HSPC-NBSGW mice (***section 3.1.9***) are functional and capable of maintaining long-term haematopoeisis, we performed serial transplantations, injecting HSPC-NBSGW total bone marrow cells harvested 20-22 weeks post-adoptive transfer into secondary female adult NBSGW mice aged 8-12 weeks (***Figure 3.1.11 (a)***). 20 weeks later successful engraftment of human leucocytes was detected in the bone marrow (***Figure 3.1.11 (b)***). We similarly assessed whether the successfully engrafted expanded human HSPCs (***section 3.1.10***) were capable of long-term haematopoeisis (***Figure 3.1.11 (c)***) and identified significantly higher engraftment in recipients of bone marrow secondarily transplanted from mice injected with CPI203-expanded HSPCs when lower numbers of initiating cells were injected (***Figure 3.1.11 (d)***).

Human leucocyte engraftment within the spleen and peripheral blood was reliably identified in recipients of bone marrow secondarily transplanted from mice injected with CPI203-expanded HSPCs (***Figure 3.1.11 (e-f)***). Engraftment of $Lin^{-}CD34^{+}$ HSPCs in the bone marrow of secondarily transplanted mice was observed at low levels in the unexpanded and control expansion groups and at high levels in the CPI203-expanded HSPC group (***Figure 3.1.11 (g)***).

Bone marrow engraftment of B cells, T cells, myeloid cells and erythrocytes similarly was present in the unexpanded HSPC group and higher in the CPI203-expanded HSPC group (***Figure 3.1.11 (h-i)***).

Altogether, these data support the capacity for long-term haematopoeitic reconstitution in the NBSGW-HSPC model and the ability of the BET inhibitor CPI203 to expand LT-HSPCs, with preserved stemness and pluripotency.

3.2. Discussion

In this chapter we have developed a novel humanised mouse model, supporting multilineage human haematopoietic reconstitution following $CD133^+$ UCB HSPC injection, without the requirement for irradiative pre-conditioning. We have also demonstrated that expansion of $CD133^+$ UCB HSPCs using a new small molecule epigenetic modifier (CPI203) does not impede the efficiency of engraftment and reconstitution but rather increases it (***Figure 3.1.10***).

In addition to mouse strain and genetic modifications, important factors to consider when developing or choosing *in vivo* HIS models include the microenvironment into which human cells seek to engraft, the route of delivery of transplanted cells, animal sex and age at the time of transplant (e.g. some necessitate neonatal or *in utero* transfer), duration of sustained human haematopoiesis following transplant, phenotype and function of long-term repopulating human cells, complications such as graft versus host disease when mature human T cells are co-transplanted, adverse effects of irradiation and the inability to reconstitute the whole human blood and immune cell profiles[195,196].

Efforts to optimise engraftment have often focussed on creating space within the murine bone marrow niche by eliminating resident murine cells and altering the microenvironment

to favour human haematopoiesis by mutating critical murine growth factor receptors as in this model (e.g. loss of c-kit receptor function (W41/Wv alleles) in NOD/SCIDIl2rγ$^{-/-}$Kit$^{W41/W41}$ (NSGW41), NOD/SCIDIl2rγ$^{-/-}$ Kit$^{Wv/+}$ (NSGWv/+), NOD/SCIDIl2rγ$^{-/-}$ Kit$^{Wv/Wv}$ (NSGWv), NOD,B6.SCID Il2rγ$^{-/-}$Kit$^{W41/W41}$ (NBSGW), NOD,Rag2$^{-/-}$Il2rγ$^{-/-}$Kit$^{Wv/Wv}$ (SRG-W41) or BALB/cRag2$^{-/-}$ Il2rγ$^{-/-}$ Kit$^{Wv/Wv}$ (BRgWv) mice), direct treatment with an anti-c-Kit receptor antibody, administration of exogenous human cytokines (e.g. BAFF), or knock-in of human cytokine genes (e.g. SCF, TPO, GM-CSF, M-CSF, IL-3 and NSG-SGM3/NSGS, MSTRG and MISTRG mice)[195,196,198,201,208,211,273-276].

The HSPC-NBSGW model presents a technically straightforward system of humanisation in which adult mice successfully engraft human HSPCs via IV injection, removing the requirement for more demanding techniques such as *in utero* injection or facial vein/intrahepatic injections into young irradiated mice. Indeed, the ability to achieve multilineage human haematopoeisis without the requirement for irradiation, co-transplantation of human haematopoietic stromal tissues or the provision of exogenous cytokines represent defining features of this model.

B cells

It is well documented that immunodeficient mice (such as NSG and BRG) humanised with UCB HSCs generate significant numbers of human B cells[277], which develop quite normally in the bone marrow. Despite this, analyses of human B and T cells generated within different HIS mice models have revealed these B cells to be developmentally blocked[255], with defective peripheral maturation and humoral responses[193,278]. Initially this was thought to result from an inability of mouse BAFF to signal human B cells, suggested by the observation that administration of rhBAFF to NOD-*Rag1^{null}Prf1^{null}* mice humanised with PBMCs increases B cell

engraftment and the ability to mount an anti-pneumococcal polysaccharide response[201]. It has been reported that pre-B and immature B cells differ from mature B cells in that they do not require BAFF for their survival [279-281]. This assertion is supported by a recent study in which expression of full-length hBAFF from cDNA in the endogenous murine locus did not improve maturation of human B cells in HIS mice[282]. We have demonstrated the development of a large proportion of mature B cells in the spleen and peripheral blood of HSPC-NBSGW mice. This is important because only mature B cells can carry out effective antigen presentation and effector function. We also identified that bone marrow cells generated within HSPC-NBSGW mice can produce hBAFF and that production can be stimulated by inflammatory cytokines such as IFN-γ (***Figure 3.1.3 (i)***). This may be an important factor supporting the maturation and survival of the sizeable mature B cell population seen to develop in this model. Indeed expression of receptors for BAFF was approximately two fold higher on mature B cells than on immature B cells (***Figure 3.1.3 (k & l)***). The use of measured concentrations of serum BAFF as a determinant of BAFF utility is controversial because consumption of BAFF by B cells leads to an inverse correlation between BAFF levels and B cell numbers[265,283,284]. We demonstrated instead the production of human BAFF by HSPC-NBSGW bone marrow cells upon stimulation with human IFNγ. We believe that expression of human BAFF and the development of a T helper cell population - from approximately 12 weeks – are significant features of this model, which aid the maturation and survival of B cells. Perhaps the third essential component in this regard is the expression of cytokines – including IL-7 – which are known to support B cell development. Future experiments to determine the presence of these cytokines in the serum of HSPC-NBSGW mice may be useful to clarify this question.

Among the mature B cells detected in this model, the majority are naïve as may be expected considering the lack of antigen exposure in the controlled environments in which these mice

are maintained. Indeed, upon exposure to antigens from transplanted allogeneic human skin, the frequency of class-switched memory B cells increased to greater levels than in unexposed mice (***Figure 3.1.3 (g-h)***). This is a promising feature because it suggests responsiveness of HSPC-NBSGW B cells to stimulation by non-self antigens and also because it suggests versatility of this model, creating possibilities to incorporate the contribution of human humoral immunity into studies of infection, autoimmunity, transplantation and cancer, where models biased toward T cell-mediated immunity fail to accurately model this component of the global immune response. Having identified a promising frequency of mature B cells, in the next chapter we will assess the functionality of these cells in the setting of transplantation.

T cells

Current transplantation models using humanised mice employ human PBMCs as the allogeneic effector cells. Following injection with PBMCs, T cells are the primary immune subpopulation that engraft and remain functional in the murine host. In BRG mice, 3-4 weeks after injection of $5x10^6$ PBMCs, over 90% of engrafted human leucocytes are $CD3^+$ T cells, divided approximately equally into $CD4^+$ and $CD8^+$ T cells and displaying an activated and/or memory phenotype. Apart from representing a disproportionately large percentage of the leucocyte repertoire typically seen in humans (approximately 5-20% of $CD45^+$), this high frequency of T cells is unfavourable because it invariably leads to lethal xenogeneic GvHD[227,228,285], the onset of which is directly correlated with the degree of human T cell engraftment. In order to prolong the short therapeutic window afforded by this model (typically 3-6 weeks post-injection) and to more closely represent the human immune system for transplantation-based studies, the development of a multilineage haematopoietic cell HIS model is desirable. We have demonstrated in HSPC-NBSGW mice the ability to generate a

model engrafting a proportionally representative frequency of human $CD3^+$ T cells, which include the different subsets of naïve and memory T cells. This contrasts with the T cell subset frequencies identified in PBMC-humanised NBSGW mice - which demonstrated negligible engraftment of naïve T cells - and more closely aligns with populations found in human peripheral blood. Engraftment of naïve T cells in addition to activated and memory T cells suggests this model might have the potential to initiate T cell responses against a wider array of pathogens than in humanised mouse models engrafted with PBMCs. The phenotypic transition from naïve to effector memory T cells was associated with a functional transition, as evidenced by increasing intracellular granzyme A expression[286]. $CD8^+$ T cells developed within this model also expressed granzyme B and perforin. Although a greater proportion of Tem cells engrafted in this model than are present in adult blood, the vast majority of recipient mice did not exhibit signs of GvHD suggesting its suitability for longer-running *in vivo* T cell experiments. Interestingly, our results demonstrate the expression of HLA class I and class II molecules on $CD3^-$ cells in the thymi of HSPC-NBSGW mice.

Human cell engraftment of the thymic microenvironment in recipient mice is necessary for *in vivo* thymic education and development of HLA-restricted human T cells[193,221]. The presence of cells capable of presenting HLA-complexed antigen to developing thymocytes may enable this model to overcome the absence of thymic human T cell selection described in other humanised mouse models, postulated to impair or exclude human alloimmune responses. The NOD/SCID/BLT system meets this requirement and supports functional human T cell development however it necessitates the procurement of human foetal tissues. In this study we demonstrate a humanised thymic microenvironment expressing both HLA class I and II molecules and a sizeable fraction of $CD4^+CD8^+$ human thymocytes, similar to that seen in humanised irradiated NSG mice and in thymus biopsies from human infants[198]. Considering

that T cells were not detectable in the peripheral blood until 12 weeks post-transplantation in the earliest instances (***Figure 3.1.2 (j)***), it seems likely that *de novo* T cell development is occurring in HSPC-NBSGW mice rather than simply proliferation of inadvertently transplanted mature cord blood MNCs. This notion may be supported by the absence of DP thymocytes in mice humanised with PBMCs, suggesting early-stage development of thymocytes may only be occurring following transplantation of haematopoietic stem cells. Transplanting FACS-sorted UCB HSPCs of high purity may help us to gain greater clarity on this issue in the future. Our observation that HSPC-NBSGW thymi are populated vast majority predominantly by HLA-expressing human $CD45^+$ cells suggests that developing human T cells may have the apparatus required to attain *in vivo* the capacity to recognise antigens in an HLA-restricted manner. This hypothesis may be formally assessed by assessing T cell receptor excision circles (TRECs) as markers for recent thymic emigrants, or by inhibiting expression of or preventing ligation of HLA molecules and subsequently assessing T cell development and allogeneic function. Additionally, future experiments to profile both the thymic microenvironment more granularly within HSPC-NBSGW mice and gene expression may help us to understand how this model is uniquely able to demonstrate features of HLA restriction without the administration of foetal tissue.

This mouse model expresses human HLA on $CD3^-$ thymic cells and consistently represents the different T cell subsets, without the requirement for delivery of foetal tissue or specific knock-in of HLA genes, overcoming a major constraint in human immunology. We hope that it therefore serves as a useful model for the assessment of *in vivo* human cellular immunity in diseases such as malignancy and infection and in transplantation.

Myeloid cells

Despite great advances in the development of experimental HIS mouse models permitting efficient development of human innate immune cells, the long-term viability of these models is unconfirmed and a long-term model supporting human innate and adaptive immunity is still desirable.

There is increasing appreciation for the importance of innate immune cells in the rejection process[26,287]. In clinical studies, leucocyte depletion (CAMPATH-1H) was shown to be insufficient to prevent renal or intestinal allograft rejection, processes demonstrated to be associated with monocytic and eosinophilic inflammation respectively[288,289]. Additionally, experimental cardiac allotransplantation experiments in alymphatic mice demonstrated immune-cell infiltration and pro-inflammatory cytokine production, highlighting the ability of innate immune cells to respond to allografts in the absence of T cells[290]. Furthermore, an array of innate immune cells such as DCs[291], NK cells[292] and mast cells[293] have been shown to display immunoregulatory properties important for tolerance induction. Findings such are these demonstrate the importance of generating HIS models capable of representing the myriad components of the human allo-response to transplantation by supporting the development of functional human innate and adaptive immune cells.

Successful engraftment of professional human APCs in a HIS mouse could also help to more accurately represent *in vivo* the human allorecognition process. Current models lacking host APCs prevent reproduction of human indirect and semi-direct allorecognition responses. We have demonstrated the engraftment of a sizeable proportion of human $CD33^+$ myeloid cells ($11.49 \pm 4.67\%$ of human leucocytes (2.5×10^5 HSPCs injected)), however this is considerably lower than the fraction found in human adult peripheral blood (~60%[204]). Engraftment of higher frequencies of myeloid cells in HSC HIS models has been described[204] however in these

models foetal liver $CD34^+$ HSCs were engrafted into newborn mice, which required irradiative preconditioning for reliable engraftment. This makes for a process significantly more technically difficult and expensive than that presented here. An additional consideration, which will be important to demonstrate in this model expressing good myeloid cell engraftment is the capacity for these cells to become activated and demonstrate function in response to antigen stimulation. This will be investigated further in Chapter 4.

Erythroid cells

Animal models capable of supporting human erythropoiesis are desirable for the assessment of biological functions of human RBCs under physiologic and disease settings, for investigating therapeutics and for evaluating protocols of *in vitro* RBC differentiation. The development of humanised mouse models capable of supporting engraftment and long-term reconstitution of erythrocytes has been fraught with difficulties.

Our results demonstrate engraftment of erythrocyte precursor cells within the bone marrow of HSPC-NBSGW mice, however erythrocytes fail to survive outside the bone marrow. We and others have determined that this occurs in part (at least) as a result of mouse macrophage-mediated phagocytosis and is reversible in the short-term following macrophage elimination. If considering the usability of HSPC-NBSGW mice for erythrocyte studies, a problem with this method is the toxicity of CloLip. In our study, three out of five mice receiving CloLip experienced weight loss, requiring them to be euthanised. This toxicity has been described in other mouse studies using CloLip[249,294] and likely relates to clearance of visceral adipose tissue macrophages (VATMs), the accumulation of which in adipose tissue is closely related to weight gain in rodent models[295,296]. Indeed, Le Bu *et al.* depleted VATMs by intraperitoneal injection of CloLip and showed that this protected mice against high-fat diet-induced obesity,

insulin resistance and hepatic steatosis. This they concluded was the result of macrophage infiltration and inflammation, which are tightly correlated with fat accumulation in adipose tissue[297]. Loss of this mechanism following CloLip treatment of mice on normal diets could potentially account for the weight loss seen in these assays. Considering this, an alternative strategy to avoid CloLip toxicity and prevent human erythrocyte phagocytosis could involve optimising the interactions between CD47 on human erythrocytes and SIRPα on mouse macrophages. CD47 is a widely expressed membrane protein that interacts with the myeloid inhibitory receptor SIRPα to stimulate downregulatory signals that inhibit phagocytosis by the host cell. Thus, CD47 functions as a "don't eat me" signal. Takenaka *et al.* identified using an unbiased positional cloning approach that mouse strains of the NOD/SCID background demonstrate superior human HSC engraftment as a result of SIRPα expression[298]. This is likely due to NOD mice expressing a highly polymorphic variant of SIRPα (in contrast to other commonly used mouse strains), with a particularly high affinity for human CD47 - higher even than that between mouse CD47 and mouse SIRPα or between human CD47 and human SIRPα[299]. Proof of the efficacy of NOD mouse SIRPα was demonstrated by breeding of the NOD *SIRPA* gene onto the BALB/c Rag2^{null}IL-2Rγ^{null} or C57Bl/6 Rag2^{null}IL-2Rγ^{null}, which alone enhanced human HSC engraftment[300,301]. This however raises the question of why in this model human erythrocytes fail to evade CD47-SIRPα mediated host macrophage phagocytosis interaction whereas other human cell types appear to be able to?

Expression levels of CD47 on the surfaces of erythrocytes may be important in this regard, with low levels affording reduced protection against phagocytosis. Experimental data on human cells has shown that CD47 expression may be lost from the surface of erythrocytes in certain conditions such as ageing or storage[302,303]. *In vivo* studies have demonstrated in both motheaten and wild type mice that reductions in CD47 expression on erythrocytes leads to

their rapid elimination[304]. In an experiment comparing engraftment of $CD47^{hi}$ vs $CD47^{lo}$ cells, sorted leukaemic cells from a human cell line ectopically expressing murine CD47 were engrafted into recipient mice. After 75 days only mice receiving $CD47^{hi}$ cells succumbed to disease and this was associated with greater infiltration of the bone marrow and spleen. In the same study, after 75 days the bone marrow cells in mice engrafted with $CD47^{lo}$ cells expressed significantly higher CD47 than the originally engrafted cells, suggesting a selection pressure exists *in vivo* for high levels of CD47 expression in this human cell line. Additionally, it is known that CD47 can exist in different conformations on the surface of erythrocytes. Studies utilising a set of antibodies directed against different conformation-dependent CD47 epitopes demonstrated different conformations of CD47 on healthy compared with sickle cell erythrocytes[305]. CD47 expression levels on HSPC-NBSGW erythrocytes have yet to be described and so we questioned whether low or aberrant expression could at least partly account for their phagocytosis. Indeed our results show that erythrocytes - which do not survive - express less CD47 than leucocytes (***Figure 3.1.7 (t)***).

Following CloLip treatment both numbers of erythrocytes and expression levels of CD47 increased significantly within the spleen (***Figure 3.1.7 (y)***). Interestingly, CloLip treatment also increased splenic phagocytes (***Figure 3.1.7 (l)***). These findings may reflect a selection pressure within the spleen, whereby erythrocytes with greater CD47 expression escape phagocytosis. This would be consistent with the observation that in the bone marrow, where CloLip treatment did not elicit a change in the frequency of murine phagocytes, no change in CD47 expression was seen. Unfortunately, we were unable to assess the effect of CloLip treatment on CD47 expression in the peripheral blood, where we saw reduced frequency of mouse macrophages.

An additional theory which may explain these findings could relate to observations suggesting that in states of stress CD47 expression can increase[306]. In support of this, CloLip treatment has been shown to produce emphysema-like histological changes in the lungs of C57BL/6 mice within 24h of injection and significant weight loss in NSG mice[307]. It is conceivable considering our findings that CloLip treatment may cause cells to become globally stressed, leading to increased CD47 expression. In addition, a recent article demonstrated how CD47 is capable of functioning as an "eat me" signal after stresses such as oxidation induce a conformational change in the protein. This change enables binding to Thrombospondin-1 (TSP-1)[308] and after this has occurred subsequent interactions between CD47 and SIRPα lead to phagocytosis. Conformation of CD47 is also of relevance to TSP-1 binding as has been shown by Isenberg *et al.* who found that TSP-1 was able to bind to CD47 on sickle cell erythrocytes but not to CD47 on healthy control erythrocytes suggesting CD47 conformation also determines capacity to bind TSP-1[309]. Further characterisation of CD47 on HSPC-NBSGW erythrocytes may therefore aid our understanding of the processes underlying erythrocyte-specific phagocytosis and reveal strategies to subvert this. However, whereas the CD47-SIRPα interaction appears to be an important factor in explaining the specific rejection of developing HSPC-NBSGW erythrocytes, there is compelling evidence supposing additional alternative explanations. One suggestion is that CD47-independent mechanisms play a considerable role in the phagocytotic process. Hu *et al.* found that human erythrocytes are significantly more rapidly cleared than CD47 KO mouse erythrocytes, indicating that human erythrocyte rejection may be induced predominantly by mechanisms other than low or absent CD47-SIRPα signalling[249]. Another suggestion is that enucleated erythrocytes are more sensitive to phagocytosis than nucleated cells[304,310]. The observation of no difference in erythrocyte prevalence within the bone marrow compared with the spleen and blood following

macrophage clearance raises interesting questions, as does the observation that CD47 expression is higher in the bone marrow than in the spleen and blood. In keeping with the latter, Nagahara *et al.* reported that in healthy human subjects CD47 expression determined by RT-PCR is almost two-fold higher in the bone marrow than peripheral blood[311]. Our results show that the bone marrow of untreated HSPC-NBSGW mice has a low abundance of murine phagocytes (***Figure 3.1.7 (l)***), which are found at similar frequencies to peripheral blood following clearance with CloLip. A combination of these factors may help to explain the persistence of erythrocytes in the bone marrow but not in peripheral tissues in the absence of CloLip treatment. It is possible that at the dose used, CloLip were unable to reach the bone marrow or to reduce the frequency of marrow-resident mouse phagocytes below that already present. This is supported by the observation that CD47 expression did not change in erythrocytes or leucocytes within the bone marrow, suggesting no alterations to the selection pressure were exerted by the treatment. However, multiple studies have demonstrated clearance of bone marrow phagocytes following CloLip treatment and so it is possible that an altered dose may increase clearance. There is also the possibility that space or biochemical constraints prevent expansion of erythrocyte numbers within the bone marrow when compared to the periphery.

Owing to the considerable morbidity associated with CloLip treatment, a method of clearing macrophages without such severe toxicity to the host is desirable. In a recent article, RBC-derived nanovesicles (RDNVs) were employed as drug nanocarriers to specifically deplete macrophages and showed superior clearance and longer term survival than CloLip (100% vs 0% at 22 days)[307]. Such an approach, which confers less toxicity to the host animal would improve welfare and may additionally enable longer running experiments to be completed.

At this point it is important to also consider the effects of macrophages in supporting erythropoiesis. It is well documented that in homeostasis and under conditions of stress macrophages play an important role in promoting RBC development[312]. Bessis and Breton-Gorius proposed that macrophages achieve this by directly transferring iron to erythroid progenitors[313] in erythroblastic islands – structures of macrophages surrounded by developing erythroblasts within the bone marrow[314]. It has yet to be determined whether cross-species reactivity exists whereby murine macrophages may support the development of hRBCs, however the observation that cobra venom factor could significantly prolong hRBC survival in mice treated with CloLip by preventing adherence of hRBCs to murine phagocytes[274] suggests that the dominant result of interactions between these cells is phagocytotic. Therefore, a potential strategy to improve RBC engraftment could involve promoting engraftment of human macrophages as well as reducing the frequency of mouse macrophages. If the development of functional human cell erythroblastic islands is as important in humanised mouse erythropoiesis as it is in humans, supporting their development may potentially help to explain why overexpression of hEPO in NBSGW mice failed to enhance hRBC engraftment[275] as they form the subsequent step – differentiation of colony-forming unit-erythroid cells into erythroblasts[315].

HSPC expansion and long-term bone marrow-repopulating capacity

HSCs are essential for long-term production of blood cells and have developed intricate molecular networks to accurately balance the processes of proliferation, differentiation, quiescence and cell death. Precise coordination of these processes is important to maintain haematopoeitic homeostasis and aberrations may alter HSC numbers and lead to reduced cellular output or potentially malignant transformation. *Ex vivo*, UCB HSCs demonstrate

extensive haematopoeitic capacity and rapidly divide in the presence of cytokine combinations. During such cellular expansions however several of these cells lose their marrow-repopulating potential. It has been reported that small molecules targeting chromatin-regulating proteins (e.g. histone deacetylase (HDAC) inhibitors and DNA demethylating agents) can overcome the loss-of-stemness exhibited by human HSCs in *ex vivo* cytokine- containing expansion cultures[316-318].

Additionally, the efficacy of BET inhibitors in the treatment of hematological and non-hematological malignancies is well documented in pre-clinical studies and as part of single or synergistic combination therapies in clinical trials. CPI203 is a BET inhibitor which has been shown to preserve 'stemness' of HSCs and prevent differentiation in part by modulating the oncogene MYC[319], overexpression of which promotes HSC differentiation at the expense of self-renewal[320]. We have demonstrated that the novel combination of CPI203 and selected cytokines can enhance the expansion of UCB HSPCs which retain long-term *in vivo* bone marrow repopulating capacity (***Figure 3.1.11***)[272]. These findings demonstrate the potential to make significant use of very small numbers of highly valuable UCB HSPCs and the ability of the HSPC-NBSGW model to support the development of cells generated with this novel expansion technique.

Our results build upon findings of other advanced HIS mouse studies and demonstrate consistent robust human haematopoietic cell engraftment and reconstitution following injection of as few as $5x10^3$ human $CD133^+$ UCB HSPCs into non-irradiated adult NBSGW recipients, in the absence of co-transplantation of additional human haematopoietic niche tissues. This model attained equivalent human $CD45^+$ bone marrow engraftment following

injection of a HSPC dose 60-fold lower than that described in comparable irradiated (irNSG) and non-irradiated (BRgWv & NSGWv) HSC HIS mouse models[198].

Importantly we have also shown that this model supports the development and maturation of human T cells, myeloid cells and NK cells in addition to B cells, producing a mouse model representing the broad spectrum of adaptive and innate immunity. This will be of particular interest in the field of transplantation, enabling models of human organ rejection to incorporate mechanisms of indirect allorecognition as well as humoral and cellular effector mechanisms.

In the next chapter, we will explore whether cells engrafting HSPC-NBSGW mice demonstrate functional capacity.

Chapter 3: Figures

Figure 3.1.1 human UCB CD133$^+$ HSPCs administered via intravenous injection at doses of 1x10^3, 5x10^3, 5x10^4 and 2.5x10^5 produce reliable leucocyte reconstitution in NOD,B6.SCID *Il2rγ$^{-/-}$ Kit$^{W41/W41}$* (NBSGW) mice. Lower human CD45$^+$ cell engraftment is seen in the bone marrow of male recipients.

Engraftment analysis of human CD133$^+$ HSCs injected into NBSGW mice.
Non-irradiated NBSGW mice were injected intravenously with 1x10^3, 5x10^3, 5x10^4 or 2.5x10^5 human CD133$^+$ HSPCs from 1 of 4 donors in 3 separate experiments. Cells were suspended in 200µl IMDM supplemented with 1% human serum albumin (HSA). n=11, n=14, n=6 and n=3 mice per group respectively. Blood samples were taken at intervals from week 2 to week 20 and analysed by FACS for the presence of live human 7AAD$^-$CD45$^+$ cells. Mice were sacrificed 20-22 weeks post-injection and spleens and bone marrow analysed by FACS for the presence of live human 7AAD$^-$CD45$^+$ cells. Mice achieving bone marrow 7AAD$^-$CD45$^+$ levels >0.1% were considered to be adequately engrafted. Data are represented as representative FACS plots demonstrating (a) human UCB 7AAD$^-$ HSPCs isolated by CD133 positive enrichment, (b) frequencies of human CD45$^+$ leucocytes (percentage of total (mouse + human) CD45$^+$ leucocytes), dot and line plot demonstrating (c) frequencies of hCD45$^+$ leucocytes in the blood at indicated time points according to dose of injected HSPCs (mean and SD shown), (d) frequencies of human leucocyte populations in the spleen, bone marrow and peripheral blood 20-22 weeks post-transplantation, (e) absolute cell numbers of human leucocyte populations in the spleen, bone marrow and peripheral blood, (f) frequencies of human leucocyte reconstitution in the bone marrow as a function of the number of hCD133$^+$ HSPCs injected. All samples successfully engrafted (>0.1% hCD45$^+$ cells in the murine bone marrow), (g) absolute numbers of human CD45$^+$ leucocytes per microliter of blood in male and female recipient mice, based on the number of injected HSPCs, (h–k) Human CD45$^+$ leucocyte frequencies (percentage of total mouse plus human CD45+ cells) and corresponding absolute numbers per bone marrow of one femur and spleen in male and female recipient mice, based on number of injected HSPCs. M- male (blue symbols), F- female (red symbols), 250x103 C – control group (mixed sex), (l) comparison of hCD45$^+$ absolute cell number and frequency in bone marrow, spleen and blood of male vs. female HSPC-NBSGW mice. Statistical analyses were performed using the Mann Whitney test (*p<0.05, ***p<0.001). In (g), two points fall below the cut-off shown for 1x10^3 cells infused. Non-statistical bars represent median values.

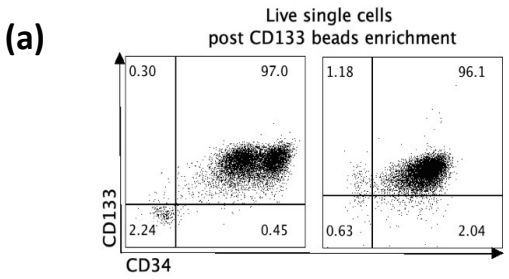

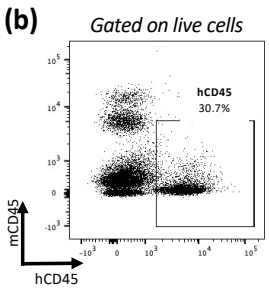

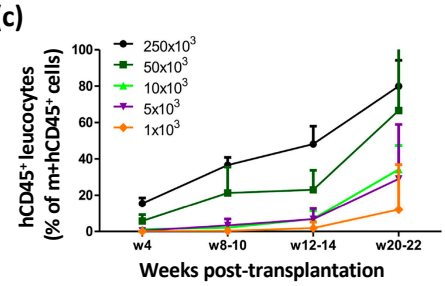

(d)

Frequencies of human leucocyte populations in the spleen, bone marrow and peripheral blood 20-22 weeks post-transplantation

		1x10³ (n=11)	5x10³ (n=7)	10x10³ (n=7)	50x10³ (n=7)	250x10³ (n=3)
spleen						
% hCD45+	mean (SD)	32.0 (39.4)	73.5 (25.4)	79.0 (10.7)	93.6 (5.3)	98.5 (0.9)
% CD19+	mean (SD)	84.6 (5.9)	86.9 (3.2)	87.5 (3.4)	85.0 (6.0)	75.1 (8.7)
% CD33+	mean (SD)	2.5 (1.0)	2.2 (1.2)	2.2 (0.6)	2.0 (1.0)	1.5 (0.3)
% CD3+	mean (SD)	1.5 (2.9)	1.8 (3.0)	2.6 (2.7)	5.3 (5.6)	14.2 (10.8)
BM						
% hCD45+	mean (SD)	35.0 (36.2)	75.5 (17.6)	64.6 (9.5)	87.8 (11.0)	97.4 (1.9)
% CD19+	mean (SD)	72.1 (17.0)	69.0 (22.5)	81.4 (9.3)	54.5 (18.8)	36.7 (3.9)
% CD33+	mean (SD)	7.9 (11.0)	11.7 (14.2)	9.0 (11.5)	25.6 (8.9)	26.4 (6.8)
% CD3+	mean (SD)	0.8 (1.1)	1.0 (1.6)	0.9 (1.5)	1.8 (2.0)	8.5 (6.7)
blood						
% hCD45+	mean (SD)	12.1 (24.7)	29.0 (30.0)	28.1 (12.8)	50.6 (31.7)	80.0 (14.2)
% CD19+	mean (SD)	50.4 (41.1)	76.6 (16.7)	85.2 (5.5)	77.1 (7.9)	51.5 (14.6)
% CD33+	mean (SD)	2.7 (3.8)	8.5 (9.9)	1.1 (1.2)	3.0 (3.5)	8.2 (3.3)
% CD3+	mean (SD)	0.4 (0.9)	1.8 (4.4)	2.8 (3.2)	7.5 (6.2)	18.4 (8.1)

hCD45⁺ as % of h+mCD45⁺, hCD19⁺, hCD33⁺, hCD3⁺ as % of hCD45⁺

(e)

Absolute cell numbers of human leucocyte populations in the spleen, bone marrow and peripheral blood.

		1x10³ (n=11)	5x10³ (n=7)	10x10³ (n=7)	50x10³ (n=7)	250x10³ (n=3)
spleen						
hCD45+	mean (SD)	873697 (1597728)	2665263 (1927842)	1762045 (1216759)	5400707 (3069853)	9575582 (3858274)
CD19+	mean (SD)	781801 (1438353)	2323283 (1684014)	1514711 (969695)	4488147 (2425023)	7308951 (3487852)
CD33+	mean (SD)	15813 (25997)	46023 (25698)	39518 (30484)	97262 (64989)	135981 (39324)
CD3+	mean (SD)	3357 (4736)	74811 (135535)	62044 (106323)	399407 (464568)	1290485 (801811)
BM						
hCD45+	mean (SD)	266284 (378622)	634043 (521090)	404888 (381261)	852015 (481297)	821951 (304156)
CD19+	mean (SD)	173734 (239825)	364826 (184394)	320377 (291311)	409470 (172648)	296236 (99304)
CD33+	mean (SD)	43122 (80370)	119812 (178873)	55818 (86370)	219477 (143491)	229085 (121670)
CD3+	mean (SD)	2178 (4208)	8083 (10125)	3869 (4519)	17083 (17397)	56467 (28179)
blood						
hCD45+	mean (SD)	16.54 (44.70)	43.57 (57.03)	17.88 (11.69)	83.61 (91.70)	92.62 (52.84)
CD19+	mean (SD)	14.14 (38.64)	33.88 (32.87)	15.15 (10.06)	64.00 (70.97)	43.11 (18.58)
CD33+	mean (SD)	0.28 (0.56)	6.30 (13.97)	0.27 (0.31)	4.83 (7.53)	6.63 (3.12)
CD3+	mean (SD)	0.03 (0.06)	2.72 (6.76)	0.61 (0.81)	6.99 (8.51)	19.92 (15.79)

Mean and standard deviations of cell numbers per spleen, femur or µl of blood

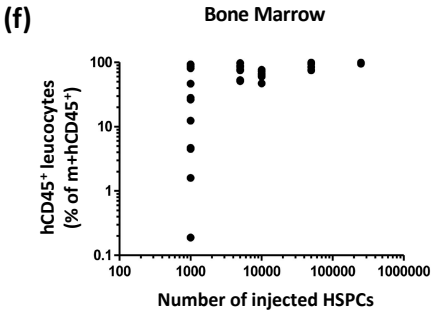

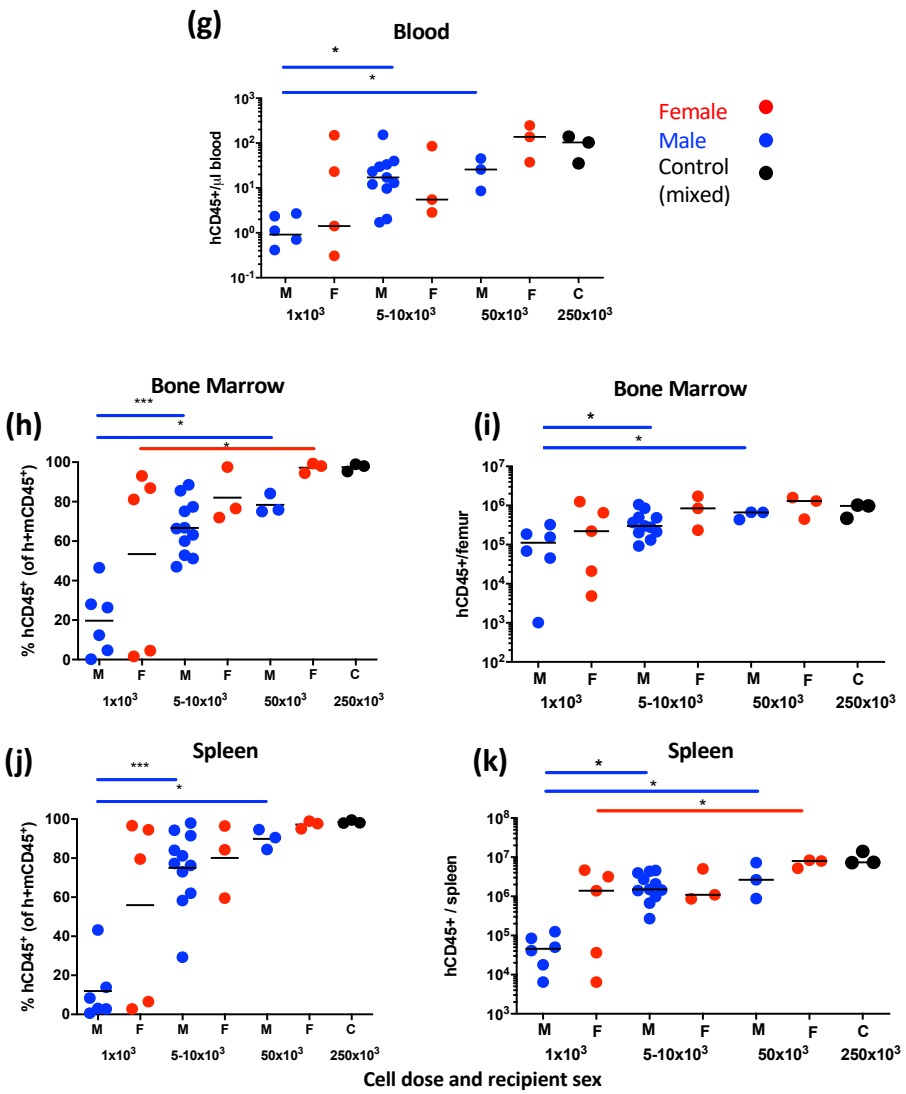

(l)

hCD133+ cells transplanted	p value for hCD45+ Chimerism in Male vs Female Recipients					
	Absolute Cell Number			Frequency		
	Peripheral Blood	Bone Marrow	Spleen	Peripheral Blood	Bone Marrow	Spleen
$1x10^3$	0.71	0.54	0.33	0.36	0.43	0.25
$5\text{-}10x10^3$	0.75	0.28	1.00	0.76	0.16	0.64
$50x10^3$	0.20	0.40	0.20	0.10	0.10	0.10

Figure 3.1.2 human UCB CD133$^+$ HSPCs administered via intravenous injection at doses of 1x10^3, 5x10^3, 5x10^4 and 2.5x10^5 produce stable multilineage leucocyte reconstitution in NOD,B6.SCID *Il2rγ$^{-/-}$ Kit$^{W41/W41}$* (NBSGW) mice.

Engraftment analysis of human CD133$^+$ HSCs injected into NBSGW mice.
Non-irradiated NBSGW mice were injected intravenously with 1x10^3, 5x10^3, 5x10^4 or 2.5x10^5 human CD133$^+$ HSCs from 1 of 4 donors in 3 separate experiments. Cells were suspended in 200µl IMDM supplemented with 1% human serum albumin (HSA). n=11, n=14, n=6 and n=3 mice per group respectively. Blood samples were analysed serially and mice were sacrificed 20-22 weeks post-injection of HSPCs. Blood, spleens and bone marrow analysed by flow cytometry for the presence of live human 7AAD$^-$CD45$^+$CD3$^+$ or 7AAD$^-$CD45$^+$CD19$^+$ or 7AAD$^-$CD45$^+$CD33$^+$ or 7AAD$^-$CD45$^+$ CD3$^-$CD56$^+$ cells. Mice achieving bone marrow 7AAD$^-$CD45$^+$ levels >0.1% were considered to be adequately engrafted. Data are represented as (a) frequencies of human B cells (hCD19$^+$), myeloid cells (hCD33$^+$) and T cells (hCD3$^+$) in the bone marrow, spleen and blood of HSPC-NBSGW mice 20-22 weeks after cell injection (50x10^3 cells), (b-d) representative flow cytometry plots of human B versus myeloid or T cell reconstitution in the (b) bone marrow, (c) spleen and (d) blood, (e-g) frequencies of human (e) B cells, (f) myeloid cells, and (g) T cells in the spleens of male (blue symbols) and female (red symbols) mice reconstituted with different numbers of HSPCs as indicated; frequencies of (h) B cells, (i) myeloid cells and (j) T cells in peripheral blood at indicated time points; (k) representative flow cytometry plot and (l) corresponding frequencies of hCD45$^+$mCD45$^-$ CD56$^+$ natural killer cells reconstituting HSPC-NBSGW bone marrow, spleens and peripheral blood (only 50x10^3 dose assessed, as shown). Bars represent median values ± IQR. Statistical significance was assessed using the unpaired Mann-Whitney test (e-g) and the Ordinary one-way ANOVA with Holm-Šídák's multiple comparisons test (l) (*p<0.05; ** p<0.01).

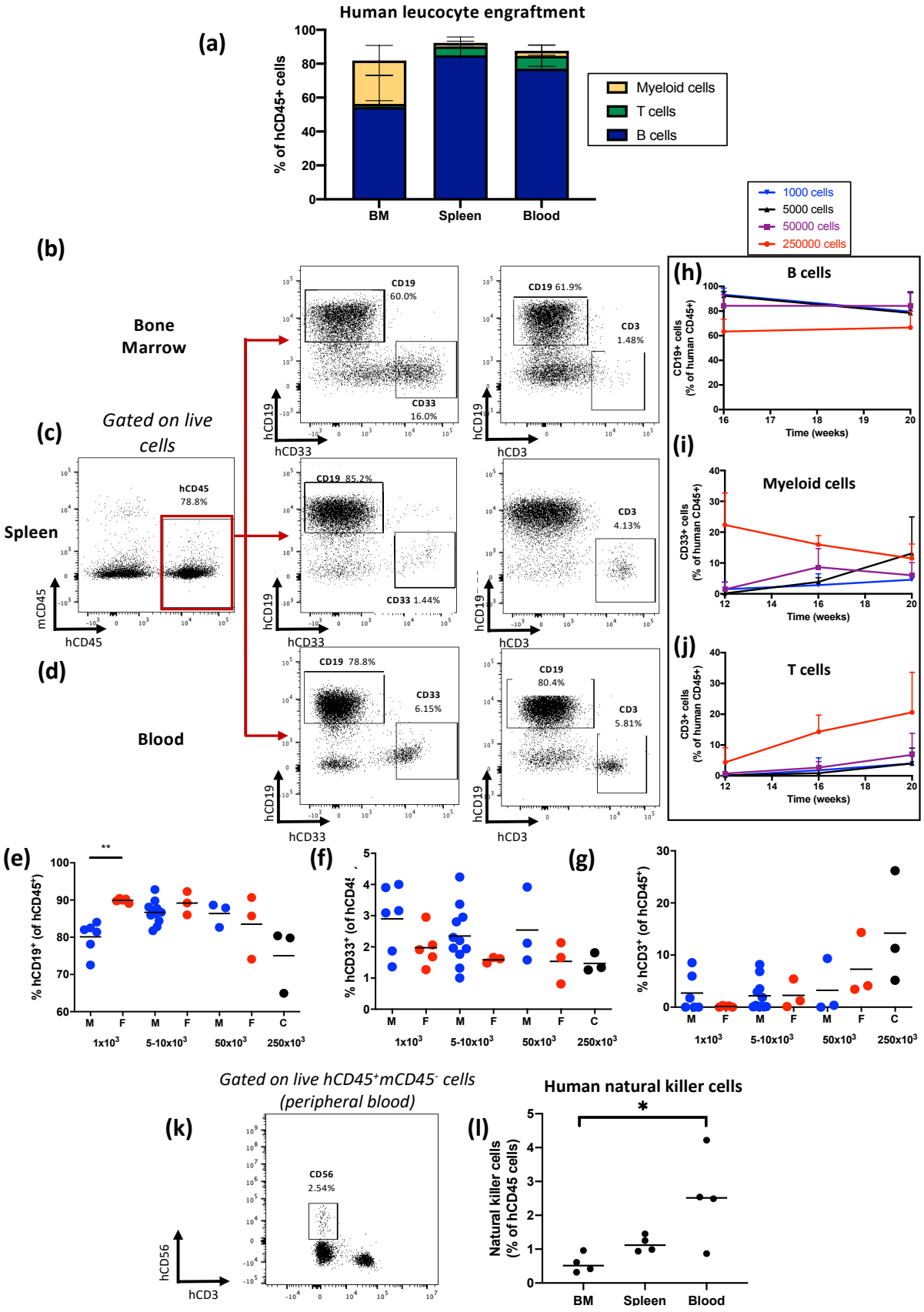
Human leucocyte engraftment
(a)
% of hCD45+ cells
Myeloid cells
T cells
B cells
BM
Spleen
Blood
(b)
Bone Marrow
(c)
Gated on live cells
Spleen
hCD45 78.8%
mCD45
hCD45
(d)
Blood
CD19 60.0%
CD33 16.0%
CD19 61.9%
CD3 1.48%
CD19 85.2%
CD33 1.44%
CD3 4.13%
CD19 78.8%
CD33 6.15%
CD19 80.4%
CD3 5.81%
hCD19
hCD33
hCD3
1000 cells
5000 cells
50000 cells
250000 cells
(h)
B cells
CD19+ cells (% of human CD45+)
Time (weeks)
(i)
Myeloid cells
CD33+ cells (% of human CD45+)
(j)
T cells
CD3+ cells (% of human CD45+)
(e)
% hCD19+ (of hCD45+)
(f)
% hCD33+ (of hCD45+)
(g)
% hCD3+ (of hCD45+)
M F M F M F C
1x10³ 5-10x10³ 50x10³ 250x10³
Gated on live hCD45+mCD45- cells (peripheral blood)
(k)
CD56 2.54%
hCD56
hCD3
Human natural killer cells
(l)
Natural killer cells (% of hCD45 cells)
BM Spleen Blood

Figure 3.1.3 human B lymphocyte engraftment and development.
Engraftment analysis of human B cells.
Non-irradiated NBSGW mice were injected intravenously with $1x10^3$, $5x10^3$, $5x10^4$ or $2.5x10^5$ human $CD133^+$ HSPCs from 1 of 4 donors in 3 separate experiments. Cells were suspended in 200µl IMDM supplemented with 1% HSA. n=11, n=14, n=6 and n=3 mice per group respectively. Mice were sacrificed 20-22 weeks post-injection of HSPCs and (a) live human $7AAD^-CD45^+CD19^+$ B cells within the bone marrow, spleen and blood were analysed by FACS for the presence of markers of (b-d) maturity (CD10 negativity) and (e-f) memory function. (g-h) Separate HSPC-NBSGW mice received an allogeneic split-thickness human skin graft and were sacrificed at the time of clinical rejection or 100 days after transplantation. Spleens were harvested concurrently and splenocytes analysed for the frequency of class-switched memory B cells. (i) $1x10^6$ thawed HSPC-NBSGW bone marrow cells were stimulated with IFN-ɣ for 36 hours in 24 well plates and analysed by FACS for intracellular expression of hBAFF. Comparison was made with unstimulated bone marrow cells. (j) HSPC-NBSGW splenocytes were analysed by FACS for surface expression of receptors to hBAFF. (k) Expression of BAFF-R was assessed in mature and immature B cells in the bone marrow, spleen and blood. (l) Expression of TACI on immature and mature splenic B cells was also analysed. Data are represented as (a) scatter plot indicating the frequency of $hCD19^+$ cells in the bone marrow (BM), spleen and peripheral blood ($50x10^3$ HSPC dose), (b) representative flow cytometric analysis of CD10 expression on human splenic B cells, (c) frequencies of mature ($CD10^-$) and immature ($CD10^+$) human B cells (BM, spleen and blood), (d) sizes of mature vs immature human splenic B cells (determined by forward scatter (FSC), (e) representative flow cytometric analysis and (f) corresponding frequencies of mature B cell subsets (BM, spleen and blood), based on IgD and CD27 expression. The red box indicates mature cells [as gated in (b)], (g) frequencies of IgD^- memory B cells in the femurs and spleens of HSPC-NBSGW mice which received allogeneic split-thickness human skin grafts 11 weeks after humanization and were sacrificed at the time of skin rejection (skin Tx) or 100 days after transplantation (no skin Tx), (h) frequencies of class-switched memory B cells in the spleens of mice which did (skin) and did not (no skin) receive allogeneic split-thickness human skin grafts. Bars represent median + IQR (c, f, h), and mean + SEM (d). Statistical significance was assessed using the paired T test (d) and the Mann-Whitney test (h, k) (*$p<0.05$; ****$p<0.0001$).

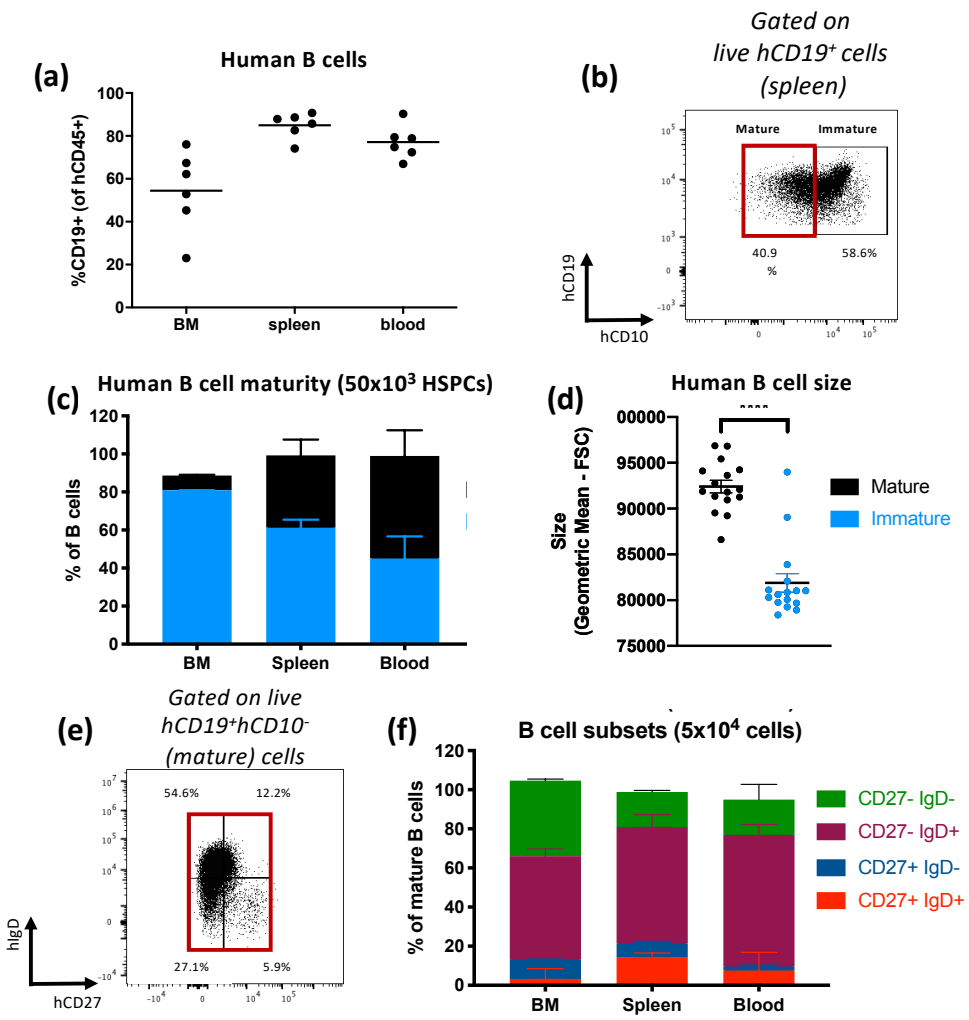
(a)
Human B cells
%CD19+ (of hCD45+)
100
80
60
40
20
0
BM
spleen
blood
(b)
Gated on
live hCD19+ cells
(spleen)
Mature
Immature
40.9
%
58.6%
hCD19
hCD10
(c)
Human B cell maturity (50x10³ HSPCs)
% of B cells
120
100
80
60
40
20
0
BM
Spleen
Blood
(d)
Human B cell size
Size
(Geometric Mean - FSC)
00000
95000
90000
85000
80000
75000
Mature
Immature
(e)
Gated on live
hCD19+hCD10-
(mature) cells
54.6%
12.2%
27.1%
5.9%
hIgD
hCD27
(f)
B cell subsets (5x10⁴ cells)
% of mature B cells
120
100
80
60
40
20
0
BM
Spleen
Blood
CD27- IgD-
CD27- IgD+
CD27+ IgD-
CD27+ IgD+

(g)

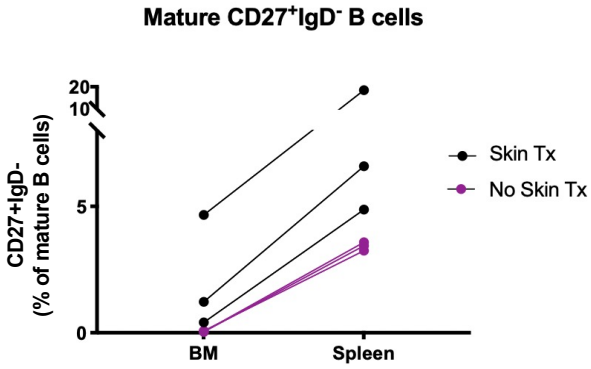
Mature CD27+IgD- B cells
CD27+IgD-
(% of mature B cells)
20
10
5
0
BM
Spleen
Skin Tx
No Skin Tx

(h)

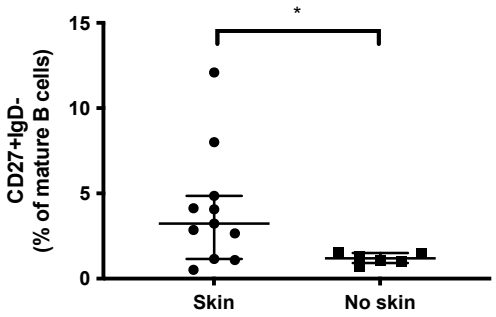
CD27+IgD-
(% of mature B cells)
15
10
5
0
*
Skin
No skin

Gated on live human CD19⁺ cells

(i)

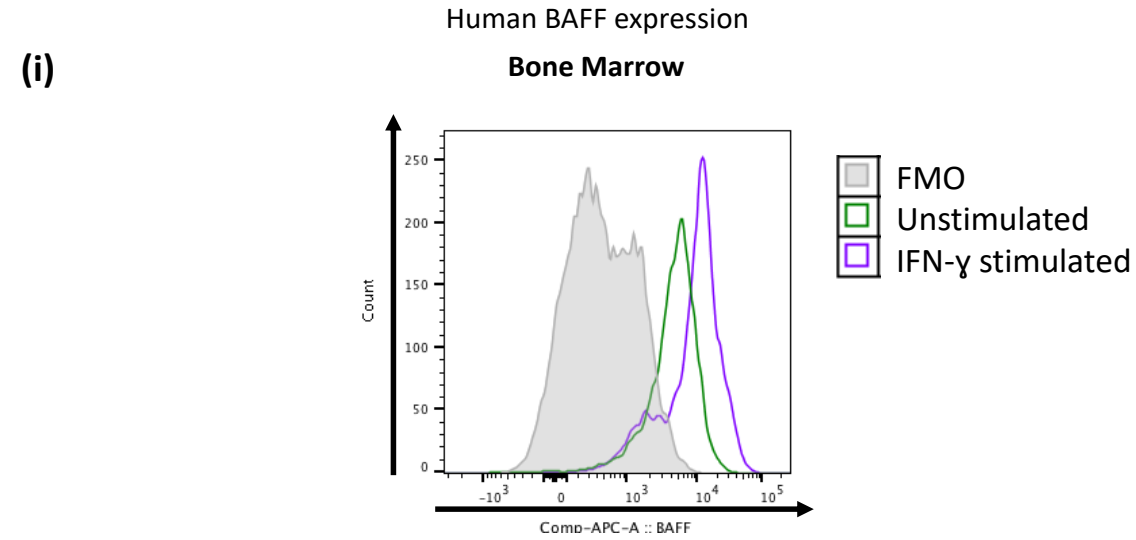

(j)

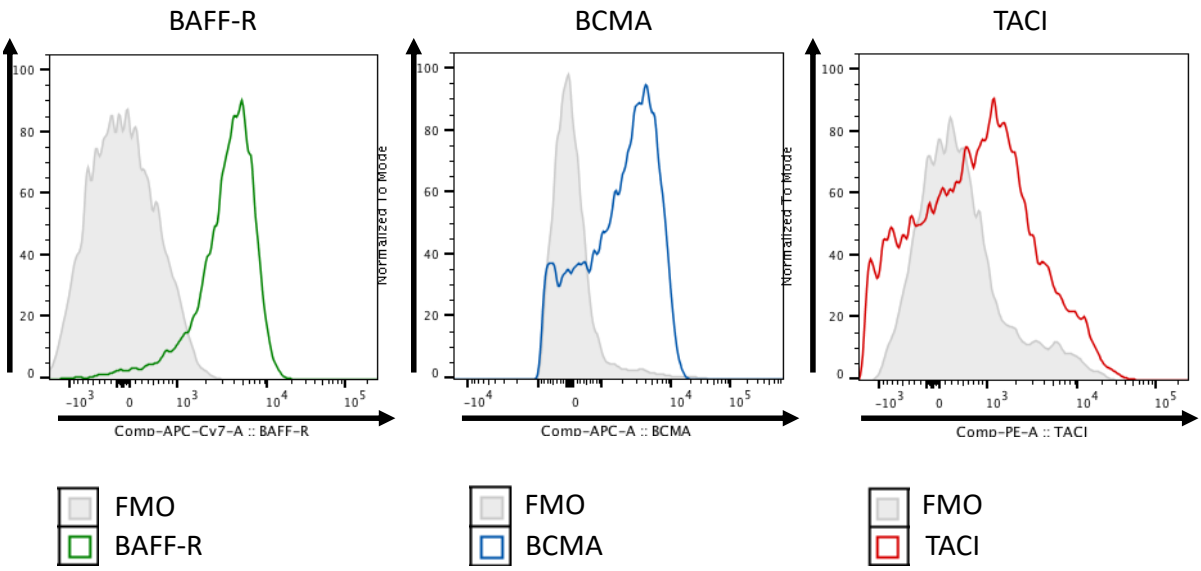

Gated on live human CD19⁺ cells

(k)

BAFF-R

BM

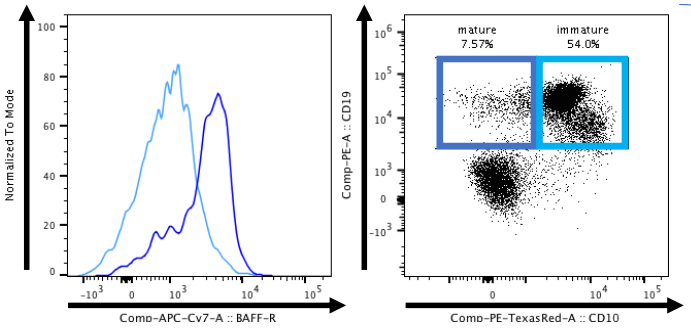

Spleen

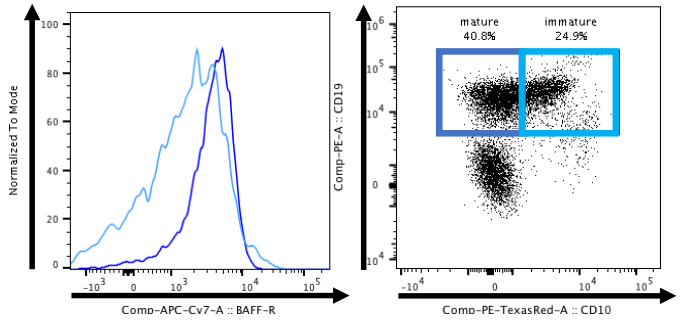

Blood

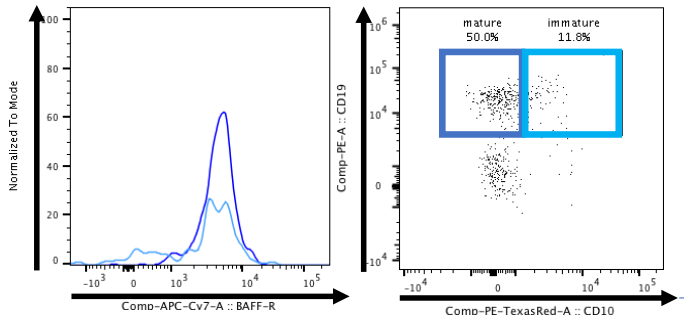

BAFF-R expression

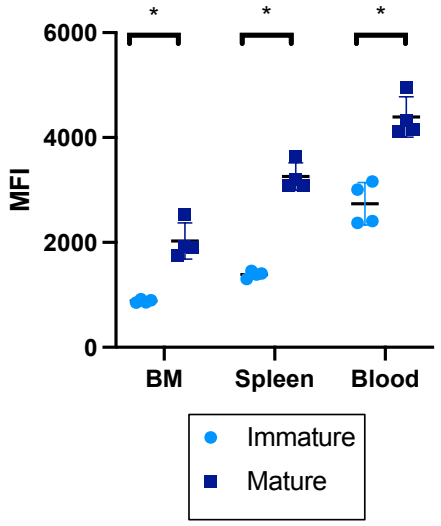

(l)

TACI

Spleen

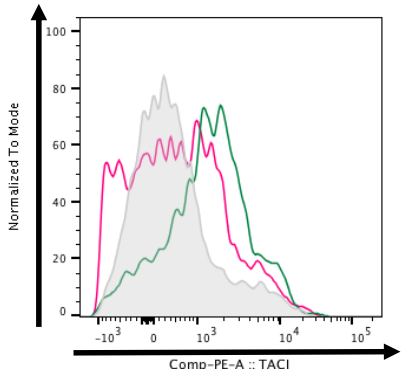

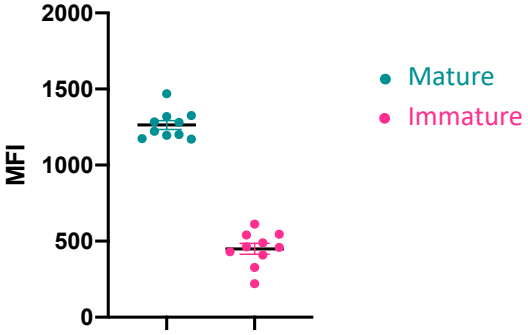

Figure 3.1.4 human T lymphocyte engraftment.
Engraftment analysis of human T cells.
Non-irradiated NBSGW mice were injected intravenously with $5x10^4$ or $2.5x10^5$ human $CD133^+$ HSPCs. Cells were suspended in 200µl IMDM supplemented with 1% HSA. Mice were sacrificed 20-22 weeks post-injection of HSPCs and harvested cells analysed by flow cytometry for the presence of (a) live human $7AAD^-CD45^+CD3^+$ T cells and (b-g) for identifiers of T cell subset (a & b - $2.5x10^5$ HSCs). (i) For comparison, thawed human PBMCs from individual donors (n=4) were analysed in an identical manner, as were (h-k) NBSGW mice injected intraperitoneally with $5x10^6$ thawed human PBMCs and harvested after 21 days (n=3). (l-m) Thawed HSPC-NBSGW (l) $CD3^+$ splenic T cells and (m) $CD8^+$ T cell subsets were analysed for intracellular expression of cytolytic proteins. Data are represented as (a) frequencies of human $CD3^+$ T cells in the BM, spleen and blood of HSPC-NBSGW mice ($50x10^3$ HSPC dose shown), (b-d) representative flow cytometric analysis of (b) CD4 and CD8 expression on live human $CD45^+CD3^+$ splenic T cells, (c) $CD8^+$ and (d) $CD4^+$ T cell subsets, determined by surface expression of CD45RA and CCR7, (e) absolute numbers of T cell subsets in spleens of NBSGW mice 20-22 weeks after humanization with $250x10^3$ $hCD133^+$ UCB HSPCs. Values shown are the means $\pm$ S.D; (f, g) frequencies of $CD8^+$ (f) and $CD4^+$ (g) splenic T cell subsets: naïve (Tn; hCD45RA+hCCR7+), Tcm (hCD45RA-hCCR7+), Tem (hCD45RA-hCCR7-) and TemRA (hCD45RA+hCCR7-) ($250x10^3$ HSPC dose shown). (h) Frequencies of CD8+ T cell subsets in peripheral blood of HSPC-NBSGW mice (black symbols), PBMC-humanised NBSGW mice (blue symbol) and human adults (red symbols); $CD3^+$ T cell subset frequencies in the (i) peripheral blood of human donors, and (j) spleen and (k) blood of NBSGW mice humanised with $5x10^6$ human PBMCs. (l-m) flow cytometric analysis and corresponding geometric mean fluorescence intensity of intracellular cytolytic protein expression. Bars indicate median values. Statistical significance was assessed using the two-way ANOVA with Tukey's multiple comparisons (*$p<0.05$; ** $p<0.01$, *** $p<0.001$, ns $p>0.05$).

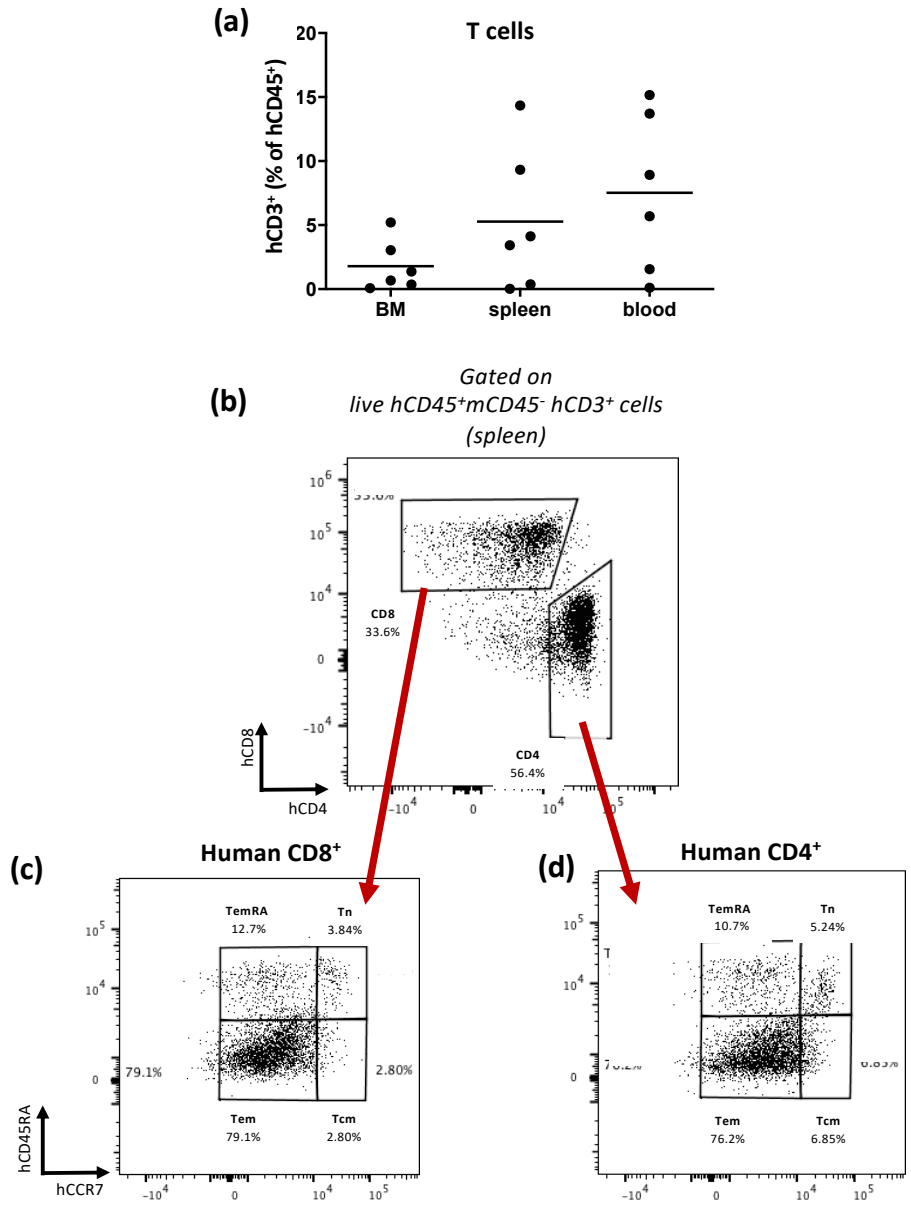

(e)

	Tn	Tcm	TemRA	Tem
Absolute number of splenic hCD4+ cells (Mean±SD)	24506±12497	68667± 54468	21609±26484	122877±123907
Absolute number of splenic hCD8+ cells (Mean±SD)	12307±3777	15413±13128	24404±23640	109980±118099

The absolute numbers of hCD4+ or hCD8+ cells in spleens of NBSGW mice 20-22 weeks after humanization with 250x10^3 hCD133+ UCB HSPCs were 237658+215304 and 162103±156083. Values shown are the means ± S.D.

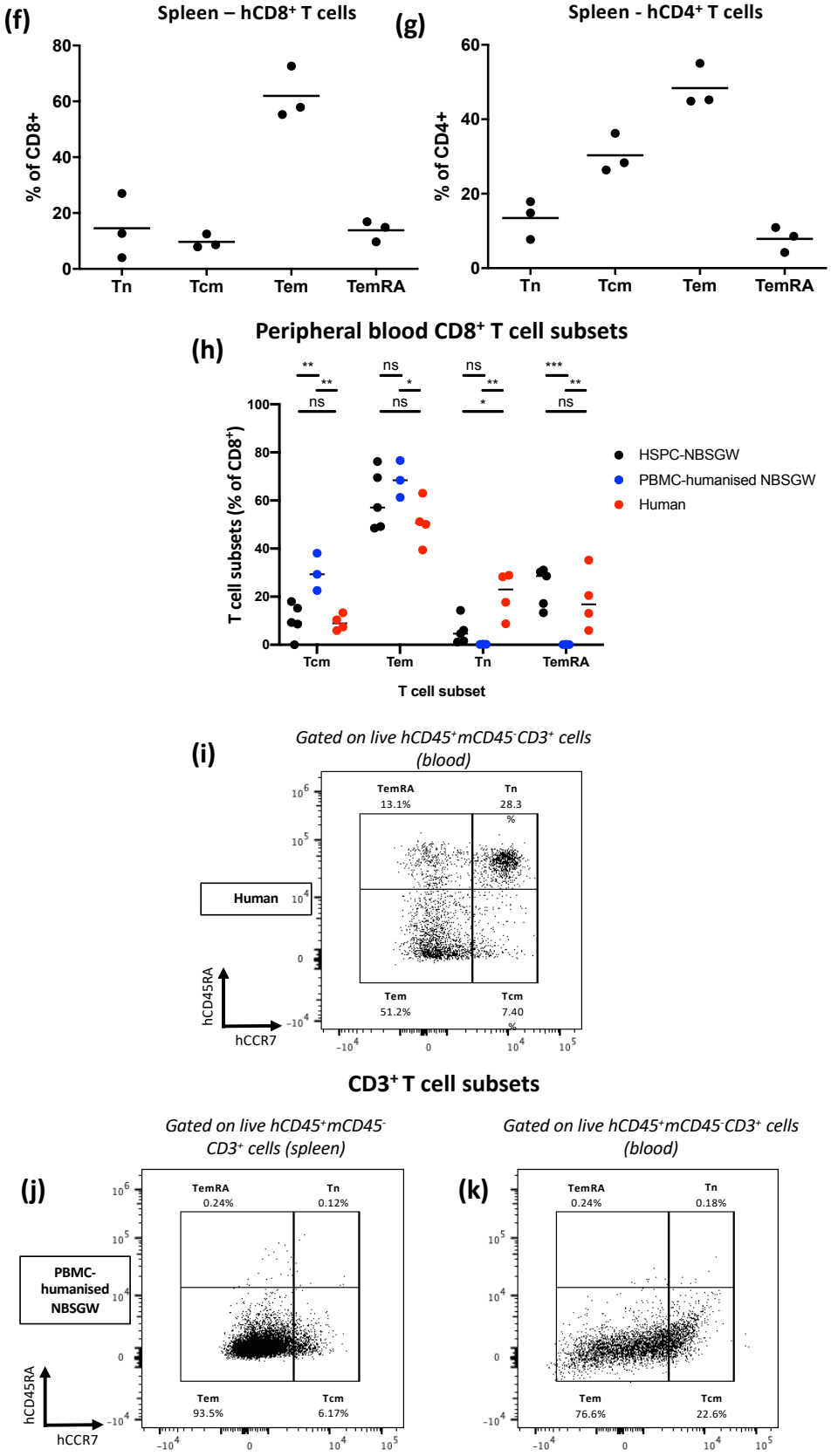
(f)
Spleen – hCD8+ T cells
% of CD8+
Tn
Tcm
Tem
TemRA
(g)
Spleen - hCD4+ T cells
% of CD4+
(h)
Peripheral blood CD8+ T cell subsets
T cell subsets (% of CD8+)
T cell subset
HSPC-NBSGW
PBMC-humanised NBSGW
Human
(i)
Gated on live hCD45+mCD45-CD3+ cells (blood)
Human
hCD45RA
hCCR7
TemRA 13.1%
Tn 28.3 %
Tem 51.2%
Tcm 7.40 %
CD3+ T cell subsets
Gated on live hCD45+mCD45- CD3+ cells (spleen)
(j)
PBMC-humanised NBSGW
TemRA 0.24%
Tn 0.12%
Tem 93.5%
Tcm 6.17%
Gated on live hCD45+mCD45-CD3+ cells (blood)
(k)
TemRA 0.24%
Tn 0.18%
Tem 76.6%
Tcm 22.6%

Gated on live human CD3⁺ splenocytes

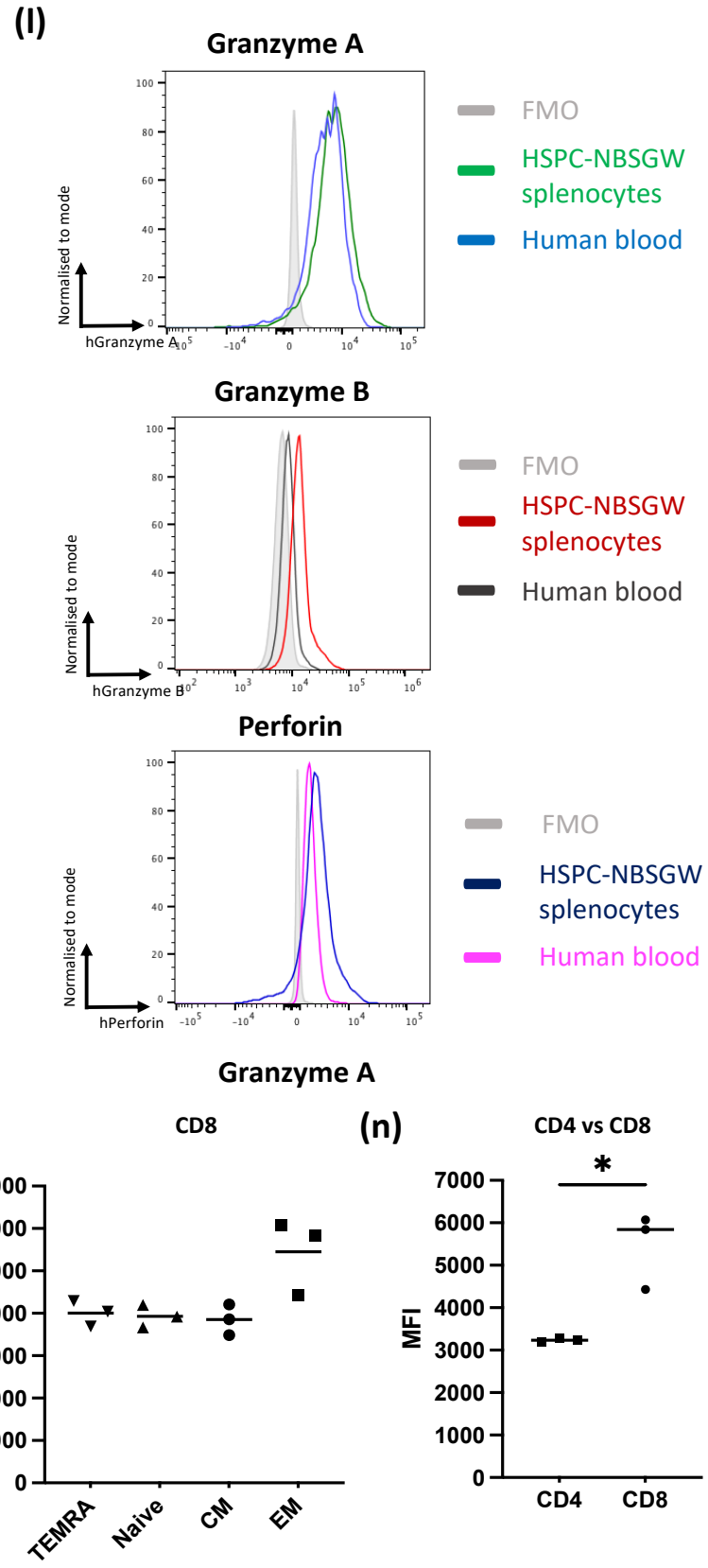

Figure 3.1.5 Human thymocyte development.
Engraftment analysis of human thymocytes.
Non-irradiated NBSGW mice were injected intravenously with $5x10^4$ or $2.5x10^5$ human $CD133^+$ HSPCs from 3 separate donors. Cells were suspended in 200µl IMDM supplemented with 1% HSA. Mice were sacrificed 20-22 weeks post-injection of HSPCs. Thymuses were harvested and thymic leucocytes analysed by flow cytometry for (a-f) expression of B and T cell markers and (i-j) HLA class I and (k-l) class II molecules. (m-n) For comparison thymuses harvested from NBSGW mice injected intraperitoneally with $5x10^6$ thawed human PBMCs 21 days earlier were analysed in an identical manner (n=3). Data are represented as (a) flow cytometric plot and (b) corresponding frequencies of human and mouse $CD45^+$ leucocytes (as percentage of mCD45 + hCD45 cells) in the thymi of HSPC-NBSGW mice ($50x10^3$ dose shown). (c-d) Representative flow cytometric analysis and (e) corresponding frequencies of single-positive CD4+, CD8+ and double-positive CD4+CD8+ human thymocytes, and (f) double-positive thymocyte engraftment following different HSPC injection doses. (g-h) B cells, T cells and thymocytes in NBSGW mice humanised with $5x10^6$ human PBMCs. (i,k) flow cytometric analyses and (j,l) corresponding frequencies of HLA class I & II expression on $CD3^-$ human thymic leucocytes. Bars represent (b, e) the mean + SEM and (f) median values. Statistical significance was assessed using the paired t test (***$p<0.001$).

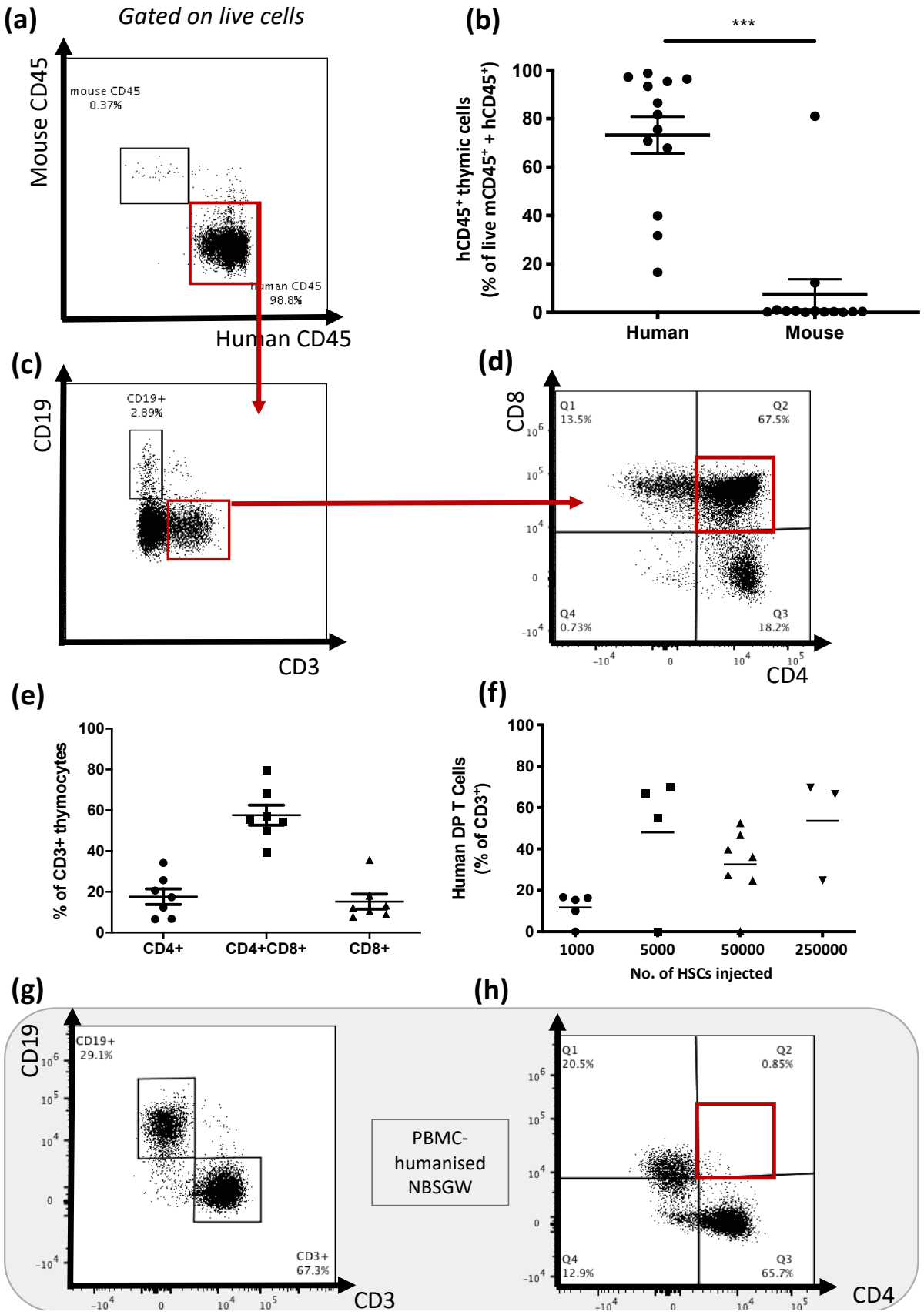
(a)
Gated on live cells
Mouse CD45
mouse CD45
0.37%
human CD45
98.8%
Human CD45
(b)
***
hCD45+ thymic cells
(% of live mCD45+ + hCD45+)
100
80
60
40
20
0
Human
Mouse
(c)
CD19
CD19+
2.89%
CD3
(d)
CD8
Q1
13.5%
Q2
67.5%
Q4
0.73%
Q3
18.2%
CD4
(e)
% of CD3+ thymocytes
100
80
60
40
20
0
CD4+
CD4+CD8+
CD8+
(f)
Human DP T Cells
(% of CD3+)
100
80
60
40
20
0
1000
5000
50000
250000
No. of HSCs injected
(g)
CD19
CD19+
29.1%
CD3+
67.3%
CD3
PBMC-
humanised
NBSGW
(h)
Q1
20.5%
Q2
0.85%
Q4
12.9%
Q3
65.7%
CD4

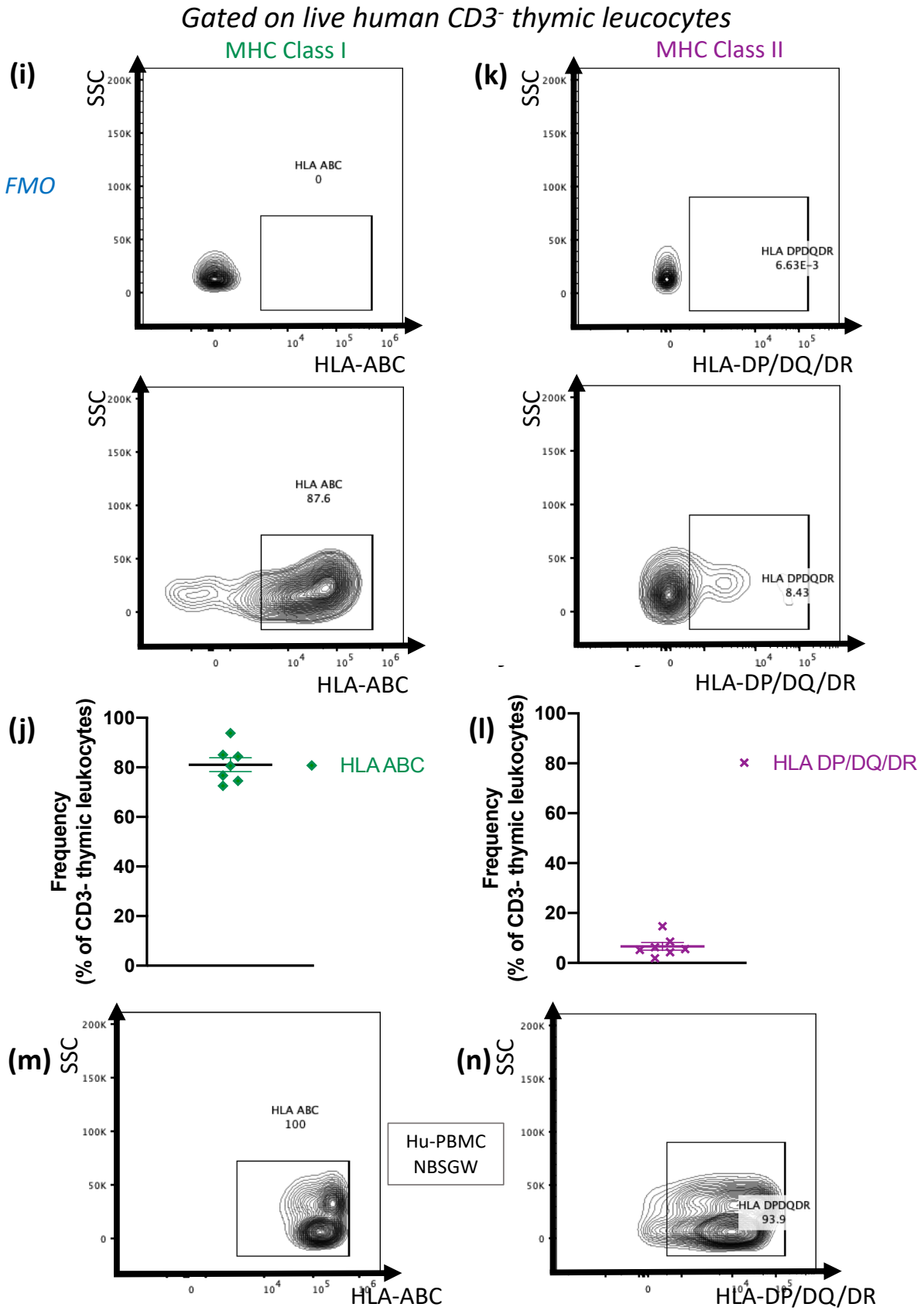
Gated on live human CD3- thymic leucocytes
MHC Class I
MHC Class II
(i)
(k)
FMO
SSC
HLA ABC
0
HLA-ABC
HLA DPDQDR
6.63E-3
HLA-DP/DQ/DR
HLA ABC
87.6
HLA DPDQDR
8.43
(j)
(l)
Frequency
(% of CD3- thymic leukocytes)
HLA ABC
HLA DP/DQ/DR
(m)
(n)
HLA ABC
100
Hu-PBMC
NBSGW
HLA DPDQDR
93.9

Figure 3.1.6 human myeloid cell engraftment.
Engraftment analysis of human $CD33^+$ cells.
(a & b) Non-irradiated NBSGW mice were injected intravenously with $1x10^7$ human PBMCs and 8 weeks later cells harvested from the BM, spleen and blood were analysed for the presence of human $CD33^+$ cells. (c) Separate NBSGW mice were injected intravenously with $1x10^3$, $5x10^3$, $5x10^4$ or $2.5x10^5$ human $CD133^+$ HSPCs from 1 of 4 donors in 3 independent experiments. Mice were sacrificed 20-22 weeks post-injection and cells harvested from the BM, spleen and peripheral blood were analysed by flow cytometry for the presence of live human $7AAD^-CD45^+CD33^+$ cells and identifiers of myeloid subsets (as indicated). Data are represented as (c) frequencies of human CD33+ myeloid cells in the BM, spleen and peripheral blood, (d-f) Representative flow cytometry plots and (g) corresponding frequencies of myeloid subsets based on CD14 and HLA-DR expression. (h) Representative flow cytometry plot and (i-j) corresponding histograms demonstrating human conventional dendritic cells (cDCs) (blue; hCD11c+hCD14-hCD33+) and human monocytes/macrophages (red; hCD14+hCD33+) in the BM of HSPC-NBSGW mice ($50x10^3$ dose shown). Histograms demonstrate high HLA-DR expression and low CD11b expression in cDCs (blue histograms) as compared with monocytes (red histograms). (k) Numbers of human cDCs (hCD11c+hCD14-hCD33+) (l) and human monocytes/macrophages (hCD14+hCD33+) in the BM of one femur in mice receiving different numbers of hUCB CD133+ HSPCs. (m-n) Representative flow cytometry plot and corresponding frequencies of $mCD45^-hCD45^+hCD33^+hCD14^-hHLA\text{-}DR^+CD11c^+$ cDCs engrafting the BM. Bars indicate median values $\pm$ IQR (C).

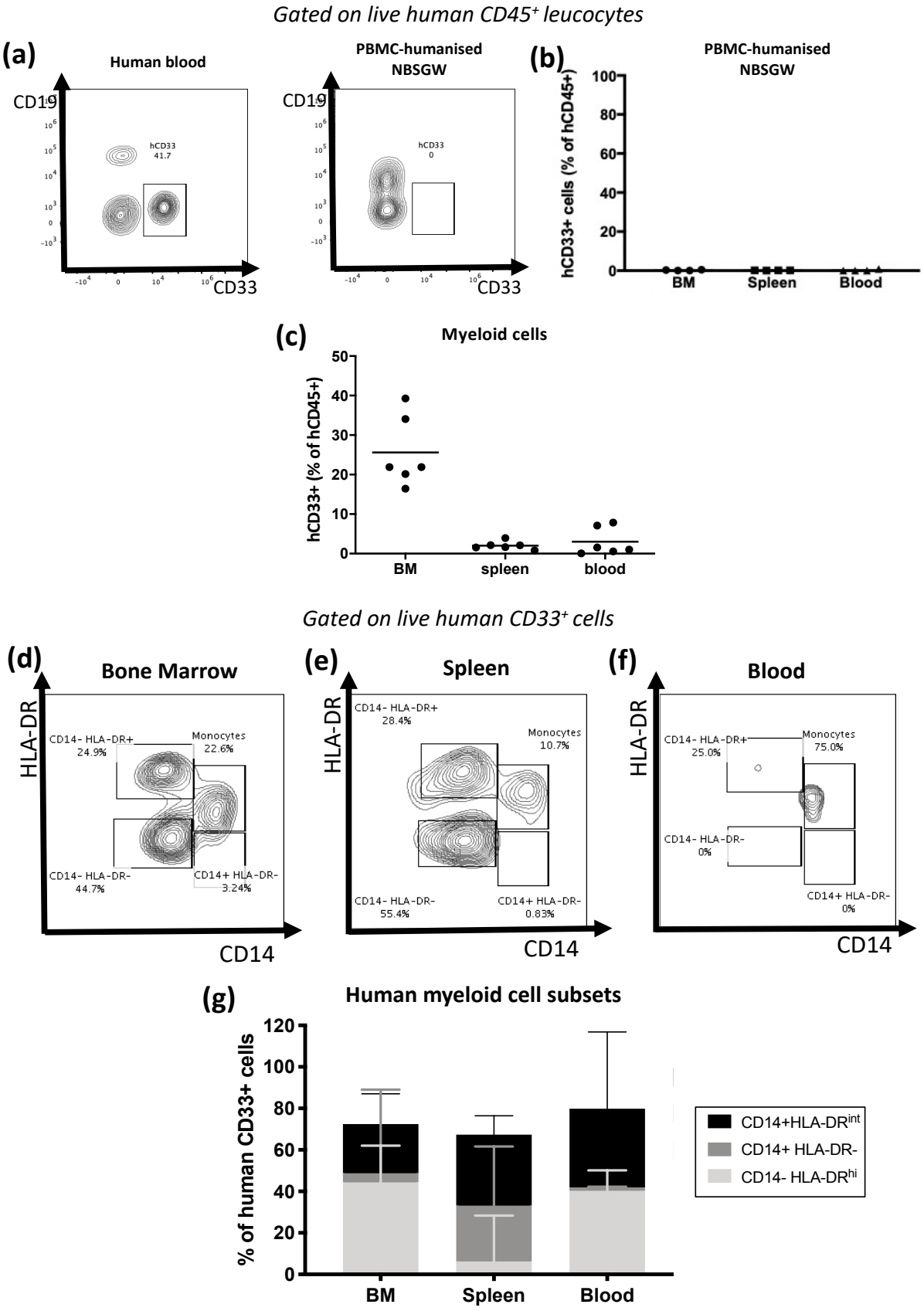
Gated on live human CD45+ leucocytes
(a)
Human blood
PBMC-humanised NBSGW
CD19
CD33
hCD33 41.7
hCD33 0
(b)
PBMC-humanised NBSGW
hCD33+ cells (% of hCD45+)
BM
Spleen
Blood
(c)
Myeloid cells
hCD33+ (% of hCD45+)
BM
spleen
blood
Gated on live human CD33+ cells
(d)
Bone Marrow
(e)
Spleen
(f)
Blood
HLA-DR
CD14
CD14- HLA-DR+ 24.9%
Monocytes 22.6%
CD14- HLA-DR- 44.7%
CD14+ HLA-DR- 3.24%
CD14- HLA-DR+ 28.4%
Monocytes 10.7%
CD14- HLA-DR- 55.4%
CD14+ HLA-DR- 0.83%
CD14- HLA-DR+ 25.0%
Monocytes 75.0%
CD14- HLA-DR- 0%
CD14+ HLA-DR- 0%
(g)
Human myeloid cell subsets
% of human CD33+ cells
BM
Spleen
Blood
CD14+HLA-DRint
CD14+ HLA-DR-
CD14- HLA-DRhi

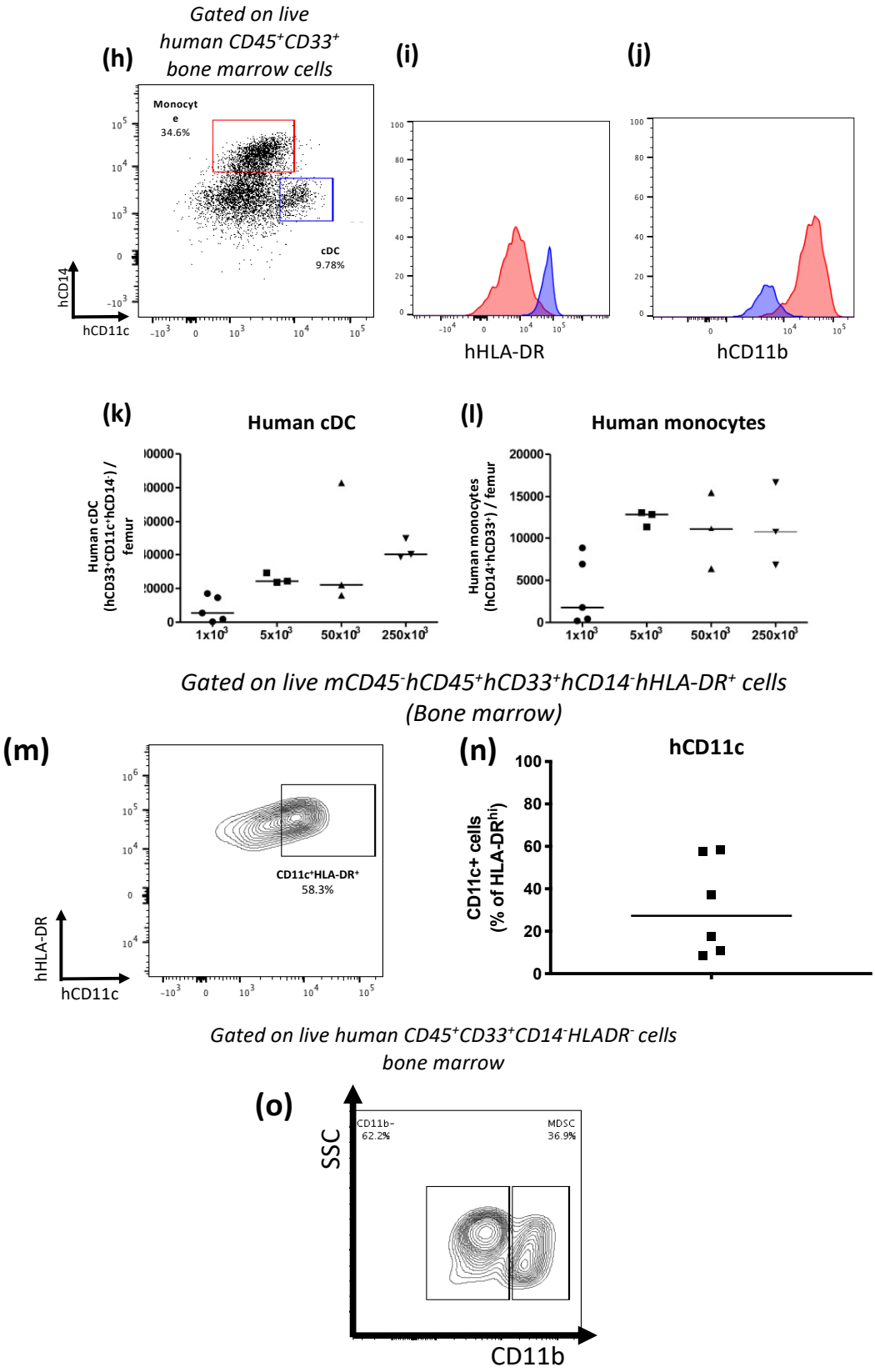
Gated on live human CD45+CD33+ bone marrow cells
(h)
Monocyte
34.6%
cDC
9.78%
hCD14
hCD11c
(i)
hHLA-DR
(j)
hCD11b
(k)
Human cDC
Human cDC (hCD33+CD11c+hCD14-) / femur
1x10^3
5x10^3
50x10^3
250x10^3
(l)
Human monocytes
Human monocytes (hCD14+hCD33+) / femur
Gated on live mCD45-hCD45+hCD33+hCD14-hHLA-DR+ cells (Bone marrow)
(m)
CD11c+HLA-DR+
58.3%
hHLA-DR
hCD11c
(n)
hCD11c
CD11c+ cells (% of HLA-DRhi)
Gated on live human CD45+CD33+CD14-HLADR- cells bone marrow
(o)
CD11b-
62.2%
MDSC
36.9%
SSC
CD11b

Figure 3.1.7 human erythroid cell engraftment.
Engraftment analysis of human erythroid lineage cells.
Non-irradiated NBSGW mice were injected intravenously with $1x10^3$, $5x10^3$, $5x10^4$ or $2.5x10^5$ human $CD133^+$ HSPCs from 1 of 2 donors in 2 separate experiments. Cells were suspended in 200µl IMDM supplemented with 1% HSA. n=5, n=3, n=3 and n=3 mice per group respectively. Mice were bled serially from 8 weeks and sacrificed 20-22 weeks post-injection of HSPCs and harvested cells analysed by flow cytometry for (a-d) the presence of $hCD45^-mCD45^-TER119^-CD235a^+$ cells, (e-k) erythroid precursor cells (following erythrocyte lysis). (l-s) To assess the effect of phagocytosis on human erythroid cell reconstitution, mouse macrophages were cleared by intravenous clodronate liposomes (CloLip) and harvested blood, spleen and BM analysed by flow cytometry for (m-p) mature and (q-s) precursor human erythroid cells. (t-w) HSPC-NBSGW leucocytes and erythrocytes were analysed for expression of CD47 20-22 weeks after humanization. (x, y) Thawed HSPC-NBSGW BM and spleen cells from mice receiving intravenous injections of CloLip or PBS and harvested 6 days later were analysed for expression of CD47. Data are represented as (a) representative flow cytometric analyses demonstrating the identification and (b) frequencies of hCD45lo/-mCD45-hCD235a+mTER119- human erythroid cells in the BM at different HSPC injection doses, (c) representative flow cytometry and (d) frequencies of hCD235+ cells in the peripheral blood at different time points following injection with increasing numbers of hUCB CD133+ HSPCs (mean ± SD shown), (e) representative flow cytometry and (f) corresponding frequencies of hCD71+hCD235lo/-, hCD71+hCD235+ and hCD71-hCD235+ erythroid precursors (in ascending order of maturity) in the BM ($50x10^3$ dose shown). (g) frequency of hCD71+hCD235-/lo and (h) hCD71+hCD235+ erythroid precursors in the BM following humanization with increasing numbers of hUCB CD133+ HSPCs. (i-k) frequencies of precursor engraftment in male (blue symbols) and female (red symbols) mice (bars represent median values), frequencies of (l) mouse CD11b+Gr1- cells in the BM, spleen and blood 5 days after CloLip treatment, (m) representative flow cytometry of human CD235+ RBCs in the blood 5 days after CloLip treatment, (n) frequency and (o) absolute number of human RBCs in the peripheral blood 5 days after CloLip treatment, (p) number of RBCs per spleen and mouse femur, (q) frequencies of hCD71+hCD235-/lo, (r) hCD71+hCD235+ and (s) hCD71-hCD235+ in the BM 6 days after CloLip/PBS treatment. (t) representative flow cytometry histogram and (u-w) corresponding geometric mean fluorescence intensities of surface CD47 expression on erythrocytes (red symbols) and leucocytes (green symbols) in (u) BM, (v) spleen and (w) blood. Symbols represent individual mice. Bars represent mean + SEM (u-y) and median values (all other graphs); Statistical significance was assessed using the paired T test (u-y) or Mann Whitney tests (ns, $p>0.5$; *, $p<0.05$; **, $p<0.01$; ***, $p<0.001$).

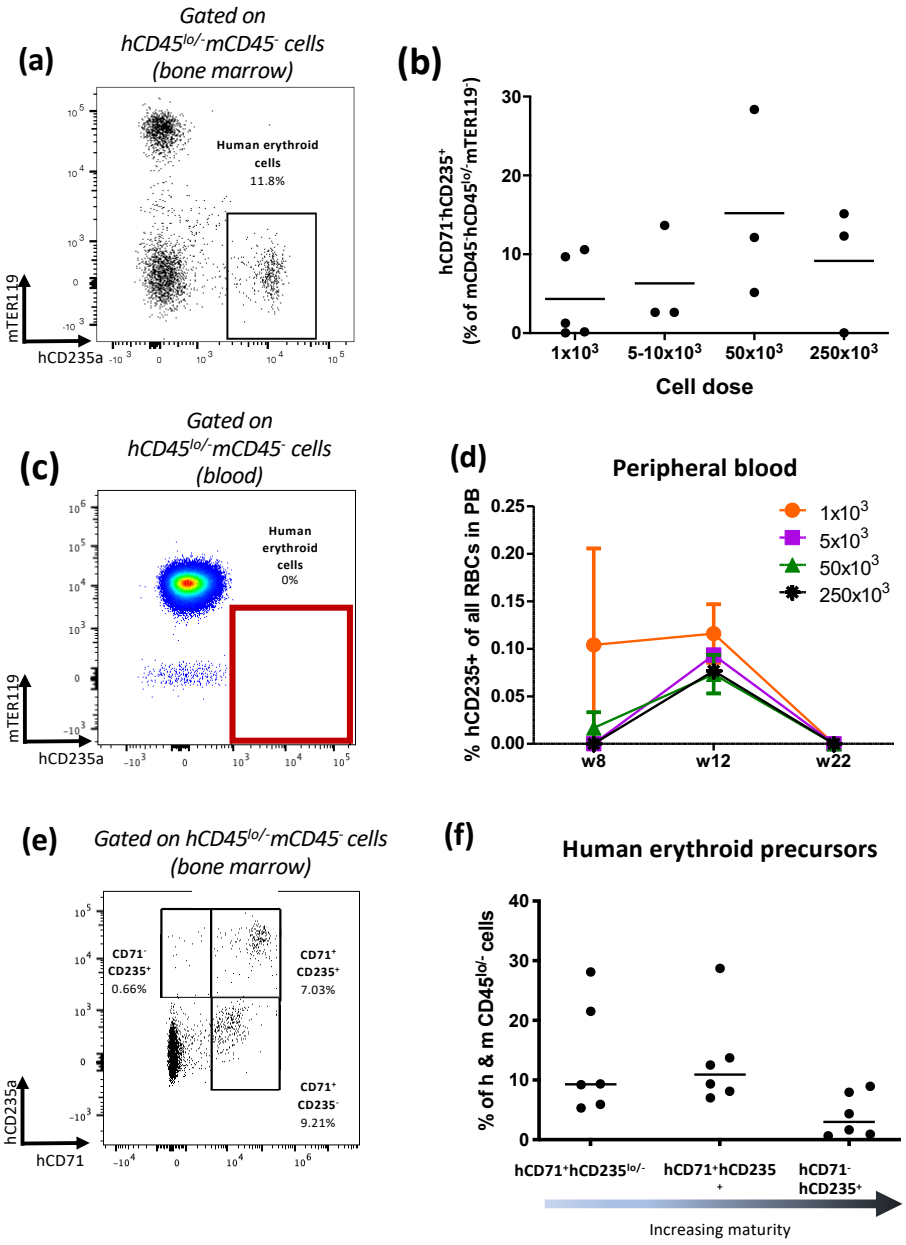
(a)
Gated on hCD45lo/-mCD45- cells (bone marrow)
Human erythroid cells 11.8%
mTER119
hCD235a
(b)
hCD71+hCD235+ (% of mCD45-hCD45lo/-mTER119-)
1x10³
5-10x10³
50x10³
250x10³
Cell dose
(c)
Gated on hCD45lo/-mCD45- cells (blood)
Human erythroid cells 0%
mTER119
hCD235a
(d)
Peripheral blood
% hCD235+ of all RBCs in PB
1x10³
5x10³
50x10³
250x10³
w8
w12
w22
(e)
Gated on hCD45lo/-mCD45- cells (bone marrow)
CD71- CD235+ 0.66%
CD71+ CD235+ 7.03%
CD71+ CD235- 9.21%
hCD235a
hCD71
(f)
Human erythroid precursors
% of h & m CD45lo/- cells
hCD71+hCD235lo/-
hCD71+hCD235+
hCD71- hCD235+
Increasing maturity

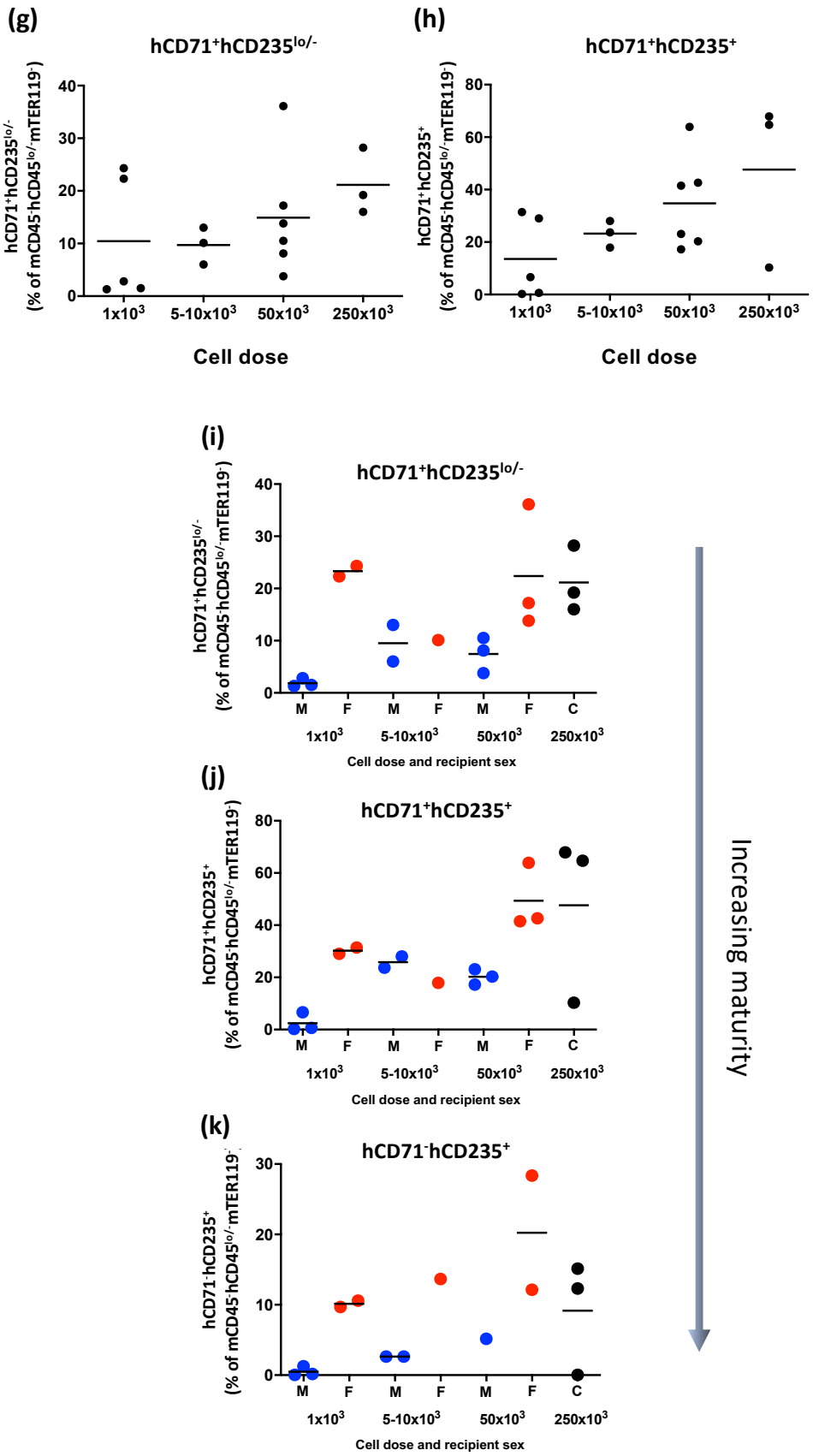
(g)
hCD71+hCD235lo/-
(% of mCD45-hCD45lo/-mTER119-)
hCD71+hCD235lo/-
0
10
20
30
40
1x10^3
5-10x10^3
50x10^3
250x10^3
Cell dose
(h)
hCD71+hCD235+
(% of mCD45-hCD45lo/-mTER119-)
hCD71+hCD235+
0
20
40
60
80
1x10^3
5-10x10^3
50x10^3
250x10^3
Cell dose
(i)
hCD71+hCD235lo/-
(% of mCD45-hCD45lo/-mTER119-)
hCD71+hCD235lo/-
0
10
20
30
40
M
F
M
F
M
F
C
1x10^3
5-10x10^3
50x10^3
250x10^3
Cell dose and recipient sex
(j)
hCD71+hCD235+
(% of mCD45-hCD45lo/-mTER119-)
hCD71+hCD235+
0
20
40
60
80
M
F
M
F
M
F
C
1x10^3
5-10x10^3
50x10^3
250x10^3
Cell dose and recipient sex
(k)
hCD71-hCD235+
(% of mCD45-hCD45lo/-mTER119-)
hCD71-hCD235+
0
10
20
30
M
F
M
F
M
F
C
1x10^3
5-10x10^3
50x10^3
250x10^3
Cell dose and recipient sex
Increasing maturity

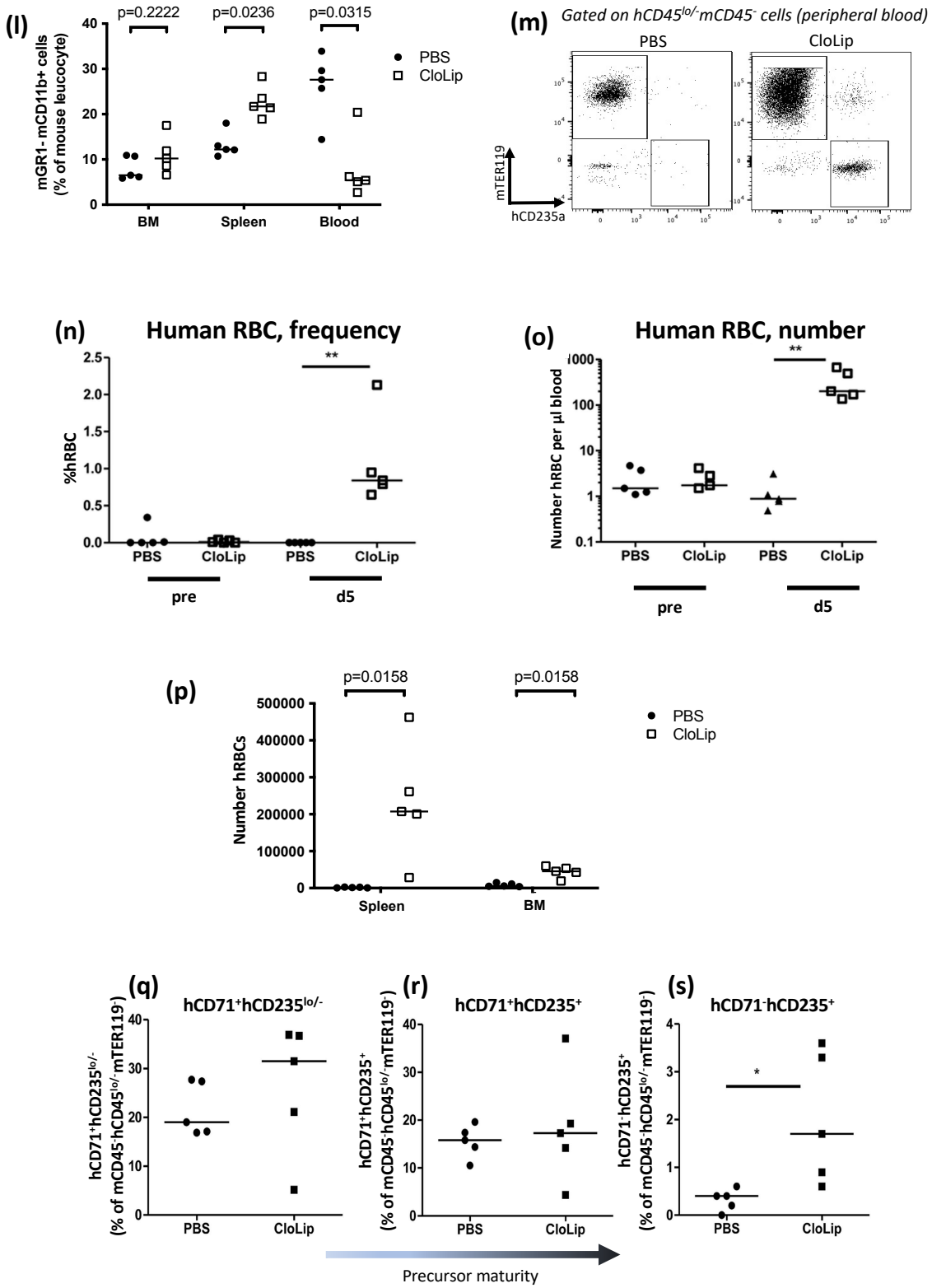
(l)
p=0.2222
p=0.0236
p=0.0315
mGR1- mCD11b+ cells (% of mouse leucocyte)
PBS
CloLip
BM
Spleen
Blood
(m)
Gated on hCD45lo/-mCD45- cells (peripheral blood)
PBS
CloLip
mTER119
hCD235a
(n)
Human RBC, frequency
%hRBC
PBS
CloLip
pre
d5
(o)
Human RBC, number
Number hRBC per µl blood
(p)
p=0.0158
p=0.0158
Number hRBCs
Spleen
BM
(q)
hCD71+hCD235lo/-
(% of mCD45-hCD45lo/-mTER119-)
(r)
hCD71+hCD235+
(s)
hCD71-hCD235+
Precursor maturity

Gated on live hCD45⁺ leucocytes or
hCD45⁻mCD45⁻TER119⁻CD235a⁺ erythrocytes

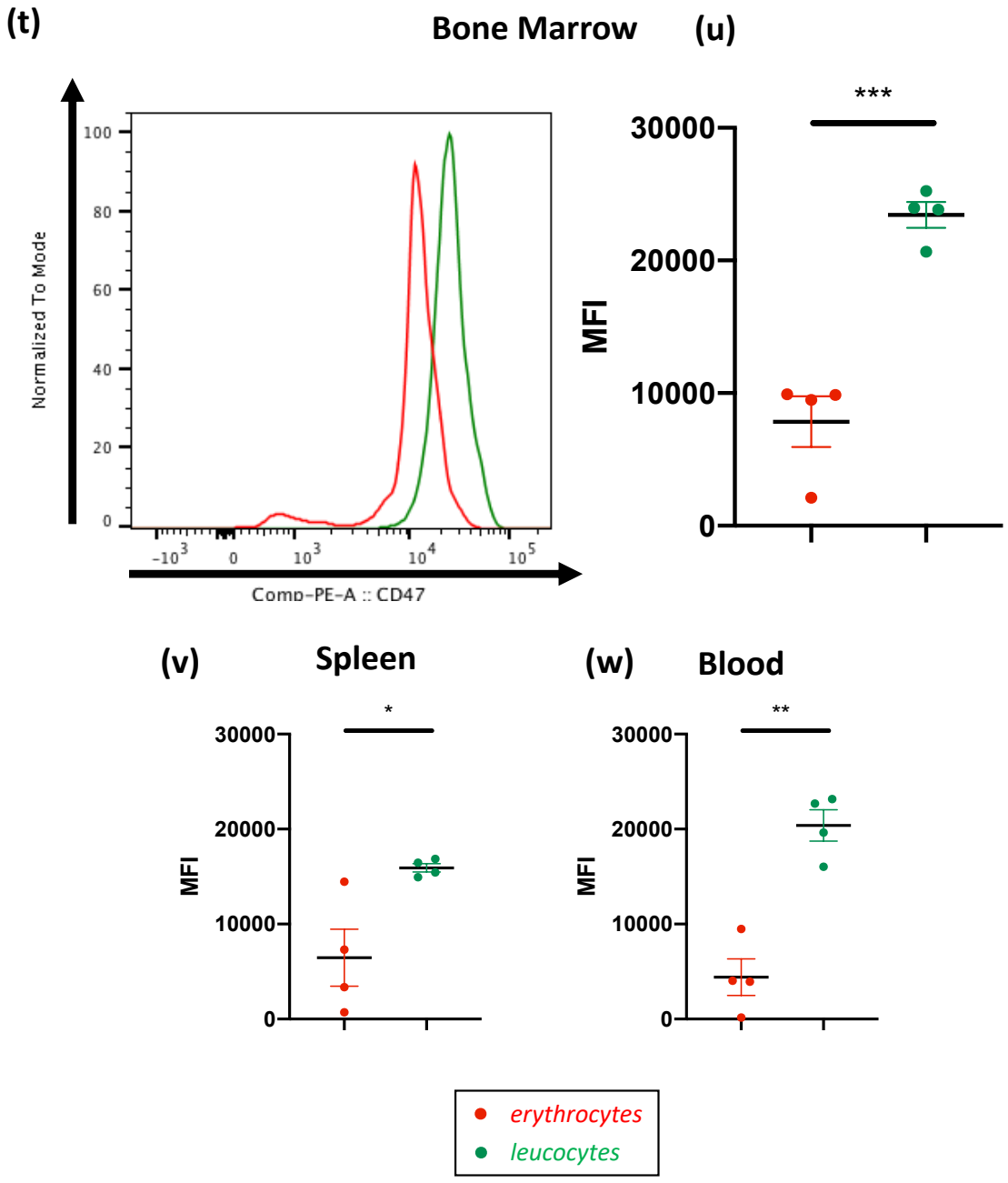

Gated on live hCD45⁺ leucocytes or
hCD45⁻mCD45⁻TER119⁻CD235a⁺ erythrocytes

(x)

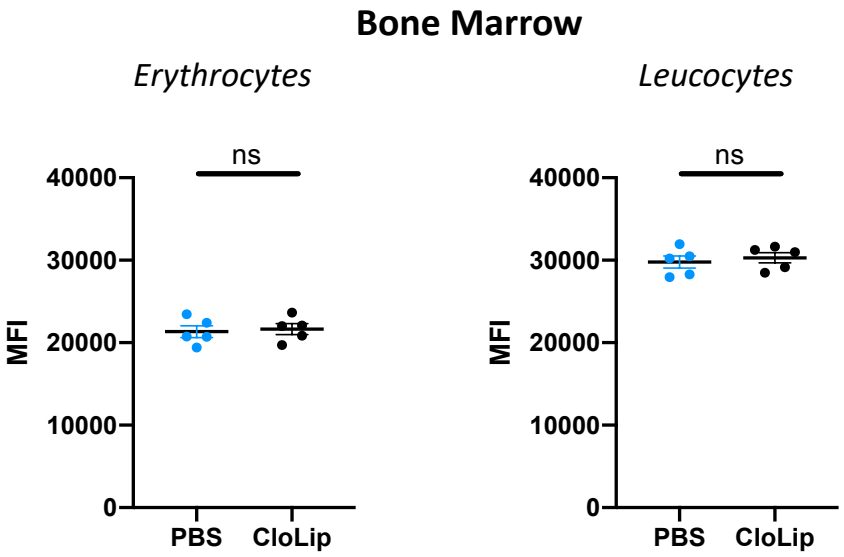

(y)

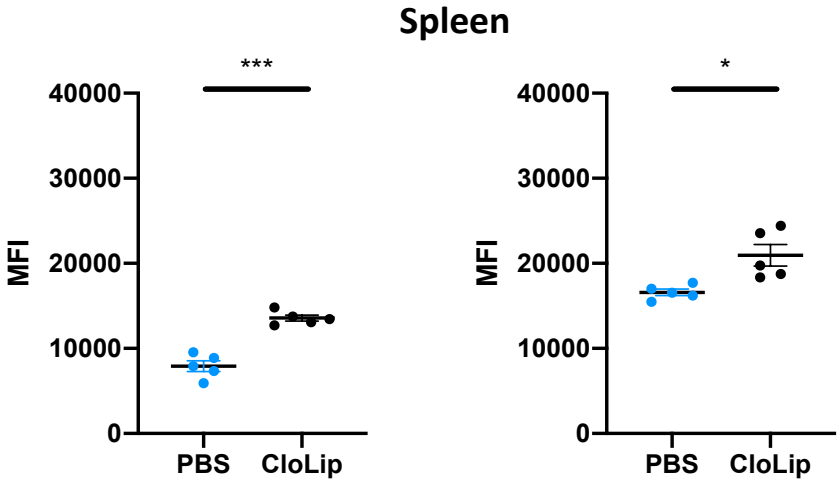

Figure 3.1.8 human thrombocyte engraftment.
Engraftment analysis of human thrombocyte lineage cells.
Non-irradiated NBSGW mice were injected intravenously with $1x10^3$, $5x10^3$, $5x10^4$ or $2.5x10^5$ human $CD133^+$ HSPCs from 1 of 2 donors in 2 separate experiments. Cells were suspended in 200µl IMDM supplemented with 1% HSA. n=5, n=3, n=3 and n=3 mice per group respectively. Mice were sacrificed 20-22 weeks post-injection of HSPCs and un-lysed cells from the BM, spleen and peripheral blood were analysed by FACS for the presence of $hCD45^-mCD45^-TER119^-CD235a^-CD61^+$ cells (a & b). To assess the effect of thrombocyte phagocytosis, mouse macrophages were cleared by intravenous CloLip at 11 weeks, which increased platelet numbers in the blood over the following 6 days (c). Data are represented as FACS plots demonstrating the gating strategy (a) and as plots indicating frequencies or numbers of platelets (b & c). Bars indicate mean values.

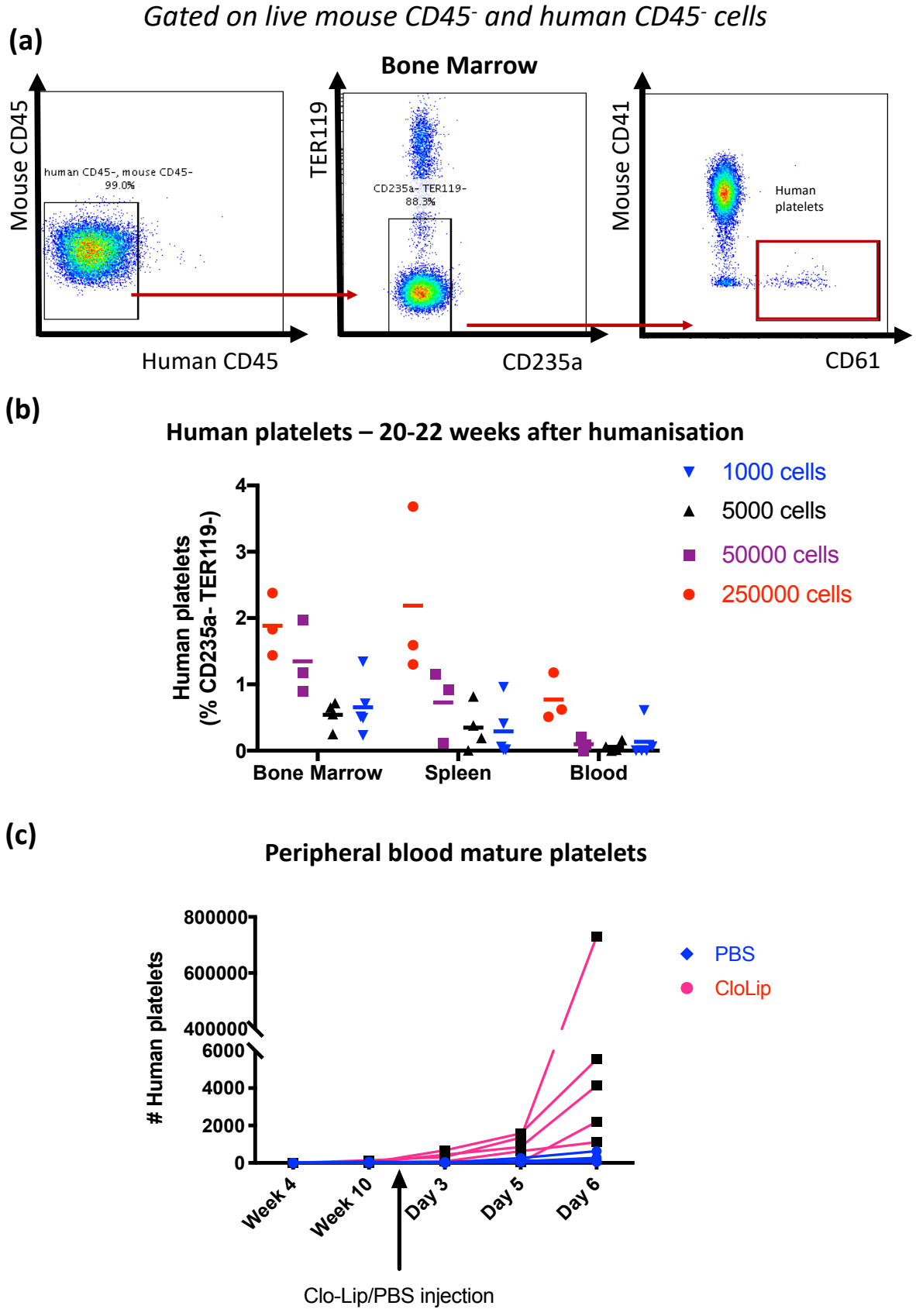
Gated on live mouse CD45- and human CD45- cells
(a)
Bone Marrow
Mouse CD45
human CD45-, mouse CD45-
99.0%
Human CD45
TER119
CD235a- TER119-
88.3%
CD235a
Mouse CD41
Human
platelets
CD61
(b)
Human platelets – 20-22 weeks after humanisation
Human platelets
(% CD235a- TER119-)
1000 cells
5000 cells
50000 cells
250000 cells
Bone Marrow
Spleen
Blood
(c)
Peripheral blood mature platelets
Human platelets
PBS
CloLip
Week 4
Week 10
Day 3
Day 5
Day 6
Clo-Lip/PBS injection

Figure 3.1.9 human HSC doses of $1x10^3$, $5x10^3$, $5x10^4$ or $2.5x10^5$ administered via intravenous injection produce reliable HSPC engraftment in the bone marrow of NOD,B6.SCID *Il2rγ*$^{-/-}$ *Kit*$^{W41/W41}$ mice.

Engraftment analysis of human $CD133^+$ HSPCs injected into NBSGW mice.
Non-irradiated NBSGW mice were injected intravenously with $1x10^3$, $5x10^3$, $5x10^4$ or $2.5x10^5$ human $CD133^+$ HSPCs from 1 of 4 donors in 3 separate experiments. Cells were suspended in 200µl IMDM supplemented with 1% HSA. n=11, n=14, n=6 and n=3 mice per group respectively. Mice were sacrificed 20-22 weeks post-injection of HSCs and BM analysed by flow cytometry for the presence of live human $7AAD^-CD45^+CD34^+Lin^-CD38^-$ cells. Human HSPC engraftment in the bone marrow of HSPC-NBSGW mice. Data demonstrated as (a-b) representative flow cytometry indicating (a) hCD34+Lin- and (b) hCD34+Lin-hCD38low\- HSPCs, (c-d) number of (c) hCD34+Lin- and (d) hCD34+Lin-hCD38low\- cells per femur in male and female recipients at the point of harvest. M-male (blue symbols), F- female (red symbols), C - $250x10^3$ – control group (mixed sex). Bars represent median values. Statistical significance was assessed using a Mann Whitney test (*p<0.05, **p<0.01).

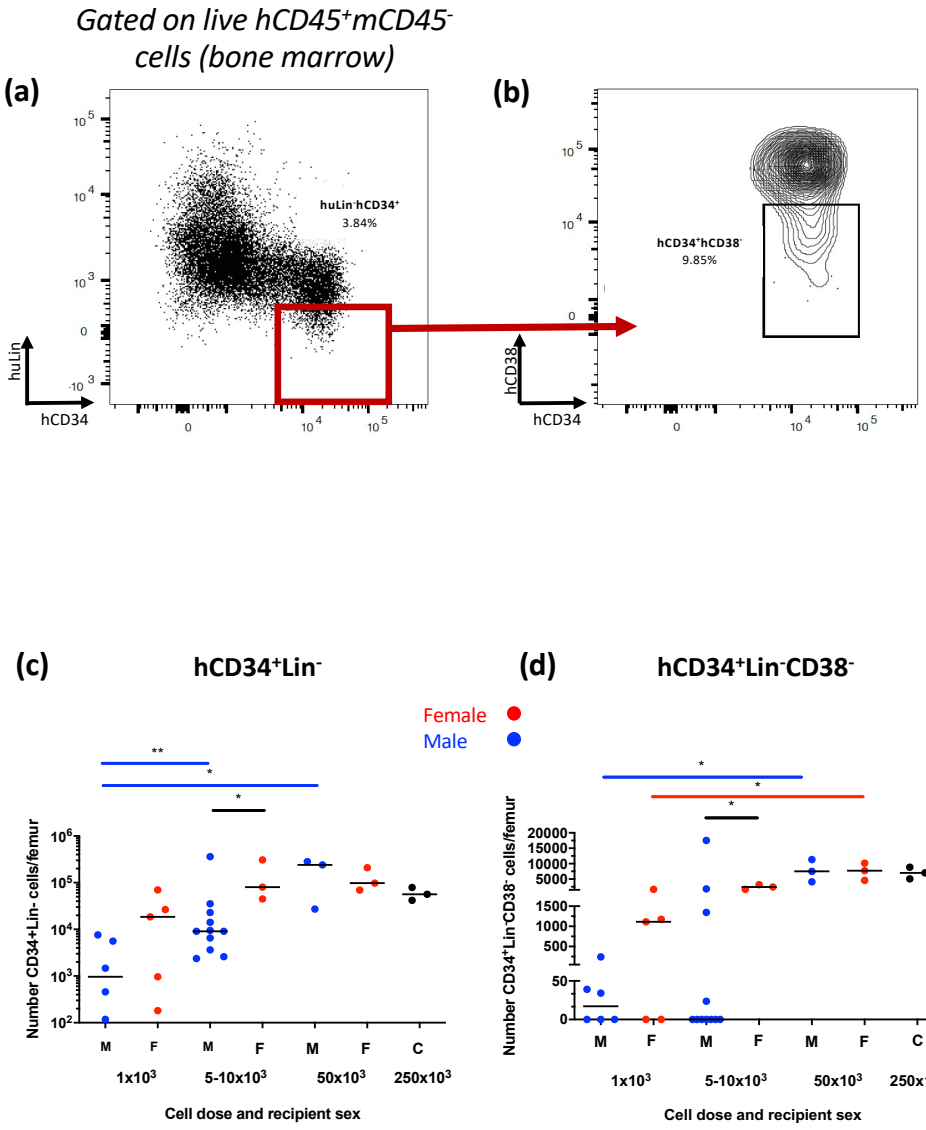
Gated on live hCD45+mCD45- cells (bone marrow)
(a)
huLin-hCD34+
3.84%
huLin
hCD34
(b)
hCD34+hCD38-
9.85%
hCD38
hCD34
(c)
hCD34+Lin-
Female
Male
Number CD34+Lin- cells/femur
M F M F M F C
1x10³ 5-10x10³ 50x10³ 250x10³
Cell dose and recipient sex
(d)
hCD34+Lin-CD38-
Number CD34+Lin-CD38- cells/femur
M F M F M F C
1x10³ 5-10x10³ 50x10³ 250x10³
Cell dose and recipient sex

Figure 3.1.10 human UCB HSC expansion does not negatively affect leucocyte engraftment.
Engraftment analysis of human $CD133^+$ HSPCs injected into NBSGW mice.
Non-irradiated NBSGW mice were injected intravenously with $1x10^4$ human $CD133^+$ HSPCs that were either unexpanded,(blue symbols), or expanded for 5 days in stem cell expansion cultures + either DMSO (expanded: vehicle control – red symbols) or the bromodomain and extra-terminal motif (BET) inhibitor CPI203 (expanded: CPI203 – black symbols). Injected cells were suspended in 200µl IMDM supplemented with 1% HSA. All mice received cells from the same HSPC donor with n=3 mice per group. Blood samples were taken at intervals from week 2 to week 20 and analysed by flow cytometry for the presence of live human (a) $7AAD^-CD45^+$ and (b) $CD3^+$, (c) $CD19^+$ or (d) $CD33^+$ cells. Mice were sacrificed 20-22 weeks post-injection of HSPCs and spleens and BM analysed as above. Data are represented as frequencies of each cell type as a percentage of human $CD45^+$ leucocytes. Bars indicate mean+SEM.

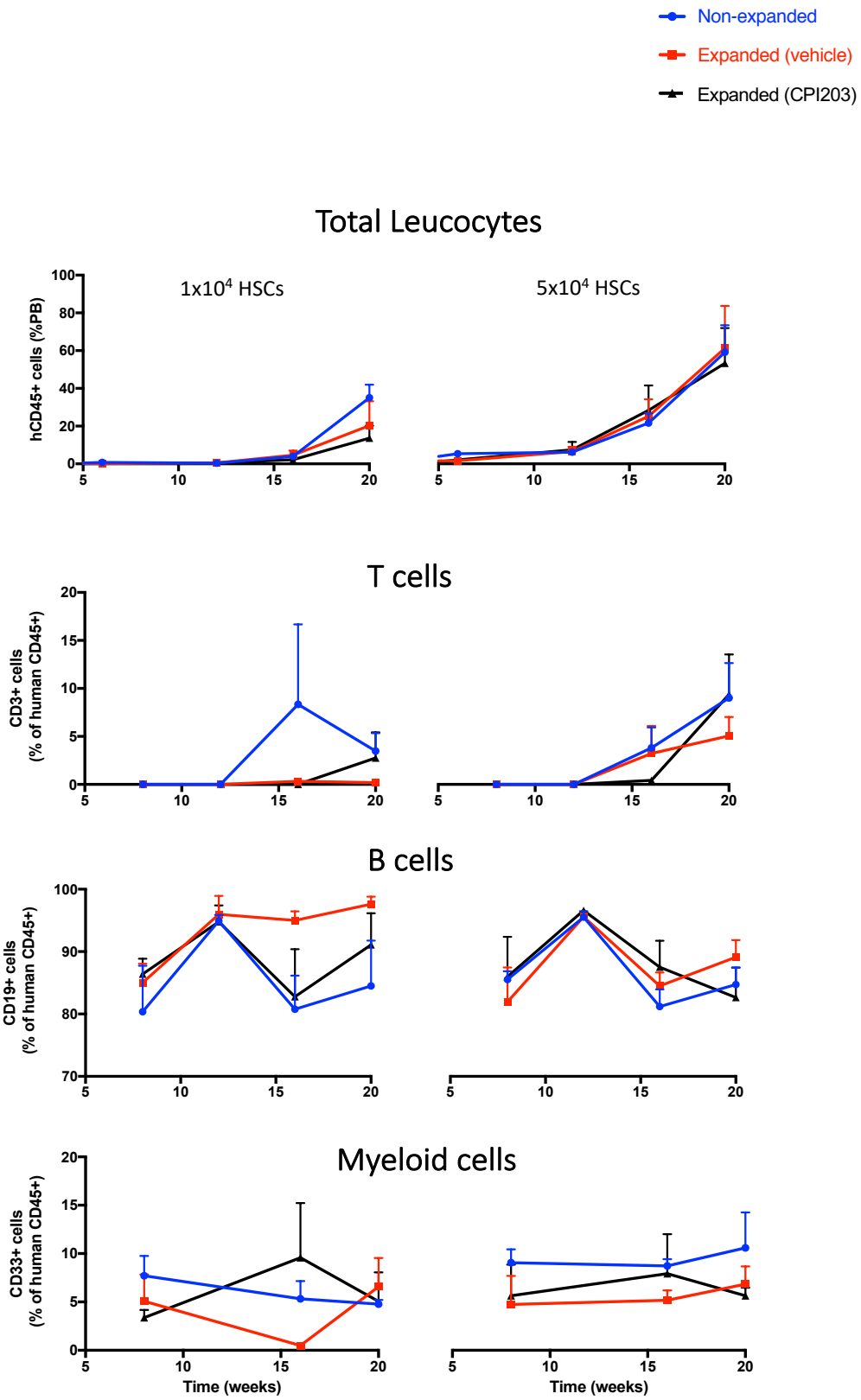
Non-expanded
Expanded (vehicle)
Expanded (CPI203)
Total Leucocytes
1x10^4 HSCs
5x10^4 HSCs
hCD45+ cells (%PB)
T cells
CD3+ cells (% of human CD45+)
B cells
CD19+ cells (% of human CD45+)
Myeloid cells
CD33+ cells (% of human CD45+)
Time (weeks)
Time (weeks)

Figure 3.1.11 HSPC-NBSGW mice demonstrate long-term reconstituting capability.
Serial transplantation engraftment analysis of human $CD133^+$ cells.
Non-irradiated NBSGW mice received a primary adoptive transfer of either 500 unexpanded human $CD133^+$ HSPCs injected intravenously, or the progeny of 500 $CD133^+$ cells expanded in stem cell expansion cultures (with stem cell factor [SCF], TPO, and FLT3L) and DMSO alone (vehicle control) or with the BET inhibitor CPI203. 20 weeks later, BM cells were harvested and secondarily transplanted intravenously (tail vein) into naïve 8-11 week old NBSGW mice. BM, spleen and peripheral blood were harvested 20 weeks later and analysed by flow cytometry. Data are represented as (a) a schematic demonstrating the timeline of transplantations, (b-d) flow cytometric analyses indicating hCD45+ leucocyte engraftment (BM) 20 weeks after primary and secondary transplantation of (b) unexpanded CD133+ HSPCS, (c) expanded CD133+ HSPCs; (d) frequencies of hCD45+ leucocyte engraftment (BM) after primary and secondary transplantation; flow cytometry and corresponding frequencies of (e-f) hCD45+ engraftment (spleen & peripheral blood); BM engraftment of (g) HSPCs, (h) T cells & B cells, (i) myeloid cells, (j) erythroid cells. Bars indicate mean+SEM. Statistical significance was assessed using the One-way ANOVA with multiple comparison (Fisher's LSD))
. N.S $p>0.05$; * $p\leq0.05$; **, $p<0.005$

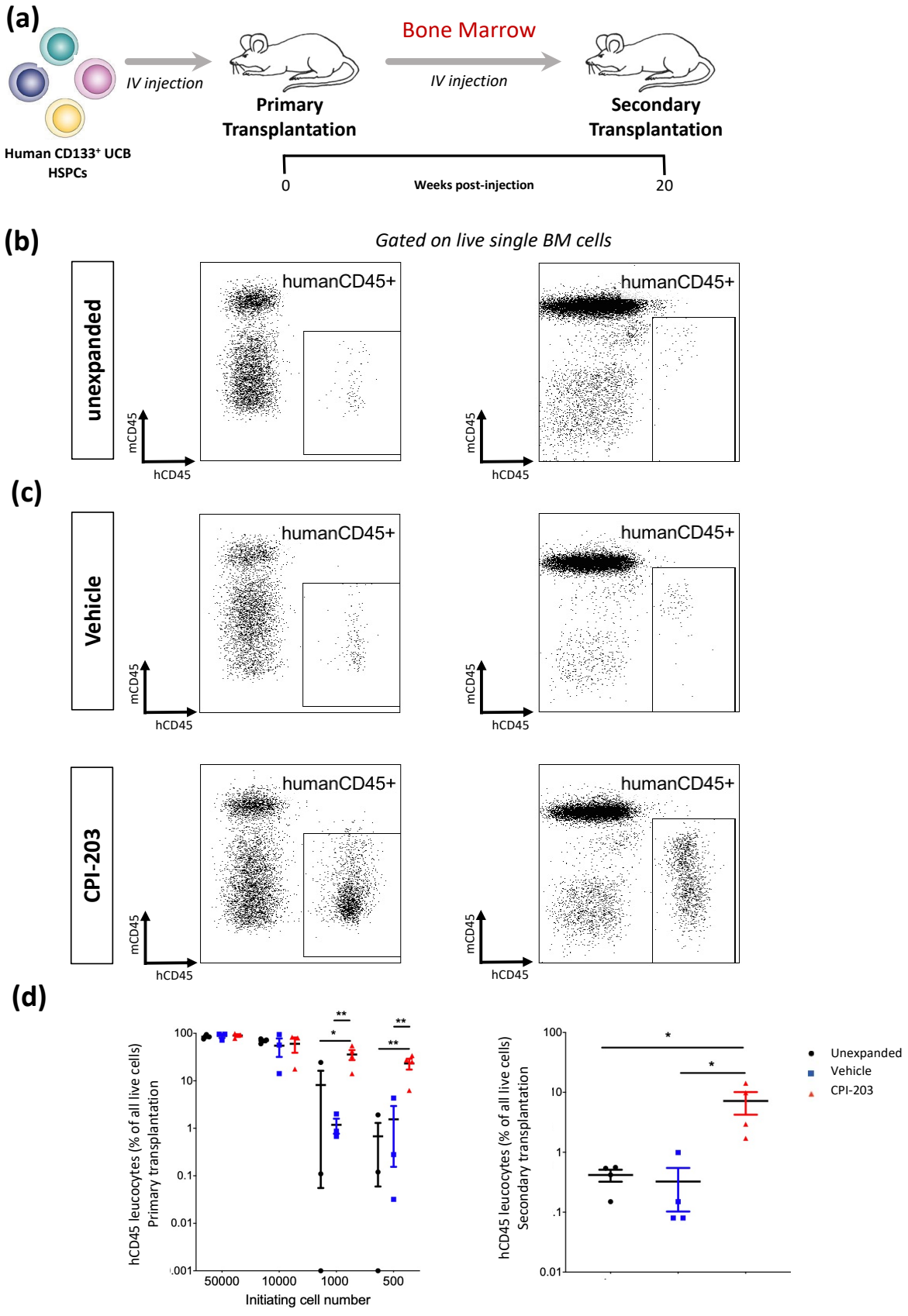
(a)
Human CD133+ UCB HSPCs
IV injection
Primary Transplantation
Bone Marrow
IV injection
Secondary Transplantation
0
Weeks post-injection
20
(b)
Gated on live single BM cells
unexpanded
humanCD45+
mCD45
hCD45
(c)
Vehicle
CPI-203
(d)
hCD45 leucocytes (% of all live cells) Primary transplantation
Initiating cell number
50000
10000
1000
500
hCD45 leucocytes (% of all live cells) Secondary transplantation
Unexpanded
Vehicle
CPI-203

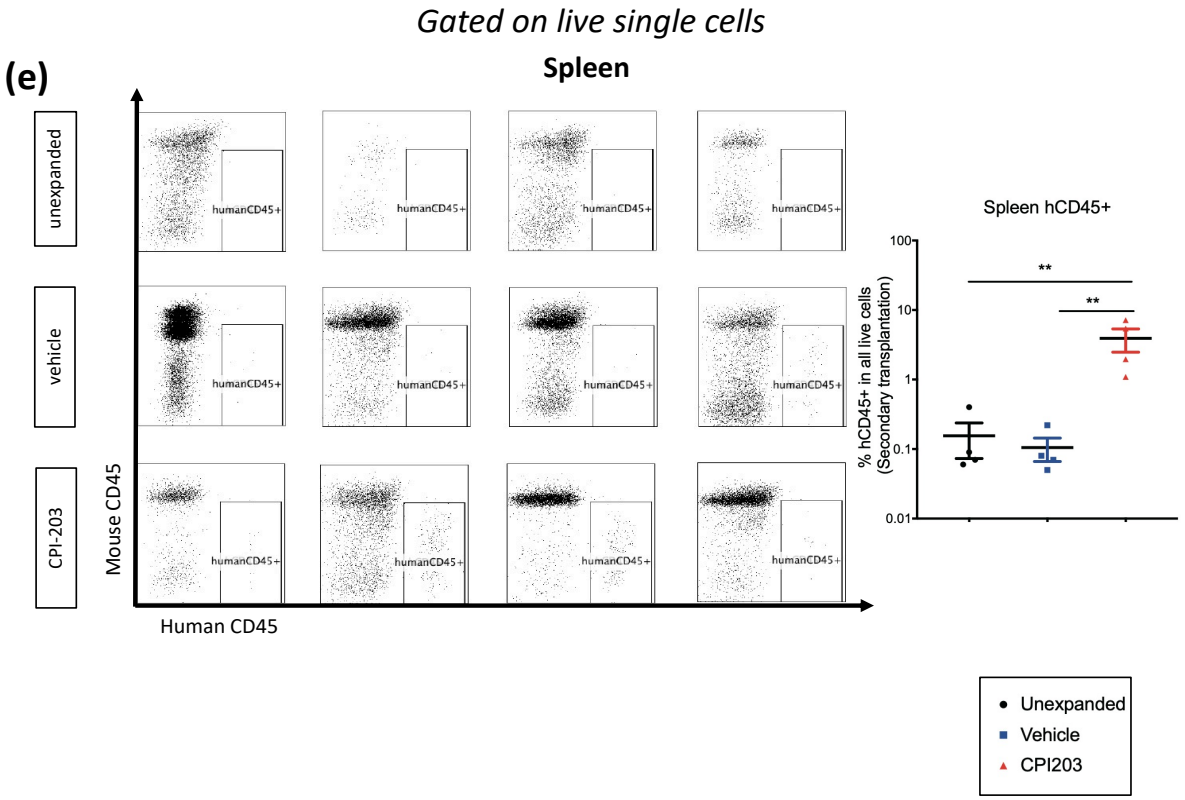
(e)
Gated on live single cells
Spleen
unexpanded
vehicle
CPI-203
humanCD45+
Mouse CD45
Human CD45
Spleen hCD45+
% hCD45+ in all live cells (Secondary transplantation)
100
10
1
0.1
0.01
**
**
Unexpanded
Vehicle
CPI203

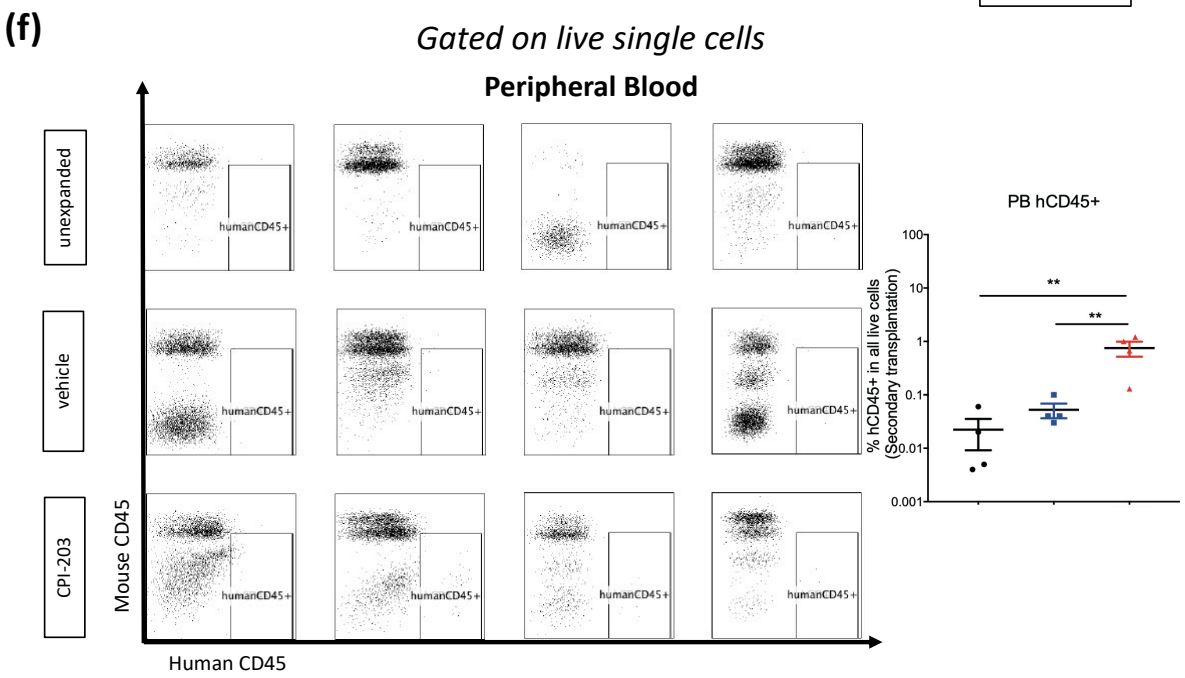
(f)
Gated on live single cells
Peripheral Blood
unexpanded
vehicle
CPI-203
humanCD45+
Mouse CD45
Human CD45
PB hCD45+
% hCD45+ in all live cells (Secondary transplantation)
100
10
1
0.1
0.01
0.001
**
**

Gated on live single human CD45+ leucocytes (bone marrow)

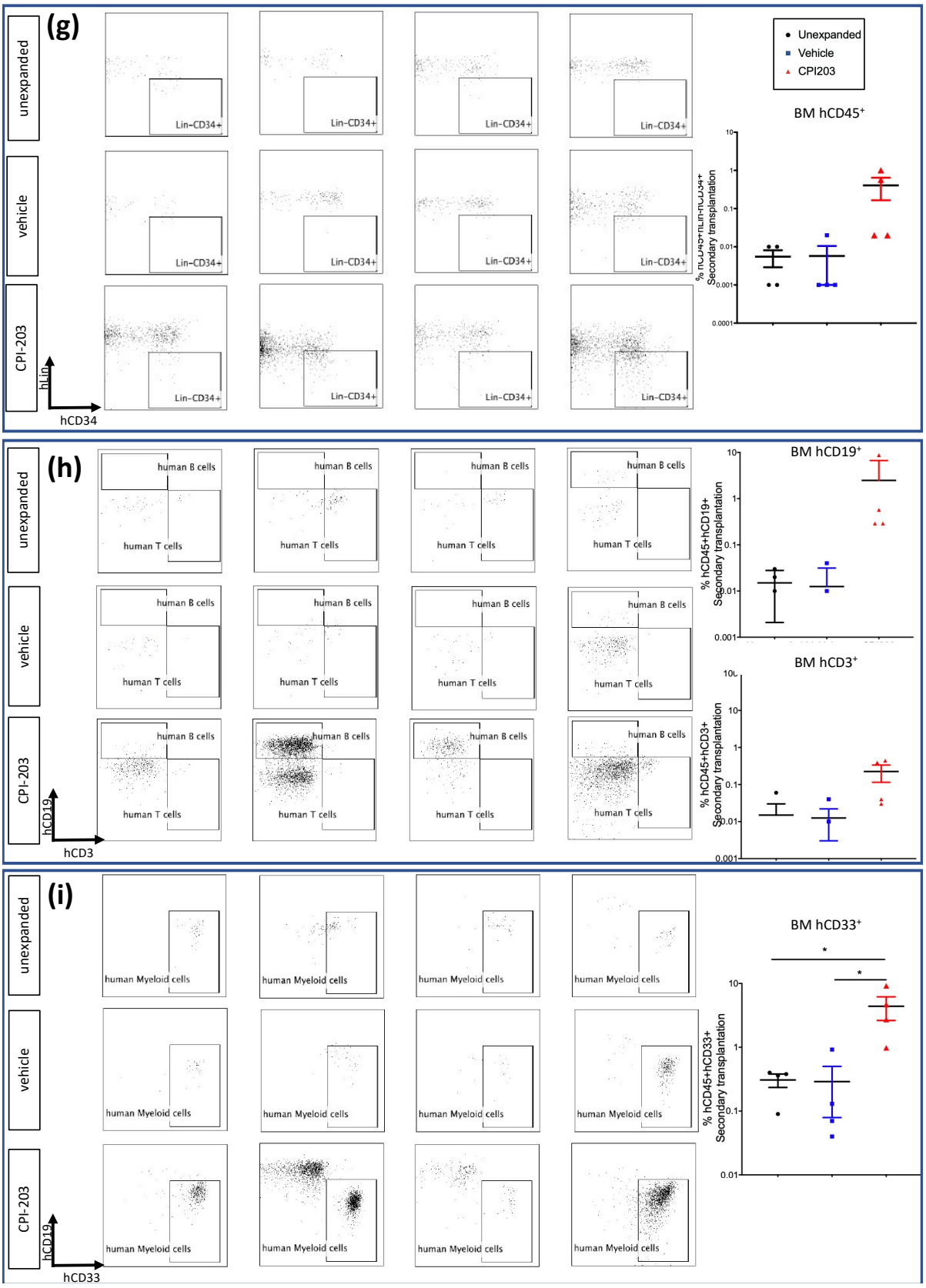

(j)

Gated on live single humanCD45-mouseCD45- cells

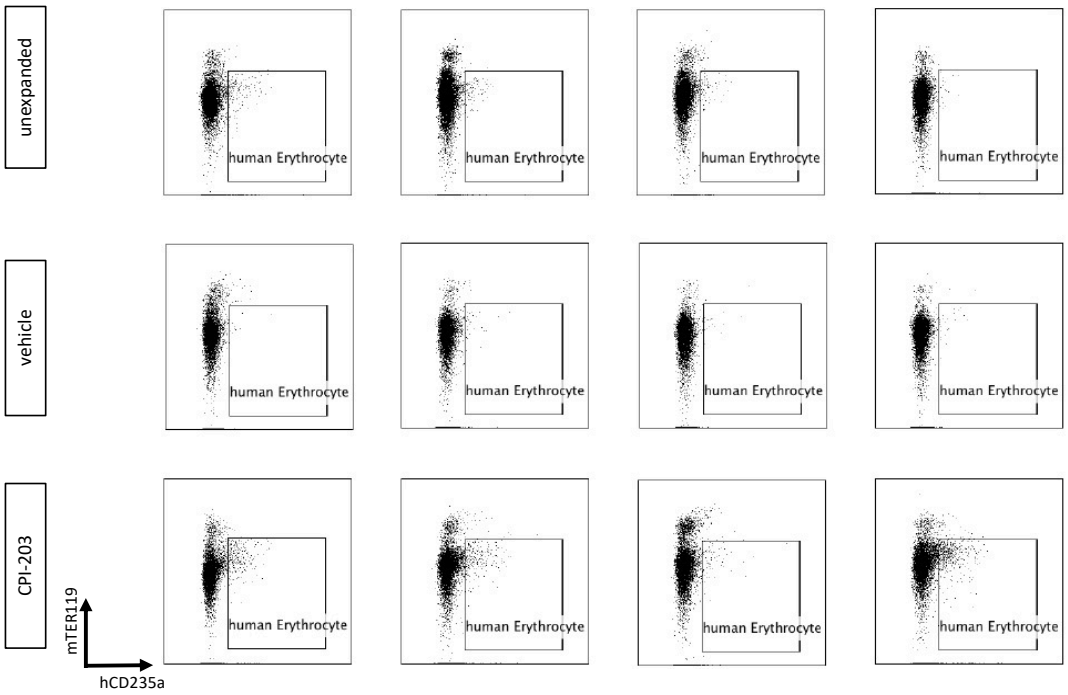

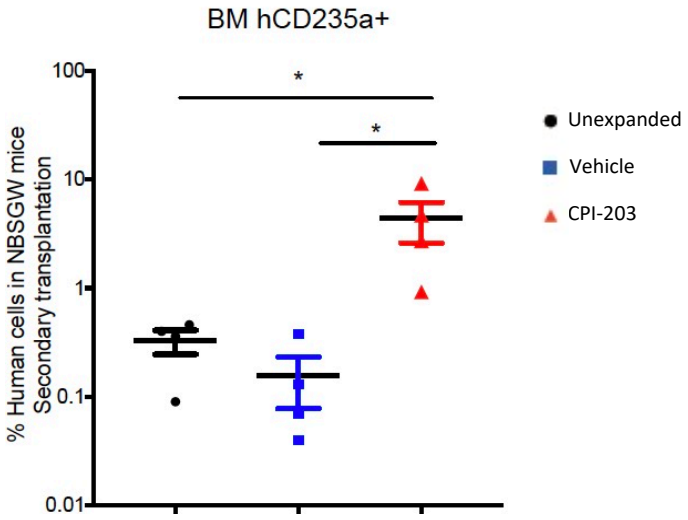

Chapter 4: Development Of A Model For The *In Vivo* Study Of Human Skin Transplant Rejection

4.0. Introduction

Skin grafting can provide desirable definitive coverage for complex and non-self-healing wounds, however in the clinical setting allogeneic skin transplantation is infrequently used and current applications are largely limited to 1) temporary coverage of freshly excised wounds, 2) as overlays on widely expanded autografts, and 3) as temporary dressings to improve recipient bed quality and vascularity prior to autografting[321]. Low usage of skin allografts is primarily due to their high susceptibility to immune rejection, which typically occurs within 20–30 days[322]. Skin allo-transplantation also occurs in the context of VCAs, following which a more complicated immunological response involving tolerogenic bone marrow cells occurs. Nonetheless, VCAs are still associated with an 85% acute rejection rate[323], which many suggest relates to high antigenicity and/or susceptibility of the skin component[324].

The clinical pathogenesis of human skin allo-rejection is incompletely understood and as such the development of safe long-term preventive therapies has yet to be realised. An abundance of experimental work has been conducted in small animal models, however the significant mechanistic gap between human and small animal immune responses hinders the translation of investigation findings to humans.

In attempts to overcome this limitation, a number of humanised mouse models of skin transplantation have been created, which support research into human skin allograft

rejection and potential therapies, without the requirement for human subjects. These models are vitally important tools, which facilitate analysis of Treg and other therapies, yet a limitation common to most models used in transplantation research is their inability to support multilineage reconstitution of functional human immune cells without the requirement for irradiative preconditioning. Cellular and tissue damage resulting from this limits the experimentation window beneath the 100-day span typically required to model human allograft rejection and necessitates the use of mature leucocytes for humanisation. The result is that though modelling of human skin allo-rejection is supported, human immune reconstitution is heavily biased toward activated and memory T cells[325], which misrepresents the immune reaction to transplantation and complicates the translatability of experimental findings. Having developed a robustly reconstituted, multilineage humanised mouse model that does not require irradiative preconditioning (chapter 3), we sought to evaluate the functionality of the human immune cells and their capacity to effect rejection of allogeneic skin grafts.

We hypothesise that HSPC-NBSGW mice can engraft human skin allografts and successfully model human skin allograft rejection macro- and microscopically. To evaluate this, we will assess the *in vivo* cellular response at the mRNA and/or protein level, and test immune cell function *in vitro*.

4.0.1. Chapter Aims

The principal aims of this chapter are to:

1) Characterise the macroscopic and microscopic features of the response to human skin allo-transplantation in NBSGW and HSPC-NBSGW mice.

2) Analyse the cellular (at the mRNA and protein level) and humoral features of human skin allograft rejection in this model

3) Investigate methods of model optimisation

4.1. Results

4.1.1. Engraftment of human skin in NBSGW and HSPC-NBSGW mice

In order to create a useable humanised mouse model of human skin allo-transplantation it is essential to demonstrate that transplanted tissue can engraft and survive *in vivo* for the full duration of the putative experiment. Factors that may affect this include host-specific factors such as xenogeneic rejection—which could occur at any time post-transplantation—and operative factors such as poor suture technique or application of dressings, following which shear forces can compromise the developing blood supply to the graft and lead to graft failure.

Our first step was to determine whether NBSGW mice support engraftment of human skin transplants, which remain healthy for at least 100 days. Healing time for transplanted human skin grafts onto BRG mice is approximately 35 days, at which point macroscopic evidence of post-operative inflammation subsides and graft revascularisation establishes, with ingrowth of vessels on the graft underside (F. Issa 2011, unpublished data).

We transplanted split-thickness human skin grafts onto the left flanks of NBSGW mice and monitored macroscopic appearances of the transplanted skin for 100 days (*Figure 4.1.1 (a)*).

After an initial inflammatory period human skin transplants 'healed-in' well by 35 days and at 100 days maintained the appearance of healthy skin, with a soft, pliable texture and without erythema, swelling or thickening (*Figure 4.1.1 (b)*). Weights remained stable in all mice (*Figure 4.1.1 (c)*) and no difference in survival rates were observed on comparison with NBSGW mice which did not receive skin transplants (*Figure 4.1.1 (d)*). Upon harvest, ingrowth of blood vessels on the graft undersides was observed, suggesting skin revascularisation had occurred (*Figure 4.1.1 (e)*). This was also suggested by the absence of shrinkage or necrosis (*Figure 4.1.1 (f)*), which we have observed in other models due to shear or excessive graft thickness, causing impaired revascularisation and ultimately graft failure in 2-3 weeks. Microscopically, skin architecture was well defined with normal epidermal and dermal thickness, a clear epidermal/dermal junction and minimal leucocyte infiltration (*Figure 4.1.1 (g)*). Importantly, no human 'passenger leucocytes' were detected in the blood or spleens of mice receiving human skin transplants (*Figure 4.1.1 (h)*).

Altogether this data suggests that the NBSGW mouse supports long-term engraftment of human skin grafts without features of rejection or graft loss, similarly to other well-characterised human-to-mouse skin transplant models.

4.1.2. Assessment of human skin transplant engraftment and rejection in humanised NBSGW (HSPC-NBSGW) mice

4.1.2.1. Macroscopic features & time-course analysis

Next, we investigated whether successfully reconstituted HSPC-NBSGW mice can support engraftment of human skin transplants and effect *in vivo* allograft rejection (*Figure 4.1.2.1*). To achieve this, we humanised 14 NBSGW mice with $5x10^4$ $CD133^+$ UCB HSPCs (HSPC-NBSGW), then 11-13 weeks later transplanted them and 3 un-humanised NBSGW control

mice with human split-thickness skin grafts (*Figure 4.1.2.1 (a)*). Grafts were observed bi-daily for macroscopic features of rejection (*Figure 4.1.2.1 (b)*). In HSPC-NBSGW mice, graft take was successful in all mice in 2 experiments. After 35 days grafts on all mice had healed in (*Figure 4.1.2.1 (b – left panel)*) and were indistinguishable macroscopically in control and experimental mice. Beyond this, skin grafts on HSPC-NBSGW mice underwent a consistent pattern of macroscopic changes that were not seen on NBSGW mice and indicate an immunological rejection response (*Figure 4.1.2.1 (b)*). This typically began with features of inflammation—characterised by skin graft swelling, thickening, and darkening in tone, the latter of which we have not typically observed in human skin grafts rejecting on albino BRG mice. Following this, skin grafts became erythematous, with patchy haemorrhages and eschar (early rejection)—typically around 40 days after transplantation. 'Late rejection' was characterised by reduction in graft size, development of a hard, crusty texture and finally over 80% graft loss (signifying the study endpoint - 'rejection') and replacement with pale scar tissue. Conversely, human skin grafts on control (NBSGW) mice survived long-term (>100 days) with no macroscopic features of rejection.

Mice with human skin grafts exhibiting features of late rejection were recorded as 'rejecters'. Where skin grafts did not demonstrate features of late rejection by the 100-day endpoint, mice were recorded as 'non-rejecters'. Mice euthanised for welfare reasons (e.g. fight injuries or illness) were recorded as 'censored'.

Over 2 experiments 10 mice (71%) developed macroscopic features of complete rejection however, 4 mice were censored prematurely (*Figure 4.1.2.1 (c) & (d)*). 5 mice were recorded as 'non-rejecters'. The median survival time was 70 days.

4.1.2.2. Histopathological features

The macroscopic features of acute human skin allograft rejection in this model were consistent with descriptions in other humanised mouse models and correlate with clinical descriptions. Microscopic features have also been defined clinically[326,327] and in experimental models[328]. To identify whether microscopic features of human skin allograft rejection are similar in the HSPC-NBSGW model, allografts from NBSGW and HSPC-NBSGW mice were examined histologically (*Figure 4.1.2.2*).

Skin samples were harvested from mice when macroscopic features of late rejection had appeared or after 100 days if rejection had not occurred. In un-rejected skins harvested from un-humanised NBSGW mice, characteristic features of normal skin were observed, with preserved architecture consisting of a thick epidermal layer with pronounced dermal papillae and minimal infiltrating leucocytes in the dermis (*Figure 4.1.2.2 (a)*).

Un-rejected skins harvested from humanised HSPC-NBSGW mice harboured altered skin microarchitecture, with shallower epidermis's, indistinct dermo-epidermal junctions and infiltrating inflammatory cells dispersed throughout the dermis (*Figure 4.1.2.2 (b)*).

Rejected allografts harvested from HSPC-NBSGW mice demonstrated substantial interstitial, perifollicular and perivascular inflammatory cell infiltrates and marked microarchitectural disruptions including significant epidermal loss and indistinct dermal-epidermal junction (*Figure 4.1.2.2 (c)*).

Altogether, these results demonstrate the capacity to reproduce characteristic macroscopic and microscopic features of acute rejection in the HSPC-NBSGW human skin allograft model.

4.1.3. Investigation of the *in vivo* human immune response to allogeneic human skin transplantation

4.1.3.1. Leucocyte response

In established humanised mouse skin allograft models, rejection is typically associated with the development (almost exclusively) of human T cell responses. Re-creation of the global human immune response to allo-stimulation requires a model capable of representing the contribution of non-T human immune cells. The HSPC-NBSGW mouse model demonstrates successful multilineage human cell haematopoeisis (chapter 3) and representative modelling of human skin allograft rejection (*section 4.1.1 & 4.1.2*). Using these attributes, we next investigated 1) whether HSPC-NBSGW human leucocytes mount measurable responses to *in vivo* allogeneic challenge and 2) whether any immune responses provoked are functional.

First, we analysed HSPC-NBSGW *in vivo* cellular responses to skin allografts by comparing human leucocyte frequencies in 'rejecters' and 'non-rejecters'. Successful peripheral blood human $CD45^+$ leucocyte reconstitution correlated significantly with allograft rejection (*Figure 4.1.3.1 (a)*), with rejecters demonstrating chimerism 6-fold higher than non-rejecters. T cells formed the most populous peripheral blood subset in rejecters, and were 20-fold more abundant than in non-rejecters (*Figure 4.1.3.1 (b)*). B cells formed the largest subset in the peripheral blood of non-rejecters. Their low frequencies in rejecters indicate an approximately reciprocal relationship with T cells in this transplant model. Myeloid cells were present in similar proportions in the presence and absence of skin allograft rejection.

4.1.3.2. T cell response

As in other humanised mouse models, T cell frequencies correlated positively with skin allograft rejection in HSPC-NBSGW mice. To study the T cell subset profiles present in rejection and non-rejection, T cell populations within spleens of allografted mice were examined by flow cytometry (*Figure 4.1.3.2 (a)*).

Both $CD4^+$ and $CD8^+$ T cells were more abundant in spleens of rejecters compared with non-rejecters (*Figure 4.1.3.2 (b)*). Of these, significantly more Tem and TemRA cells were observed in rejecters (*Figure 4.1.3.2 (c) & (d)*). Numbers of other subsets were greater in rejecters however these differences were not significant.

4.1.3.3. B cell response

We identified that the frequency of HSPC-NBSGW B cells is significantly lower in spleens of mice demonstrating skin allograft rejection (*Figure 4.1.3.1 (b)*). We also found spleens of skin allograft recipients to harbour greater proportions of class-switched memory B cells than un-transplanted HSPC-NBSGW mice (*Figure 3.1.3 (h)*). To evaluate the B cell response to skin allografting more closely, we assessed splenic B cell maturity in the presence and absence of rejection (*Figure 4.1.3.3*).

Similar frequencies and numbers of $CD10^-$ mature B cells were identified in rejecters and non-rejecters (*Figure 4.1.3.3 (a)*). A trend of greater abundance of class-switched memory B cells was seen in rejecters however, this was not statistically significant (p=0.1143) (*Figure 4.1.3.3 (b)*).

4.1.3.4. Myeloid cell response

Myeloid cells are present in low frequencies in skin transplanted mice and no differences were observed in the blood of 'rejecters' and 'non-rejecters' (*Figure 4.1.3.1 (b)*). To evaluate whether any differences in key myeloid subsets may accompany rejection we assessed the monocyte and conventional dendritic cell compositions in HSPC-NBSGW bone marrow.

Conventional dendritic cells were significantly more numerous in rejecters (*Figure 4.1.3.4 (b)*). Frequencies of both subtypes were non-significantly higher in rejecters (*Figure 4.1.3.4 (c)*).

4.1.4. *In vitro* investigation of HSPC-NBSGW leucocyte function following allogeneic skin transplantation

4.1.4.1 *In vitro* effector T cell function

We identified an association between high HSPC-NBSGW human T cell frequencies and human skin allograft rejection *in vivo* (*Figure 4.1.3.1 (b)*). To explore the functional characteristics of these T cells, we compared the effects of *in vitro* stimulation with those in human peripheral blood T cells. $CD3^+$ T cells were harvested from spleens of mice 'rejecters' and assessed for their ability to respond to αCD3/αCD28 stimulation and to allogeneic re-challenge with peripheral blood APCs from the skin allograft donor (*Figure 4.1.4.1 (a)*). Polyclonal αCD3/αCD28 stimulation triggered a characteristic proliferative response, demonstrated by dilution of violet proliferation dye (*Figure 4.1.4.1 (b)*). Allogeneic re-challenge triggered proliferation of ~10% of T cells (*Figure 4.1.4.1 (c)*). To determine whether this effect was truly representative of a second set allo-response, we additionally assessed responses to third party allogeneic human APCs (PBMC- or bone marrow-derived) and NBSGW bone marrow cells from another mouse (*Figure 4.1.4.1 (c)*). There was minimal T cell proliferation following co-culture with allogeneic human APCs.

In addition to intracellular cytolytic enzyme expression (*Figure 3.1.4 (l-n)*) and proliferative responsiveness to stimulation, we investigated whether HSPC-NBSGW T cells have the capacity for effector cytokine production. Splenic T cells were stimulated *in vitro* (with the same conditions as above) for 72-96h (*Figure 4.1.4.1 (d)*), then culture supernatants were isolated and Th1, Th2 and Th17 cytokine concentrations quantified by cytometric bead array.

Th1 cytokine concentrations were significantly higher in supernatants from wells of polyclonally-stimulated T cells compared with unstimulated T cells (*Figure 4.1.4.1 (e)*). Th2 and Th17 cytokines were most prominently upregulated following allogeneic re-challenge with APCs from the skin donor. Similarly to T cell proliferative responses, 3rd party allo-antigen stimulation did not significantly increase cytokine concentrations.

4.1.4.2 *In vitro* B cell function

In HSPC-NBSGW mice, we identified human B cells developing to maturity, including class-switched memory cells, which are more populous in human skin allograft recipients (chapter 3). To determine whether these cells are capable of effector function, we investigated their capacity to produce human antibodies.

Surface antibody expression on HSPC-NBSGW splenic human B cells was assessed by flow cytometry (*Figure 4.1.4.2 (a)*). IgD and IgM were consistently identified on mature B cells, with IgM in particular demonstrating a similar expression pattern to mature human peripheral blood B cells (*Figure 4.1.4.2 (b)*). IgG and IgA expression profiles were also similar to human peripheral blood B cells. In keeping with human blood profiles, mature B cells expressed more IgA/IgG and less IgM than immature B cells, suggesting antibody class-switching may be occurring in this group of B cells (*Figure 4.1.4.2 (c)*). To evaluate whether following skin allografting HSPC-NBSGW B cells can secrete antibodies (particularly IgG), plasma total IgG concentrations were measured (*Figure 4.1.4.2 (d)*). IgG was significantly higher in the plasma of 'rejecters' than 'non-rejecters' (*Figure 4.1.4.2 (e-f)*). Where sufficient plasma remained, antibody subtypes were subsequently analysed by cytometric bead array (*Figure 4.1.4.2 (g)*). In humanised mice without skin transplant only IgD and IgM were detected. In skin-allografted HSPC-NBSGW mice IgD expression was significantly lower in

'rejecters' than 'non-rejecters'. IgM expression was higher in 'rejecters', as were IgG1, IgG3 and IgG4. Expression of these subsets was only significantly raised in plasma of skin-allografted 'rejecter' HSPC-NBSGW mice (*Figure 4.1.4.2 (g)*) ($p<0.001$ - $p<0.05$). In non-skin-allografted NBSGW and BRG mice humanised with $5x10^6$ PBMCs, plasma IgD expression was similar to HSPC-NBSGW mice, whereas IgM and IgG subtype expression was significantly higher, at levels close to human serum.

Altogether, this pattern of broad human immunoglobulin expression, with reduced IgD and increased in IgM and IgG expression in HSPC-NBSGW mice rejecting skin allografts indicates the potential for specific human B cell responses to be mounted in response to antigen challenge within this model.

4.1.4.3 *In vitro* antigen presenting function

To determine the functional capacity of HSPC-NBSGW human myeloid cells, we first evaluated whether co-culture with allogeneic leucocytes could stimulate myeloid cells and trigger antigen presenting responses. Thus, HSPC-NBSGW bone marrow leucocytes were co-cultured with allogeneic human peripheral blood $CD3^+$ T cells for 18 hours, then expression of activation and antigen presentation markers were analysed by flow cytometry (*Figure 4.1.4.3 (a)*).

Myeloid cells upregulated expression of the stimulatory markers CD80 and CD86 (*Figure 4.1.4.3 (b)*) as well as protein and lipid antigen presentation molecules (*Figure 4.1.4.3 (c)*). Comparable responses were observed in $CD45^+$ leucocytes derived from human bone marrow and peripheral blood (*Figure 4.1.4.3 (b-c, right)*).

We then assessed the ability of HSPC-NBSGW myeloid cells to stimulate allogeneic human T cells. In separate experiments, irradiated HSPC-NBSGW human $CD45^+$ bone marrow leucocytes harvested from 'rejecters' were co-cultured for 72 hours with allogeneic human PBMCs or allogeneic HSPC-NBSGW splenic T cells and stimulation assessed by T cell proliferation (*Figure 4.1.4.3 (d)*). HSPC-NBSGW bone marrow stimulation triggered proliferation in both human peripheral blood and HSPC-NBSGW T cells and in frequencies characteristically observed in human *in vitro* allogeneic stimulation assays (*Figure 4.1.4.3 (e)*).

4.1.4.4 mRNA analysis

Molecular mechanisms that participate in human organ transplant rejection are best inferred from mRNAs expressed in biopsies. This is because the proteins they correspond with often have low expression profiles and short half-lives, whereas small non-coding RNAs have low specificity.

We utilised NanoString multiplex nucleic acid hybridisation technology to evaluate RNA expression in skin and spleens harvested from skin-allografted HSPC-NBSGW mice and interrogate the immune processes involved in rejection. We began by assessing the expression of leucocyte profiling genes in skin and spleens harvested from HSPC-humanised 'rejecters' and 'non-rejecters', and non-humanised (skin only) mice (*Figure 4.1.4.4 (a)*). Expression was highest in spleens and skins harvested from *rejecters*, and this was considerably greater than in samples harvested from *non-rejecters* and *skin only* mice. Next, we performed principal component analysis of expression of immunity-related genes to evaluate similarities and disparities between groups (*Figure 4.1.4.4 (b)*). Samples within experimental groups demonstrated clustering of gene expression profiles, indicating that similar processes had occurred in each mouse. We also observed skin *non-rejecters* and *skin*

only mice clustering together, suggesting similar gene expression in skin of these mice. We then evaluated differential expression of genes involved in immune pathways associated with rejection (*Figure 4.1.4.4 (c)*). Across most immune pathways we similarly observed clustering of the highest gene expression scores in spleens and skins from *rejecters*, and the lowest scores in non-rejected skins from both *non-rejecters* and *skin only* mice. Notably, in both *rejecters* and *non-rejecters,* immune senescence-related genes were expressed more highly in skins than in spleens. This may be in keeping with the role of senescence as a programme of cell-intrinsic stress responses, programmed to induce stable cell-cycle arrest and prevent injured cells from propagating further tissue damage[329]. Next, we interrogated the expression of genes involved in adaptive and innate immune functions (*Figure 4.1.4.4 (d-g) and (h-j)* respectively). This was particularly pertinent because support for multilineage human leucopoiesis is an important feature of the HSPC-NBSGW model. Regarding adaptive pathways associated with cytotoxic and regulatory functions, and specifically with pathways of T and B cell functions, we observed highest gene expression in spleens and skins from *rejecters* and lowest expression in spleens and skins from *non-rejecters* and *skin only mice*. Among cytotoxicity pathways, several genes encoding cytolytic enzymes (including Granzymes and Perforin) were substantially upregulated in *rejecters* (*Figure 4.1.4.4 (d)*). Innate system-related genes involved in antigen processing (e.g. TAP1), antigen presentation and NK cell functional pathways (e.g. KLR family genes) were similarly expressed most abundantly in spleens and skins from *rejecters* and least abundantly in unrejected skins (*Figure 4.1.4.4 (h-j)*). Cell type mRNA analysis—which profiles cells based on characteristic gene expression patterns—demonstrated expression of macrophage profiling genes to be substantially higher in skins and spleens from *rejecters* than *non-rejecters*. These patterns of gene expression suggest that high expression of similar immune cell profiles and functional

pathways occurs in spleens and skins during rejection. Having identified this, we then sought to analyse differential gene expression more granularly, using volcano plots to delineate how significant disparities are for individual genes. In *non-rejecters*, we identified 26 genes with greater expression in spleens than skins, and 9 with lower expression (*Figure 4.1.4.4 (k)*). Genes expressed more abundantly in the skin included some involved in complement (c1r,C1s), leucocyte chemotaxis (CXCL12), inflammation and apoptosis (IFI27) and connective tissue repair (COL3A1- encoding type 3 collagen protein). Genes expressed more abundant in spleens related to myriad functions, including many relating to lymphocyte activity (e.g. CD79b & IRF4). Comparison of skins harvested from *rejecters* and *non-rejecters* demonstrated significantly higher expression of 15 genes in rejected skins and lower expression of 1 gene (*Figure 4.1.4.4 (l, n & o)*). This was in contrast with spleens in which no significant differences in individual gene expression were found between *rejecters* and *non-rejecters* (*Figure 4.1.4.4 (l, n & o)*). Interestingly, most genes with significantly higher expression in rejected skins encode proteins with important functions in innate immunity. These include phagocytosis-related proteins (CYBB), α and β chains of antigen presenting HLA class II molecules (-DP, -DQ and -DR) and their chaperone protein HLA-DM, migration and adhesion molecules (e.g. AMICA1 and ITGB2) and signalling proteins (IL2RG) (*Figure 4.1.4.4 (n)*), suggesting the importance of innate immunity and its representation in models of human skin transplant rejection.

Altogether these results demonstrate significant upregulation of recognised pathways of both afferent and efferent immunity in the HSPC-NBSGW model of human transplant allorejection. This supports the applicability of the HSPC-NBSGW mouse as a representative model for pre-clinical *in vivo* investigations of human immunity.

4.1.5. Assessment of the NBSGW murine immune cell response to human skin transplantation

NBSGW mice are specifically engineered to lack T, B and NK cells and are "genetically-myeloablated", providing the capacity to support engraftment and reconstitution of human HSPCs and mature immune cells. Despite these major immune deficiencies, murine innate cells such as granulocytes and macrophages are still produced, which may have an impact on human skin grafts in our model. It has previously been shown in non-humanised NSG mice that mouse GR-1^{+} cells can infiltrate human skin grafts and actively participate in graft destruction[330]. Having already demonstrated that there is not a significant cellular infiltrate into human skin grafts transplanted onto NBSGW mice (*Figure 4.1.2.2*), we aimed to determine whether engrafted human HSPCs and skin transplants stimulate murine innate cells within mouse spleens.

Following humanisation, splenic NBSGW murine immune cells do not significantly proliferate in response to engrafted human cells and there is no difference in frequencies between HSPC-NBSGW skin allograft recipients and non-recipients (*Figure 4.1.5 (a-c)*). Frequencies of Gr-1^{+} granulocytes were not significantly raised in humanised HSPC-NBSGW mice and human skin engraftment did not produce an additive effect (*Figure 4.1.5 (a)*). Frequencies of myeloid DCs and macrophages were higher in HSPC-NBSGW mice with skin allografts than in unhumanised mice (*Figure 4.1.5 (b&c)*). Additionally, activation marker expression on mouse innate cells was not increased in recipients of human HSPCs or human skin grafts (*Figure 4.1.5 (d)*).

Altogether these results suggest that following humanisation of NBSGW mice, murine innate responses appear to be small and without significant cellular activation. Skin allo-transplantation onto HSPC-NBSGW mice is associated with higher frequencies of innate cells.

Further characterisation of these cells may provide insight into potential effects of importance to this model.

4.1.6. Rejection of human skin transplants in PBMC-humanised NBSGW mice and comparison with HSPC-NBSGW mice and PBMC-humanised BRG mice

PBMC-humanised (also known as PBL-humanised) mouse models have been used widely in *in vivo* investigations of transplant immunology. Notably, they have enhanced our understanding of human transplant rejection and the effects of treatments including Treg therapy. Owing to their reliability, these models represent a suitable benchmark against which new models can be compared. To our knowledge there are currently no published studies utilising PBMC-humanised NBSGW mice in studies of immunology or oncology. BRG mice humanised with PBMCs are well recognised in transplant studies[219]. We therefore sought to determine whether humanisation of NBSGW mice with PBMCs (as observed in Chapter 3) can lead to comparable functional human immune responses.

Human skin grafts were transplanted onto adult NBSGW and BRG mice and 35 days later $5x10^6$ allogeneic human PBMCs were injected intraperitoneally (*Figure 4.1.6 (a)- top panel*). Complete macroscopic rejection occurred in 6 PBMC-humanised NBSGW mice but not in control mice, suggesting that this model is suitable for use in investigations of human skin transplant rejection (*Figure 4.1.6 (b)*). Survival analysis demonstrated a median survival time of 45 days. This was longer than PBMC-humanised BRG mice (28.5 days). A comparison of skin allograft rejection in PBMC models and HSPC-NBSGW mice (*Figure 4.1.6 (a)- bottom panel*) was conducted to assess for temporal differences, which may influence model choice. From the time of skin transplantation, the MST of the HSPC-NBSGW model was 71 days, 26 days longer than the PBMC-humanised NBSGW and 43.5 days longer than PBMC-humanised BRG

model. 3 PBMC-humanised NBSGW mice and 4 HSPC-NBSGW mice developed weight loss and were censored (*Figure 4.1.6 (c)*).

4.1.6.1. Human leukocyte profiles in HSPC-NBSGW, PBMC-humanised NBSGW and PBMC-humanised BRG mice following rejection of human skin allografts

Leucocyte profiles in spleens and bone marrow of PBMC-humanised NBSGW, PBMC-humanised BRG and HSPC-NBSGW mice on which skin allograft rejection had occurred was then assessed (*Figure 4.1.6.1*).

Total leucocyte reconstitution in spleens was similar among all groups, with slightly greater reconstitution in HSPC-NBSGW mice (*Figure 4.1.6.1 (a)*). However, like PBMC-humanised mice which did not receive skin allografts, T cells formed the vast majority of splenic human leucocytes in both PBMC-humanised NBSGW and PBMC-humanised BRG mice (*Figure 4.1.6.1 (b)*), with negligible splenic B cells (*Figure 4.1.6.1 (c)*) and no bone marrow myeloid cells (*Figure 4.1.6.1 (d)*). Despite low B cell frequencies, we did identify antibodies in the serum of PBMC-humanised mice which rejected skin allografts (*Figure 4.1.2.2 (c)*).

Altogether these results demonstrate more robust and multilineage leucocyte reconstitution in HSPC-NBSGW mice demonstrating rejection of human skin allografts, and leucocyte profiles in PBMC-humanised NBSGW mice that are similar to the well known PBMC-humanised BRG model.

4.1.7. Assessment of allogeneic human skin transplant rejection in HSPC-NBSGW mice receiving UCB HSPCs ± MNCs

Having observed reliable reconstitution in HSPC-NBSGW mice and successful rejection of allogeneic human skin transplants, we sought to investigate the potential to increase the

speed and frequency of complete allograft rejection in order to enhance data acquisition and reduce the duration of experiments. Having determined that leucocyte chimerism correlates with rejection dynamics in this model, we augmented leucocyte frequency in an attempt to enhance rejection. HSPCs form only a small proportion of leucocytes acquirable from UCB units and yielding sufficient numbers to inject into multiple mice for rejection experiments can be challenging. To get around this, 11-13 weeks after humanisation with UCB HSPCs, we injected $CD45^{+}CD34^{-}$ MNCs derived from the same UCB unit and 2 weeks later transplanted allogeneic human skin and monitored for rejection (*Figure 4.1.7 (a)*). Our hypothesis was that additive MNC-transplantation may augment leucocyte numbers directly and increase chimerism by providing mature cytokine-producing leucocytes to enhance HSPC differentiation and proliferation.

Skin allograft rejection occurred more quickly in mice transplanted with MNCs in addition to HSPCs, with the median survival time of 39 vs 94 days (*Figure 4.1.7 (b & c*). Macroscopic features of rejection were indistinguishable between the groups.

4.1.7.1. Human leucocyte profiles in UCB HSPC+MNC-humanised NBSGW mice on which human skin allografts rejected

Cellular analysis showed no difference in CD45 chimerism in the bone marrow and spleen between MNC-recipients and non-recipients (*Figure 4.1.7.1 (a)-(c)*). Bone marrow myeloid cell frequencies and numbers were also equivalent between the two groups (*Figure 4.1.7.1 (d)&(e)*). Lower frequencies and numbers of B cells were found in spleens of MNC-recipients compared with HSC-only recipients. Reciprocal increases in T cell frequencies and numbers were observed (*Figure 4.1.7.1 (f)-(h)*).

This data suggests that addition of UCB MNCs serves predominantly to enhance T cell frequencies at the expense of B cell reconstitution and without significant effects on myeloid cells or overall leucocyte reconstitution.

4.1.7.2. Human T cell subset profiles in UCB HSC +/- MNC-humanised NBSGW mice on which human skin allografts rejected

Having identified faster human skin allograft rejection in HSPC+MNC-NBSGW mice, which was associated with increased T cell frequencies and numbers, we assessed T cell subsets.

Higher T cell frequencies, particularly $CD3^+CD8^+$ T cells were observed (*Figure 4.1.7.2 (a)&(b)*). In rejecters, the majority of splenic T cells were $CCR7^-$ Tem cells (both $CD4^+$ and $CD8^+$) (*Figure 4.1.7.2 (c)-(e)*). In mice humanised only with HSPC-NBSGW mice, greater diversity was seen, with TemRA cells forming a significant proportion of the T cell repertoire, however in MNC-recipients T cells were almost exclusively $CCR7^-CD45RA^-$ Tem.

4.1.7.3. Human B cell subset profiles in UCB HSPC +/- MNC-humanised NBSGW mice on which human skin allografts rejected

Skin allograft rejection in MNC-recipients was associated with lower frequencies of $CD19^+$ B cells than MNC non-recipients (*Figure 4.1.7.3 (a-b)*). The majority of B cells in these mice however, were $CD10^-$ mature B cells (*Figure 4.1.7.3 (c)*), and frequencies of $CD27^+IgD^-$ memory B cells were non-significantly higher (*Figure 4.1.7.3 (d)*).

This suggests that in the context of rejection at least, additive humanisation with UCB MNCs may skew human B cell populations toward predominantly mature phenotypes.

4.1.7.4. Human myeloid cell subset profiles in UCB HSPC +/- MNC-humanised NBSGW mice on which human skin allografts rejected

Lower frequencies of myeloid cells were observed in MNC-recipient rejecters (*Figure 4.1.7.4 (a)&(b)*). Additionally, lower frequencies of $CD11c^+$ dendritic cells were observed in the bone marrow of MNC-recipients than HSPC-NBSGW rejecters (*Figure 4.1.7.4 (c)*).

4.2. Discussion

In this chapter we have developed on successful multilineage humanisation in the HSPC-NBSGW mouse model by investigating functionality of the reconstituting human immune cells.

Allogeneic transplant rejection is a complex process involving several immune cells and non-immune cells (e.g. platelets), which participate in coordinated activation and effector phases. Both hostile attacks against allografts and protective regulatory responses have been demonstrated by a wide range of innate and adaptive immune cells. Experimental animal models have provided the bulk of understanding of immunological responses to transplantation. Most of such studies have been conducted in mice engineered with deficiencies in cells of particular interest. This method provides valuable information about the functions of specific cells in relative isolation within controlled environments, however it is prudent to consider that engineered experimental conditions may limit our understanding of the functions these cells produce within a genetically replete organism. It is also important to appreciate translational limitations that result from incomplete crossover between murine and human biological systems. The development of humanised *in vivo* mouse models that are

capable of supporting multilineage functional immune systems could help to overcome some of these limitations.

Another important endeavour in transplantation research is the establishment of a multilineage humanised model that can represent the *in vivo* immune cell repertoire more closely than the PBL models popularly used. This because the preponderance of mature T cells in these models is liable to skew experimental representation of the human allo-response.

We have presented evidence of functional innate and adaptive immune responses in a humanised mouse model of complete skin allo-rejection. A notable feature of this model is the capacity to re-create human allorecognition *in vivo.* This highly sought-after property creates the potential to expand current understanding of human transplant rejection and enhance capacity to develop and test therapies more accurately in a representative *in vivo* setting. Furthermore, its more expansive modelling of immune pathways broadens the range of targets that may be exploited in pre-clinical therapeutics research.

The ability to re-create reliable human alloresponses *in vivo* depends in large part on the ability of donor APCs to present donor antigen to T cells in the context of donor HLA molecules (direct allorecognition), and host APCs to present donor antigen in the context of self-HLA molecules (indirect allorecognition). We have demonstrated *in vivo* rejection of human skin allografts, which is associated with significant upregulation of genes encoding antigen presentation molecule expression, macrophage, NK cell and complement function. We also demonstrated *in vitro* expression of activation and antigen presentation molecules in HSPC-NBSGW myeloid cells co-cultured with allogeneic human antigen, and their capacity to present antigen to allogeneic T cells, triggering proliferation. Investigation of the capacity for indirect antigen presentation is discussed in chapter 6.

Regarding the efferent limb of allorecognition (T cell recognition of HLA-antigen complexes), in addition to demonstrating engraftment of HLA-expressing thymic cells (Chapter 3), we have demonstrated *in vivo* rejection of human skin allografts, which is mediated in part by T cells that demonstrate specific memory responses against skin donor antigen. These T cells did not respond to murine antigen, potentially reflecting a degree of HLA restriction in developing HSPC-NBSGW T cells. In theory, HLA-expressing thymic cells may impose HLA restriction on developing thymocytes undergoing positive selection, providing a survival signal only to thymocytes binding HLA molecules with appropriate affinity[331]. HLA restriction has been formally investigated through assessment of T cell populations with intact TCRαβ gene rearrangements, allowing "untested" preselection TCRs to be sampled for the presence or absence of inherent MHC reactivity by germline-encoded recognition motifs. This has been achieved using either mice lacking expression of MHC class I and II molecules, in which thymocytes are blocked at the $CD4^+CD8^+TCR\alpha\beta^+$ stage[332-334] or TCRα mice[335], which are unable to express TCRs.

Another notable feature we discovered in the HSPC-NBSGW skin transplantation model was the significant difference in abundance of T cells in spleens and peripheral blood in the context of rejection. In keeping with the evidence from other animal and human studies, rejection in the HSPC-NBSGW model primarily associated with activation of responses effected directly and indirectly by T cells–T cell-mediated rejection (TCMR). It is well documented that antigen from grafted tissue triggers activation and proliferation of allo-specific T cells and initiates a cascade of effector elements that mediate graft injury and rejection. The major role of antigen-specific $CD8^+$ CTLs in rejection is well established. In studies where infiltrating CTLs were eluted from rejecting human renal allografts, Strom *et al*

demonstrated the role of cytolysis in cellular rejection[336]. In *in vivo* mouse experiments, Rosenberg *et al* demonstrated adoptive transfer of $CD8^+$ effector T cells to induce rejection of MHC class I-mismatched skin transplants[337]. The $CD8^+$ response can be initiated by priming and activation of CTLs following recognition of peptides presented in the context of MHC-class I, but these peptide antigens also serve as targets for mature cytolytic effectors. In HSPC-NBSGW mice, we observed higher numbers of $CD8^+$ T cells (particularly Tem & Tcm) in 'rejecters' than in 'non-rejecters'. This may be in keeping with *in vitro* observations of memory (but not naïve) T cells becoming activated during co-culture with human skin microvessel endothelial cells[338].

Within 72h of activation of CTL precursors, perforin and granzyme-containing cytotoxic granules are formed. Upon identification of the target cell, granules fuse with the effector cell membrane and extrude their contents into the immunological synapse[339]. Following this, perforins assemble into polyperforins and insert into the target cell membrane to facilitate uptake of granzymes via the granzyme exocytosis (GE) pathway. Upon entry into the target cells, granzyme B triggers apoptosis through a number of different pathways such as direct cleavage of procaspase-3[340]. In keeping with this, we demonstrated that CTL's developing within the HSPC-NBSGW mouse produce perforin, granzyme A and B (Chapter 3). Following stimulation, expression of genes encoding cytolytic proteins were upregulated in rejecters.

The allo-specific CTL pathway is a significant mode of delivery of precise antigen-specific killing, as reflected by the demonstration of apoptotic cells in biopsies of rejecting allografts[341]. However, studies in which $CD8^+$ T cell depletion has not prevented rejection[342] suggest that other effector mechanisms of rejection are importantly involved. NK cells are historically known to be the primary effector cells of rejection after MHC-mismatched bone marrow transplantation[343,344], but have only recently gained recognition as important

effectors in solid organ transplant rejection[345]. In a skin transplantation study, $Rag^{-/-}$ mice lacking T and B cells rejected allografts upon activation of NK cells exposed to IL-15, however rejection did not occur in $Rag^{-/-}\gamma c^{-/-}$ mice lacking NK cells[53]. Our mRNA data demonstrated genes characterising NK cells to co-cluster with cytotoxic function and to be more highly expressed in both the skins and spleens of rejecters. Future studies that assess the expression of cytolytic molecules and the Fc receptor CD16 (characteristic in ABMR) would be useful to confirm the capacity of this model to experimentally represent the important contribution of NK cells to the human response to allo-transplantation.

Another important effector limb of the T cell response to transplantation is the delayed-type hypersensitivity (DTH) response, mediated primarily by alloantigen-specific $CD4^+$ Th1 cells[346]. These cells secrete cytokines such as TNF and IFN-γ in response to alloantigen stimulation, producing pro-inflammatory responses including activation of monocytes and macrophages, which commonly infiltrate rejecting allografts. Following activation, cytokine and chemokine production is amplified further and proteolytic enzymes, nitric oxide and other soluble factors are released perpetuating the local inflammatory response. It has been suggested through adoptive transfer experiments that allo-specific DTH responses alone are sufficient to reject skin grafts. Early experiments by Dalloul *et al* in which $CD4^+$ T cells from $CD8^{-/-}$ mice were adoptively transferred into SCID mice transplanted with MHC class I or II-disparate allogeneic skin showed Th1-mediated rejection without direct cytotoxicity[347]. Valujskikh[348] and later Brennan and colleagues[349] showed – via adoptive transfer of Th1 allo-reactive cell lines and TCR transgenic $CD4^+$ T cells respectively - that Th1 allo-reactive cells recognising donor MHC peptides via the indirect pathway can reject allogeneic skin grafts with typical Th1 DTH profiles, reproducible by subcutaneous injection of donor antigen[348].

We have demonstrated Th1, Th2 and Th17 functionality of HSPC-NBSGW T cells both in response to CD3/CD8 co-stimulation and following repeated challenge with specific donor antigen. Whereas Th cell cytokine production in HIS mice has been reported in models such as the huNSG mouse[350], an additional prospect of the HSPC-NBSGW model in transplant research is the potential to incorporate interactions between human Th cells and innate immune cells as seen in DTH responses and eosinophil-mediated rejection promoted by IL-4 and IL-5[351-353]. Perhaps more significantly, it provides the potential to recapitulate the pivotal interactions between Th cells and mature B cells. It has previously been shown that although the Th2 cytokine profile generally limits DTH and cell-mediated immunity, it is capable of inducing antibody-mediated rejection. This may be of particular importance in developing a more representatively complete humanised allo-response because in humans the third major pathway of rejection (in addition to CTL and DTH) is the allo-antibody response[346]. Antibody production is predominantly a function of B cells, however allo-reactive $CD4^+$ T cells are vitally important mediators of B cell growth, differentiation and antibody secretion. Antibodies secreted bind MHC antigens expressed on endothelial cells and trigger responses involving complement, which activate and recruit inflammatory cells that effect graft injury. Allo-antibodies may also be bound at their Fc receptors by NK cells and macrophages, promoting target cell lysis by ADCC. We have demonstrated that following stimulation *in vitro* HSPC-NBSGW T cells produce Th2 cytokines. We have also detected human IgG in HSPC-NBSGW mouse serum, with quantities rising significantly higher in the serum of 'rejecters' than 'non-rejecters'. Considering also that 'rejecters' had on average four times more class-switched memory B cells in their spleens than 'non-rejecters', there is the suggestion of a causal association between transplantation, B cell activation, class-switching and allograft rejection. Importantly, 'rejecters' combined higher numbers of mature B cells with higher T cell

frequencies, suggesting that the rejection process in this model might be ABMR or a combination of ABMR and TCMR. Future studies to confirm the presence of ABMR in HSPC-NBSGW mice by assessing the presence of donor-specific allo-antibodies (DSAs), staining for complement products (e.g. C4d[354]) and immunostaining for Ig and complement may be useful to confirm this.

Importantly, we demonstrate that although murine immune cells within HSPC-NBSGW mice may be more populous following xenografts, there were no significant stimulatory responses to these tissues. Lack of a murine activated immune phenotype that could suggest a contribution to human skin graft rejection affords us greater confidence in the experimental rejection observed being the result of a human cell allo-response.

The significantly different rejection dynamics seen between PBMC-humanised NBSGW and PBMC-humanised BRG mice are particularly interesting because the cellular engraftment frequencies and IgG expression levels in the two models are very similar. As no other models of human skin allo-transplantation have yet been described in NBSGW mice, identifying a species-specific cause of this is difficult. A plausible explanation would involve differences in the frequency of Tem cells, which consistently appear to be the main effectors of rapid skin allograft rejection in humanised mice. Other possibilities include differences in the cytokine microenvironments within the different mouse strains, responses of murine cells to xenografted cells and tissues and clinical interpretations of rejection based on differences in skin and fur colour. Of importance, rejection in HSPC-humanised mice occurred more slowly than in PBMC-humanised mice. This is likely to reflect the lower frequency of mature effector lymphocytes in the more balanced HSPC-NBSGW model. It could also suggest varying levels of cellular functionality or engraftment efficiency between the models or the participation of tolerogenic cells.

We also demonstrate the potential for allograft rejection to be accelerated by additive humanisation with MNCs derived from the same UCB unit used for primary humanisation. Accelerated rejection can increase convenience from an experimental standpoint, however this appeared to come at the expense of robust multilineage reconstitution. With reduced B cell and diminished myeloid compartments, the immune cell profiles of HSPC-NBSGW+MNC mice consisted predominantly of memory T cells, aligning more closely with the PBMC-humanised NBSGW model. This may reflect inhibition of B cell, myeloid progenitor ± immature cell reconstitution and survival by engrafting mature MNCs. This assertion would correspond with reports of suppressed HSC proliferation and differentiation following transplantation with syngeneic lymphocytes[355]. The causative mechanism here was homeostatic expansion of allo-reactive T cells, inducing a proinflammatory environment expressing IL-6, TGFβ, TNFα and IFNγ, which suppress haematopoiesis through blocked lineage commitment[356], impaired cell division[357], and induced programmed cell death[358]. Additionally, inflammation can damage cellular components of host stem cell niches[359], and create a bone marrow environment inhospitable for haematopoiesis. To assess this, in future experiments humanisation with MNCs prior to skin allo-transplantation could prevent inflammation-mediated inhibition of haematopoiesis and potentially support it as initially hypothesised[360]. Success could promote accelerated allo-rejection, while preserving *de novo* HSPC-mediated multilineage reconstitution.

In summary, in this chapter we have built upon the observation of human multilineage reconstitution in the HSPC-NBSGW model by demonstrating functionality of each of the major immune cell types in the context of allograft rejection. In doing so, we have identified RNA expression profiles that correlate with upregulated cytotoxicity, antigen presentation and B

cell function. This technically undemanding and functionally representative model may have great utility, widening access to reliable *in vivo* representations of human allo-transplantation.

Chapter 4: Figures

Figure 4.1.1 Engraftment of human skin in HSPC-NBSGW mice.
Engraftment analysis of human skin transplanted onto NOD,B6.SCID *Il2rγ*$^{-/-}$ *Kit*$^{W41/W41}$ (NBSGW) mice. (a) 1 cm^2 split-thickness skin grafts procured from excess abdominal free flap tissue from a single donor were transplanted onto the left flanks of NBSGW mice. Comparator mice did not receive skin grafts. Schematic outline shown (b) Representative photographs demonstrating human skin graft take and healing, as assessed macroscopically bi-daily until day 100. (c) Graphical representations of mouse weights and (d) survival as serially recorded. (e) Representative photographs demonstrating vasculature on graft undersides, assessed at graft harvest; (f) Representative photograph of a failing human skin graft demonstrating central necrosis; (g) Representative photomicrograph of a human skin graft harvested at day 100, stained with hematoxylin and eosin, demonstrating normal skin microarchitecture. The histology shown is representative of 6 stained sections from each of n=3 mice. (h) Representative flow cytometric analysis of human donor 'passenger' leucocytes within murine lymphoid organs and peripheral blood (spleen shown).

(a)

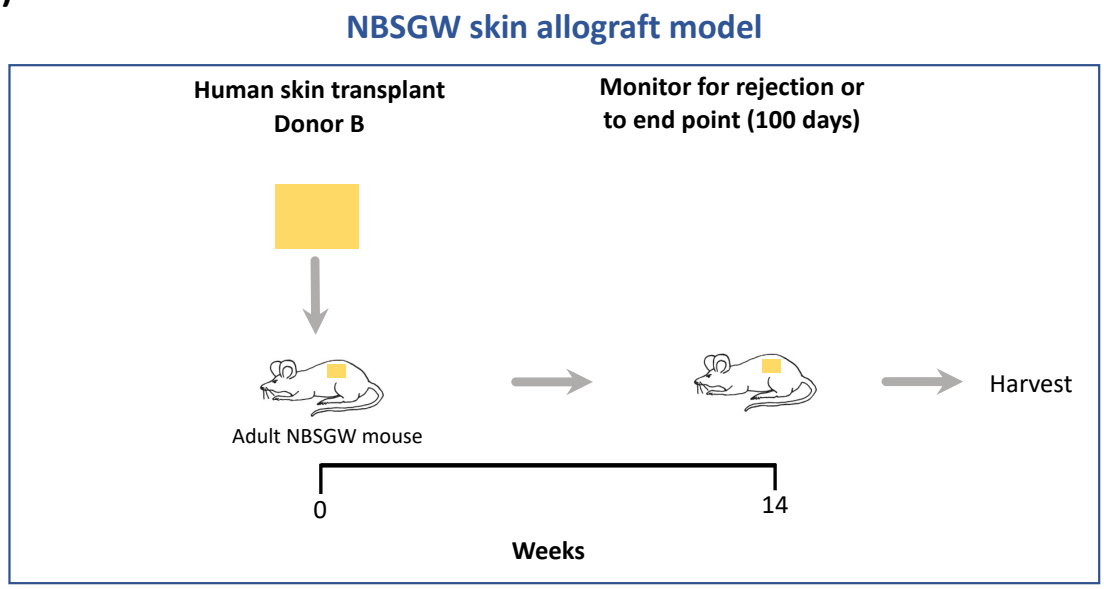
NBSGW skin allograft model
Human skin transplant
Donor B
Monitor for rejection or
to end point (100 days)
Adult NBSGW mouse
Harvest
0
14
Weeks

(b)


Day 10
Day 35
Day 100

(c)

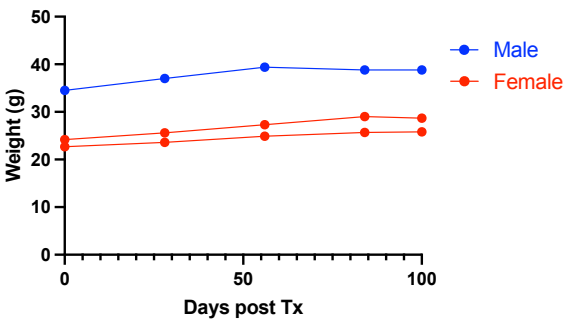

(d)

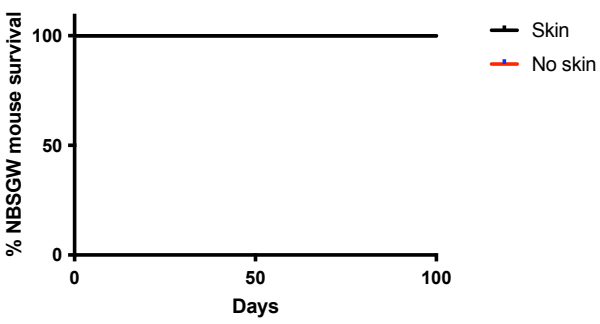

(e)

Day 100

(f)

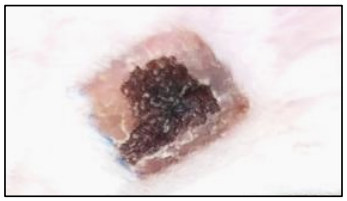

(g)

(h)

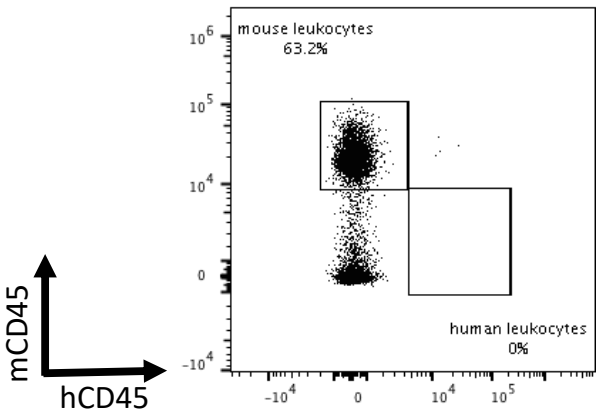

Figure 4.1.2.1 Macroscopic features and time-course of human skin allograft rejection in NBSGW and HSPC-NBSGW mice.

Analysis of rejection of human skin allografts on un-humanised NOD,B6.SCID *Il2rγ*$^{-/-}$ *Kit*$^{W41/W41}$ (NBSGW) and humanised (HSPC-NBSGW) mice.

NBSGW mice were injected intravenously with 200µl IMDM (NBSGW) or 5x10^4 human CD133$^+$ UCB HSPCs suspended in 200µl IMDM (HSPC-NBSGW). In each individual experiment, all mice received cells from the same HSPC donor. 11-13 weeks later 1 cm^2 split-thickness skin grafts procured from excess abdominal free flap tissue from a single donor were transplanted onto the left flank of mice in both groups. Grafts were monitored bi-daily and harvested when they had either developed features of late rejection or reached 100 days (the experimental endpoint) - (a) schematic outline shown. (b) Representative photographs demonstrating macroscopic features of skin graft rejection. (c) Kaplan Meier curves demonstrating survival of human skins transplanted onto NBSGW and HSPC-NBSGW mice; (d) table indicating numbers of mice per group, graft survival, numbers censored and median survival time (MST). Statistical significance was assessed using the Log-rank (Mantel-Cox) test (**, $p<0.01$).

(a) HSPC-NBSGW skin transplant rejection - experimental Plan

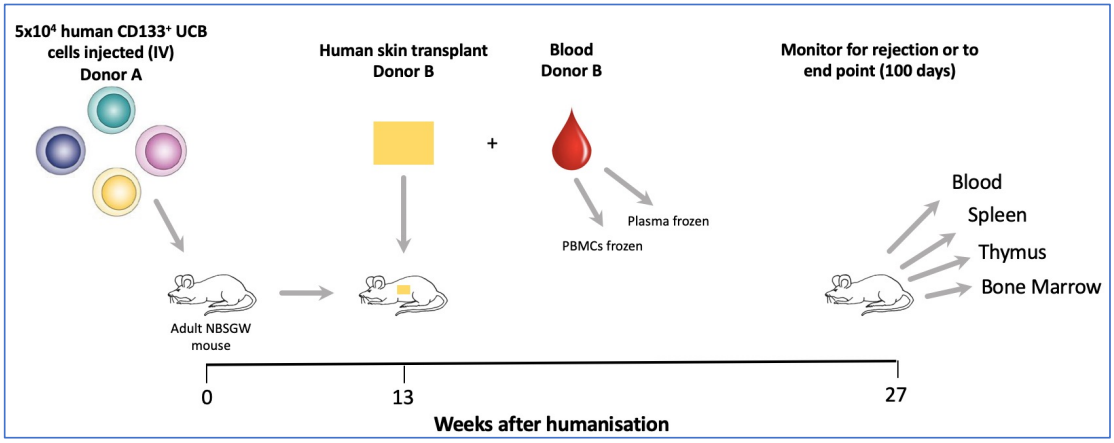

(b) Graft rejection – macroscopic features

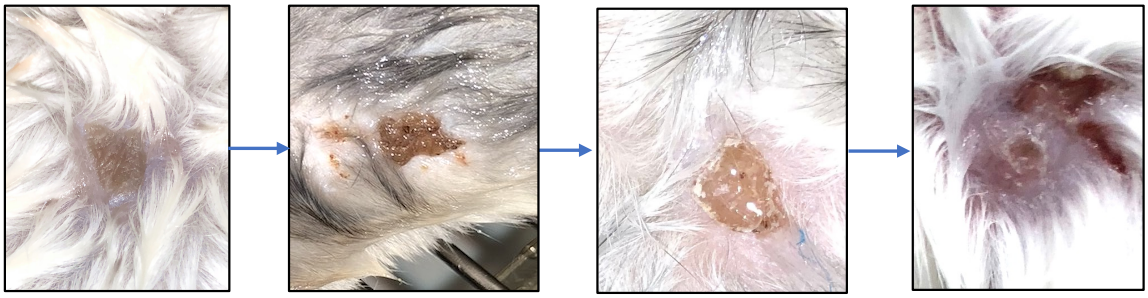

Early post-Tx | Inflammation | Early rejection | Late rejection

(c) Graft rejection – Timeline

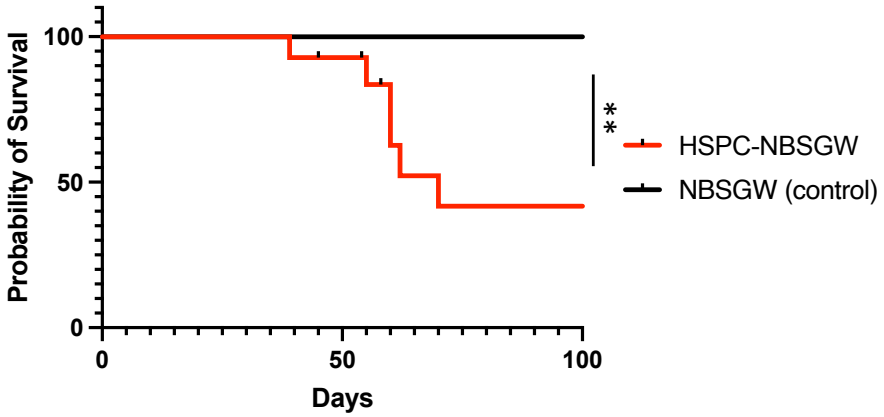

(d)

Group	N	Graft survival (days)	Censored (day)	MST
HSPC-NBSGW	14	39, 55, 60, 60, 62, 70, 100, 100, 100, 100	4 (45, 45, 54, 58)	70
NBSGW	3	100, 100, 100	0	100

Figure 4.1.2.2 Microscopic features of human skin allograft rejection in NBSGW and HSPC-NBSGW mice.
Histological analysis of human skin allografts harvested from un-humanised NOD,B6.SCID *Il2rγ*$^{-/-}$ *Kit*$^{W41/W41}$ (NBSGW) and humanised (HSPC-NBSGW) mice.
Human skin grafts transplanted onto NBSGW and HSPC-NBSGW mice were harvested following development of features of late rejection or at 100 days (the experimental endpoint) in the absence of late features, then snap frozen in OCT. Skins were subsequently cross-sectioned in 6µm slices using a cryostat, air-dried, fixed, stained with haematoxylin and eosin (H&E) and examined microscopically. Data is represented as photomicrographs of H&E-stained histology slides demonstrating (a) un-rejected skin harvested from a NBSGW mouse, (b) unrejected skin harvested from a HSPC-NBSGW mouse, and (c) rejected skin harvested from a HSPC-NBSGW mouse – black arrows indicate blood vessels.

NBSGW – not rejected

(a)

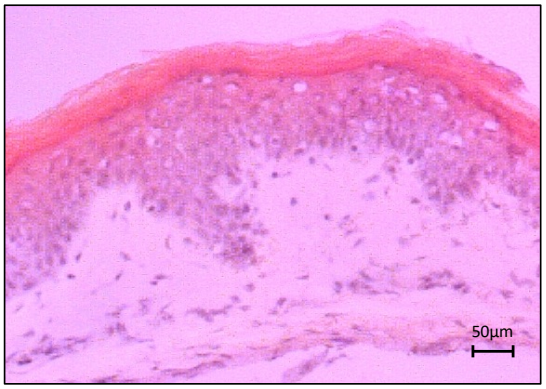

HSPC-NBSGW – not rejected

(b)

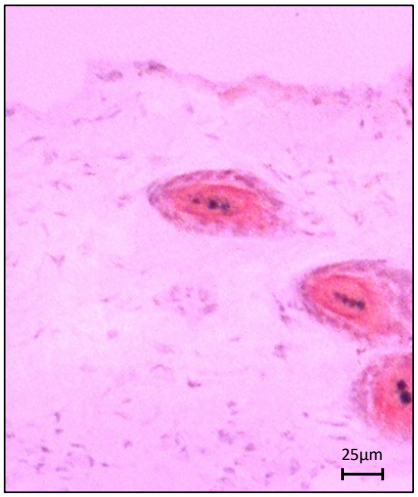

HSPC-NBSGW - rejected

(c)

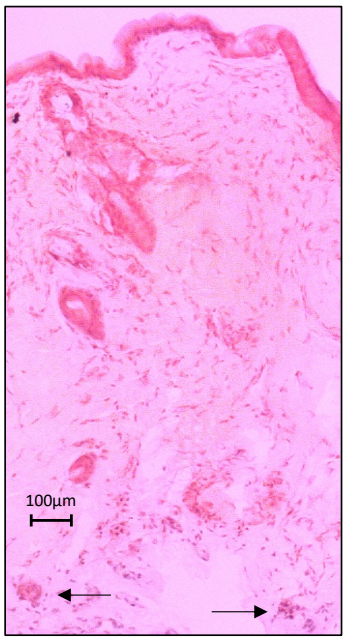

Figure 4.1.3.1 *In vivo* leucocyte responses to allogeneic human skin transplantation in HSPC-NBSGW mice are different in rejection vs non-rejection

Analysis of human leucocyte frequencies in HSPC-NBSGW mice following allogeneic human skin transplantation.

HSPC-NBSGW mice humanised 11-13 weeks earlier with $5x10^4$ human $CD133^+$ UCB HSPCs, received 1 cm^2 split-thickness skin grafts procured from excess abdominal free flap tissue. Grafts were monitored bi-daily and harvested when they had developed features of late rejection or at 100 days (the experimental endpoint). Peripheral blood leucocytes were analysed by flow cytometry for the presence of live human (a) $7AAD^-CD45^+$ leucocytes, (b) $7AAD^-CD45^+CD3^+$ or $7AAD^-CD45^+CD19^+$ or $7AAD^-CD45^+CD33^+$ cells. Frequencies of each cell type shown. Bars indicate means +/- SEM. Statistical significance was assessed using the unpaired T test (ns, $p>0.05$; *, $p<0.05$; **, $p<0.01$; ***, $p<0.001$). Results of 2 independent experiments. In each individual experiment, all mice received HSPCs from the same donor and skin from a single non-autologous donor.

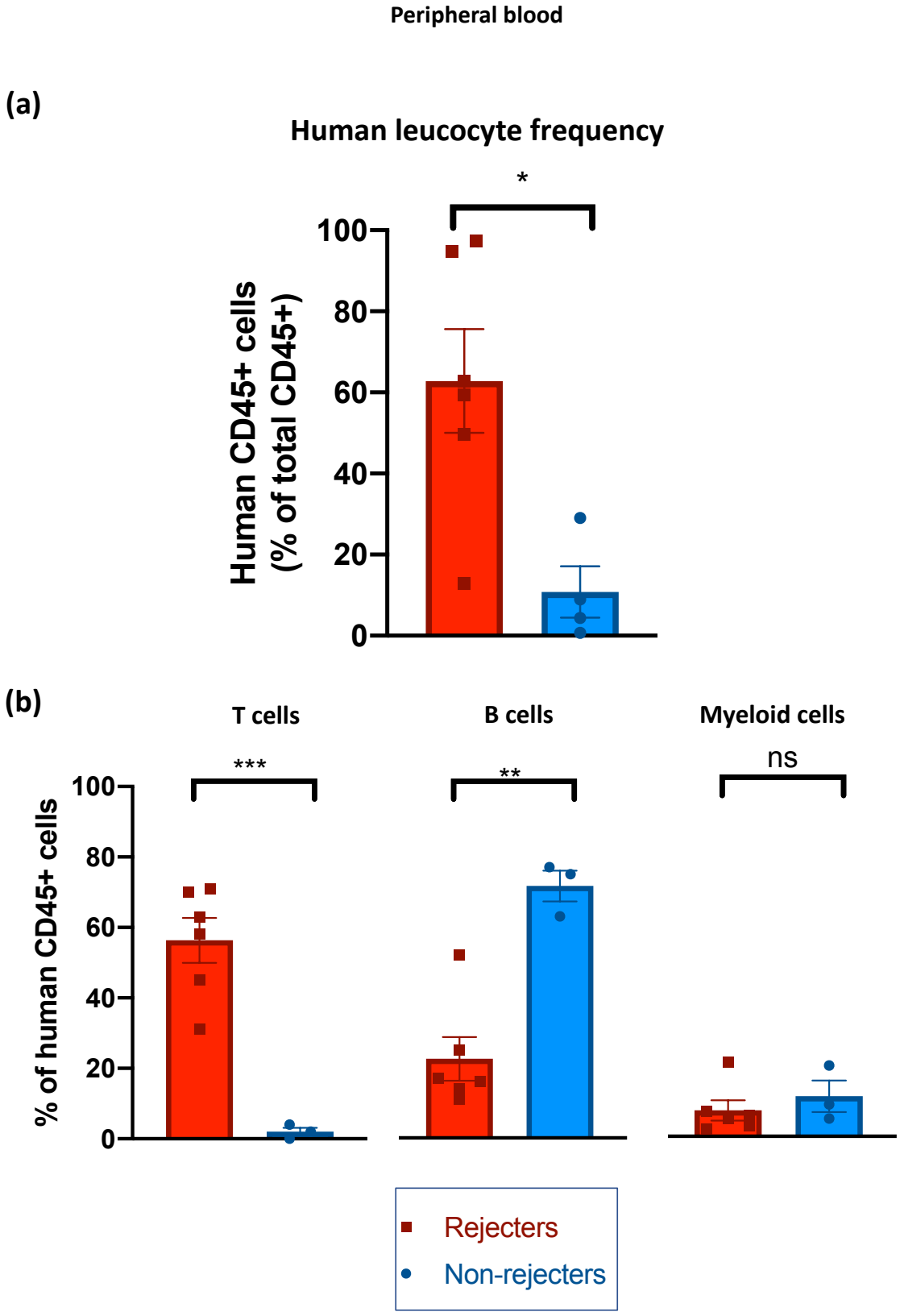
Peripheral blood
(a)
Human leucocyte frequency
*
Human CD45+ cells
(% of total CD45+)
100
80
60
40
20
0
(b)
T cells
B cells
Myeloid cells
***
**
ns
% of human CD45+ cells
100
80
60
40
20
0
Rejecters
Non-rejecters

Figure 4.1.3.2 *In vivo* T cell responses to allogeneic human skin transplantation in HSPC-NBSGW mice – greater numbers of effector memory T cells are seen in rejection.
Analysis of human T cell subset frequencies in HSPC-NBSGW mice following allogeneic human skin transplantation.
HSPC-NBSGW mice humanised 11-13 weeks earlier with $5x10^4$ human $CD133^+$ UCB HSPCs, received 1 cm^2 split-thickness skin grafts procured from excess abdominal free flap tissue. Grafts were monitored bi-daily and harvested when they had developed features of late rejection or at 100 days (the experimental endpoint).
T cells from harvested spleens were analysed by flow cytometry for the presence of live human (a) & (b) $7AAD^-CD45^+CD3^+CD4^+/CD8^+$ cells and (c) & (d) for identifiers of T cell subset.
(a) Data are represented as FACS plots demonstrating the gating strategy and (b)-(d) numbers of each subtype per mouse spleen. Bars indicate median + IQR. Statistical significance was assessed using the two-tailed Mann-Whitney test (*, $p<0.05$).
Tem – Effector memory T cells ; TemRA – T effector memory cells expressing CD45RA ; Tcm – Central memory T cells

(a)

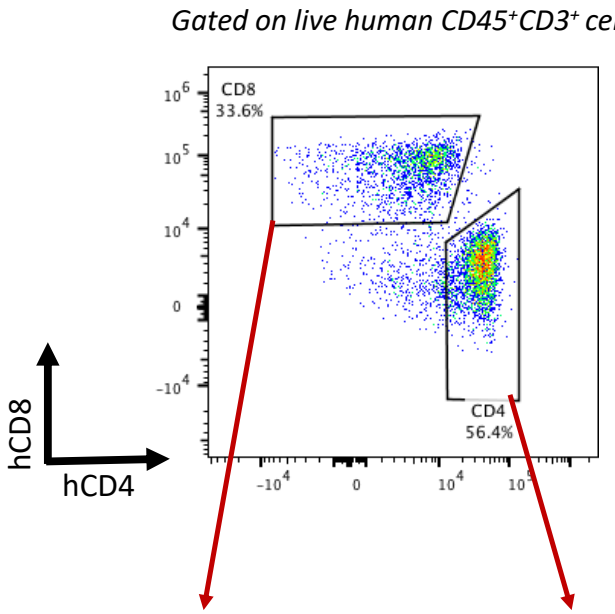
Gated on live human CD45⁺CD3⁺ cells
CD8
33.6%
CD4
56.4%
hCD8
hCD4

(b)

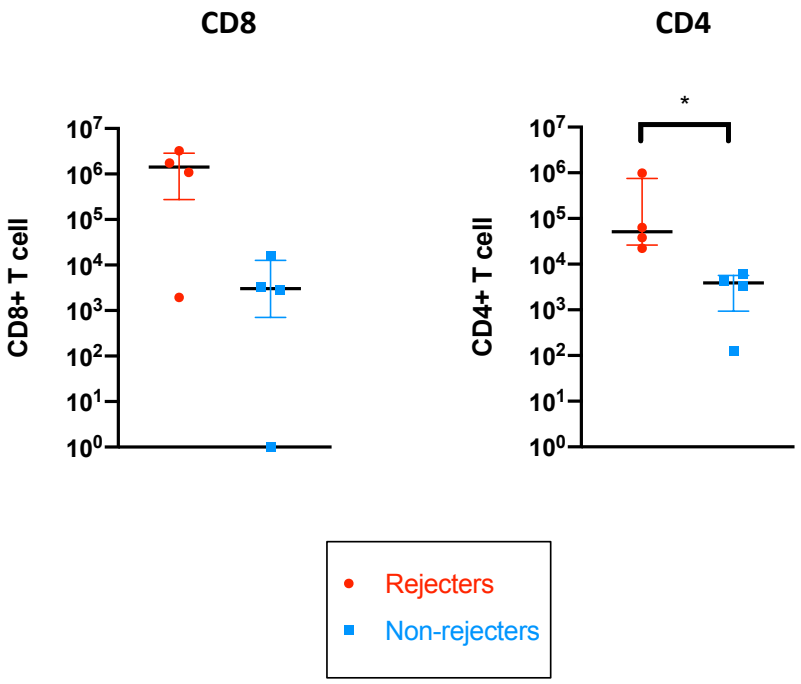
CD8
CD4
CD8+ T cell
CD4+ T cell
*
Rejecters
Non-rejecters

(c)

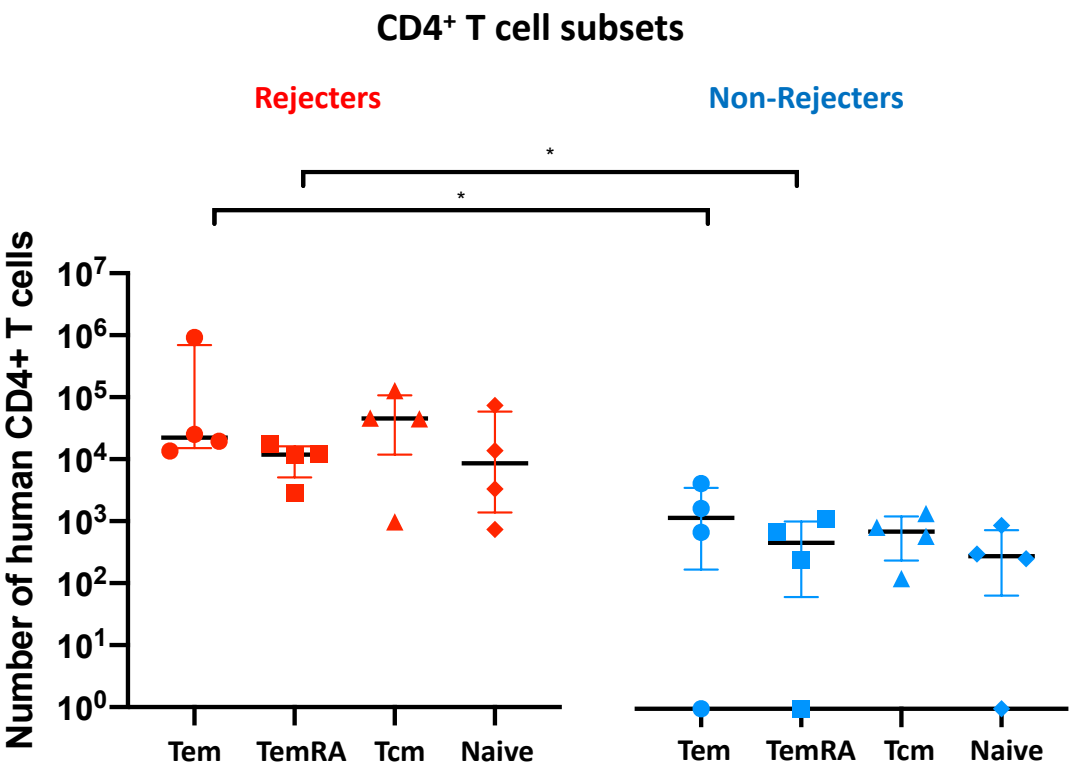
CD4+ T cell subsets
Rejecters
Non-Rejecters
*
*
Number of human CD4+ T cells
10^7
10^6
10^5
10^4
10^3
10^2
10^1
10^0
Tem
TemRA
Tcm
Naive
Tem
TemRA
Tcm
Naive

(d)

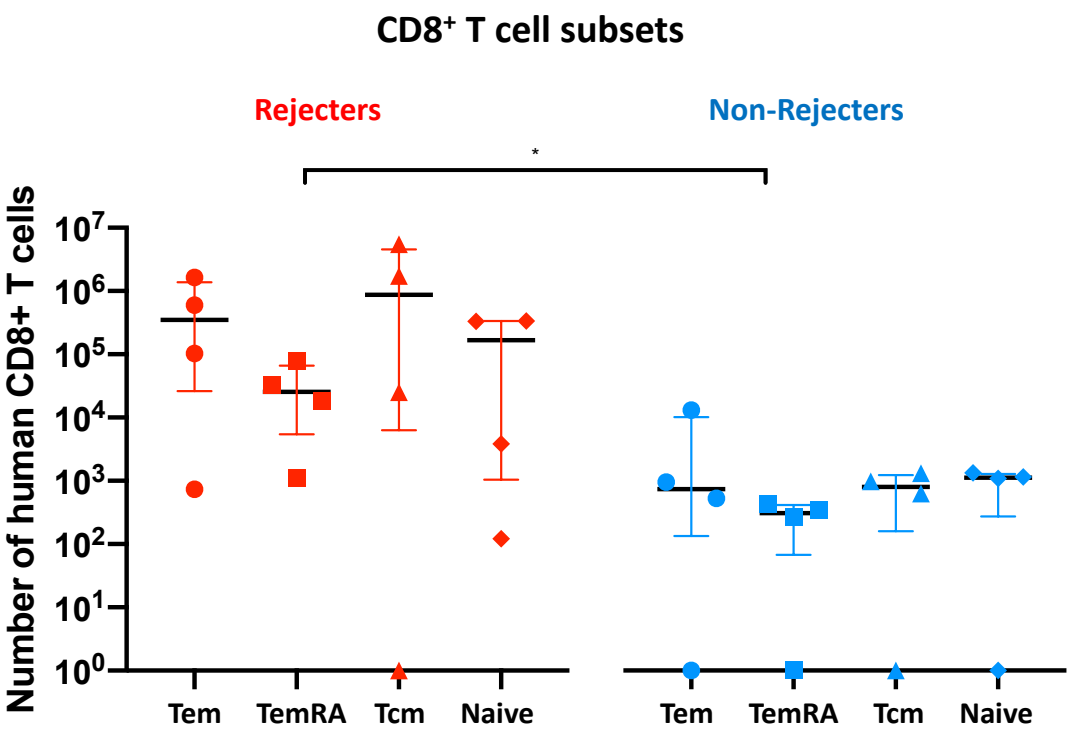
CD8+ T cell subsets
Rejecters
Non-Rejecters
*
Number of human CD8+ T cells
10^7
10^6
10^5
10^4
10^3
10^2
10^1
10^0
Tem
TemRA
Tcm
Naive
Tem
TemRA
Tcm
Naive

Figure 4.1.3.3 *In vivo* B cell responses to allogeneic human skin transplantation in HSPC-NBSGW mice.
Analysis of human B cell subset frequencies in HSPC-NBSGW mice following allogeneic human skin transplantation.
HSPC-NBSGW mice humanised 11-13 weeks earlier with $5x10^4$ human $CD133^+$ UCB HSPCs, received 1 cm^2 split-thickness skin grafts procured from excess abdominal free flap tissue. Grafts were monitored bi-daily and harvested when they had developed features of late rejection or at 100 days (the experimental endpoint).
B cells from harvested spleens were analysed by flow cytometry for the presence of (a) live human $7AAD^-CD45^+CD3^+CD10^-$ (mature) B cells and (b) $7AAD^-CD45^+CD3^+CD10^-CD27^+IgD^-$ (class-switched memory) B cells. Data are represented as FACS plots demonstrating the gating strategy and plots indicating the numbers of each cell subtype per mouse spleen. Bars indicate the median + IQR.

Gated on live human CD45⁺CD19⁺ cells

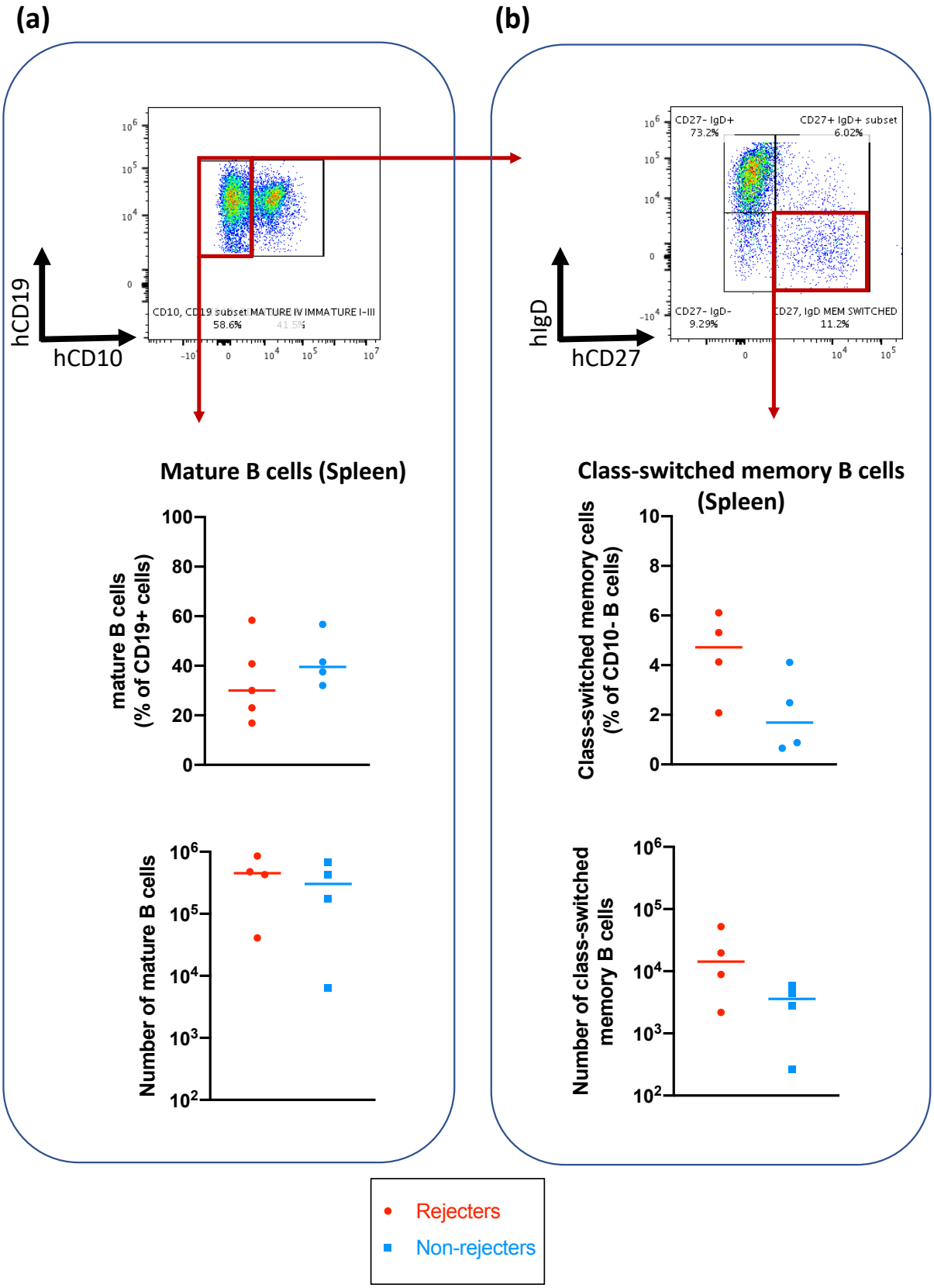

Figure 4.1.3.4 *In vivo* myeloid cell response to allogeneic human skin transplantation in HSPC-NBSGW mice.

Analysis of human myeloid cell subset frequencies in HSPC-NBSGW mice following allogeneic human skin transplantation.

HSPC-NBSGW mice humanised 11-13 weeks earlier with $5x10^4$ human $CD133^+$ UCB HSPCs, received 1 cm^2 split-thickness skin grafts procured from excess abdominal free flap tissue. Grafts were monitored bi-daily and harvested when they had developed features of late rejection or at 100 days (the experimental endpoint).

Myeloid cells within the bone marrow of harvested femurs were analysed by flow cytometry for the presence of live human $7AAD^-CD45^+CD33^+CD11c^-CD14^+$ (monocytes) and $7AAD^-CD45^+CD33^+CD14^-CD11c^+$ (cDCs) cells.

Data are represented as (a) a FACS plot demonstrating the gating strategy, (b) numbers and (c) frequencies of monocytes and cDCs per 2 mouse femurs. Bars indicate the median + IQR. Statistical significance was assessed using the two-tailed Mann-Whitney test (*, $p<0.05$).

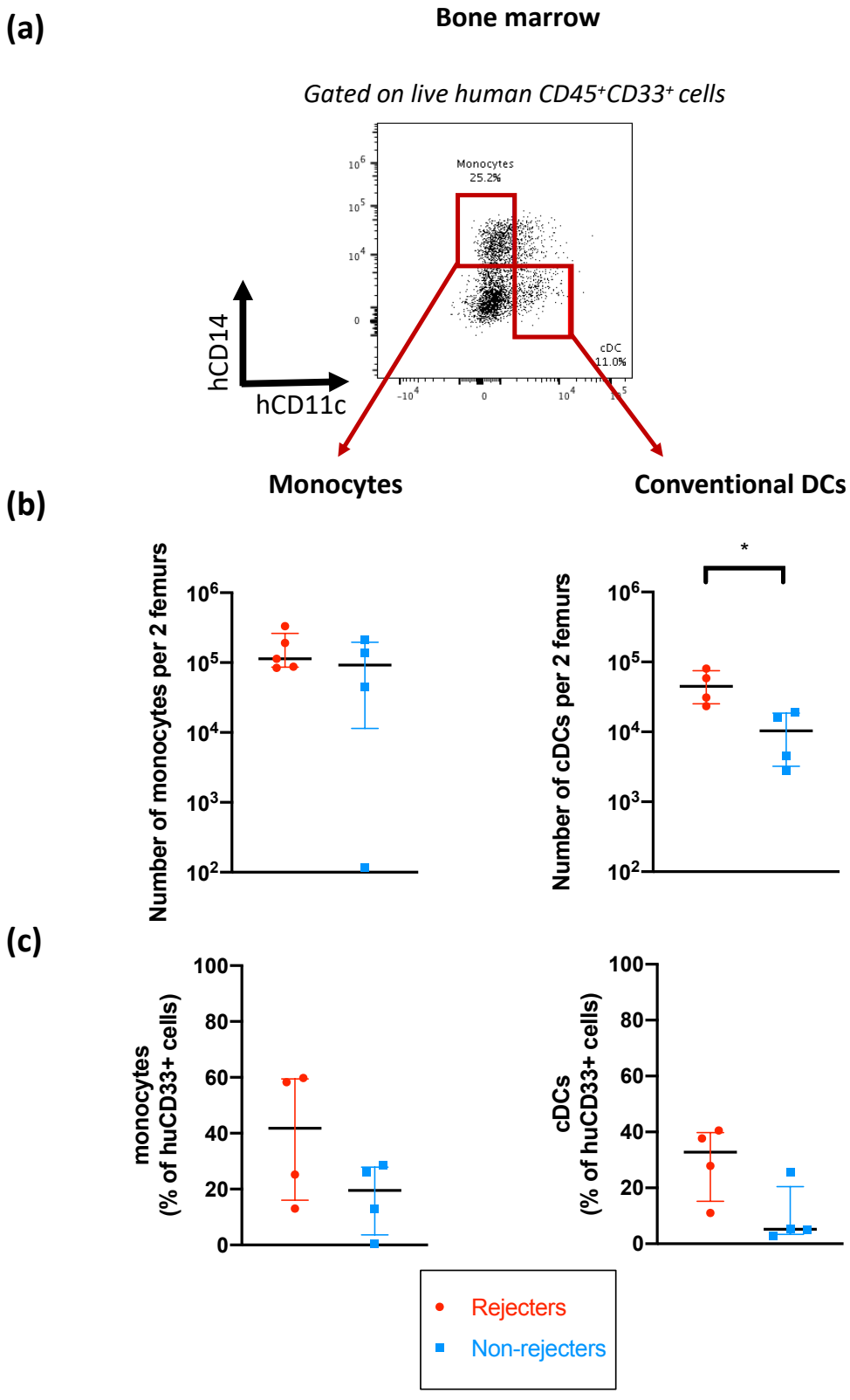
(a)
Bone marrow
Gated on live human CD45+CD33+ cells
Monocytes
25.2%
cDC
11.0%
hCD14
hCD11c
Monocytes
Conventional DCs
(b)
Number of monocytes per 2 femurs
Number of cDCs per 2 femurs
*
(c)
monocytes
(% of huCD33+ cells)
cDCs
(% of huCD33+ cells)
Rejecters
Non-rejecters

Figure 4.1.4.1 *In vitro* function of HSPC-NBSGW leucocytes harvested from mice receiving allogeneic human skin transplants – T cell effector functions can be demonstrated following stimulation.

Analysis of functional capacity of HSPC-NBSGW human T cells harvested from spleens of mice on which allogeneic human skin transplants had rejected.

(a) Following *in vivo* rejection of human skin allografts, $CD3^+$ T cells from harvested spleens were isolated by magnetic bead separation and labelled with violet proliferation dye (VPD). T cells were stimulated for 72-96h by either αCD3/αCD28 beads, allogeneic $CD3^-$ PBMCs (derived from the skin donor), pooled allogeneic 3rd party $CD3^-$ PBMCs, NBSGW bone marrow cells or human bone marrow cells (all irradiated). (b)&(c) HSPC-NBSGW T cell proliferation was assessed flow cytometrically by measuring VPD dilution. (d)&(e) Following stimulation, culture supernatants were harvested and T helper (Th) 1, 2 and 17 cytokine concentrations evaluated by cytometric bead array.

Data are represented as (a)&(d) schematic outlines of the experiments, (b)&(c) FACS histograms indicating VPD dilution of proliferating T cells and (e) cytokine concentrations within culture supernatants. Bars indicate means + SEM. Statistical significance was assessed using the two-tailed unpaired T-test (*, $p<0.05$; **, $p<0.01$; ***, $p<0.001$).

(a) Experimental Plan

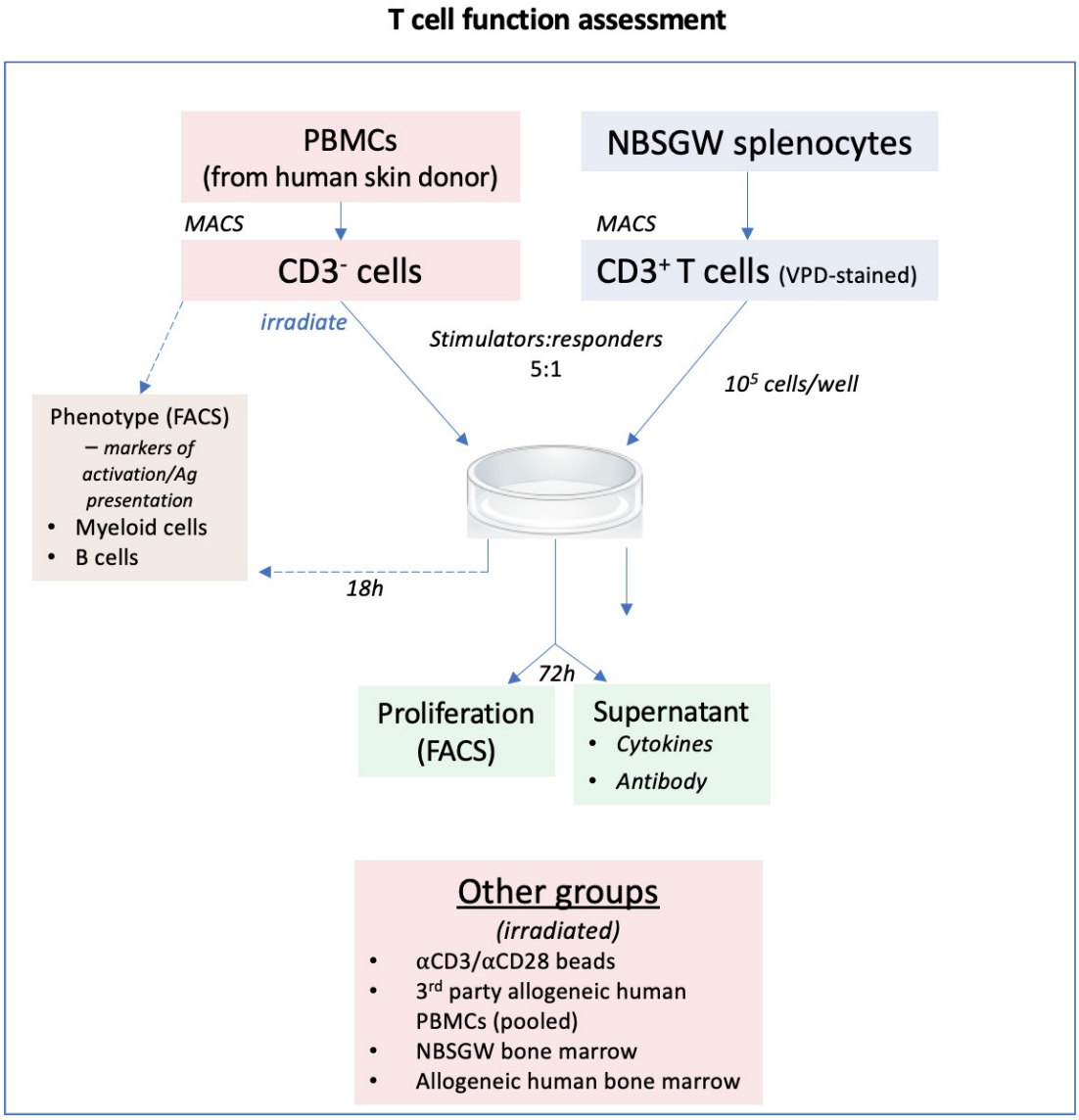

T cell function - proliferation

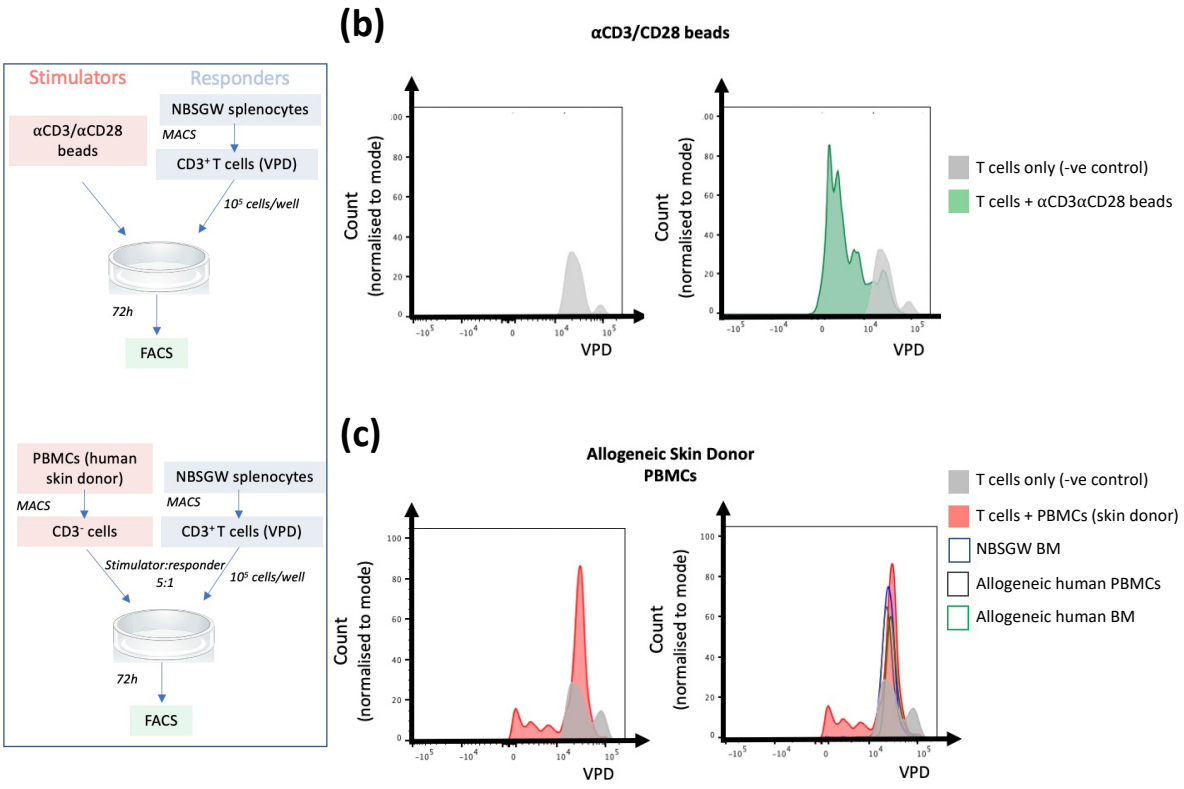

T cell function assessment – cytokine production

(d)

Experimental Plan

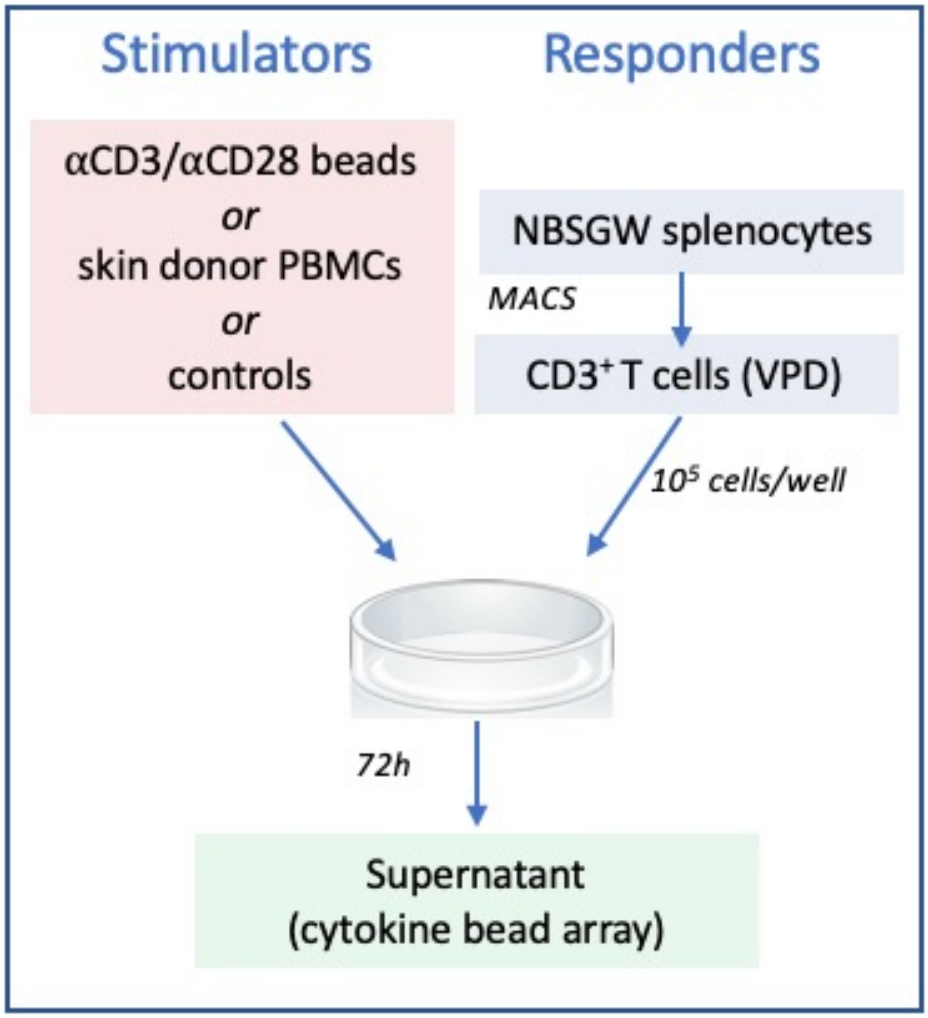

T cell function assessment – cytokine production

(e)

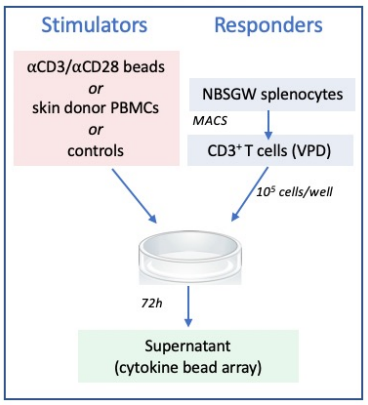

Th1 cytokines

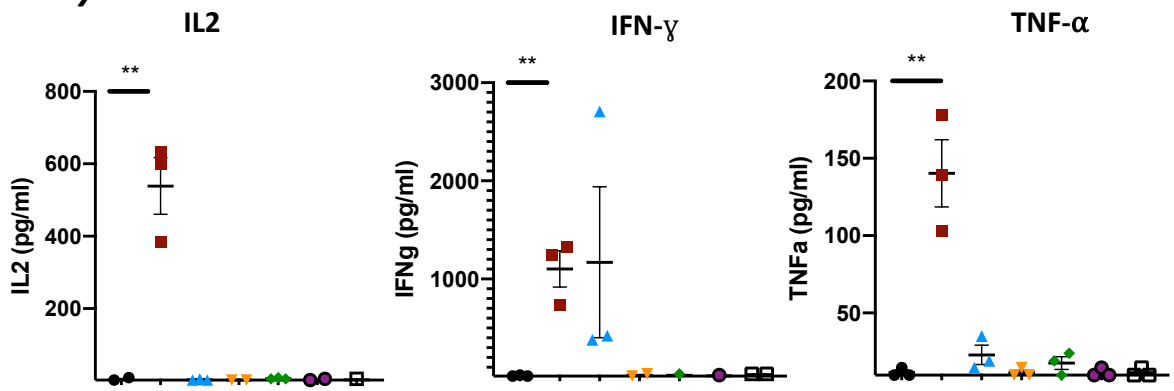

Th2 cytokines

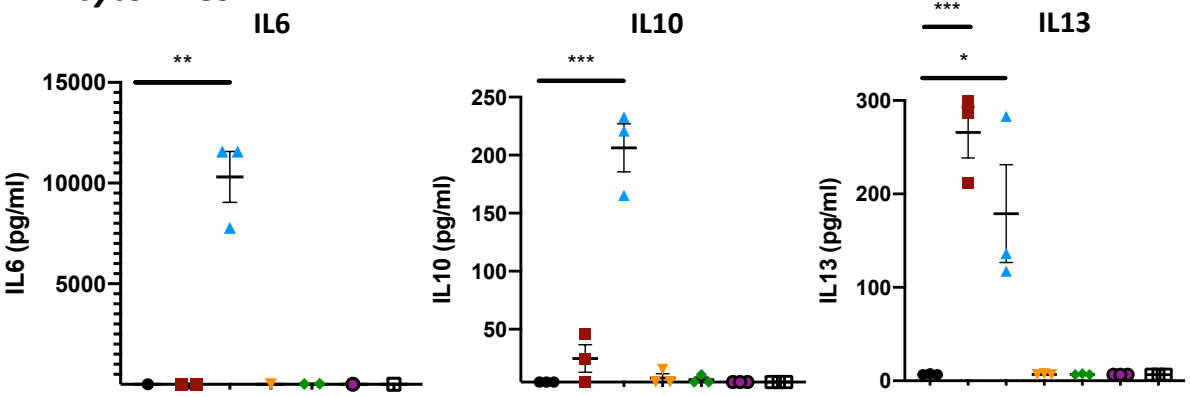

Th17 cytokines

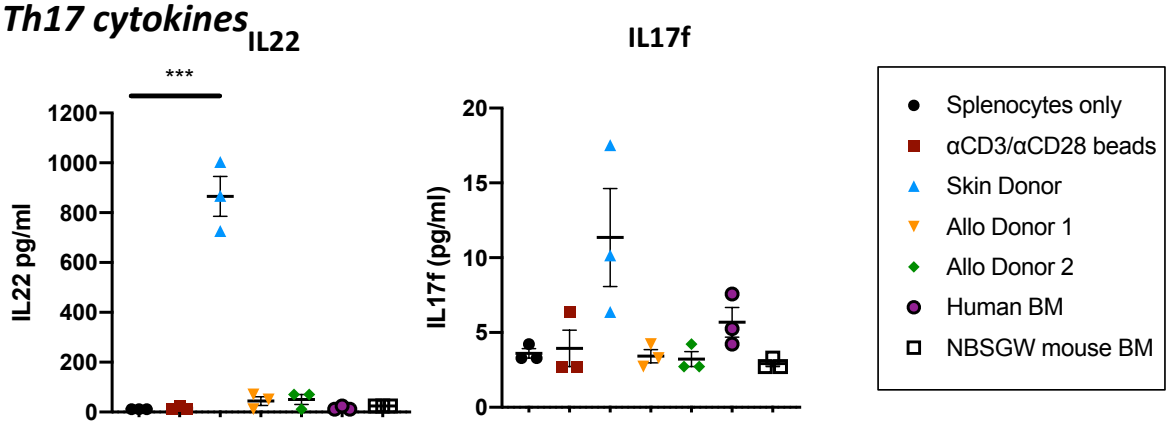

Figure 4.1.4.2 *In vitro* function of HSPC-NBSGW leucocytes harvested from mice receiving allogeneic human skin transplants – B cell effector function.
Analysis of functional capacity of HSPC-NBSGW human B cells harvested from spleens of human skin-allografted mice.
Spleens were harvested when late features of skin graft rejection were macroscopically visible or after 100 days in the absence of rejection. (a)&(b) Surface expression of IgA, IgD, IgM and IgG antibodies were assessed by flow cytometry and compared with PBMCs. (c) Surface expression of IgM and IgG/IgA on mature (CD10-) and immature (CD10+) HSPC-NBSGW B cells and PBMCs – geometric mean fluorescence intensity (MFI) indicated in boxes. (d-f) Human antibody concentrations in the plasma were evaluated by cytometric bead array in 'rejecters' and 'non-rejecters'. (g) Plasma immunoglobulin subtypes were analysed further by cytometric bead array, comparing plasma from NBSGW mice, human plasma, HSPC-NBSGW 'rejecters', HSPC-NBSGW 'non-rejecters', NBSGW and BRG mice humanised 3 weeks earlier with $5x10^6$ human PBMCs (PBMC-humanised NBSGW and PBMC-humanised BRG).
Data are represented as schematic outlines of the experiments (a, d, g), FACS histograms (b, c, e) and plasma immunoglobulin concentrations (f) and geometric mean fluorescence intensity (g). Bars indicate the mean + SEM. Statistical significance was assessed using the two-tailed unpaired T-test (*, $p<0.05$; **, $p<0.01$; ***, $p<0.001$; ****, $p<0.0001$; ns, $p>0.05$).

B cell function – surface antibody expression

a)

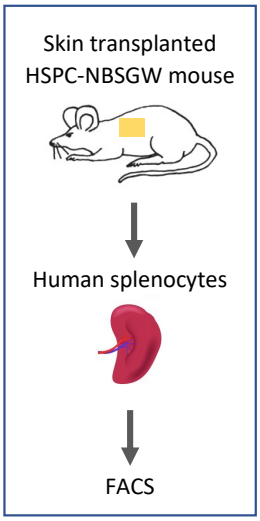

b) *Gated on live hCD45⁺CD19⁺CD10⁻ HSPC-NBSGW splenocytes*

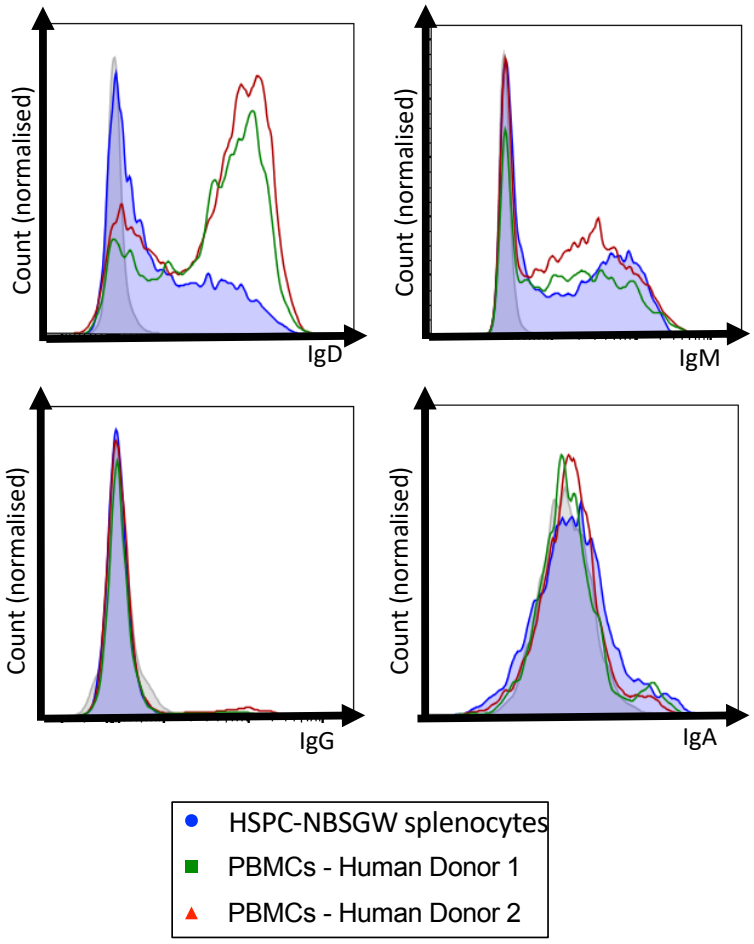

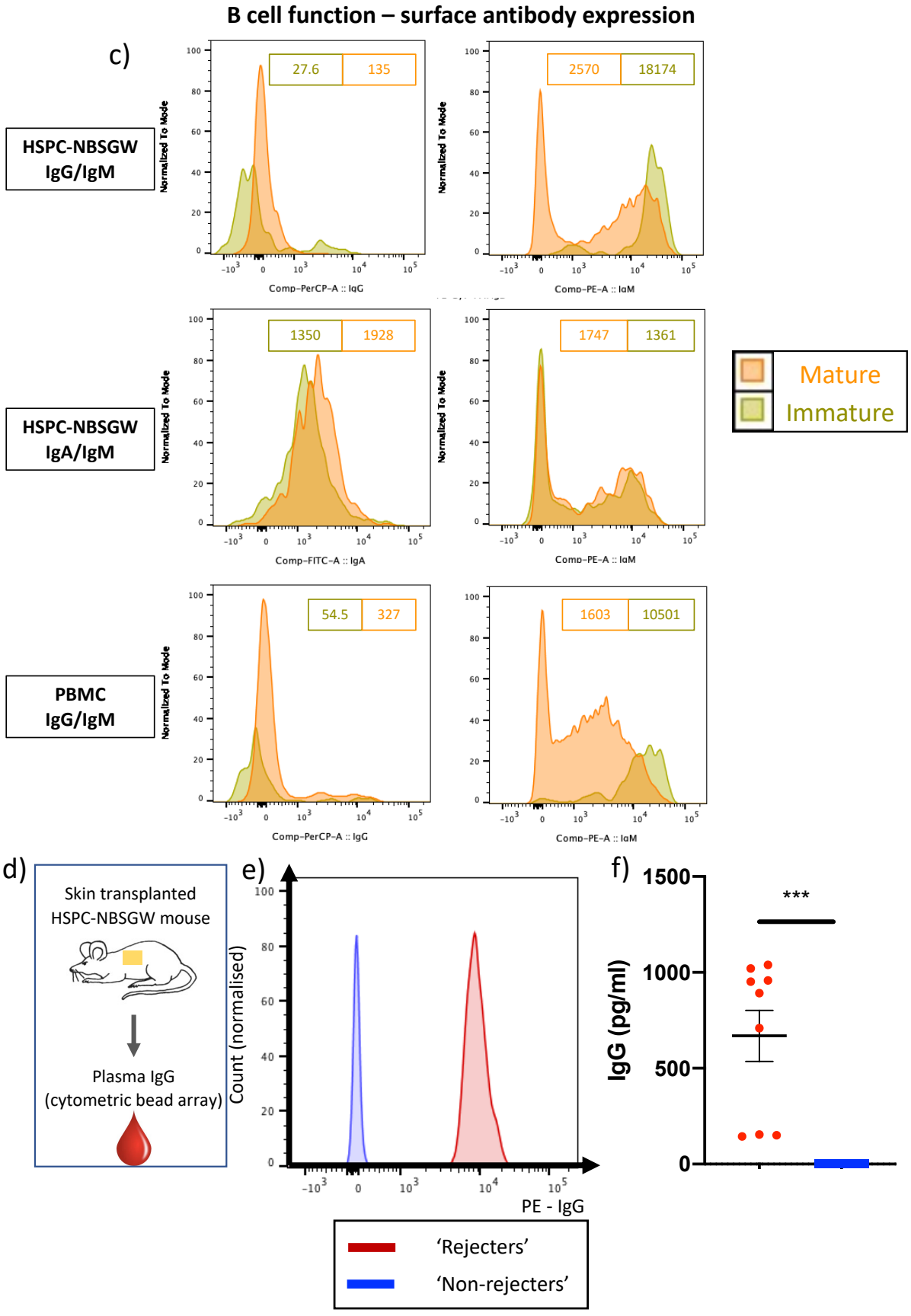
B cell function – surface antibody expression
c)
HSPC-NBSGW IgG/IgM
HSPC-NBSGW IgA/IgM
PBMC IgG/IgM
27.6
135
2570
18174
1350
1928
1747
1361
54.5
327
1603
10501
Normalized To Mode
Comp-PerCP-A :: IgG
Comp-PE-A :: IgM
Comp-FITC-A :: IgA
Mature
Immature
d)
Skin transplanted HSPC-NBSGW mouse
Plasma IgG (cytometric bead array)
e)
Count (normalised)
PE - IgG
'Rejecters'
'Non-rejecters'
f)
IgG (pg/ml)
***

g)

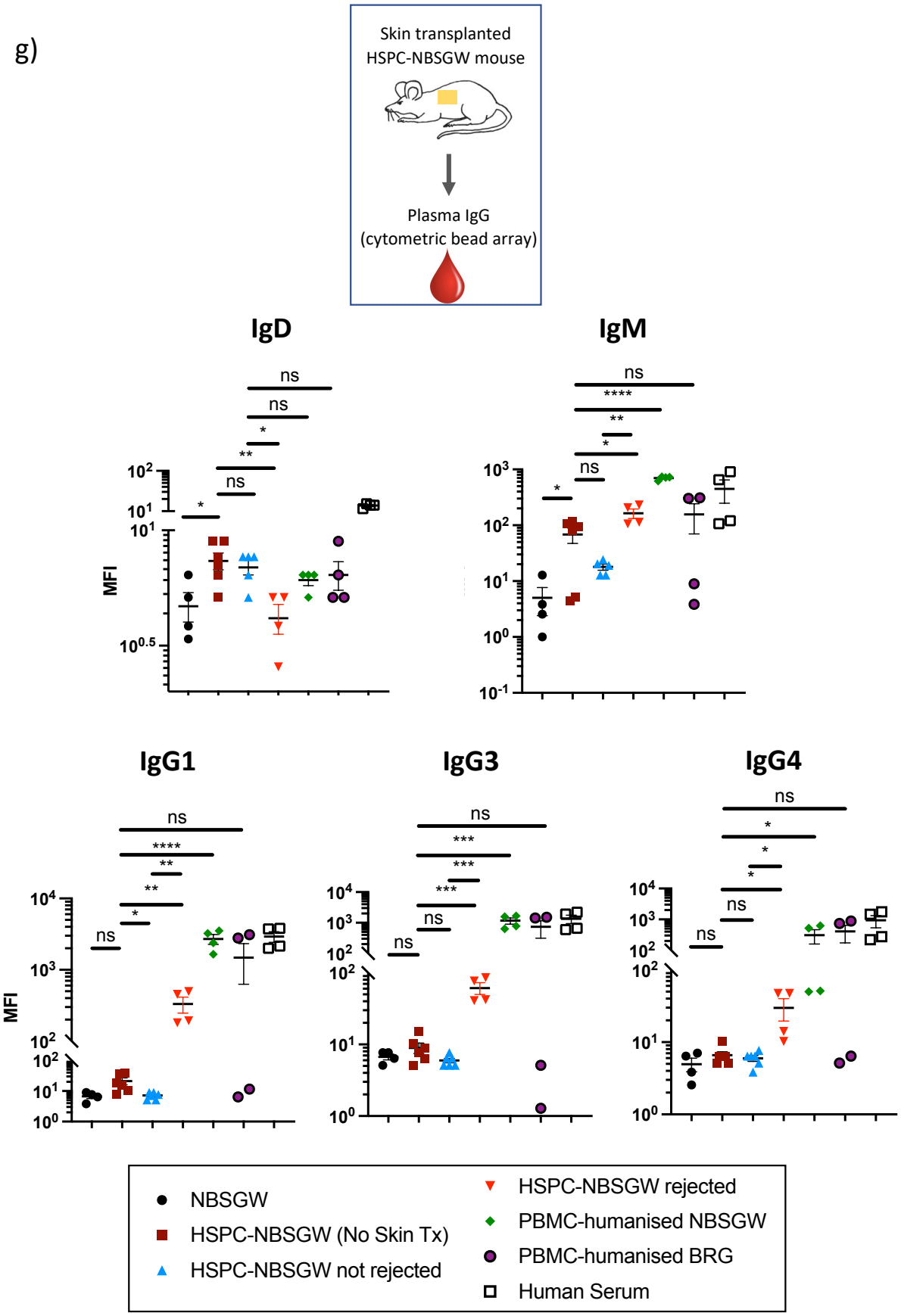
Skin transplanted
HSPC-NBSGW mouse
Plasma IgG
(cytometric bead array)
IgD
IgM
IgG1
IgG3
IgG4
MFI
NBSGW
HSPC-NBSGW (No Skin Tx)
HSPC-NBSGW not rejected
HSPC-NBSGW rejected
PBMC-humanised NBSGW
PBMC-humanised BRG
Human Serum

Figure 4.1.4.3 In vitro function of HSPC-NBSGW leucocytes harvested from mice receiving allogeneic human skin transplants – APCs can be activated and trigger proliferation of allogeneic T cells.

Analysis of the functional capacity of human myeloid cells harvested from the bone marrow of human skin-allografted HSPC-NBSGW mice.

Bone marrow was harvested from femurs of HSPC-NBSGW mice 20-22 weeks after humanisation with $5x10^4$ human $CD133^+$ UCB HSPCs. (a) Human $CD45^+$ leucocytes were isolated by magnetic bead separation (MACS) and co-cultured for 18h with MACS-separated $CD3^+$ T cells from allogeneic human PBMCs. For comparison, human bone marrow-derived and human peripheral blood-derived $CD45^+$ leucocytes were similarly co-cultured with allogeneic $CD3^+$ T cells. Surface expression of (b) activation markers (CD80 & CD86) and (c) antigen presentation molecules (CD1a and HLA-DR) was assessed by flow cytometry. (d-e) Antigen presenting capacity of HSPC-NBSGW APCs was assessed by measuring T cell proliferation (VPD dilution) of allogeneic human PBMCs and HSPC-NBSGW splenic T cells following 5 days of co-culture.

Data are represented as (a)&(d) schematic outlines of the experiments, FACS histograms (b, c & e) and geometric mean fluorescence intensities (MFIs) of (b & c) expressed surface markers or (e) VPD dilution. Bars indicate median values. Statistical significance was assessed using the one-way ANOVA with multiple comparisons (*, $p<0.05$; **, $p<0.01$; ***, $p<0.001$; ****, $p<0.0001$).

(a)

Experimental Plan

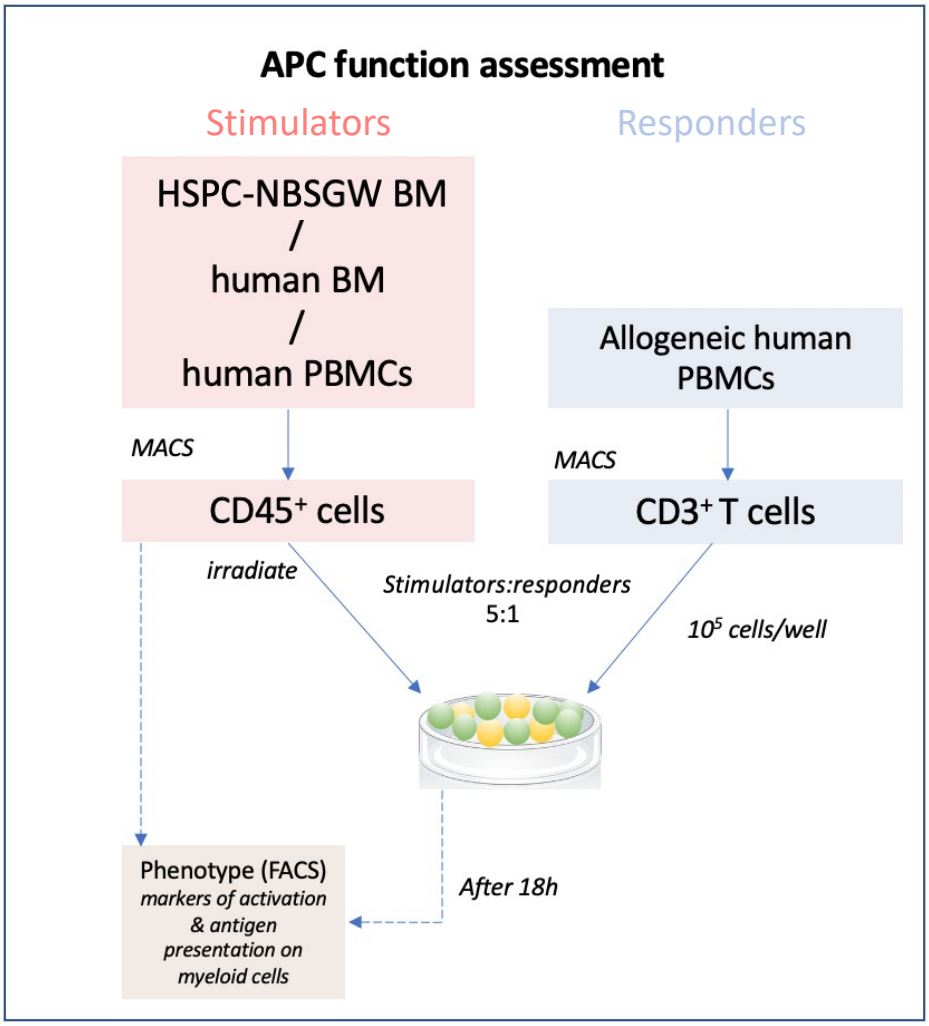

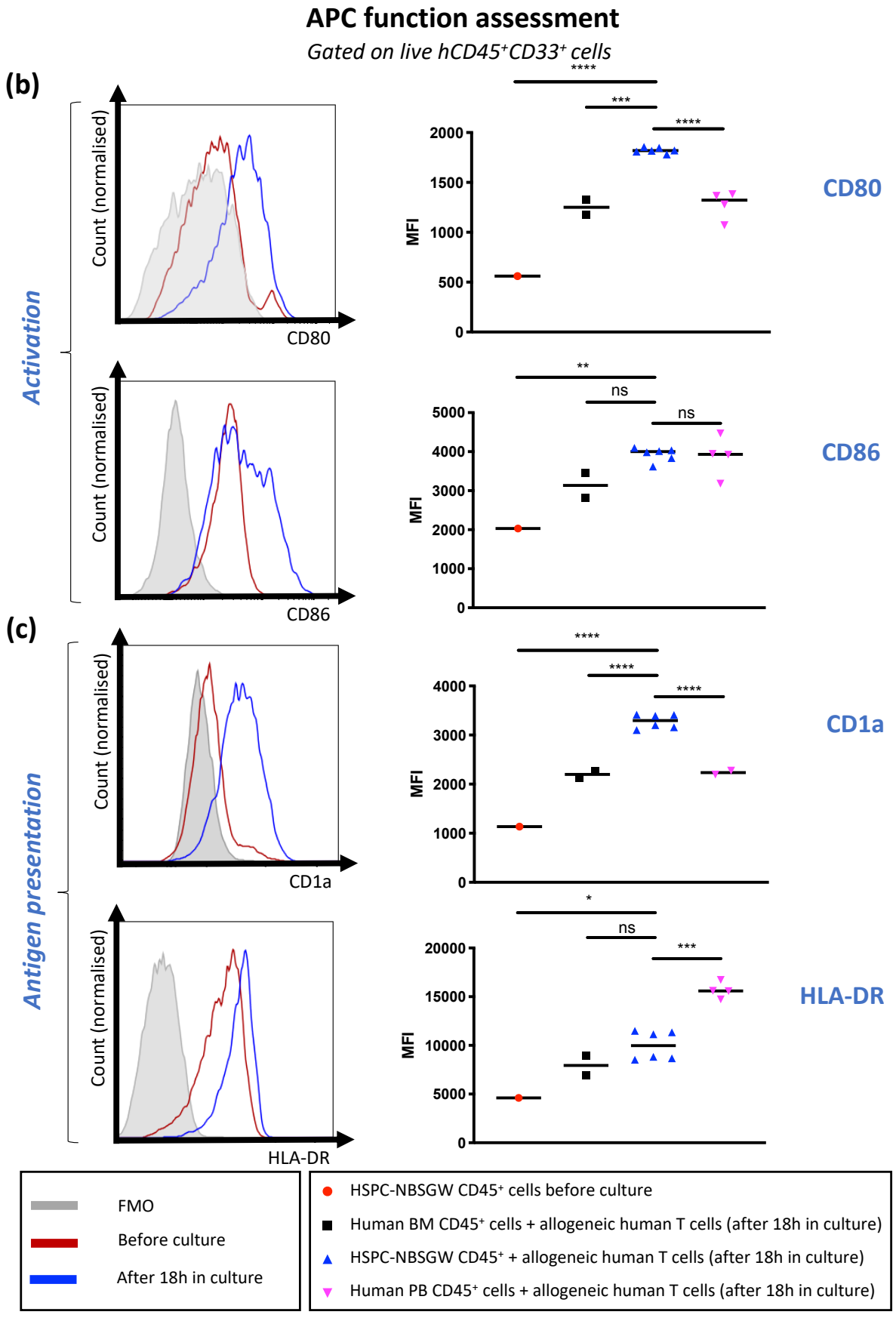
APC function assessment
Gated on live hCD45+CD33+ cells
(b)
Activation
Count (normalised)
CD80
CD86
MFI
CD80
CD86
(c)
Antigen presentation
CD1a
HLA-DR
FMO
Before culture
After 18h in culture
HSPC-NBSGW CD45+ cells before culture
Human BM CD45+ cells + allogeneic human T cells (after 18h in culture)
HSPC-NBSGW CD45+ + allogeneic human T cells (after 18h in culture)
Human PB CD45+ cells + allogeneic human T cells (after 18h in culture)

(d)

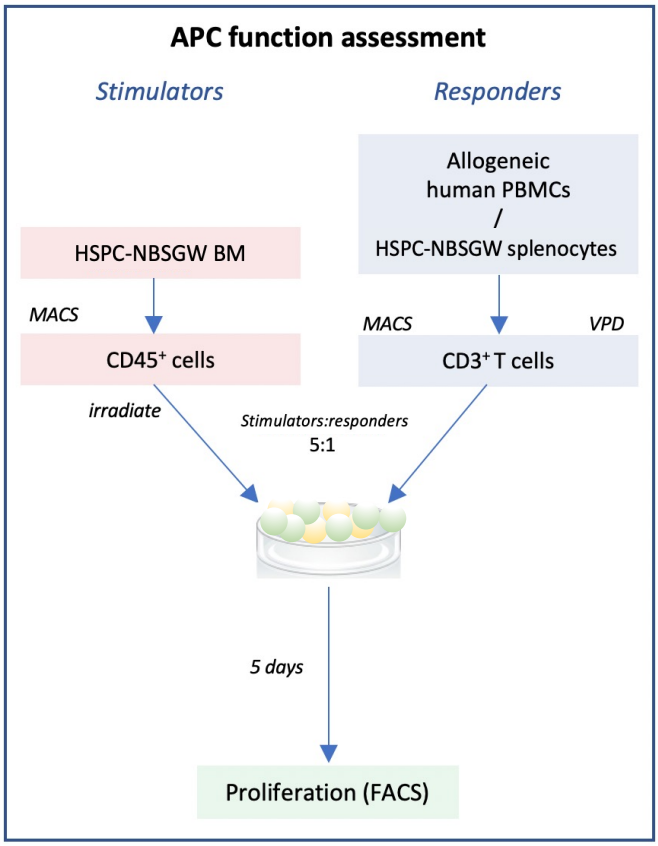

(e) **HSPC-NBSGW CD45⁺ stimulators vs 3rd party allogeneic human T cell responders**

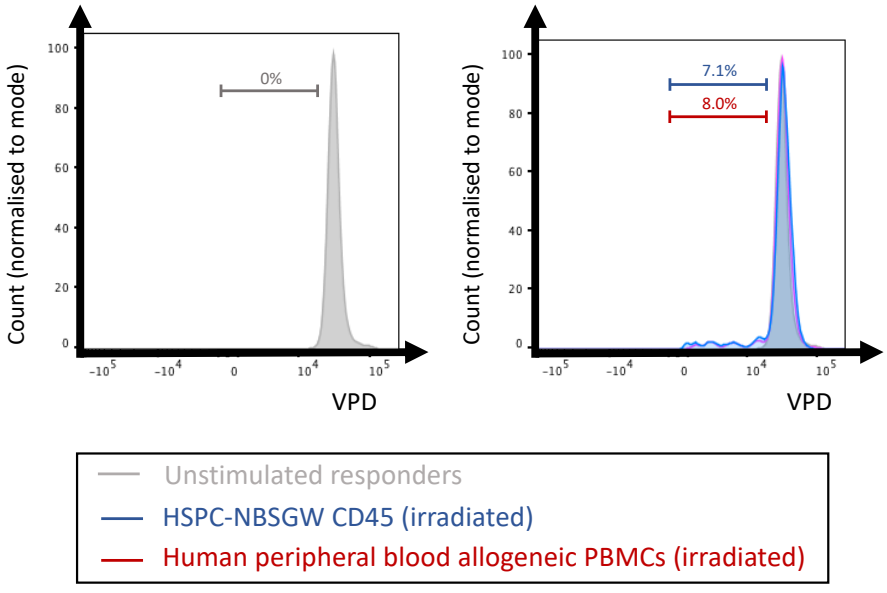

Figure 4.1.4.4 Nanostring mRNA analysis of HSPC-NBSGW spleens and human skin allografts harvested from transplant recipients.
Analysis of spleen and skin mRNA profiles in rejection, non-rejection and control (NBSGW) mouse recipients of human skin allografts.
Spleens and human skin grafts were harvested when late features of skin graft rejection were macroscopically visible or after 100 days in the absence of rejection. RNA was extracted from thawed skin and spleen samples and analysed by Nanostring.
Data are represented as (a & j) Covariate plots comparing the abundance of genes characteristic of leucocytes (a) and macrophages (j) in the different experimental groups; (b) Principal components analysis, plotting the first 4 principal components of gene expression data against each other, with colours delineating the covariates as indicated; (c) Pathway scores heatmap - measuring alterations in gene expression in various immune pathways, which indicate how pathway scores cluster together and change across samples—orange indicates high scores; blue indicates low scores.; (d-i) Heatmaps of normalised data, scaled to give all genes equal variance, generated via unsupervised clustering. Scores are displayed on the same scale via a Z-transformation; (k-m) Volcano plots displaying differential gene expression (log2 fold change) and significance (-log10(p-value)) between the covariates (indicated in blue). Highly statistically significant genes fall at the top of the plot above the horizontal lines (adjusted p values), and highly differentially expressed genes fall to either side. Horizontal lines indicate various False Discovery Rate (FDR) thresholds or p-value thresholds if there is no adjustment to the p-values. Coloured genes indicate resulting p-values below the given FDR threshold; Light and dark grey boxes indicate numbers of significantly upregulated (light) and downregulated (dark) genes; (o&p) Tables indicating properties of genes most significantly upregulated (o) or downregulated (p) in rejected vs non-rejected skins (as in (k)).

(a)

Leucocyte genes expressed in rejection vs non-rejection

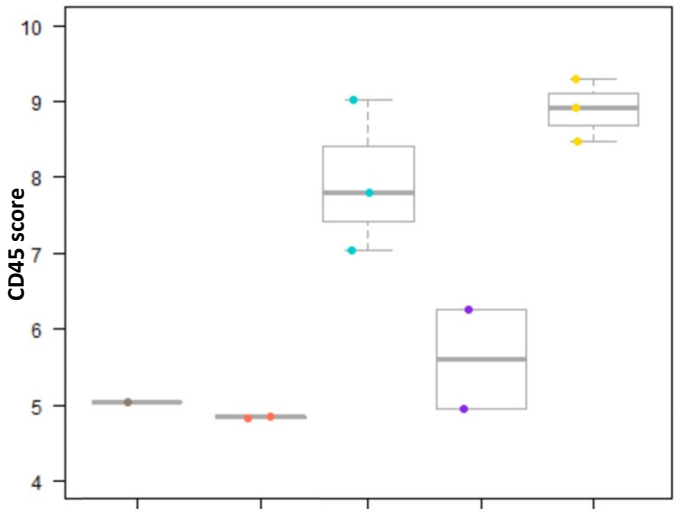

(b)

Principal Components Analysis

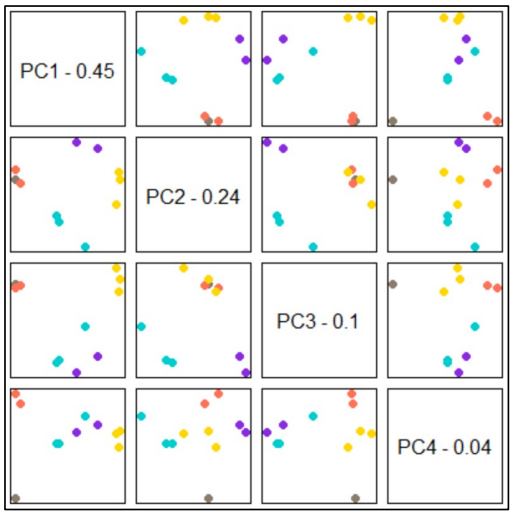

(c)

Immune pathway-related gene expression

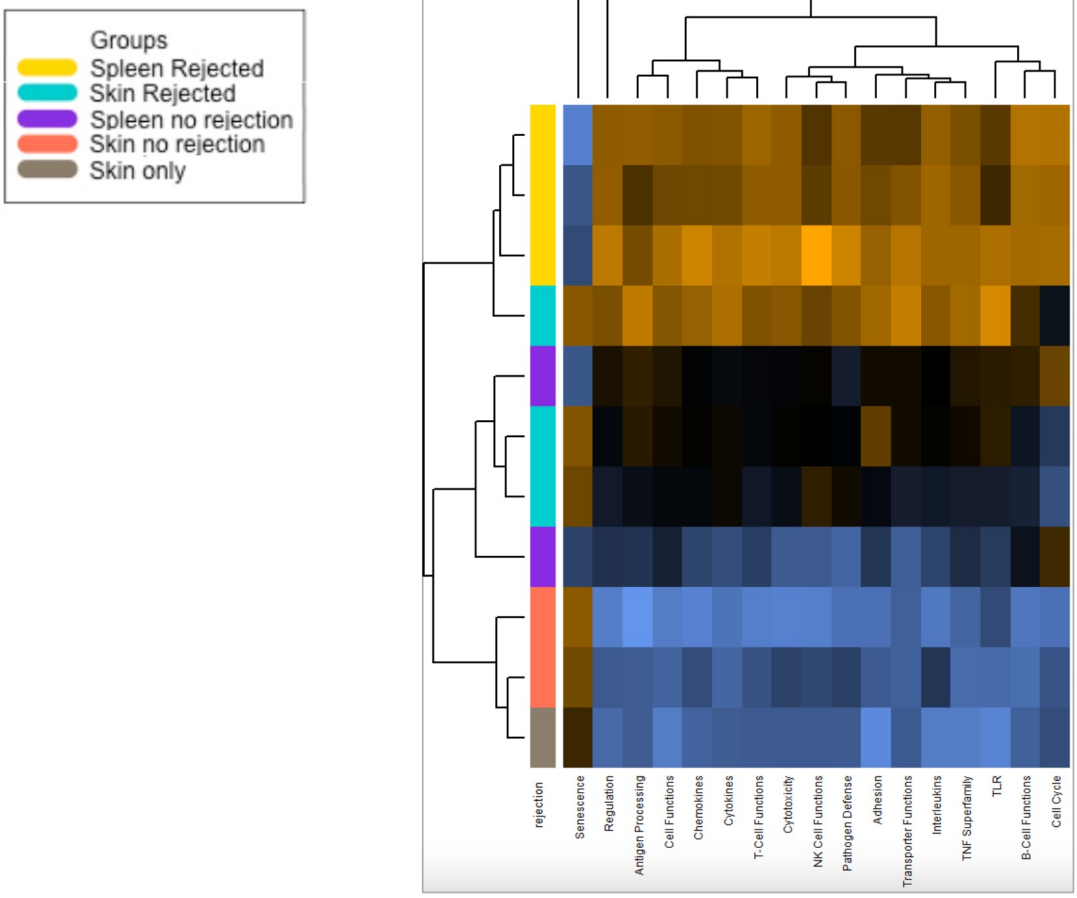

Adaptive immune function

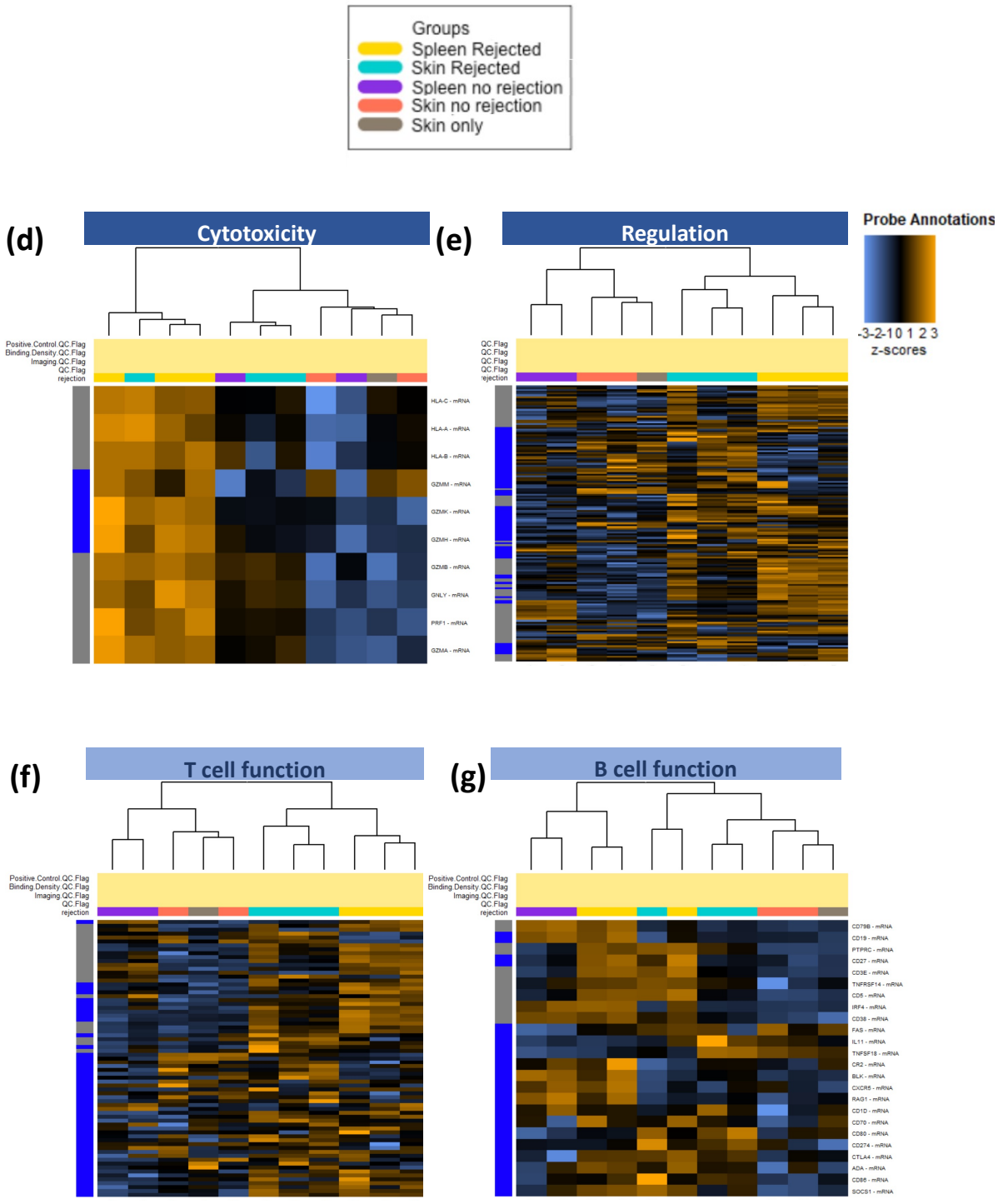

Innate immune function

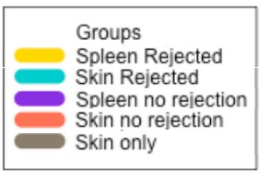

(h) **Antigen processing**

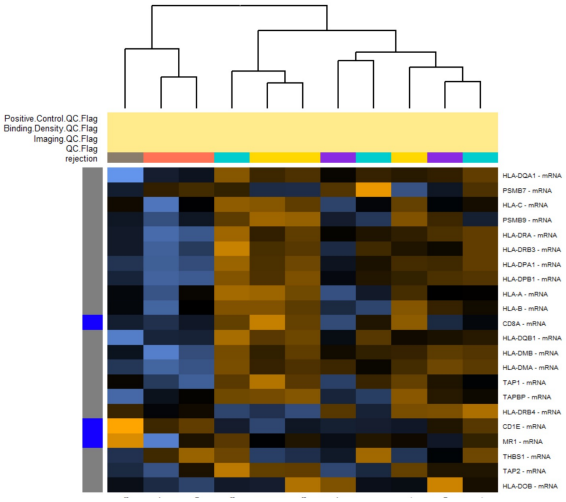

(i) **NK cell function**

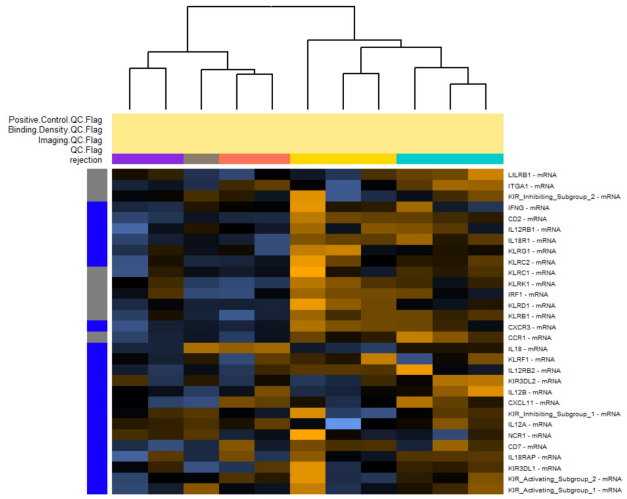

(j) **Macrophage profile**

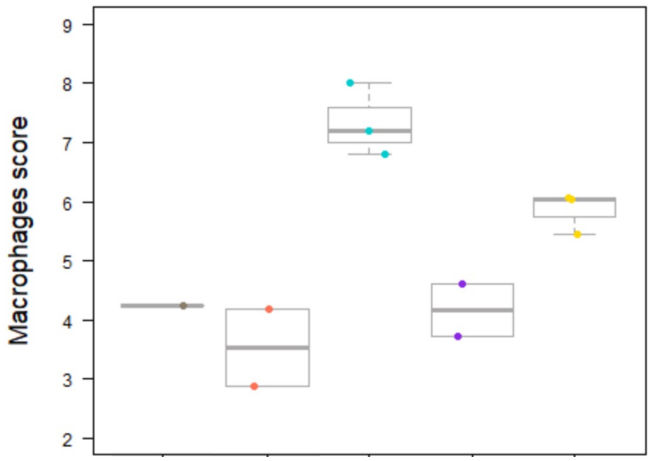

Differential mRNA expression

(k)

Non-rejection (spleen) vs non-rejection (skin)

↑ 26
↓ 9

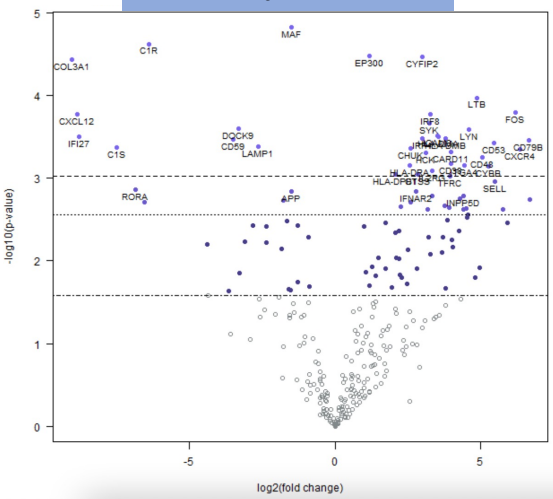

(l)

Rejection (skin) vs Non-rejection (skin)

↑ 15
↓ 1

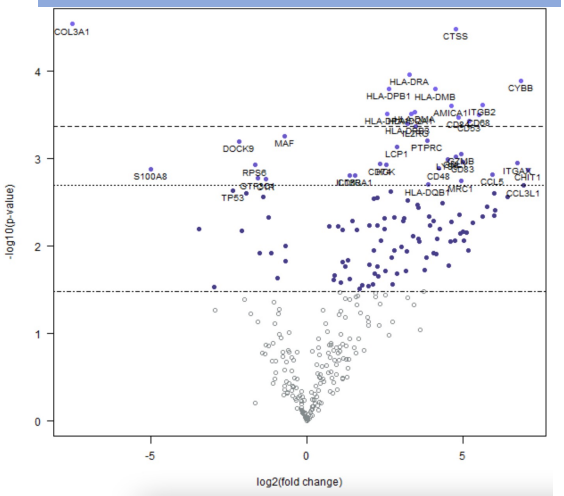

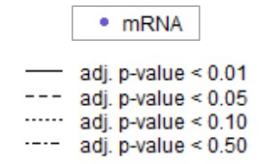

Genes upregulated
Genes downregulated

(m)

Rejection (spleen) vs non-rejection (spleen)

↑ 0
↓ 0

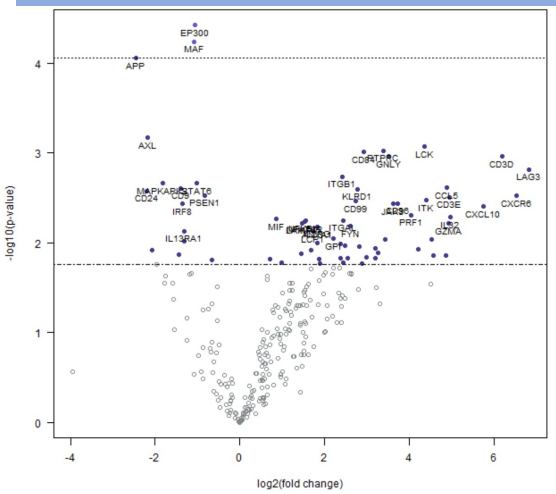

(n) Genes upregulated in rejected skin allografts

Gene	Protein	Function	References	*B.Y.* *p* value
CTSS	Cathepsin S	• Degrades antigenic protein for MHC II presentation • Drives alloimmunity in kidney rejection	Lei, 2020 Halloran, 2017	0.0303
HLA-DRA	HLA Class II, DR Alpha Chain	• Complexes with HLA-DRB & displays antigen peptides on APCs for recognition by TCRs on HLA-DR-restricted $CD4^+$ T cells • Guides ag-specific Th effector function- antibody-mediated response & macrophage activation • Mismatch is an independent risk factor for *de novo* DSAs and T-cell–mediated rejection	Halleck, 2016	0.0482
CYBB	Cytochrome B-245 Beta Chain	• Primary component of the phagocyte microbicidal oxidase system • Expressed by macrophages in biopsies of rejected heart Tx • Upregulated in murine cutaneous GvHD post-HSCT • Potential marker of IFNγ effect in rejecting murine allografts	Halloran, 2018 Sugerman, 2004 Famulski, 2006	0.0482
HLA-DPB1	HLA Class II, DP Beta 1 Chain	• Part of a heterodimer of an alpha (DPA) and a beta chain (DPB), which presents peptides derived from endocytosed extracellular proteins • Strong immunogenicity post-HSCT & effective targets of GvL reactivity • Expression informs risk of GvHD post-matched & mismatched HSCT	Stevanovic, 2012 Herr, 2017 Petersdorf, 2020	0.0482
HLA-DMB	HLA Class II, DM Beta Chain	• Chaperone protein with a critical role in catalysing CLIP release from newly synthesised class II molecules, freeing the peptide binding site for acquisition of antigenic peptides • Associated with AMR in kidney transplantation	In-Wha Kim, 2018	0.0482
ITGB2	Integrin Subunit Beta 2	• Participates in leucocyte adhesion & cell-surface mediated signalling • Combines with ITGAM and ITGAX to form complement receptors 3 & 4 • Overexpressed in kidney Tx TCMR, marking DCs & MΘs	Vonbrunn 2021	0.0482
AMICA1 (JAML)	Adhesion Molecule Interacting With CXADR Antigen 1	• Controls leucocyte migration & activation • Activates gamma-delta T-cells in tissue homeostasis, repair and healing	Verdino, 2011	0.0482
HLA-DMA	HLA Class II, DM Alpha Chain	• Chaperone protein with a critical role in catalysing CLIP release from newly synthesised class II molecules, freeing the peptide binding site for acquisition of antigenic peptides • Allorecognition, T cell proliferation & cytotoxic responses reduced in DMA ko murine heart allograft model • Commonly upregulated in biopsy-based gene expression studies across solid-organ transplantation	Felix, 2000 Chen 2010	0.0482
HLA-DQA1	HLA Class II, DQ Alpha 1 Chain	• Part of a heterodimer of an alpha (DQA) and a beta chain (DQB), which presents peptides derived from endocytosed extracellular proteins • Chronic AMR	Nakamura, 2019 Lee, 2016	0.0482
HLA-DPA1	HLA Class II, DP Alpha 1 Chain	• Part of a heterodimer of an alpha (DPA) and a beta chain (DPB), which presents peptides derived from endocytosed extracellular proteins • AMR in kidney Tx	Goral 2007	0.0482
CD68	CD68	• Expressed by monocytes and tissue macrophages • Localizes to lysosomes and endosomes • Scavenger receptor - clears cellular debris, promotes phagocytosis, and mediates recruitment & activation of MΘs • Associated with kidney Tx ABMR & correlates with severity of TCMR	Bergler 2016	0.0482
CD84	CD84	• Signalling lymphocyte activation molecule (SLAM) family member • Innate & adaptive signalling • Acute & chronic AMR	Chong, 2020	0.0482
CD53	CD53	• Transduction of CD2-generated signals in T & NK cells • Expressed in kidney Tx TCMR • May shift NK cell responses from effector function toward proliferation	Liu, 2019	0.049
HLA-DRB3	HLA Class II, DR Beta 3 Chain	• Only present in a subset of individuals • Complexes with HLA-DRA & displays antigen peptides on APCs for recognition by TCRs on HLA-DR-restricted $CD4^+$ T cells • Associated with formation of DSAs in kidney Tx AR	Habets, 2018	0.0492
IL2RG	Interleukin 2 Receptor Subunit Gamma	• Important signalling component of interleukin receptors, including -2, -4, -7 and -21 • Overexpressed in liver Tx rejection	Inkinen, 2005 Spivey, 2011	0.0492

(o) Genes downregulated in rejected skin allografts

Gene	Protein	Function	References	*B.Y.* *p* value
COL3A1	Collagen type 3 alpha 1	• Encodes type 3 collagen – increased expression in AR kidney biopsies • Upregulated in cardiac allograft rejection • Source of collagen in cardiac fibrosis in human cardiac allografts • Pro-fibrotic in small intestine rejection	Ling 2010 Christopher 2003 Pichler 2012 Hünerwadel 2018	0.0303

Figure 4.1.5 NBSGW innate cellular responses to human HSPCs and allogeneic skin transplantation.

Analysis of murine leucocyte frequencies and activation status in un-humanised NOD,B6.SCID *Il2rγ*$^{-/-}$ *Kit*$^{W41/W41}$ (NBSGW) and humanised (HSPC-NBSGW) mice which did and did not receive allogeneic human skin transplants.

Spleens from NBSGW mice, and HSPC-NBSGW mice ± human skin allografts were harvested at the time of skin allograft rejection or 20-22 weeks post-humanisation (for non-skin grafted mice) and the equivalent time point (NBSGW mice). Thawed Spleens were analysed by flow cytometry for markers of murine monocytes/neutrophils/eosinophils 7AAD^{-} mCD45^{+}mGR-1^{+}mCD11b^{+}, myeloid DCs 7AAD^{-}mCD45^{+}mCD11b^{+}mCD11c^{+}, lymphoid DCs 7AAD^{-}mCD45^{+}mCD11b^{-}mCD11c^{+}, 7AAD^{-}mCD45^{+}mF4/80^{+}mCD11b^{+}, and expression of the activation marker mCD80.

Data are represented as (a-c) FACS plots demonstrating gating strategies, with corresponding frequencies of each cell subtype, and (d) a FACS histogram and geometric mean fluorescence intensities of mCD80 expression. Bars indicate median values. Statistical significance was assessed using the one-way ANOVA with multiple comparisons (*, $p<0.05$; ns, $p>0.05$).

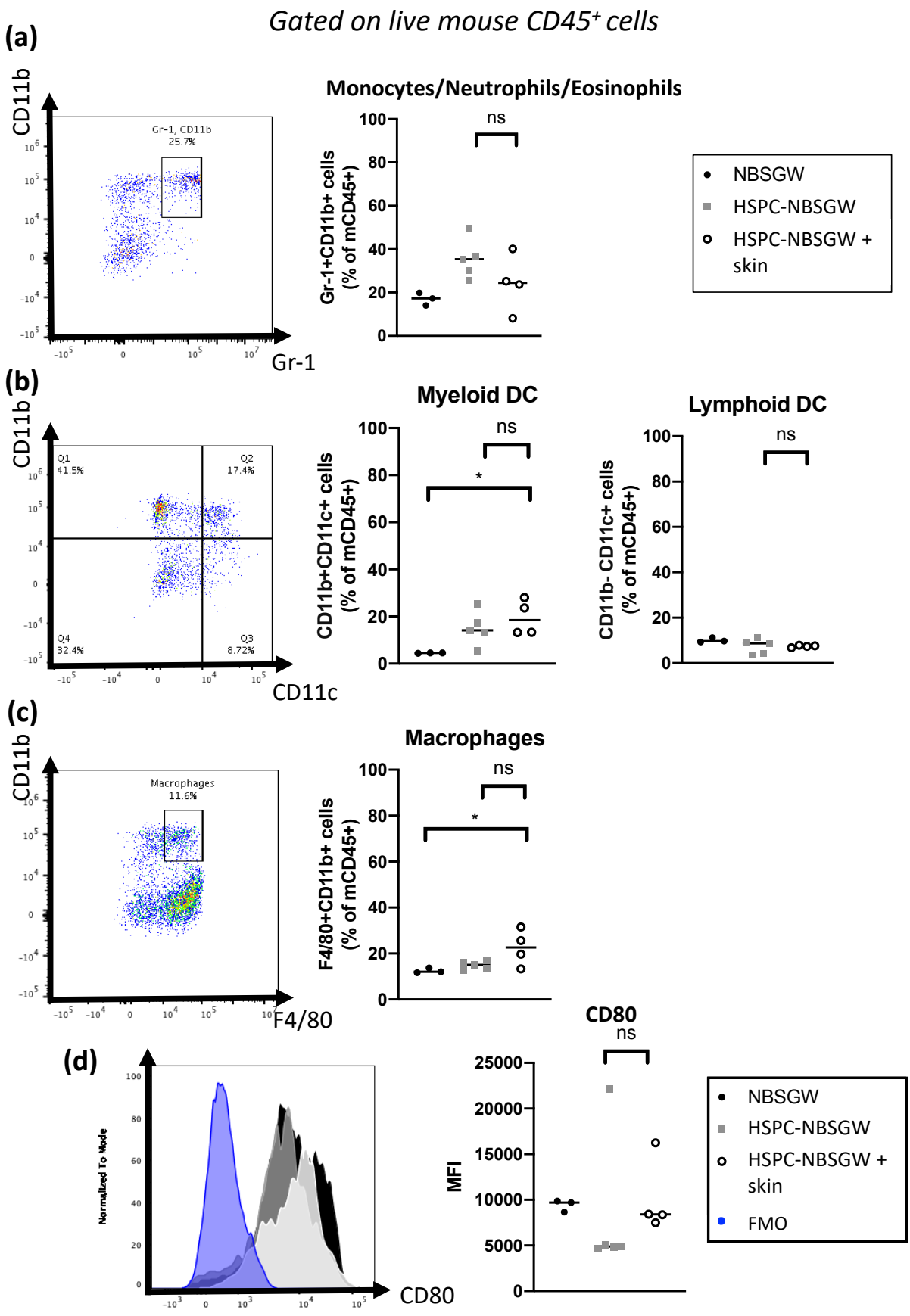
Gated on live mouse CD45+ cells
(a)
CD11b
Gr-1, CD11b
25.7%
Gr-1
Monocytes/Neutrophils/Eosinophils
Gr-1+CD11b+ cells
(% of mCD45+)
ns
NBSGW
HSPC-NBSGW
HSPC-NBSGW + skin
(b)
CD11b
Q1
41.5%
Q2
17.4%
Q4
32.4%
Q3
8.72%
CD11c
Myeloid DC
CD11b+CD11c+ cells
(% of mCD45+)
ns
*
Lymphoid DC
CD11b- CD11c+ cells
(% of mCD45+)
ns
(c)
CD11b
Macrophages
11.6%
F4/80
Macrophages
F4/80+CD11b+ cells
(% of mCD45+)
ns
*
(d)
Normalized To Mode
CD80
CD80
MFI
ns
NBSGW
HSPC-NBSGW
HSPC-NBSGW + skin
FMO

Figure 4.1.6 Allogeneic human skin transplant rejection in HSPC-NBSGW mice vs PBMC-humanised NBSGW mice and PBMC-humanised BRG mice.
Comparison of human skin allograft rejection on NOD,B6.SCID *Il2rγ*$^{-/-}$ *Kit*$^{W41/W41}$ (NBSGW) mice humanised with UCB HSPCs (HSPC-NBSGW) vs PBMCs (PBMC-humanised NBSGW) and BALB/c-Rag2$^{-/-}$cγ$^{-/-}$ mice (PBMC-humanised BRG).
NBSGW mice were injected intravenously with 200µl IMDM supplemented with 1% HSA (Skin only, no cells) or 5x10^4 human CD133$^+$ HSPCs suspended in 200µl IMDM supplemented with 1%% HSA (HSPC-NBSGW). 3 independent experiments, mice received cells from one of 3 HSPC donors. 11-13 weeks later 1 cm^2 split-thickness skin grafts procured from excess abdominal free flap samples from a single donor were transplanted onto mice in both groups.
For PBMC-humanised NBSGW mice and PBMC-humanised BRG mice, 1 cm^2 split-thickness skin grafts were transplanted onto mice and allowed to heal-in for 5 weeks, after which time 5x10^6 allogeneic human PBMCs from a single donor were suspended in 200µl complete medium and injected intraperitoneally. Grafts were monitored bi-daily and harvested when they had developed features of late rejection or at 100 days (experimental end-point).
Data are represented as (a) schematic outlines of experiments, (b) Kaplan-Meier survival curves indicating the MST and (c) a table indicating study groups. Statistical significance was assessed using the Log-rank (Mantel-Cox) test (**, p<0.01; ***, p<0.001; ****, p<0.0001).

(a)

PBMC-humanised NBSGW / PBMC-humanised BRG skin allograft models

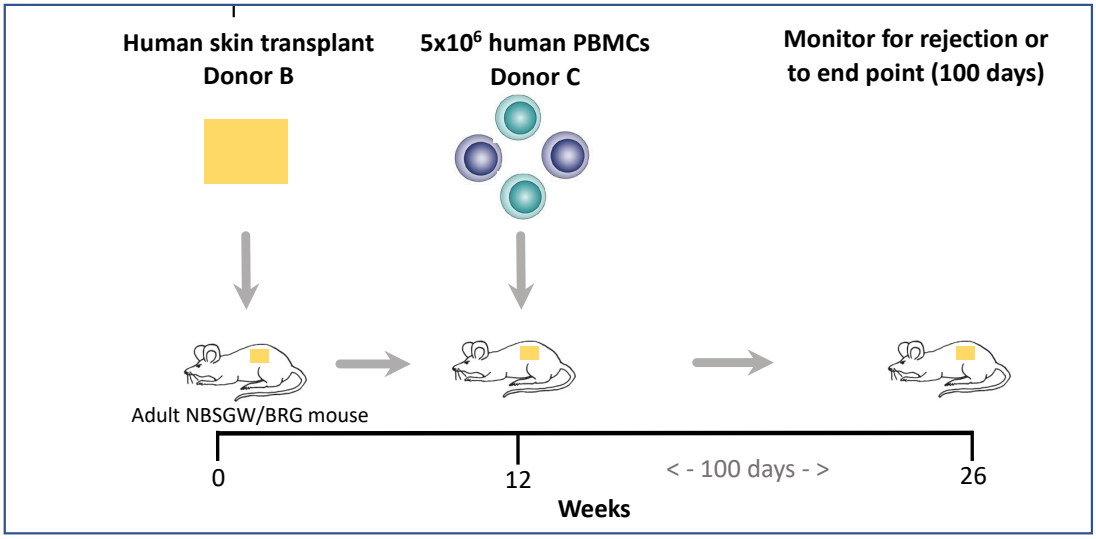

HSPC-NBSGW skin allograft model

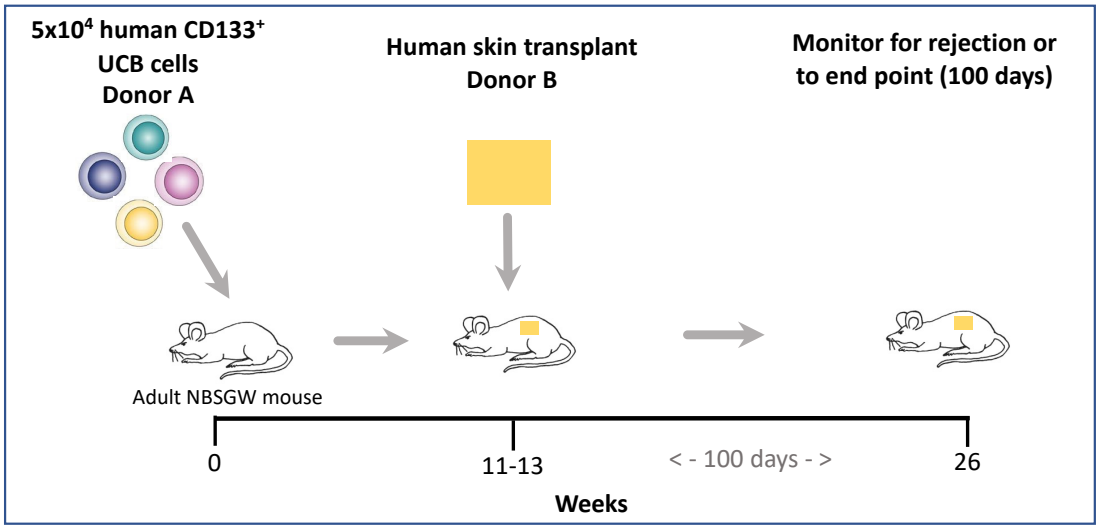

Skin allograft rejection in HSPC-NBSGW vs PBMC-humanised mice

(b)

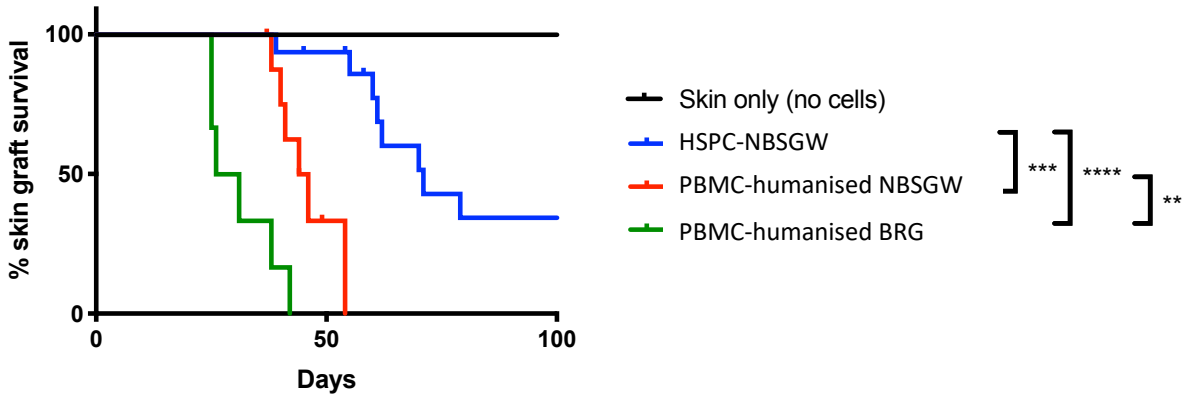

(c)

Group	N	Graft survival (days)	Censored (day)	MST
Skin only (no cells)	3	100, 100, 100	0	100
HSPC-NBSGW	16	39, 55, 60, 61, 62, 70, 72, 79, 100, 100, 100, 100	4 (45, 45, 54, 58)	71
PBMC-humanised NBSGW	9	38, 40, 44, 54, 41, 46	3 (37, 44, 49)	45
PBMC-humanised BRG	6	25, 25, 27, 31, 38, 42	0	28.5

Figure 4.1.6.1 Cellular profiles in HSPC-NBSGW, PBMC-humanised NBSGW & PBMC-humanised BRG mice following rejection of allogeneic human skin transplants.
Comparison of human immune cells in spleens and bone marrow of NOD,B6.SCID *Il2rγ*$^{-/-}$ *Kit*$^{W41/W41}$ (NBSGW) mice and NBSGW mice humanised with UCB HSPCs (HSPC-NBSGW) vs PBMCs (PBMC-humanised NBSGW) and BALB/c-Rag2$^{-/-}$cγ$^{-/-}$ mice (PBMC-humanised BRG) following skin allograft rejection.
Cells from mouse spleens and bone marrow were analysed by flow cytometry for the presence of (a) live human 7AAD^{-}CD45^{+}, (b) 7AAD^{-}CD45^{+}CD3^{+}, (c) 7AAD^{-}CD45^{+}CD19^{+} or (d) 7AAD^{-}CD45^{+}CD33^{+} cells.
Data are represented as frequencies of human (a) CD45^{+} leucocytes (percentage of total (mouse + human) CD45^{+} leucocytes), (b) CD3^{+} T cells, (c) CD19^{+} B cells, and (d) CD33^{+} myeloid cells. Bars indicate mean +/- SEM. Statistical significance was assessed using the one-way ANOVA with Tukey's multiple comparisons test (**, $p<0.01$; ***, $p<0.001$).

(a)

CD45

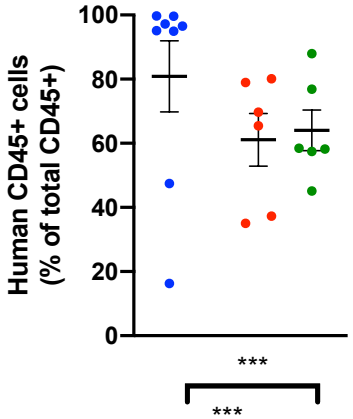

(b)

CD3

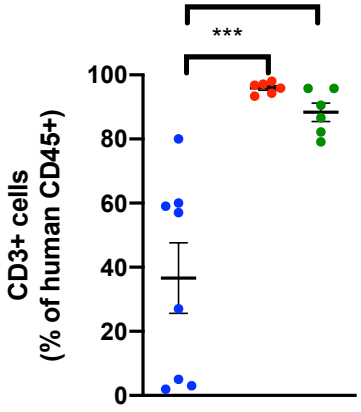

(c)

CD19

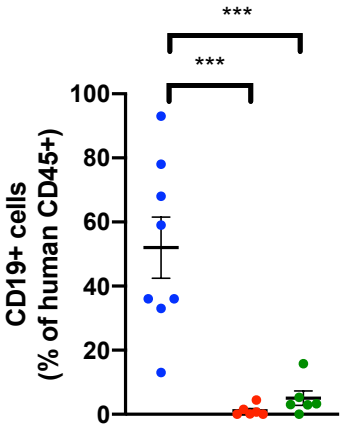

(d)

CD33

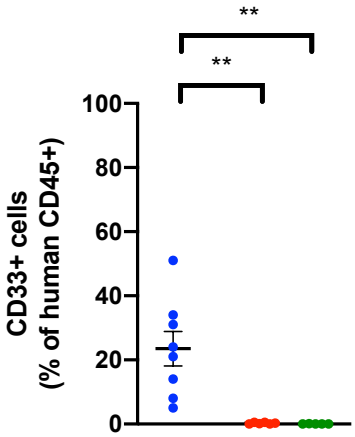

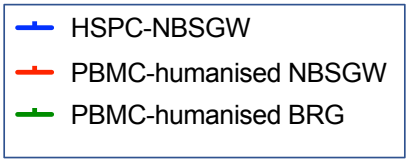

Figure 4.1.7 Allogeneic human skin transplant rejection in NBSGW mice humanised with UCB HSCs +/- MNCs

Analysis of rejection of human skin allografts on NOD,B6.SCID *Il2rγ*$^{-/-}$ *Kit*$^{W41/W41}$ (NBSGW) mice, and HSPC-NBSGW mice with or without subsequent additive transplantation of human CD45^{+}CD34^{-} UCB mononuclear cells (MNCs).

Adult NBSGW mice were injected intravenously with 5x10^{4} human CD133^{+} UCB HSPCs suspended in 200µl IMDM supplemented with 1% HSA (HSPC-NBSGW). 13 weeks later some mice received injections of 5x10^{6} thawed human CD45^{+}CD34^{-} MNCs from the same UCB unit (HSPC+MNC-NBSGW) or 200µl IMDM supplemented with 1% HSA (HSPC-NBSGW). In each individual experiment, mice received cells from one of two HSPC donors. 2 weeks later 1 cm^{2} split-thickness skin grafts procured from excess abdominal free flap samples from a single donor were transplanted onto mice in both groups. Grafts were monitored bi-daily and harvested when they had developed features of late rejection or at 100 days (experimental end-point). Time-course of rejection in HSC and HSC+MNC groups are shown.

Data are represented as (a) a schematic outline of the experiment, (b) a survival curve indicating the MST and (c) a table indicating study groups. Statistical significance was assessed using the Log-rank (Mantel-Cox) test (**, $p<0.01$).

(a)

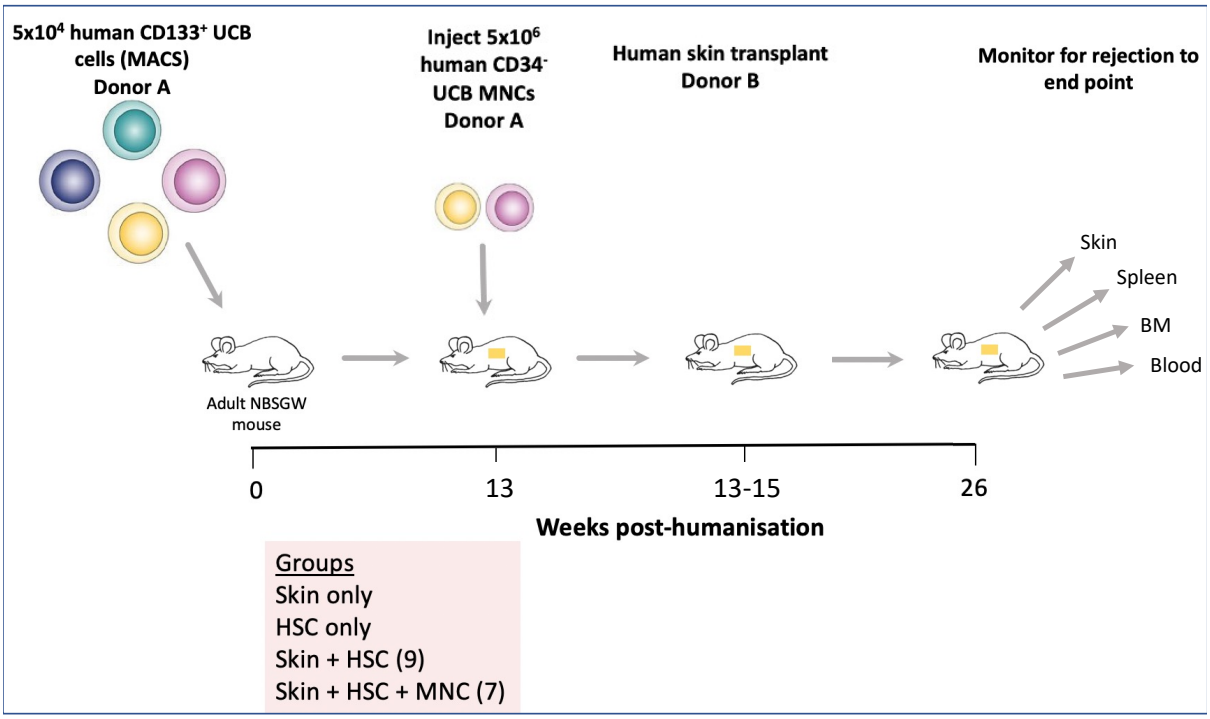

(b)

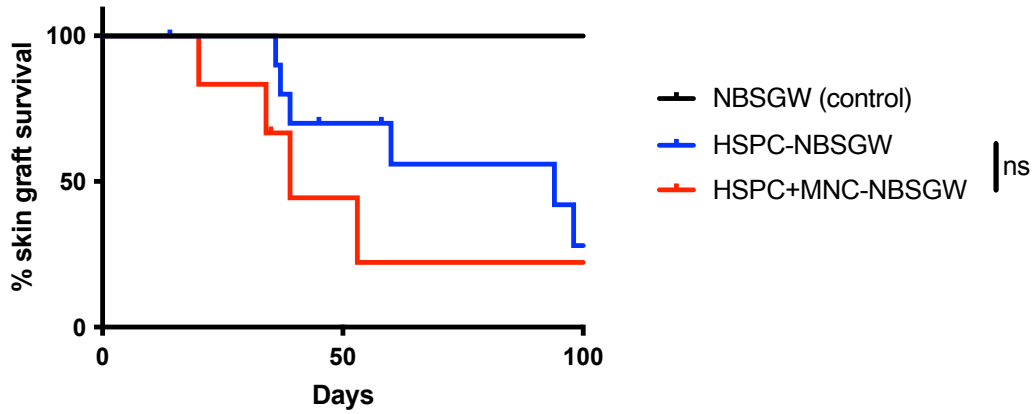

(c)

Group	N	Graft survival (days)	Censored (day)	MST
Skin only (no cells)	3	100, 100, 100	0	100
HSPC-NBSGW	11	36, 37, 39, 60, 94, 98, 101, 101	4 (14, 45, 58)	94
HSPC+MNC-NBSGW	6	20, 34, 39, 53, 100	1 (35)	39

Figure 4.1.7.1 Human leucocyte profiles in UCB HSPC +/- MNC-humanised NBSGW mice on which human skin allografts rejected

Analysis of bone marrow and splenic human $CD45^+$ leucocytes in HSPC-NBSGW mice with or without subsequent additive transplantation of human $CD45^+CD34^-$ UCB mononuclear cells (MNCs) following rejection of human skin allografts.

Adult NBSGW mice were injected intravenously with $5x10^4$ human $CD133^+$ UCB HSPCs suspended in 200µl IMDM supplemented with 1% HSA (HSPC-NBSGW). 11-13 weeks later some mice received injections of $5x10^6$ thawed human $CD45^+CD34^-$ MNCs from the same UCB unit (HSPC+MNC-NBSGW) or 200µl IMDM supplemented with 1% HSA (HSPC-NBSGW). In each individual experiment, mice received cells from one of two HSPC donors. 2 weeks later 1 cm^2 split-thickness skin grafts procured from excess abdominal free flap samples from a single donor were transplanted onto mice in both groups. Grafts were monitored bi-daily and harvested when they had developed features of late rejection or at 100 days (experimental end-point). Bone marrow and splenic cells were analysed by flow cytometry for the presence of live human (a & b) $7AAD^-CD45^+$, (c & d) $7AAD^-CD45^+CD33^+$, (f & g) $7AAD^-CD45^+CD19^+$, (f & h) $7AAD^-CD45^+CD3^+$ cells.

Data are represented as (a) ,(c), (f) FACS plots demonstrating the gating strategy, and frequencies and (b), (d), (g), (h) numbers of each cell subtype per mouse spleen. Bars indicate mean +/- SEM. Statistical significance was assessed using the unpaired T test (*, $p<0.05$; **, $p<0.01$; ns, $p>0.05$).

Total human CD45⁺ leucocytes

Gated on live cells

(a)

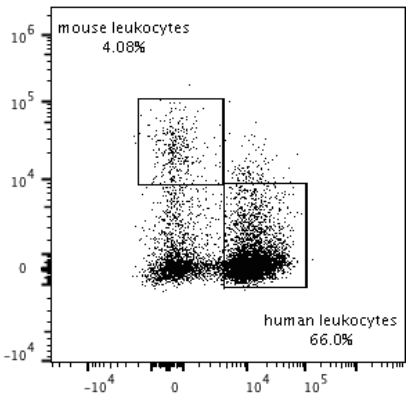

Bone Marrow CD45+ leucocytes

(b)

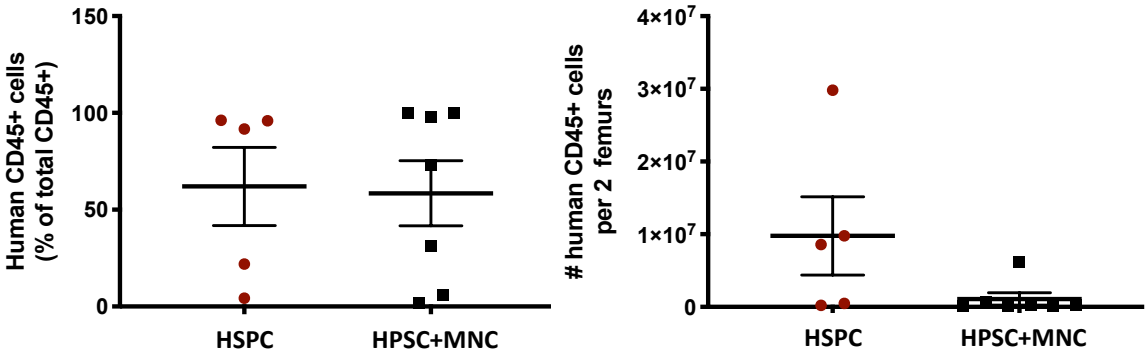

Spleen CD45+ leucocytes

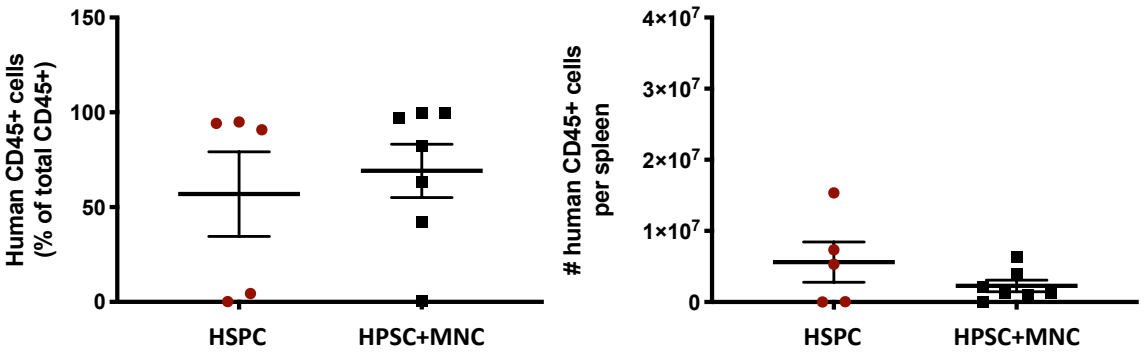

Human Myeloid cells

Gated on live human CD45⁺ cells

(c)

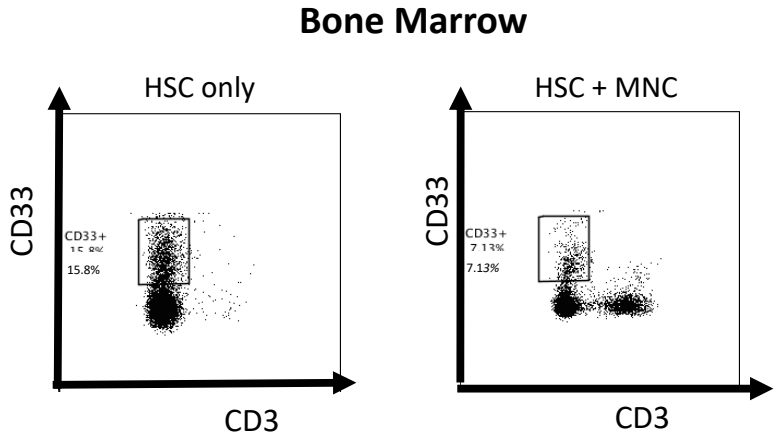

(d)

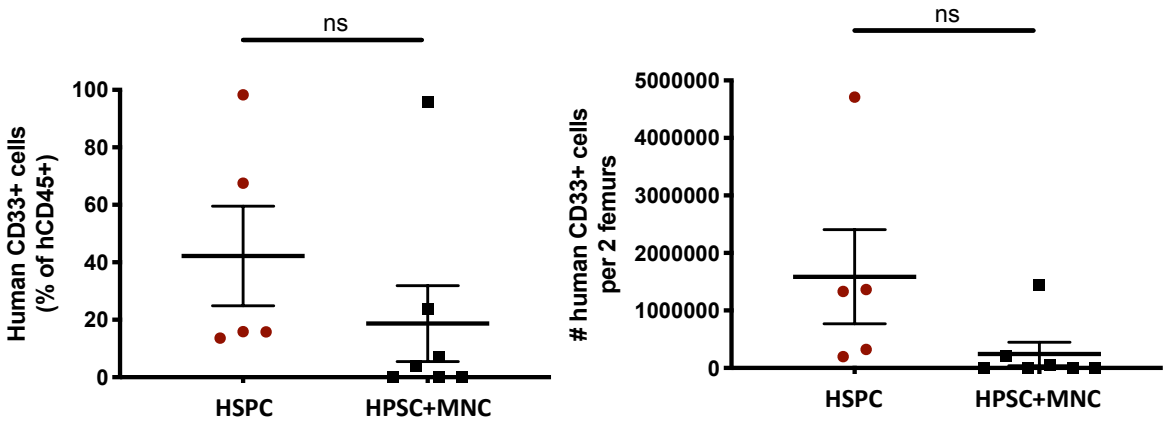

Human B and T cells

Gated on live human CD45⁺ cells

Spleen

(f)

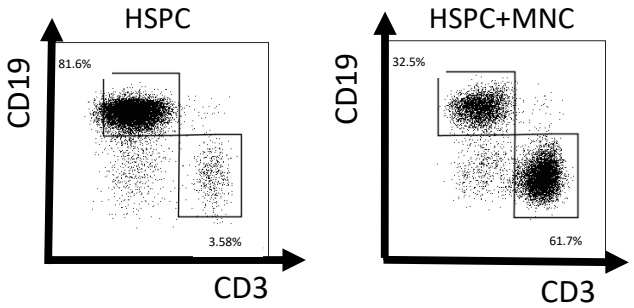

(g)

B cells

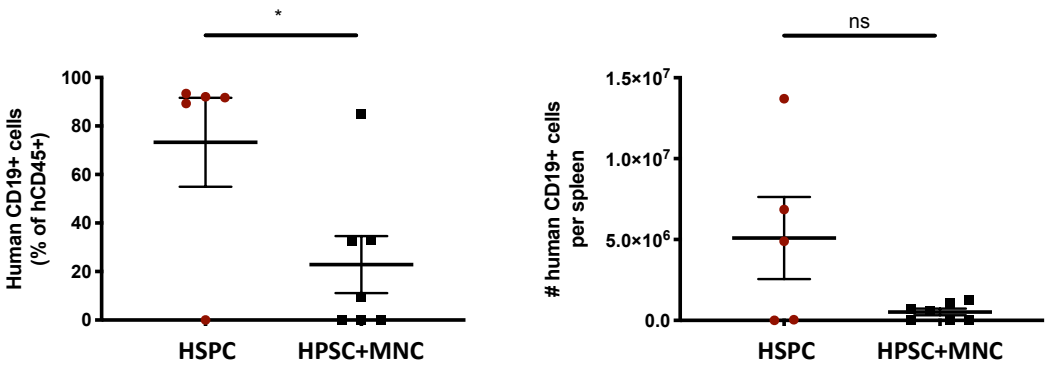

(h)

T cells

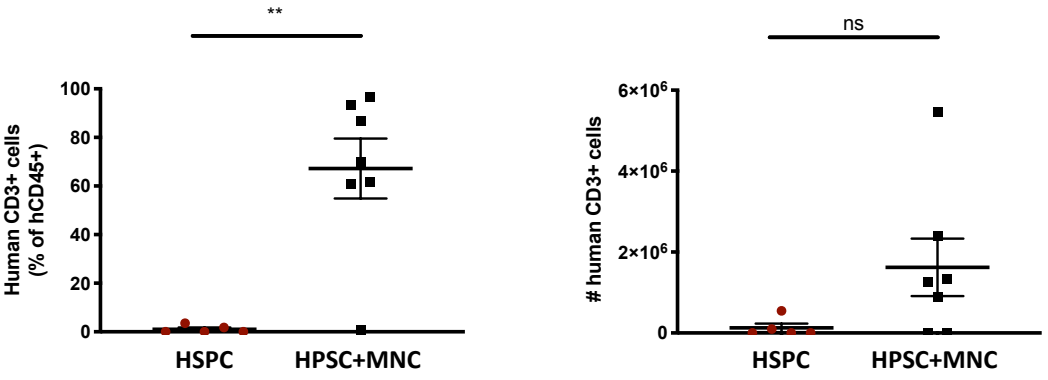

Figure 4.1.7.2 Human T cell subset profiles in UCB HSPC +/- MNC-humanised NBSGW mice on which human skin allografts rejected

Analysis of splenic human $CD3^+$ T cells in UCB HSPC and HSPC+MNC- humanised NBSGW mice following rejection of human skin allografts.

Adult NBSGW mice were injected intravenously with $5x10^4$ human $CD133^+$ HSCs suspended in 200µl IMDM supplemented with 1%% HSA (HSPC-NBSGW). 11-13 weeks later some mice received injections of $5x10^6$ thawed human $CD45^+CD34^-$ MNCs from the same UCB unit (HSPC+MNC-NBSGW) or 200µl IMDM supplemented with 1% HSA (HSPC-NBSGW). In each individual experiment, mice received cells from one of two HSPC donors. 2 weeks later 1 cm^2 split-thickness skin grafts procured from excess abdominal free flap samples from a single donor were transplanted onto mice in both groups. Spleens were harvested when skin allografts had developed features of late rejection or at 100 days (experimental end-point). Cells were analysed by flow cytometry for the presence of live human (a & b) $7AAD^-CD45^+CD3^+$ $CD8^+$ or $CD8^-$ T cells and among these (c & d), Tcm, Tn, TemRA and Tem cells.

Data are represented as (a & c) FACS plots demonstrating the gating strategy and (b, d & e) frequencies and numbers of each cell subtype per mouse spleen. Bars indicate mean +/- SEM. Statistical significance was assessed using the unpaired T test (*, $p<0.05$; **, $p<0.01$).

Spleen

(a)

Gated on live cells

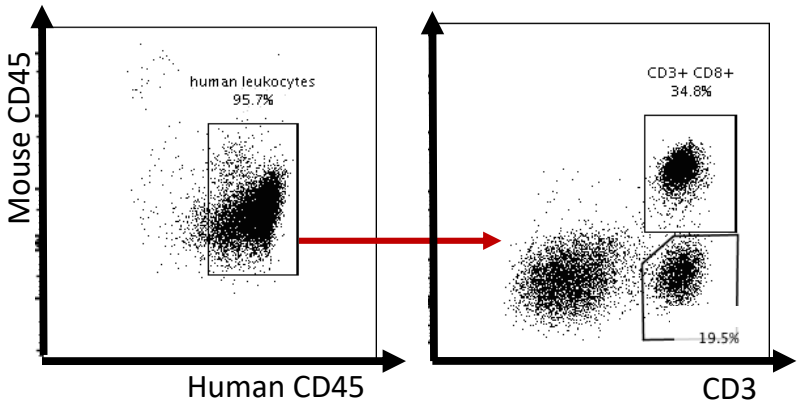

(b)

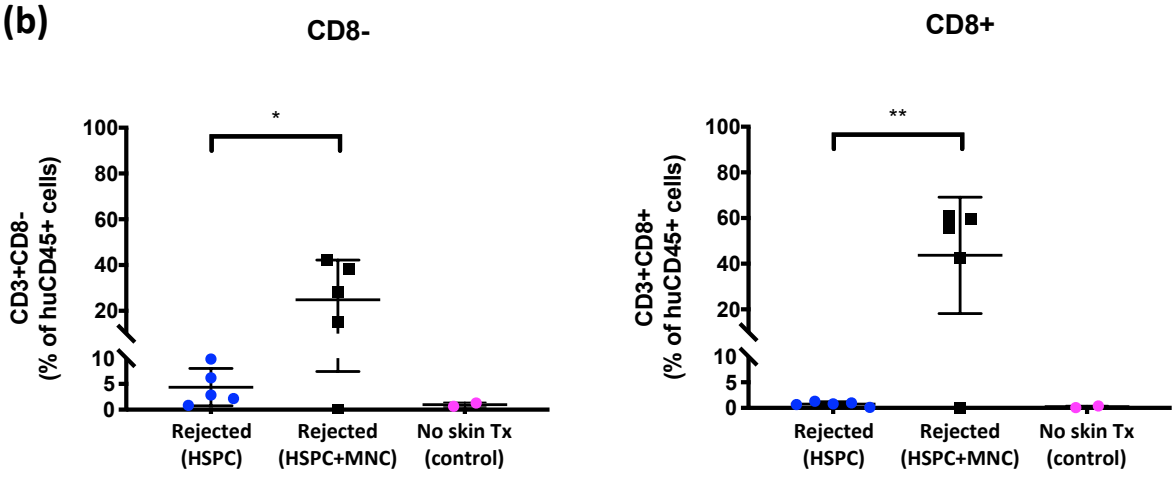

Comparing cell populations in mice which rejected skin Tx

(c) *Gated on live cells*

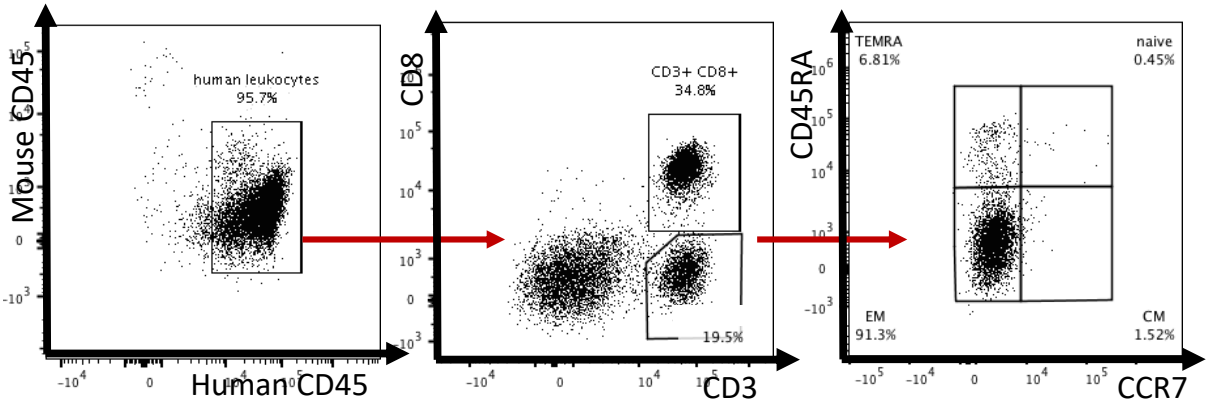

(d) **CD8⁻ subsets (Spleen)**

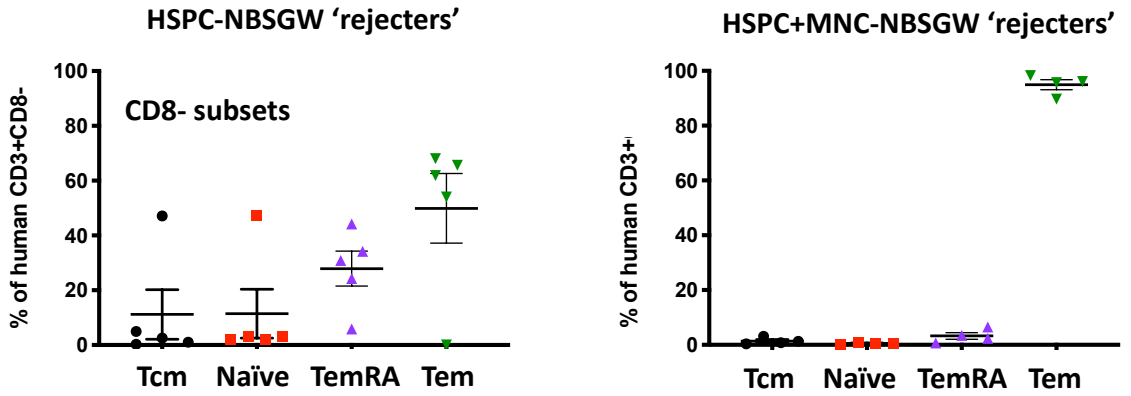

(e) **CD8⁺ subsets (Spleen)**

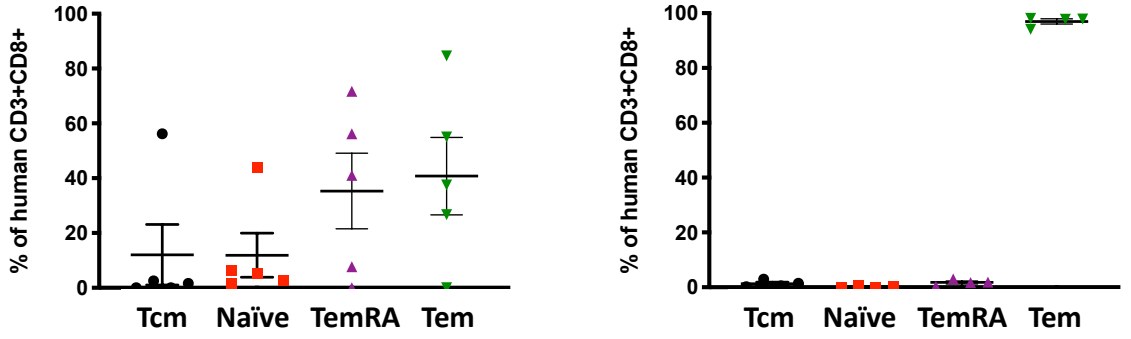

Figure 4.1.7.3 Human B cell subset profiles in UCB HSPC +/- MNC-humanised NBSGW mice on which human skin allografts rejected

Analysis of splenic human $CD19^+$ B cells in UCB HSPC and HSPC+MNC-humanised NBSGW mice following rejection of human skin allografts.

12 adult NBSGW mice were injected intravenously with $5x10^4$ human CD133+ HSPCs suspended in 200µl IMDM supplemented with 1% HSA (HSPC-NBSGW - pink symbols). 11-13 weeks later 4 mice received injections of $5x10^6$ thawed human $CD45^+CD34^-$ MNCs (HSPC+MNC-NBSGW) from the same UCB unit and 5 received 200µl IMDM supplemented with 1% HSA (HSPC-NBSGW). In each individual experiment, mice received cells from one of two HSPC donors. 2 weeks later 1 cm^2 split-thickness skin grafts procured from excess abdominal free flap samples from a single donor were transplanted onto HSPC-NBSGW (blue symbols) and HSPC+MNC-NBSGW (black symbols) mice. Spleens were harvested when skin allografts had developed features of late rejection or at 100 days (experimental end-point). Cells were analysed by FACS for the presence of (a & b) live human $7AAD^-CD45^+CD19^+$, $7AAD^-CD45^+CD19^+CD10^-$ mature and $7AAD^-CD45^+CD19^+CD10^-IgD^-CD27^+$ memory B cells .

Data are represented as (a) FACS plots demonstrating the gating strategy and (b-d) frequencies of the respective B cell subtypes. Bars indicate mean +/- SEM. Statistical significance was assessed using the unpaired T test (*, $p<0.05$; ****, $p<0.0001$; ns, $p>0.05$).

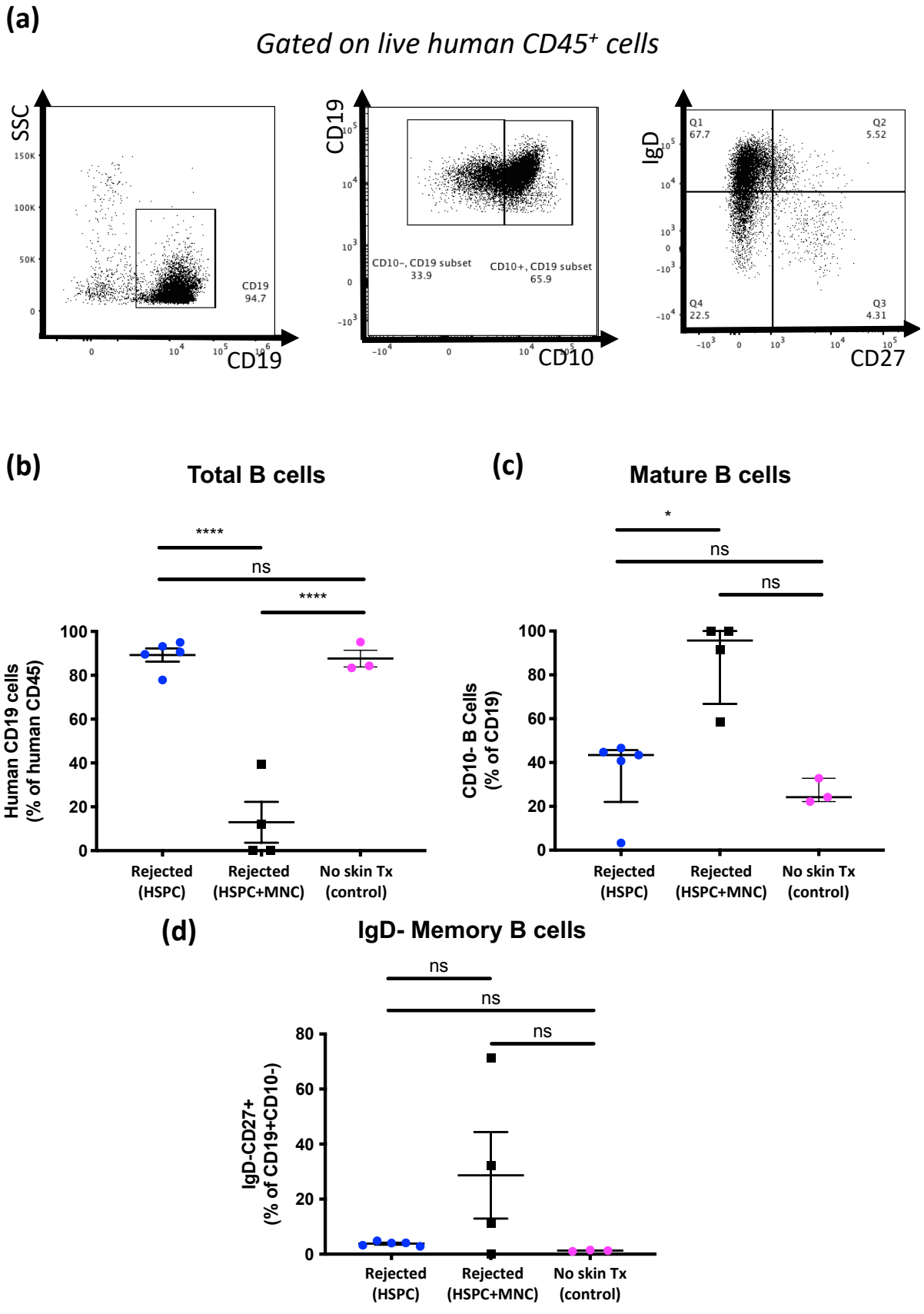
(a)
Gated on live human CD45+ cells
SSC
CD19
CD19
94.7
CD19
CD10
CD10−, CD19 subset
33.9
CD10+, CD19 subset
65.9
IgD
CD27
Q1
67.7
Q2
5.52
Q4
22.5
Q3
4.31
(b)
Total B cells
Human CD19 cells
(% of human CD45)
****
ns
****
Rejected
(HSPC)
Rejected
(HSPC+MNC)
No skin Tx
(control)
(c)
Mature B cells
CD10- B Cells
(% of CD19)
*
ns
ns
(d)
IgD- Memory B cells
IgD-CD27+
(% of CD19+CD10-)
ns
ns
ns

Figure 4.1.7.4 Human myeloid cell subset profiles in UCB HSPC +/- MNC-humanised NBSGW mice on which human skin allografts rejected

Analysis of splenic human $CD33^+$ myeloid cells in UCB HSPC and HSPC+MNC- humanised NBSGW mice following rejection of human skin allografts.

Adult NBSGW mice were injected intravenously with $5x10^4$ human CD133+ HSPCs suspended in 200µl IMDM supplemented with 1% HSA (HSPC-NBSGW - pink symbols). 11-13 weeks later some mice received injections of $5x10^6$ thawed human $CD45^+CD34^-$ MNCs from the same UCB unit (HSPC+MNC-NBSGW – black symbols) or 200µl IMDM supplemented with 1% HSA (HSPC-NBSGW – blue symbols). In each individual experiment, mice received cells from one of two HSPC donors. 2 weeks later 1 cm^2 split-thickness skin grafts procured from excess abdominal free flap samples from a single donor were transplanted onto mice in both groups. Bone marrow cells were harvested when skin allografts had developed features of late rejection or at 100 days (experimental end-point). Cells were analysed by flow cytometry for the presence of (a & b) live human $7AAD^-CD45^+CD33^+CD11c^+$ dendritic cells.

Data are represented as (a) FACS plots demonstrating the gating strategy and (b) frequencies of dendritic cells. Bars indicate mean +/- SEM. Statistical significance was assessed using the one-way ANOVA (*, $p<0.05$; ns, $p>0.05$).

(a) *Gated on live human CD45⁺CD33⁺ cells*

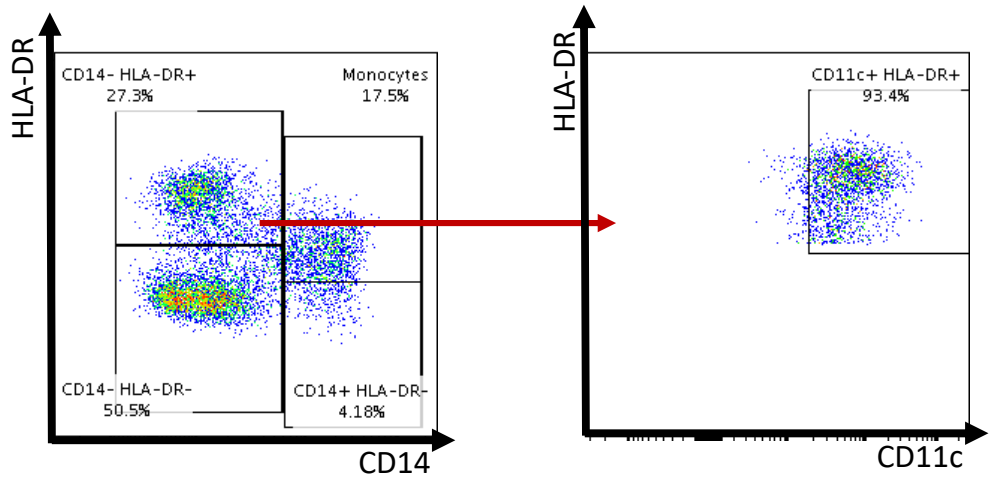

(b)

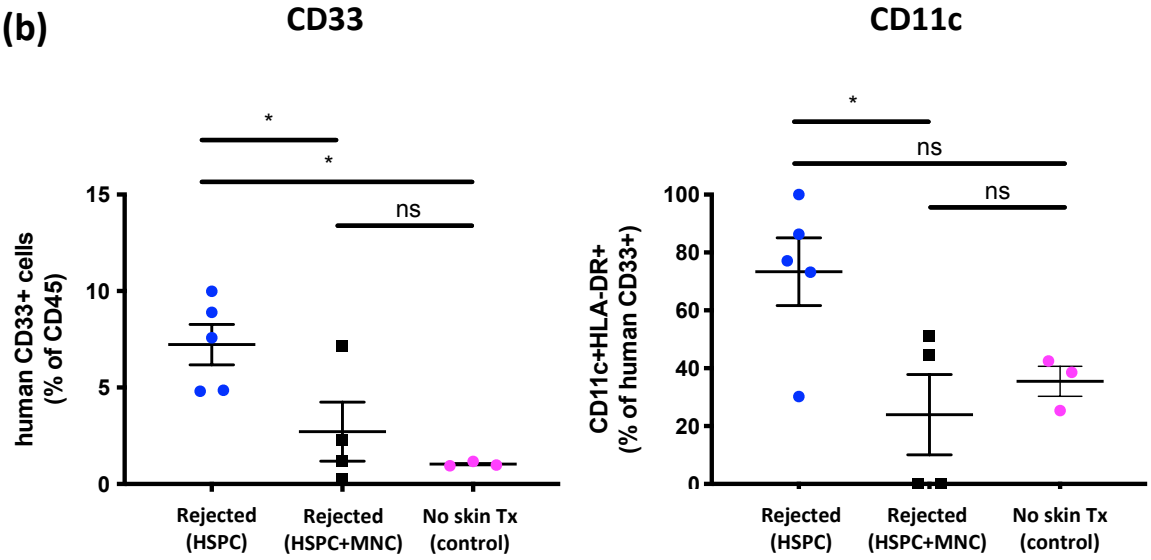

Chapter 5: CCR4 And CCR8-Expressing Regulatory T Cells In The Immunoregulation Of Human Skin Transplant Rejection

5.1. Introduction

Human regulatory T cells (Tregs) comprise a subset of $CD4^+CD25^+$ T cells expressing the transcription factor FOXP3, which are capable of inhibiting effector T cell function. Experimental and early short-term clinical data suggest Tregs to be a promising therapy for the safe control of transplant rejection[219,361-363]. Targeting of immunomodulatory therapies is of particular interest, and studies have demonstrated enhanced suppressive activity in allotransplantation models when antigen-specific T cell receptors[364] or homing receptors are present on ex-vivo expanded Treg[365]. Chemokine receptors are classically known to function as attractants of immune cells to target areas of immune surveillance or pathology. The chemokine receptor CCR4 is expressed on the surface of Th2 cells and Tregs and is implicated in trafficking of these cells to nonlymphoid organs and tumors expressing their cognate ligands CCL17 and CCL22[366]. Clinical trials are currently investigating the potential to inhibit migration of Tregs into tumours such as cutaneous T cell lymphoma, by blockading CCR4 with the anti-CCR4 monoclonal antibody Mogamulizumab[367]. CCR8 is another chemokine receptor expressed on highly suppressive Tregs. Cells exhibiting CCR8 demonstrate chemotaxis toward CCL1, and CCR8 has also been described to be highly prevalent on tumor-resident Tregs[183,368]. In health, these chemokine receptors are found on skin-resident T cells. Skin-homing capabilities of Tregs bearing these receptors suggest the potential for use in the prevention of skin transplant rejection. The mechanisms responsible for the suppressive capacity of these

Treg subsets however are not fully understood and have yet to be explored in the setting of transplantation. The desire for optimal suppressive potency, coupled with reasonable theoretic concerns about adverse effects following adoptive transfer of high Treg doses fuels efforts to identify highly stable and suppressive Tregs, which could facilitate the use of lower doses. This could additionally reduce both the timescale for production of expanded cells and the associated costs. Additionally, methods of focused targeting of adoptively transferred Tregs to sites of desirable function could enhance therapeutic potency and limit the potential for systemic toxicity.

We hypothesise that expression of CCR4 and CCR8 identify highly suppressive subpopulations of human Tregs that may be used to enhance Treg cellular therapy

5.1.1. Chapter aims

1) Evaluate CCR4 and CCR8 expression on human Tregs and assess the suppressive capacities of these cells.
2) Develop a humanised mouse model to aid *in vivo* characterisation of human T cell trafficking and function

5.2. Results

5.2.1. A minority of peripheral blood Tregs express surface CCR4 and CCR8

Tregs expressing CCR4 and CCR8 have been reported to migrate into several types of tumours[167,172-176], and are thought to impair tumour-directed cytotoxicity. Antibody-

mediated depletion of these cells enhances the anti-tumour immune response[167]. To determine whether suppressive intratumour phenotypes associated with high CCR4 and CCR8 expression reflects generally higher expression on Tregs than Tconvs in peripheral blood, we analysed blood samples from healthy donors **(*Figure 5.2.1)*.** Tregs expressed higher CCR4 and CCR8 than Tconvs **(*Figure 5.2.1 (a-d)*)**. Expression of both receptors was primarily on $CD45RA^-$ memory Tregs **(*Figure 5.2.1 (e-f)*),** and CCR4/CCR8 co-expression was exclusively found on Tregs **(*Figure 5.2.1 (e)*).**

These results demonstrate that in the peripheral blood of healthy individuals Tregs constitutively express higher CCR4 and CCR8 than Tconvs and suggest this is not a tumour-specific phenotype.

5.2.2. Expanded $CCR4^+$ and $CCR8^+$ Tregs demonstrate greater *in vitro* suppressive capacity than $CCR4^-$ and $CCR8^-$ Tregs

Having identified that CCR4 and CCR8 are more abundant on unstimulated Tregs than Tconvs, we investigated whether the suppressive phenotypes associated with $CCR4^+$ [167] and $CCR8^+$ [183] Tregs related solely to efficient recruitment of Tregs or perhaps to high suppressive capacity of these subsets.

As individual healthy donor blood cones contain insufficient numbers of Tregs to support assessment of Treg suppressive function, we isolated Tregs before expanding them by polyclonal stimulation in *in vitro* expansion cultures (high-concentration αCD3/αCD28 beads + IL-2) **(*Figure 5.2.2 (a) & Figure 5.2.3 (a)*).** Following 14 days of expansion and 2 days of resting, 70% of Tregs were $CCR4^+$ **(*Figure 5.2.2 (b)*)** and 31% of these were memory type. 14% of expanded Tregs expressed CCR8- a modest increase compared with pre-stimulation **(*Figure***

5.2.3 (b)*)**. Expanded Tregs were then sorted into $CCR4^+$, $CCR4^-$ and $CCR8^+$ and $CCR8^-$ fractions (Figure 5.2.2 (c)-(d)***) and (***Figure 5.2.3 (c)-(d)***) respectively, and assessed for their ability to suppress the proliferation of polyclonally-stimulated autologous PBMC responders (***Figure 5.2.2 (e)***) and (***Figure 5.2.3 (d)***). $CCR4^+$ and $CCR8^+$ Tregs were more potent suppressors of T cell proliferation than $CCR4^-$ and $CCR8^-$ Tregs respectively (***Figure 5.2.2 (f) – (i)***) and (***Figure 5.2.3 (e) – (h)***), suggesting that the suppressive capacity of these Treg subsets is conferred by mechanisms beyond the chemotactic recruitment afforded by CCR4 and CCR8.

5.2.3. $CCR4^+$ Tregs prolong human skin allograft survival

Having identified superior capacity of $CCR4^+$ Tregs to suppress *in vitro* proliferation of allogeneic T cells, we hypothesised that this may translate *in vivo* and help prevent human skin allograft rejection. To assess this, we transplanted human split-thickness skin grafts onto immunodeficient BALB/c-$Rag2^{-/-}c\gamma^{-/-}$ mice, allowed them to heal in for five weeks, then injected allogeneic human PBMCs intraperitoneally, alone or with expanded-sorted low dose of $CCR4^+$ or $CCR4^-$ Tregs from the same blood donor (***Figure 5.2.4 (a)***). Skin allografts were observed for the development of macroscopic features of late rejection ***(Figure 5.2.4 (b)).*** Upon development of these features—or after 100 days if rejection did not occur, mice were sacrificed (as in Chapter 4). Injection of human $CCR4^+$ Tregs in addition to PBMCs significantly prolonged skin allograft survival (MST 66 days), compared with injection of human PBMCs and $CCR4^-$ Tregs (MST 42 days, p=0.0445), and following injection of human PBMCs alone (MST 31 days, p=0.0153) (***Figure 5.2.4 (c) & (d)***).

These results suggest that *ex vivo*-expanded autologous $CCR4^+$ Tregs prevent PBMC-mediated destruction of human skin allografts *in vivo* and do so with greater efficacy than $CCR4^-$ Tregs.

5.2.4. CCR8$^+$ Tregs prolong human skin allograft survival but not significantly more than CCR8$^-$ Tregs

Similarly to CCR4$^+$ vs CCR4$^-$ Tregs, CCR8$^+$ Tregs were more suppressive of allogeneic T cell proliferation *in vitro* than CCR8$^-$ Tregs. We examined whether this suppressive capacity translates into *in vivo* prevention of allogeneic human skin transplant rejection (as in section 5.2.3.). Both CCR8$^+$ and CCR8$^-$ Tregs administered with PBMCs **(*Figure 5.2.5 (a)*)** prolonged human skin allograft survival compared with PBMCs alone (MST 48 days *cf.* 25 days, p=0.0046 and 31 days *cf.* 25 days, p=0.0153 respectively) **(*Figure 5.2.5 (b-d)*).** CCR8$^+$ Tregs promoted long-term survival (beyond 100days) in 2 out of 5 skin allografts. Grafts on these mice remained soft, pliable and demonstrated no macroscopic evidence of inflammation. However, the overall MST was not significantly extended compared with CCR8$^-$ Tregs (MST 48 days *cf.* 31 days, *p*=0.2040).

This data suggests that *ex vivo*-expanded autologous CCR8$^+$ Tregs act to prevent PBMC-mediated destruction of human skin allografts *in vivo* however with equivalent efficacy to CCR8$^-$ Tregs.

5.2.5. Effects of low-dose polyclonal stimulation on Tregs

5.2.5.1. Treg CCR4 expression

Expression of the CCR4 receptor is known to be upregulated upon stimulation in certain inflammatory environments[369]. Following expansion with high-dose polyclonal stimulation (3:1 ratio of Tregs:αCD3αCD28 beads), expression of CCR4 is substantially greater **(*Figure 5.2.2 (b)*)** than on unstimulated peripheral blood Tregs **(*Figure 5.2.1 (a)*).** This is associated with high suppressive capacity *in vitro* **(*Figure 5.2.2 (f-i)*)** and *in vivo* **(*Figure 5.2.4 (c-d)*).** We

therefore sought to evaluate the effects of a more physiological dose of polyclonal stimulation on $CCR4^+$ expression on Tregs **(*Figure 5.2.6 (a)*).** Considering also that chemokines themselves can stimulate T cells[370] and enhance chemokine receptor expression through a positive feedback loop[369], we additionally assessed the effect on CCR4 expression of adding recombinant human CCL17/22.

Unexpanded Tregs were sorted into $CCR4^-$ (naïve) and $CCR4^+$ fractions, then stimulated for 14 days in a 5:1 Treg:αCD3/αCD28 beads ratio, with low-dose IL-2 ± rhCCL17/22 **(*Figure 5.2.6 (a–c)*)**. CCR4 expression was analysed bi-daily by flow cytometry **(*Figure 5.2.6 (d)*).** Early post-stimulation, $CCR4^-$ (naïve) Tregs transiently gained CCR4 expression and proliferated rapidly, however by day 6 expression was lost **(*Figure 5.2.6 (e-f)*).** Addition of rhCCL17/22 appeared to additively increase the number of $CCR4^+$ Tregs, however this effect was similarly transient and modest. Expression on sorted $CCR4^+$ Tregs was more prolonged. Proliferation of CCR4-expressers was continuous to day 10, with the majority of Tregs maintaining $CCR4^+$ expression, however this fell thereafter and at day 14 expression was lower than in expanded Tregs. In our expansion cultures, we have previously determined that re-stimulation at day 7/14 produces optimal numbers of suppressive Tregs. To identify whether re-stimulation also affects Treg CCR4 expression, we analysed CCR4 expression during expansion **(*Figure 5.2.6 (g)*).** Similarly to Tregs receiving low-dose stimulation, Tregs in expansion cultures transiently upregulated CCR4 expression, however following re-stimulation CCR4 expression increased and remained persistently high on the majority of Tregs **(*Figure 5.2.6 (h)*).**

This suggests that CCR4 expression on Tregs increases upon activation and becomes persistent following repeat exposure to activating stimuli, especially when the high stimulation dose is used.

5.2.5.2. Treg CCR8 expression

As above, unexpanded Tregs were sorted into $CCR8^-$ and $CCR8^+$ fractions **(*Figure 5.2.7 (a) – (c)*)** and stimulated *in vitro* with αCD3/αCD28 beads (5:1 ratio of Tregs:beads) **(*Figure 5.2.7 (d) & (e)*).** Following stimulation, $CCR8^-$ Tregs did not gain expression of CCR8 and $CCR8^+$ Treg rapidly lost expression **(*Figure 5.2.7 (f)-(g)*).** In contrast, High-dose polyclonal stimulation caused a transient upregulation of CCR8 expression **(*Figure 5.2.7 (h)*),** but unlike CCR4, this was not sustained after re-stimulation.

This data indicates that CCR8 expression is not responsive to Treg activation and that expanding $CCR8^+$ Tregs is not as achievable as it is for $CCR4^+$ Tregs.

5.2.6. $CCR4^+$ Tregs demonstrate higher expression of FOXP3 and CD27 than $CCR4^-$ Tregs

Tregs are heterogenous cells with functional capabilities that vary between subsets. A number of cell surface and intracellular proteins are known to be expressed by Tregs with high suppressive capacity. To investigate whether the superior suppression demonstrated by $CCR4^+$ vs $CCR4^-$ Tregs may be associated with expression of these functional proteins, we analysed expression levels in expanded human Tregs by flow cytometry **(*Figure 5.2.8 (a)*).**

We identified significantly greater expression of intracellular FOXP3 ($p=0.0123$) and surface CD27 ($p= 0.0227$), LAG3 ($p=0.0038$) and TIGIT ($p=0.0387$) on expanded $CCR4^+$ Tregs compared with $CCR4^-$ Tregs **(*Figure 5.2.8 (b-e)*),** together with lower expression of CD154 (CD40L) ($p=0.0037$) **(*Figure 5.2.8 (f)*).** Treg function critically depends on stable expression of the transcription factor $FOXP3^{371}$ **(*Figure 5.2.8 (g)*)**, and downregulation of FOXP3-as can occur due to pro-inflammatory cytokines-can cause Tregs to lose suppressive function and secrete pro-inflammatory cytokines[372,373]. $CD27^+$ Tregs have been shown to be potent suppressors

and express a transcriptome profile of archetypal Tregs[374]. In fact, high expression of CD27 can be used to isolate potent *in vitro*-expanded Tregs. LAG3, a MHC class II-binding CD4 homologue, has been shown to be a marker of highly suppressive Tregs[375,376]. Its specific mechanisms of regulation have not bene fully elucidated however it is thought to interfere with dendritic cell maturation and suppress T cell activation. TIGIT provides co-inhibitory signalling through CD155, inhibits IL12 production and induces regulatory IL10 production[377]. A consensus over the role of the co-stimulatory molecule CD154 (CD40L) in Tregs is yet to be reached. Though its pro-inflammatory activity on Tconvs is well established, CD154 expression has been described as a marker of highly suppressive antigen-reactive nTregs. A recent report suggests that following re-stimulation, $CD154^-$ Tregs are part of a subset of epigenetically stable antigen-activated Tregs[378]. These findings suggest that in addition to chemokine-mediated homing, $CCR4^+$ expression may help to identify Tregs with greater regulatory capacity and lineage stability.

5.2.7. $CCR8^+$ Tregs express several suppressive markers differently to $CCR8^-$ Tregs

Having identified correlation between the superior suppressive capacity of $CCR4^+$ Tregs and expression of proteins found abundantly on highly suppressive Tregs **(*Figure 5.2.8*),** we similarly analysed co-expression of these markers on expanded $CCR8^+$ and $CCR8^-$ Tregs **(*Figure 5.2.9 (a)*).** Expression of CD27 ($p=0.0142$), FOXP3 ($p=0.0008$) and CD154(CD40L) ($p=0.0452$) was significantly higher on $CCR8^+$ Tregs than $CCR8^-$ Tregs **(*Figure 5.2.9 (b-d)*).** Functions of the relevant proteins **(*Figure 5.2.8 (g)*)** are discussed in section 5.2.6.

5.2.8. Assessing leucocyte homing *in vivo*: model development

5.2.8.1. Chemotaxis via CCR4-CCL17/22 axis

The CCR4–CCL17/22 axis is known to play a vital role in Treg migration. An abundance of $CCR4^+$ Tregs have been described in tumour microenvironments rich in CCL17 and CCL22[175,379-383] and in laboratory studies of transplant rejection. Considering CCR4 expression on expanded Tregs is high, we hypothesised that replicating localised chemokine expression may preferentially attract expanded Tregs and promote immunoregulation if concentrated beneath a skin allograft.

To pilot this, we treated extracellular matrix-based hydrogels (Matrigel) with increasing doses of CCL17/22 (200μl total volume), injected them subcutaneously into the flank of BRG mice and subsequently assessed the migration of intravenously injected human PBMCs into treated Matrigels vs untreated controls, which were injected into the contralateral flank ***(Figure 5.2.9.1. (a)).*** After 4 days Matrigels were harvested and leucocytes analysed by flow cytometry. Although with increasing chemokine dose, leucocyte migration into treated Matrigels increased modestly **(*Figure 5.2.9.1. (b)*)**, substantial chemotaxis was not observed. We considered that though chemotaxis may be stimulated by localised chemokine expression in this model, the absence of an inflammatory microenvironment (e.g. as seen post-transplantation) may limit leucocyte migration one may expect following skin transplantation surgery.

5.2.8.2. Simulating an inflammatory microenvironment increases mouse leucocyte chemotaxis in a murine model

Following skin transplantation surgery, leucocytes in the inflammatory microenvironment become stimulated and increase expression of cytokine and chemokine receptors. We hypothesised that simulating an inflammatory microenvironment using pro-inflammatory cytokines may replicate this and enhance leucocyte migration into chemokine-treated Matrigels. As a feasibility trial, we conducted this experiment in immunocompetent mice, and treated Matrigels with recombinant mouse (rm) CCL1, CCL22 and MCP1 chemokines (to attract multilineage mouse leucocytes) and/or rmIFNγ, then injected them subcutaneously into the flanks of mice **(*Figure 5.2.9.2. (a)*)**. Substantial leucocyte migration was observed **(*Figure 5.2.9.2. (b)*).** Significant increases in leucocyte migration only occurred into Matrigels treated with both chemokines and IFNγ - *cf.* control Matrigels ($p<0.0001$), *cf.* Matrigels treated with chemokines alone ($p=0.0077$) and *cf.* IFNγ alone ($p=0.0007$) **(*Figure 5.2.9.2. (c)*).** Among the migratory leucocytes we identified T cells, B cells and myeloid cells **(*Figure 5.2.9.2. (d)*).**

This data suggests the feasibility of the *in vivo* localised chemotaxis model and that inflammatory signalling and chemokine expression are required to effect leucocyte migration.

5.2.8.3. Simulating an inflammatory microenvironment also increases human leucocyte chemotaxis

Having optimised a model to promote localised chemoattraction of murine leucocytes using cytokine and IFNγ-impregnated Matrigels, we applied this protocol to assess migration of human PBMCs. Using recombinant human CCL17/22, CCL1 and/or IFNγ-treated Matrigels, we repeated experiment 5.2.8.2 in BRG mice, with human PBMCs to replace murine leucocytes **(*Figure 5.2.9.3. (a)*).** As in 5.2.8.2, significant leucocyte migration was only observed into

Matrigels co-treated with chemokines and IFNγ **(*Figure 5.2.9.3. (a)*).** Migration was substantially lower into Matrigels were treated with either agent alone **(*Figure 5.2.9.3. (b)*).** Among the human leucocytes migrating into Matrigels we identified both $CD4^+$ and $CD8^+$ human T cells **(*Figure 5.2.9.3. (c)*).**

5.2.8.4. The *in vivo* chemotaxis model can be used to attract human Tregs

To be able to utilise the *in vivo* chemotaxis model for the prevention of skin allograft rejection, recruitment of Tregs is likely to be essential. Having demonstrated the capacity to chemoattract human T cells using cytokines and chemokines, to assess Treg recruitment, we adoptively transferred PBMCs and expanded Tregs into BRG mice (as in the humanised mouse model of skin transplantation above) and 3 weeks later injected Matrigels treated with rhCCL22 and rhIL2, (which is preferentially consumed by Tregs and provides important stimulation) **(*Figure 5.2.9.4. (a)*).** Matrigels treated with chemokines and IL2 promoted greater migration of leukocytes into Matrigels than both control (untreated) and IL2-treated Matrigels **(*Figure 5.2.9.4. (b)*).** Additionally, greater numbers of Tregs were detected in CCL17/22-IL2 Matrigels than controls, however this was not significantly significant ($p=0.0697$, $n=3$) **(*Figure 5.2.9.4. (c)*).** Nonetheless, this result suggests that the *in vivo* chemotaxis model is capable of recruiting Tregs to the site of chemokine/cytokine expression.

5.2.9. Matrigels treated with CCL22 injected beneath skin allografts are capable of prolonging graft survival

Having demonstrated localised human Treg chemotaxis (section 5.2.8.4), we hypothesised that administration of chemokine-treated Matrigels in the humanised mouse model of skin transplantation may prolong human skin allograft survival. To test this, we transplanted full-thickness human skin grafts onto BALB/c-Rag2$^{-/-}$cγ$^{-/-}$ mice and allowed them to heal for five weeks **(*Figure 5.2.10 (a)*).** Full-thickness skin grafts were used instead of split-thickness grafts in order to prevent secondary contraction—which we observed in split-thickness skin grafts following subcutaneous injection of Matrigels—causing grafts to shrink, and obscuring macroscopic interpretation of rejection. Following allograft healing, allogeneic human PBMCs were injected intraperitoneally, with or without Tregs (from the same donor). Four weeks later, Matrigels treated with or without rhCCL22 were injected subcutaneously beneath the grafts **(*Figure 5.2.10. (b) & (c)*).** Grafts were monitored bi-daily until they developed macroscopic features of late rejection (as previously described) **(*Figure 5.2.10. (d)*)** or to 100 days.

In the presence of Matrigels, Tregs maintained their ability to prolong allograft survival (PBMC + Matrigel MST 32 days *cf.* PBMC + Treg + Matrigel MST 52 days, p=0.0082) **(*Figure 5.2.10. (e) & (f)*)**. The presence of Matrigels did not affect graft survival in mice injected with human Tregs (PBMC + Treg MST 48 days *cf.* PBMC + Treg + Matrigel MST 52 days, p=0.6154). Matrigels treated with CCL22 significantly prolonged allograft survival and led to long-term survival (MST>100 days) in 4 of 6 mice. Upon harvest, Matrigels were tethered to the under surface of skin grafts and blood vessels traversing between the two could be observed **(*Figure 5.2.10. (g)*).**

These results suggest that expression of CCL17/22 beneath skin allografts can prolong human skin allograft survival. This is likely to result from augmented chemotactic recruitment of Tregs and suppression of the human allo-rejection response.

5.3. Discussion

Treg therapy is an established therapeutic option for the prevention of allogeneic human transplant rejection. Currently, the use of polyclonally expanded total Tregs from peripheral blood forms the mainstay of the clinical application in transplantation. Whereas the evidence base for the efficacy of this therapy is strong, the goal of obviating the requirement for immunosuppressive drugs has not yet been achieved. This in part reflects difficulties associated with the extensive expansion of Tregs required for therapeutic applications, and the need to determine optimal Tregs in terms of safety and suppressive function. It is well documented that the Treg population is functionally heterogenous, encompassing a broad spectrum of suppressive mechanisms capable of controlling various inflammatory immune responses[384]. We recently identified differences in suppressive capacities of Tregs based on the expression of markers such as CD27, CD70[374] and ST2[385].

In this chapter we investigated the relationship between expression of CCR4 and CCR8, and the suppressive capacity of Tregs. We demonstrate that in human blood, CCR4 and CCR8 are expressed more common on Tregs than Tconvs. This interesting finding may go some way toward explaining the disproportionate recruitment of $CCR4^+$ and $CCR8^+$ Tregs into the tumour microenvironment of several cancers, which is associated with a reduced antitumour immune response. The pathogenesis of cancers such as adult T cell lymphoma/leukaemia[172], breast cancer[173], non-Hodgkins lymphoma[174], head and neck cancer[175] and melanoma[167,176] derive in part from microenvironmental enrichment of chemokines such as CCL1, CCL17 and CCL22, which attract immunosuppressive cells including Tregs. This has influenced researchers to explore augmentation of anti-tumour immune activity through exploitation of tumour-specific chemokine axes. To counteract the immunosuppressive effect of CCR4-

mediated Treg migration in non-Hodgkin's lymphoma, CD30 chimeric antigen receptor T cells (CAR-T) have been engineered to co-express CCR4, which enhanced homing and anti-tumour immunity[386]. T cell transduction has been similarly employed to enhance adoptive cell transfer, redirecting cytotoxic immunity towards CCL22 producing pancreatic cancer[387]. In contrast with the burgeoning experimental utility of chemokine receptor-engineered leucocytes, the use of exogenous chemokines to attract cells of interest tends to have predominantly been described in *in vitro* studies[388]. However, in light of reported successes in the use of CCR4 inhibition to abrogate Treg-mediated immunosuppression in cancer[389], we sought to investigate whether augmenting the CCL22-CCR4 axis could increase the suppressive capacity of Tregs. In doing so, we demonstrated that following expansion, Tregs expressing CCR4 and CCR8 suppress *in vitro* proliferation of polyclonally stimulated Tconvs significantly more than $CCR4^-$ and $CCR8^-$ Tregs respectively. The close proximity of these cells in 96-well plates suggests that the enhanced suppressive capacity observed does not solely relate to migratory function. However, considering CCL17 and CCL22 are expressed at high levels in skin[390-392], it is reasonable to suspect that the significantly prolonged survival of allogeneic human skin transplants following adoptive transfer of expanded $CCR4^+$ Tregs compared with expanded $CCR4^-$ Tregs relates to the skin-homing capacity of CCR4. Following this experiment, we sought to investigate whether we could increase the frequency of CCR4-expressing Tregs. To achieve this, we stimulated human Tregs *in vitro* and observed a transient two-fold increase in $CCR4^+$ Treg numbers by day 4 and again at day 10. Transient upregulation of CCR4 and CCR8 mRNA following CD3/CD28 stimulation on a Th2 clone has previously been described[393]. To assess the effects of prolonged stimulation on CCR4 expression levels (as is likely to occur following allo-transplantation), we then tracked expression over two weeks of Treg expansion (with high-dose stimulation) and identified that

re-stimulation sustains high-expression of CCR4, which persists after freezing. Having developed a large population of $CCR4^+$ Tregs with potent suppressive capacity, we then explored the potential to employ the chemoattractant properties of CCR4 and thus boost migration of adoptively transferred expanded human Tregs to desired sites of action. To achieve this, we developed a model of localised chemokine expression in which Matrigel hydrogels were functionalised by impregnation with recombinant chemokines and injected subcutaneously. In developing this model, we discovered that *in vivo* chemoattraction of unstimulated human PBMCs only occurs to a measurable degree in the presence of stimulatory cytokines. We interpreted this to suggest that stimulation—as would occur following injury, inflammation, infection or surgery—is required to support a robust chemotactic motility response. This would be in keeping with published stimulation experiments**.** and the results presented here, which showed CCR4 expression to increase following Treg stimulation through CD3 and CD28 in the presence of IL2. Having demonstrated human Treg chemotaxis in this model, our next step was to incorporate our functionalised Matrigels into the humanised mouse model of human skin transplantation. Thus, CCL17/22-impregnated Matrigels were injected beneath human skin allografts at a time point when early macroscopic features of allograft rejection typically arise in the skin allograft model (~28 days). This treatment significantly prolonged allograft survival compared with standard Treg adoptive transfer therapy. Unfortunately, owing to disruptions caused by the COVID-19 pandemic, it was not possible to perform further cellular analyses on samples from long-term surviving mice. Additionally, a confirmatory experiment which included a group of CCL22+Mogamulizumab-treated Matrigels had to be terminated early. Ideally, I would have evaluated the cellular composition of both skins and Matrigels harvested from mice, as well as mRNA expression profiles by NanoString.

Due to the biocompatibility, biodegradability and cell-supportive microenvironment of Matrigel, it was a suitable material to utilise in our conceptual analysis of localised therapeutic chemotaxis. Additionally, use of a hydrogel-type scaffold afforded the potential for removal should adverse reactions thought to relate to the hydrogel have occurred. However, despite Matrigels widespread use in biological investigations, limitations such as inter-batch variability can affect reproduction of results. In consideration of this, to optimise reliability, our *in vivo* experiments were replicated with Matrigels of different batch numbers for each repeat. Additionally, considering Matrigel is derived from mouse sarcoma, it is feasible that pathogen transmission and immunogenicity could occur and therefore subsequent experimentation and clinical application of this model will utilise an alternative scaffold material such as Matriderm. This clinically approved acellular collagen-elastin dermal matrix is commonly used in reconstructive surgery beneath split-thickness skin grafts and could incorporate CCL17/22-fortified solution into its rehydration step.

A wave of recent research has developed an abundance of alternative synthetic scaffolds with tuneable mechanical, biological and degradative properties as well as options for biofunctionalisation that can create bespoke microenvironments for specific therapeutic needs[394]. An issue in the short-to-medium term may be the prohibitive cost of some such scaffolds, which may limit clinical uptake.

By demonstrating inhibited Tconv proliferation *in vitro* and longer graft survival with $CCR4^+$ Tregs *in vivo*, our results indicate that the CCR4 axis confers high-level Treg-mediated suppression through chemotactic and non-chemotactic mechanisms. Through studies of cancer, it has become increasingly appreciated that chemokine functions extend beyond typical migration-related processes and include atypical functions that do not directly activate

motility pathways[395]. For example, certain chemokines have been implicated directly in increasing the expression of checkpoint blockade molecules (e.g. PD-L1) on tumour cells, thus reducing the effectiveness of the anti-tumour immune response[395]. Expression of chemokines also affects cellular phenotype and disease progression. For example, CXCL12, CXCR4, and CXCR7-expressing pancreatic tumours have been shown to exhibit lower focal expression of Ki-67 than common (control) tumours, partially explaining lower proliferative potential *in vivo*[396].

We explored differences in the phenotypes and functionality of CCR4/CCR8-expressing Tregs and identified disparities in the expression of functional proteins that are unrelated to motility processes. Two proteins expressed more frequently on expanded $CCR4^+$ and $CCR8^+$ Tregs were FOXP3 and CD27. *FOXP3* is the master regulator of Treg suppressive capacity and Treg function is dependent on stable FOXP3 expression[371]. Studies have shown loss of FOXP3 expression to be associated with reduced suppressive capacity and conversion into Th cell phenotypes with the capacity to secrete inflammatory cytokines[397,398] (e.g. IFNγ, IL2 and IL17). CD27 is a costimulatory receptor for T cells and its expression has been shown to positively correlate with Treg suppressive potency[374,399,400]. These results correlate with a report showing FOXP3 expression to be greater on highly suppressive CD27-expressing cells[374]. Differential expression of other suppression associated Treg markers was identified on $CCR8^+$ Tregs, including CD154, which shows lower surface expression on $CCR4^+$ compared with $CCR4^-$ Tregs and interestingly higher expression on $CCR8^+$ than $CCR8^-$ Tregs. The disparate effects of CD154 expression on Treg function is not fully understood, with reports describing CD154 positivity and negativity as markers of highly suppressive Tregs in different contexts. From our results, it may be reasonable to suggest that lower CD154 expression as seen in our more potently suppressive $CCR4^+$ Tregs may represent the more regulatory phenotype. It is possible

that this may relate to difficulties in isolating pure CCR8$^+$ Tregs and possibly to the pro-inflammatory cytokine secreting potential described even in suppressive CD154$^+$ Tregs[401]. LAG3, which is expressed on both induced Tregs and activated natural Tregs at higher levels than on activated effector T cells[375], was more abundant on CCR4$^+$ Tregs. A potent suppressive co-inhibitor, it is necessary for Treg-mediated control of T cell homeostasis[402], inhibiting T cell expansion through various mechanisms including blocking of the interaction with MHC class II[403].

Altogether, the results in this chapter demonstrate the high potency of CCR4$^+$ Tregs and present a practical method of targeting immune-regulatory function to the site of skin allo-transplantation. Techniques such as these could help to reduce the number of Tregs required in adoptive cell therapies without reducing treatment efficacy. This carries the potential to reduce the potential for off-target effects and the time and cost of producing Tregs for adoptive transfer.

Chapter 5: Figures

5.2.1. Expression of CCR4 and CCR8 is more abundant on human $CD4^+$ Tregs than $CD4^+$ Tconvs. Expression is predominantly seen on memory $CD4^+$ Tregs.

Comparison of surface (a & c) CCR4, (b & d) CCR8 and (e) dual ($CCR4^+CCR8^+$) expression on healthy human peripheral blood Tregs and Tconvs.

Thawed PBMCs were analysed by flow cytometry to evaluate frequencies of (a) live human $7AAD^-CD45^+CD3^+CD25^+CD127^{lo}CCR4^+$ Tregs and $7AAD^-CD45^+CD3^+CD4^+CD25^-CCR4^+$ Tconvs. (b) CCR8 expression was similarly analysed on $7AAD^-CD45^+CD3^+CD25^+CD127^{lo}CCR8^+$ Tregs and $7AAD^-CD45^+CD3^+CD4^+CD25^-CCR8^+$ Tconvs. (c) CCR4 and (d) CCR8 expression on naïve and memory Treg subtypes was analysed by CD45RA expression. (e) Dual ($CCR4^+CCR8^+$) expression on Tregs and Tconvs.

Data are represented as (a & c) frequencies of (a) $CD4^+CCR4^+$ Tregs and Tconvs and (c) $CD4^+CCR8^+$ Tregs and Tconvs (as percentages of total $CD4^+$ Tregs and total $CD4^+$ Tconvs respectively); and (b & d) representative corresponding histograms. (e & f) flow cytometric analyses of naïve and memory subtypes. (g) Frequencies of $CD4^+CCR8^+$ Tregs and Tconvs. Bars indicate mean +/- SEM. Statistical significance was assessed using the paired t-test (*, $p<0.05$; **, $p<0.01$; ****, $p<0.0001$).

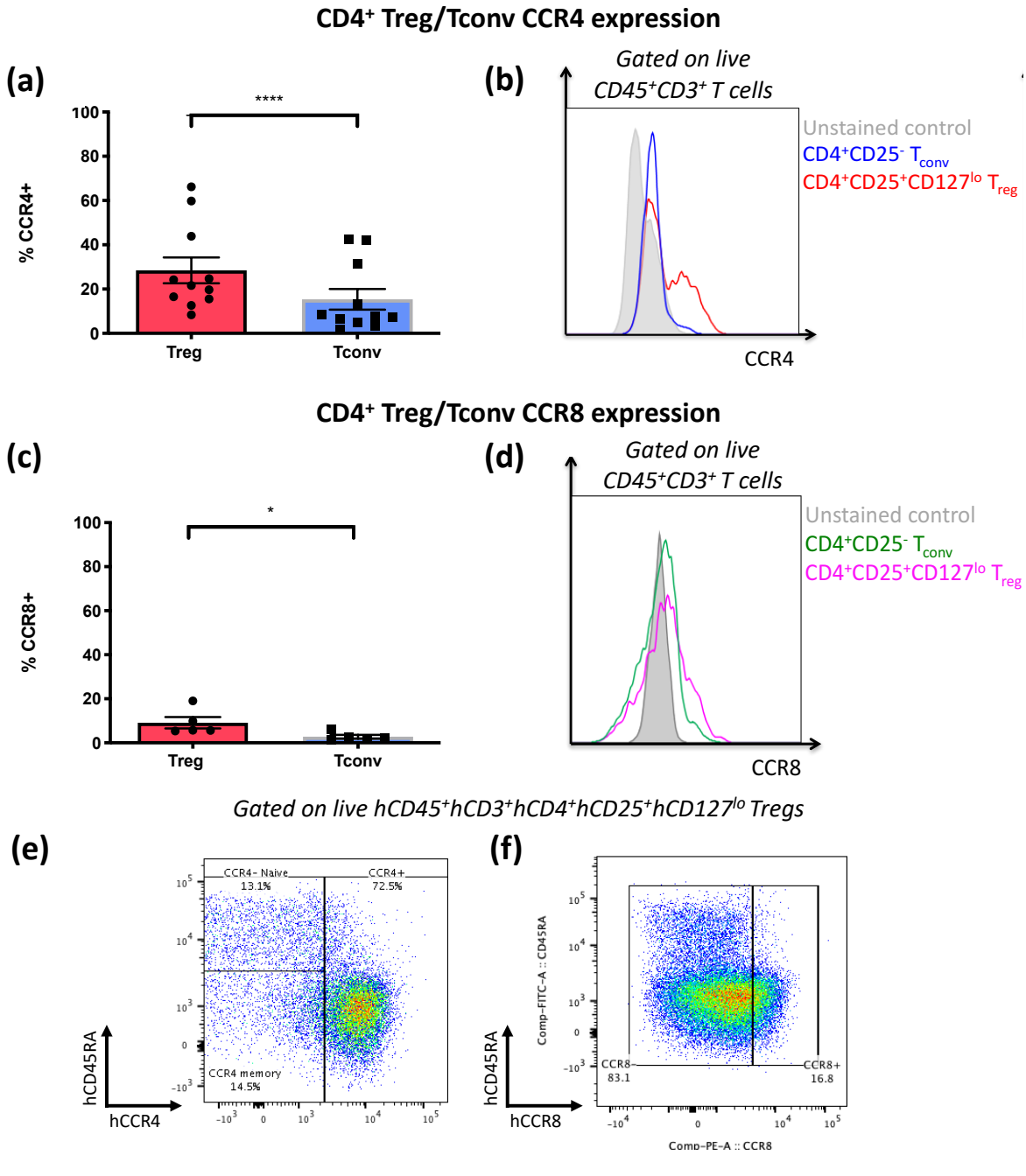
CD4+ Treg/Tconv CCR4 expression
(a)
****
% CCR4+
100
80
60
40
20
0
Treg
Tconv
(b)
Gated on live
CD45+CD3+ T cells
Unstained control
CD4+CD25- Tconv
CD4+CD25+CD127lo Treg
CCR4
CD4+ Treg/Tconv CCR8 expression
(c)
*
% CCR8+
100
80
60
40
20
0
Treg
Tconv
(d)
Gated on live
CD45+CD3+ T cells
Unstained control
CD4+CD25- Tconv
CD4+CD25+CD127lo Treg
CCR8
Gated on live hCD45+hCD3+hCD4+hCD25+hCD127lo Tregs
(e)
CCR4- Naive
13.1%
CCR4+
72.5%
CCR4 memory
14.5%
hCD45RA
hCCR4
(f)
Comp-FITC-A :: CD45RA
CCR8-
83.1
CCR8+
16.8
hCD45RA
hCCR8
Comp-PE-A :: CCR8
(g)
CD4+ T cell CCR4/CCR8 co-expression
**
% CCR4+CCR8+
100
80
60
40
20
0
Treg
Tconv

Figure 5.2.2. $CCR4^+$ Tregs are more suppressive than $CCR4^-$ Tregs *in vitro*. Comparison of the capacity for expanded $CCR4^+$ and $CCR4^-$ Treg to suppress *in vitro* proliferation of stimulated Tconvs.

(a) PBMCs isolated from the blood of healthy human donors underwent $CD25^+$ MACS bead enrichment, FACS sorting into $7AAD^-CD45^+CD3^+CD25^+CD127^{lo}$ Treg, and 14-day expansion by αCD3αCD28 bead stimulation (at D0 & D7) in complete human media + rhIL-2 (1000U/ml). Following 2 days of rest in complete human medium supplemented with rhIL-2 (200U/ml) (b) CCR4 expression was assessed, (c) expanded Tregs were sorted into $CCR4^+$ and $CCR4^-$ fractions, and (d) purity of the sorted cells was analysed. (e) Allogeneic human T cells were enriched using CD3-selective MACS beads (positive selection), labelled with violet proliferation dye (VPD), then $1x10^5$ T cells were stimulated with $2x10^4$ αCD3αCD28 beads and co-cultured with reducing doses of Treg for 72-78h in triplicate wells. T cell proliferation was measured by VPD dilution and analysed by flow cytometry (f) - (i). n=4

Data are represented as schematics demonstrating the experimental outline (a) & (e), a (b) frequencies of $CCR4^+$ and $CCR4^-$ Tregs following expansion and resting, (c-d) FACS plots indicating (c) sorting gates (red dashed lines) and (d) sort purities, (f & h) histograms demonstrating T cell proliferation (indicated by VPD dilution) for (f) CD8+ Tconvs & (h) CD4+ Tconvs, (g & i) division indices (DI) of T cells cultured without Tregs (black bars), with $CCR4^+$ Treg (red bars) and $CCR4^-$ Tregs (blue bars) at the Tconv:Treg ratios specified. Bars represent SD. Statistical significance was assessed using the Ordinary one-way ANOVA with Tukey's multiple comparisons test (*, $p<0.05$; **, $p<0.01$; ***, $p<0.001$; ****, $p<0.0001$; ns, $p>0.05$).

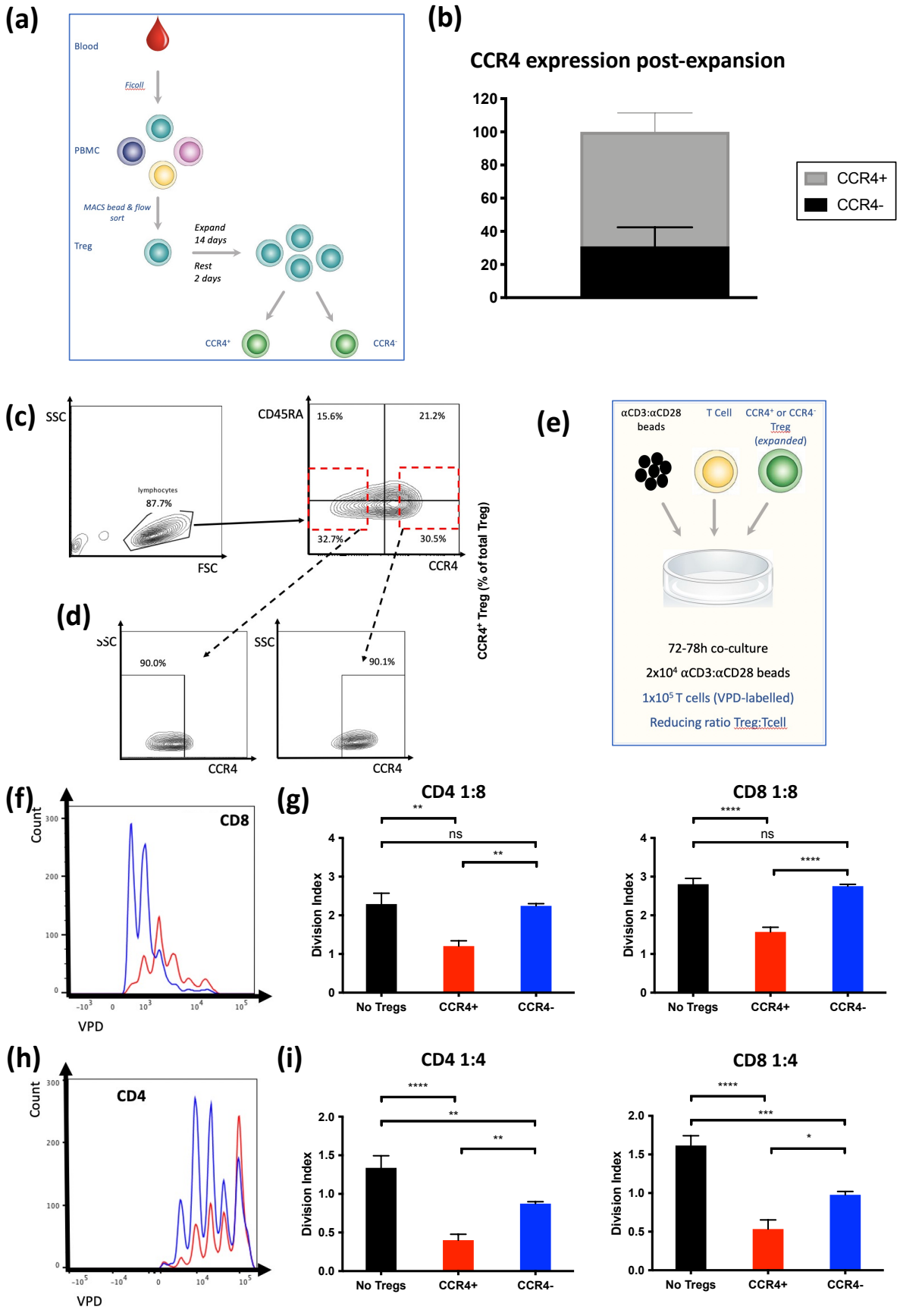
(a)
Blood
Ficoll
PBMC
MACS bead & flow sort
Treg
Expand 14 days
Rest 2 days
CCR4+
CCR4-
(b)
CCR4 expression post-expansion
120
100
80
60
40
20
0
CCR4+
CCR4-
(c)
SSC
FSC
lymphocytes
87.7%
CD45RA
15.6%
21.2%
32.7%
30.5%
CCR4
CCR4+ Treg (% of total Treg)
(d)
SSC
90.0%
90.1%
CCR4
CCR4
(e)
αCD3:αCD28 beads
T Cell
CCR4+ or CCR4- Treg (expanded)
72-78h co-culture
2x10^4 αCD3:αCD28 beads
1x10^5 T cells (VPD-labelled)
Reducing ratio Treg:Tcell
(f)
Count
CD8
VPD
(g)
CD4 1:8
CD8 1:8
Division Index
ns
No Tregs
CCR4+
CCR4-
(h)
Count
CD4
VPD
(i)
CD4 1:4
CD8 1:4
Division Index
No Tregs
CCR4+
CCR4-

Figure 5.2.3 CCR8$^+$ Tregs are more suppressive than CCR8$^-$ Tregs *in vitro*.
Comparison of the capacity for expanded CCR8$^+$ and CCR8$^-$ Treg to suppress *in vitro* proliferation of stimulated Tconvs.
(a) PBMCs isolated from the blood of healthy human donors underwent CD25$^+$ MACS bead enrichment, FACS sorting into 7AAD$^-$CD45$^+$CD3$^+$CD25$^+$CD127^{lo} Treg, and 14-day expansion by αCD3αCD28 bead stimulation (at D0 & D7) in complete human media + rhIL-2 (1000U/ml). Following 2 days of rest in complete human medium supplemented with rhIL-2 (200U/ml) (b) CCR8 expression was assessed, (c) expanded Tregs were sorted into CCR8$^+$ and CCR8$^-$ fractions, and purity of the sorted cells was analysed. (d) Allogeneic human T cells were enriched using CD3-selective MACS beads (positive selection), labelled with violet proliferation dye (VPD), then 1x10^5 T cells were stimulated with 2x10^4 αCD3αCD28 beads and co-cultured with reducing doses of CCR8$^+$ or CCR8$^-$ Tregs for 72-78h in triplicate wells. T cell proliferation was measured by VPD dilution and analysed by flow cytometry (e) - (h). n=4
Data are represented as (a) & (d) schematics demonstrating the experimental outline, (b) frequencies of CCR8$^+$ and CCR8$^-$ Tregs following expansion and resting, (c) FACS plots indicating sort purities, (e & g) histograms demonstrating T cell proliferation (indicated by VPD dilution) for CD8+ Tconvs & CD4+ Tconvs, (f & h) division indices (DI) of T cells cultured without Tregs (black bars), with CCR8$^+$ Tregs (red bars) and CCR8$^-$ Tregs (blue bars) at the T cell:Treg ratios specified. Bars represent SD. Statistical significance was assessed using the Ordinary one-way ANOVA with Tukey's multiple comparisons test (*, p<0.05; **, p<0.01; ***, p<0.001; ****, p<0.0001; ns, p>0.05).

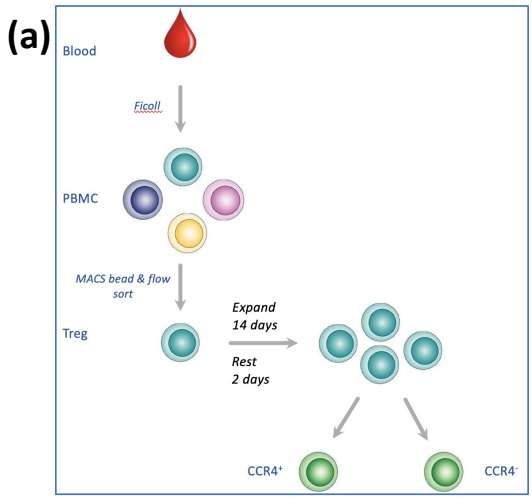
(a)
Blood
Ficoll
PBMC
MACS bead & flow sort
Treg
Expand 14 days
Rest 2 days
CCR4+
CCR4-

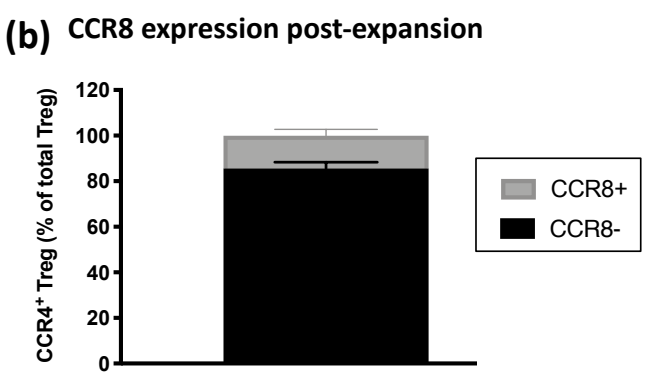
(b) CCR8 expression post-expansion
CCR4+ Treg (% of total Treg)
120
100
80
60
40
20
0
CCR8+
CCR8-

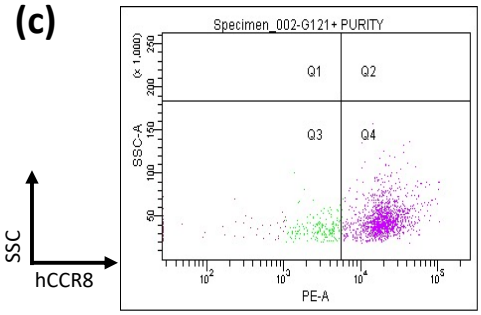
(c)
Specimen_002-G121+ PURITY
Q1
Q2
Q3
Q4
SSC-A
PE-A
SSC
hCCR8

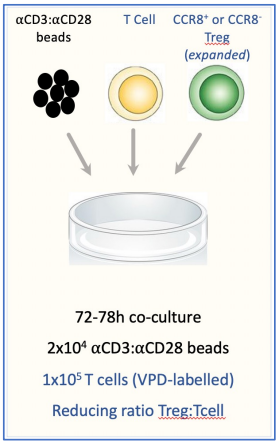
(d)
αCD3:αCD28 beads
T Cell
CCR8+ or CCR8- Treg (expanded)
72-78h co-culture
2x10⁴ αCD3:αCD28 beads
1x10⁵ T cells (VPD-labelled)
Reducing ratio Treg:Tcell

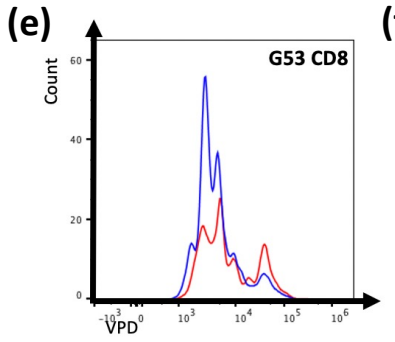
(e)
G53 CD8
Count
VPD

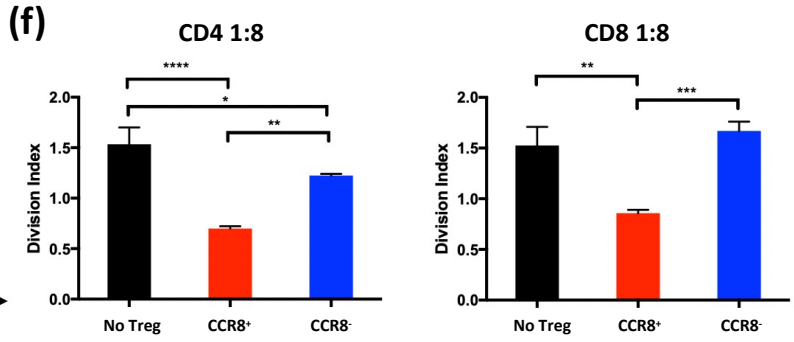
(f)
CD4 1:8
CD8 1:8
Division Index
No Treg
CCR8+
CCR8-

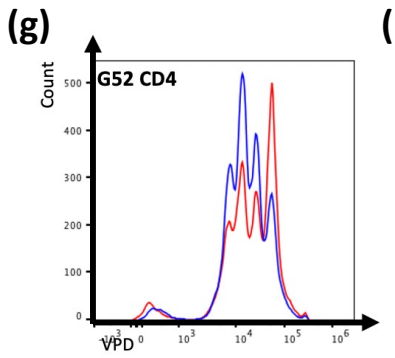
(g)
G52 CD4
Count
VPD

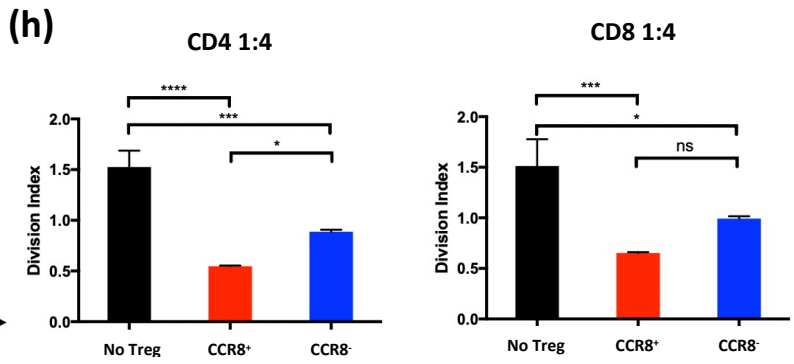
(h)
CD4 1:4
CD8 1:4
Division Index
No Treg
CCR8+
CCR8-
ns

Figure 5.2.4 CCR4$^+$ Tregs prolong human skin allograft survival.
Comparison of human skin allograft rejection on BALB/c-Rag2$^{-/-}$cγ$^{-/-}$ (BRG) mice humanised with PBMCs and CCR4$^+$ or CCR4$^-$ Tregs.
BRG mice received 1 cm^2 split-thickness skin grafts procured from excess abdominal free flap tissue from a single donor. (a) Skin grafts were allowed to heal-in for 5 weeks, then 5x10^6 allogeneic human PBMCs suspended in 200µl RPMI were injected intraperitoneally either alone or with and 1x10^6 CCR4$^-$ or CCR4$^+$ expanded-sorted Tregs. (b) Grafts were monitored bi-daily and harvested when they had developed features of late rejection or at 100 days (experimental end-point). (c) Time-course analysis of rejection is shown together with (d) the number of mice per group, survival time, censored mice and MSTs.
Data from 2 independent experiments. In each experiment, mice received leucocytes from one of 2 human blood donors. Data represented as (a) a schematic outline of the experiment, (b) photographs demonstrating macroscopic features of rejection, (c) survival curves indicating the Median survival times (MSTs) for mice humanised with PBMCs alone (black line), or with CCR4$^-$ or CCR4$^+$ Tregs (blue and red lines, respectively); (d) a table indicating study groups. Statistical significance was assessed using the Log-rank (Mantel-Cox) test (*, $p<0.05$; ns, $p>0.05$).

(a)

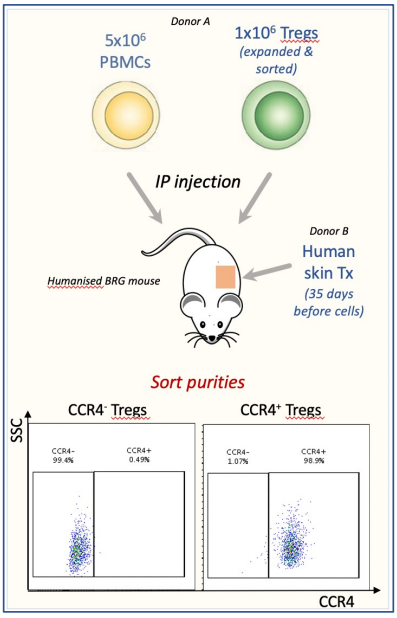

(b)

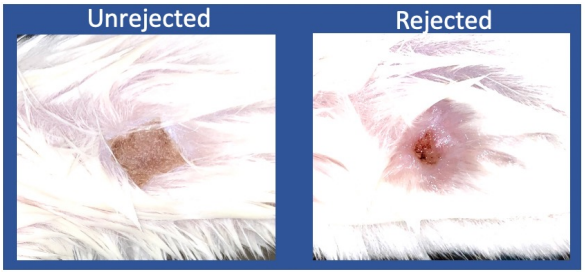

(c)

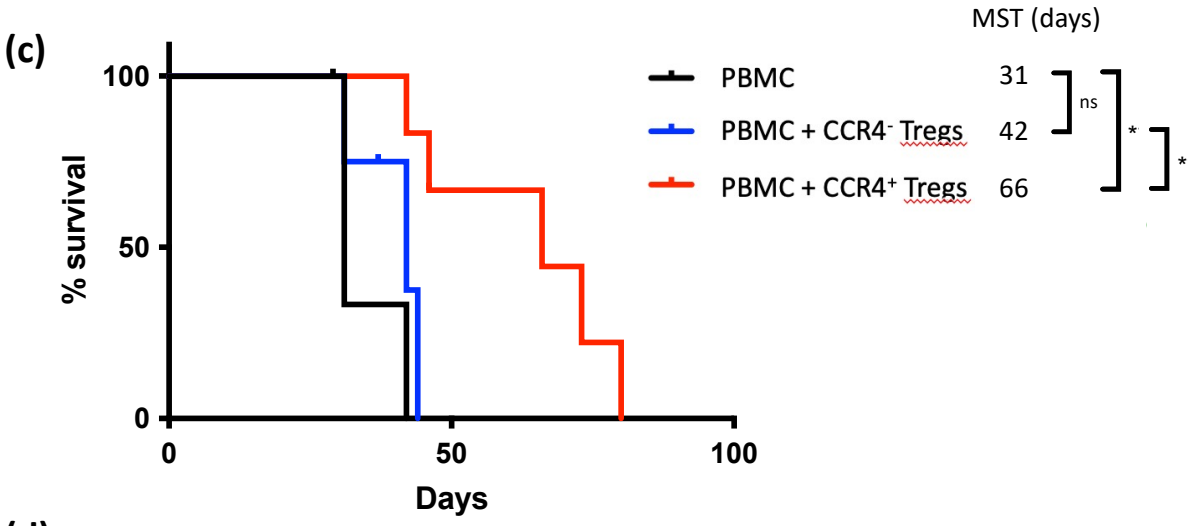

(d)

Group	n	Survival (days)	Censored (day)	MST (days)
PBMC	4	31, 31, 42	1 (29)	31
PBMC + CCR4⁻ Tregs	4	31, 42, 44	1 (37)	42
PBMC + CCR4⁺ Tregs	6	42, 46, 66, 73, 80	1 (46)	66

Figure 5.2.5 $CCR8^+$ and $CCR8^-$ Treg prolong human skin allograft survival equivalently. Comparison of human skin allograft rejection on BALB/c-$Rag2^{-/-}c\gamma^{-/-}$ (BRG) mice humanised with PBMCs and $CCR8^+$ or $CCR8^-$ Tregs.
BRG mice received 1 cm^2 split-thickness skin grafts procured from excess abdominal free flap tissue from a single donor. (a) Skin grafts were allowed to heal-in for 5 weeks, then $5x10^6$ allogeneic human PBMCs suspended in 200µl RPMI were injected intraperitoneally either alone or with and $1x10^6$ $CCR4^-$ or $CCR4^+$ expanded-sorted Tregs. Grafts were monitored bi-daily and harvested when they had developed features of late rejection (***Figure 5.2.4. (b)***) or at 100 days (experimental end-point). (b) Time-course analysis of rejection is shown together with (c) the number of mice per group, survival time and MST.
Data from 2 independent experiments. In each experiment, mice received leucocytes from one of 2 human blood donors. Data represented as (a) a schematic outline of the experiment, (b) survival curves indicating the Median survival times (MSTs) for mice humanised with PBMCs alone (black line), or with $CCR4^-$ or $CCR4^+$ Tregs (blue and red lines, respectively); (c) a table indicating study groups. Statistical significance was assessed using the Log-rank (Mantel-Cox) test (*, $p<0.05$; **, $p<0.01$; ns, $p>0.05$).

(a)

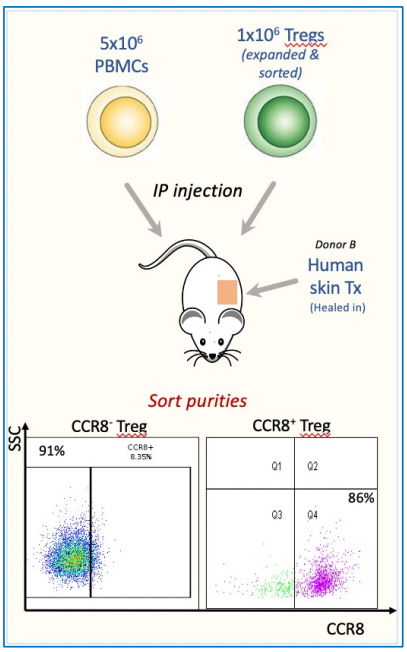

(b)

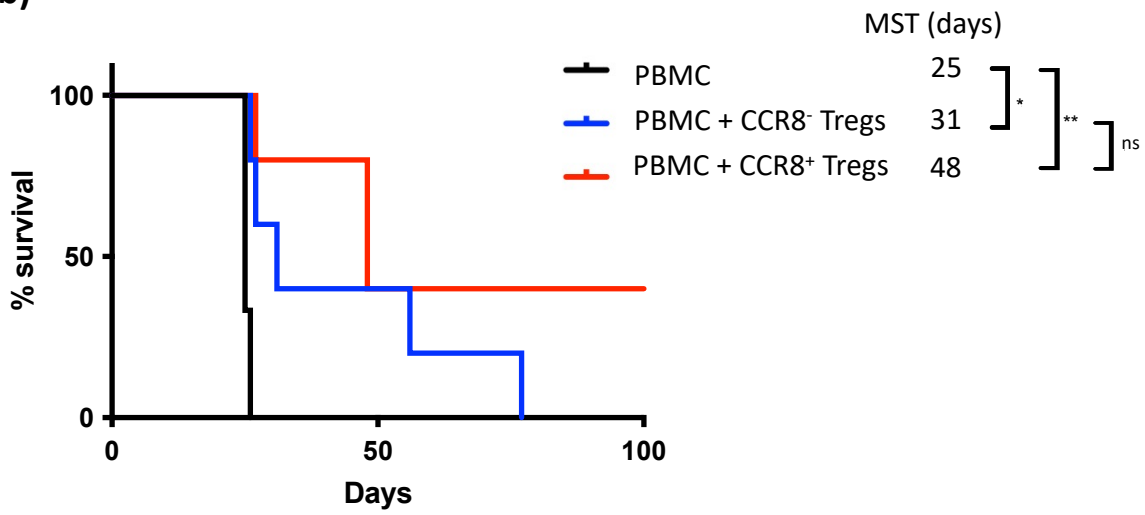

(c)

Group	n	Survival (days)	Censored (days)	MST (days)
PBMC	3	25, 25, 26	0	25
PBMC + CCR8⁻ Tregs	5	26, 27, 31, 56, 77	0	31
PBMC + CCR8⁺ Tregs	5	27, 48, 48, 100, 100	0	48

Figure 5.2.6 Dynamics of CCR4 expression following polyclonal stimulation of Tregs. Analysis of Treg CCR4 expression following stimulation with αCD3αCD28 beads recombinant human IL-2, and the chemokines CCL17/22.
$1x10^5$ FACS-sorted $7AAD^-CD45^+CD3^+CD25^+CD127^{lo}CD45RA^+CCR4^+$ and $7AAD^-CD45^+CD3^+CD25^+CD127^{lo}CCR4^-$ Tregs were separately cultured in complete media, in the presence of recombinant human IL-2 (200U/ml) and stimulated with $2x10^4$ αCD3αCD28 T cell activator beads (1:5 Treg:bead ratio), with or without recombinant human CCL17/22 for 14 days (a-c). CCR4 expression was analysed bi-daily by flow cytometry (d-f). n=4. Separately, $7AAD^-CD45^+CD3^+CD25^+CD127^{lo}$ Tregs undergoing expansion by culturing in complete media, in the presence of recombinant human IL-2 (1000U/ml) and stimulated at Day 0 and 7 with αCD3αCD28 T cell activator beads in a 1:3 Treg:bead ratio for 14 days were analysed for CCR4 expression (g-h). n=3.
Data are represented as (a & g) schematics demonstrating the experimental outline, (b-d) flow cytometric analyses demonstrating (b) the gating strategy used to sort $CCR4^+$ and $CCR4^-$ Tregs, (c) purity of sorted Tregs, and (d) staining of stimulated Tregs (+ unstained control); (e, f & h) time course analyses indicating (e) numbers and (f & g) frequencies of human $CCR4^+$ Tregs (as percentages of total $CD4^+$ Tregs). Bars indicate means +/- SD. Statistical significance was assessed using the Ordinary one-way ANOVA with Tukey's multiple comparisons test (*, $p<0.05$).

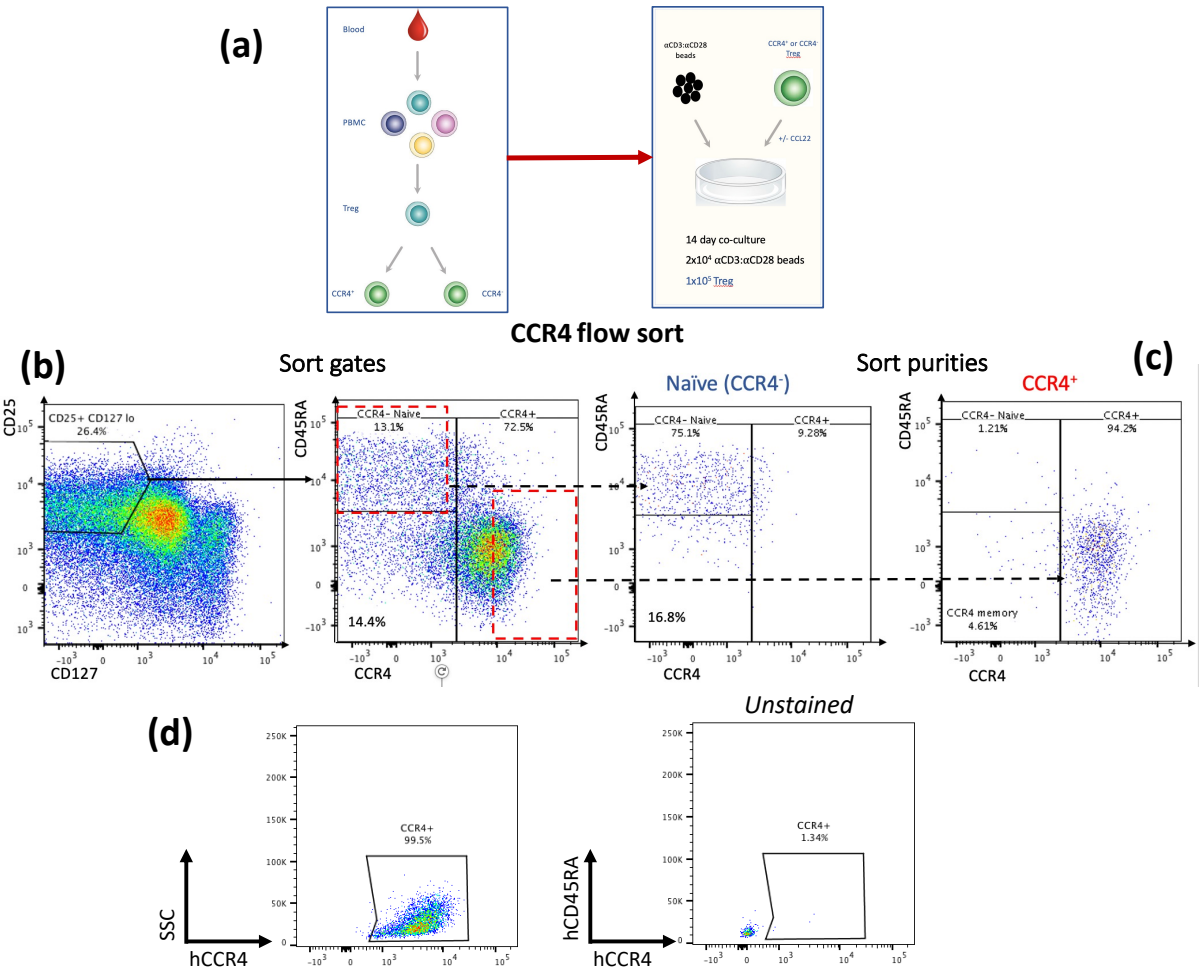
(a)
Blood
PBMC
Treg
CCR4+
CCR4-
αCD3:αCD28 beads
CCR4+ or CCR4- Treg
+/- CCL22
14 day co-culture
2x10⁴ αCD3:αCD28 beads
1x10⁵ Treg
CCR4 flow sort
(b)
Sort gates
Sort purities
(c)
Naïve (CCR4-)
CCR4+
CD25
CD127
CD25+ CD127 lo
26.4%
CD45RA
CCR4
CCR4- Naive
13.1%
CCR4+
72.5%
14.4%
CCR4- Naive
75.1%
CCR4+
9.28%
16.8%
CCR4- Naive
1.21%
CCR4+
94.2%
CCR4 memory
4.61%
(d)
Unstained
SSC
hCCR4
CCR4+
99.5%
hCD45RA
CCR4+
1.34%
Stimulation of naïve (CCR4-) vs CCR4+ sorted Tregs
(e)
No. of CCR4+ cells
Days post-stimulation
(f)
% CCR4+ cells
Days post-stimulation
Naive + Chemokine
Naive
CCR4+ Chemokine
CCR4+
n=4
CCR4 expression following high-dose polyclonal stimulation of sorted total Tregs
(g)
αCD3:αCD28 beads
Treg
14-day co-culture
1x10⁵ Treg
αCD3:αCD28 beads (D0 & D7)
(1:3 Treg:bead ratio)
Analysis: CCR4 expression
(h)
begin proliferating
restimulation
CCR4+ Treg (% of total Treg)
Day
Donor 1
Donor 2
Donor 3
n=3

Figure 5.2.7 Dynamics of CCR8 expression following polyclonal stimulation of Treg. Analysis of Treg CCR4 expression following stimulation with αCD3αCD28 beads and recombinant human IL-2.
$7AAD^{-}CD45^{+}CD3^{+}CD25^{+}CD127^{lo}CD45RA^{+}CCR8^{+}$ and $7AAD^{-}CD45^{+}CD3^{+}CD25^{+}CD127^{lo}CCR8^{-}$ Tregs were sorted from whole Tregs by FACS (a)-(c). $1x10^{5}$ Tregs from each group were separately cultured in complete media, in the presence of recombinant human IL-2 (200U/ml) and stimulated with $2x10^{4}$ αCD3αCD28 T cell activator beads (1:5 cell:bead ratio), for 14 days (d). CCR8 expression was analysed bi-daily by FACS (e)-(g). n=4. Separately $7AAD^{-}CD45^{+}CD3^{+}CD25^{+}CD127^{lo}$ Tregs undergoing expansion by culturing in complete media, in the presence of recombinant human IL-2 (1000U/ml) and stimulated at Day 0 and 7 with αCD3αCD28 T cell activator beads in a 1:3 cell:bead ratio for 14 days were analysed for CCR8 expression by FACS (h). n=3.
Data are represented as schematics demonstrating the experimental outline (a) & (d), FACS plots demonstrating the gating strategy used to sort $CCR8^{+}$ and $CCR8^{-}$ Tregs (b), the purity of sorted Tregs (c), and staining of stimulated Tregs (+ unstained control) (e), and as a time course analysis indicating the number (f) and frequencies (g) & (h) of human $CCR8^{+}$ Treg (as percentages of total $CD4^{+}$ Treg). Bars indicate mean +/- SD. Statistical significance was assessed using the unpaired t test (**, $p<0.01$).

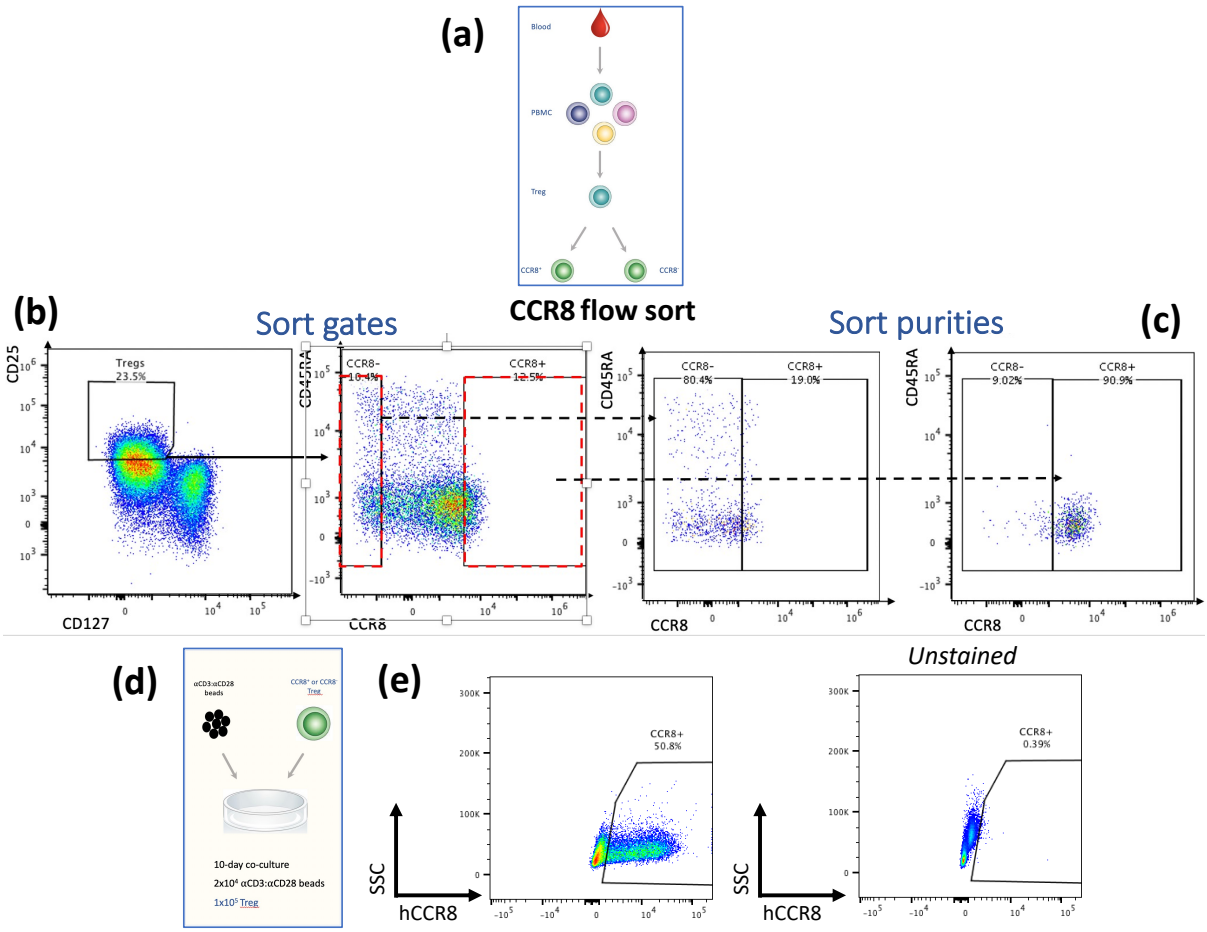
(a)
Blood
PBMC
Treg
CCR8+
CCR8-
(b)
Sort gates
CCR8 flow sort
Sort purities
(c)
Tregs
23.5%
CD25
CD127
CD45RA
CCR8
CCR8-
10.4%
CCR8+
12.5%
CCR8-
80.4%
CCR8+
19.0%
CCR8-
9.02%
CCR8+
90.9%
(d)
αCD3:αCD28 beads
CCR8+ or CCR8- Treg
10-day co-culture
2x10⁴ αCD3:αCD28 beads
1x10⁵ Treg
(e)
Unstained
CCR8+
50.8%
CCR8+
0.39%
SSC
hCCR8
Stimulation of CCR8⁺ vs CCR8⁻ sorted Treg
(f)
No of CCR8+ cells
Days post-stimulation
(g)
% CCR8+ cells
Days post-stimulation
CCR8+
CCR8-
**
n=4
CCR8 expression following high-dose polyclonal stimulation of sorted total Treg
(h)
CCR8⁺ Treg (% of total Treg)
restimulation
Day
Donor 1
Donor 2
Donor 3

Figure 5.2.8 CCR4$^+$ Tregs express markers associated with greater regulatory function & Treg stability.

Comparison of functional marker expression on CCR4$^+$ and CCR4$^-$ Tregs.

(a) Thawed, expanded human Tregs were analysed by flow cytometry for expression of markers expressed by highly suppressive Tregs.

Data are represented as (a) a schematic demonstrating the experimental outline, geometric mean fluorescence intensities (MFIs) of (b) CD27, (c) FOXP3, (d) LAG3, (e) TIGIT and (f) CD154) on CCR4$^+$ (red symbols) and CCR4$^-$ (blue symbols) Tregs; (g) functional information about the differentially expressed markers. Black lines link samples from the same donor. Statistical significance was assessed using the Paired t test (*, $p<0.05$; **, $p<0.01$).

Experimental outline – analysis of Treg suppressive markers

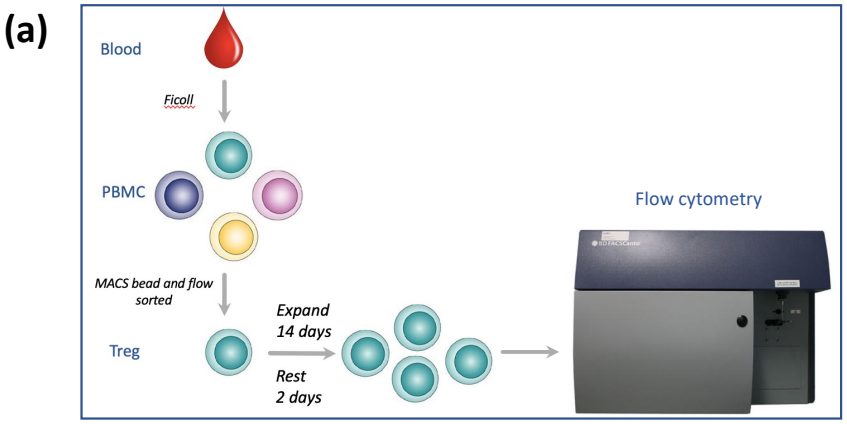

Expression levels of Treg suppressive markers

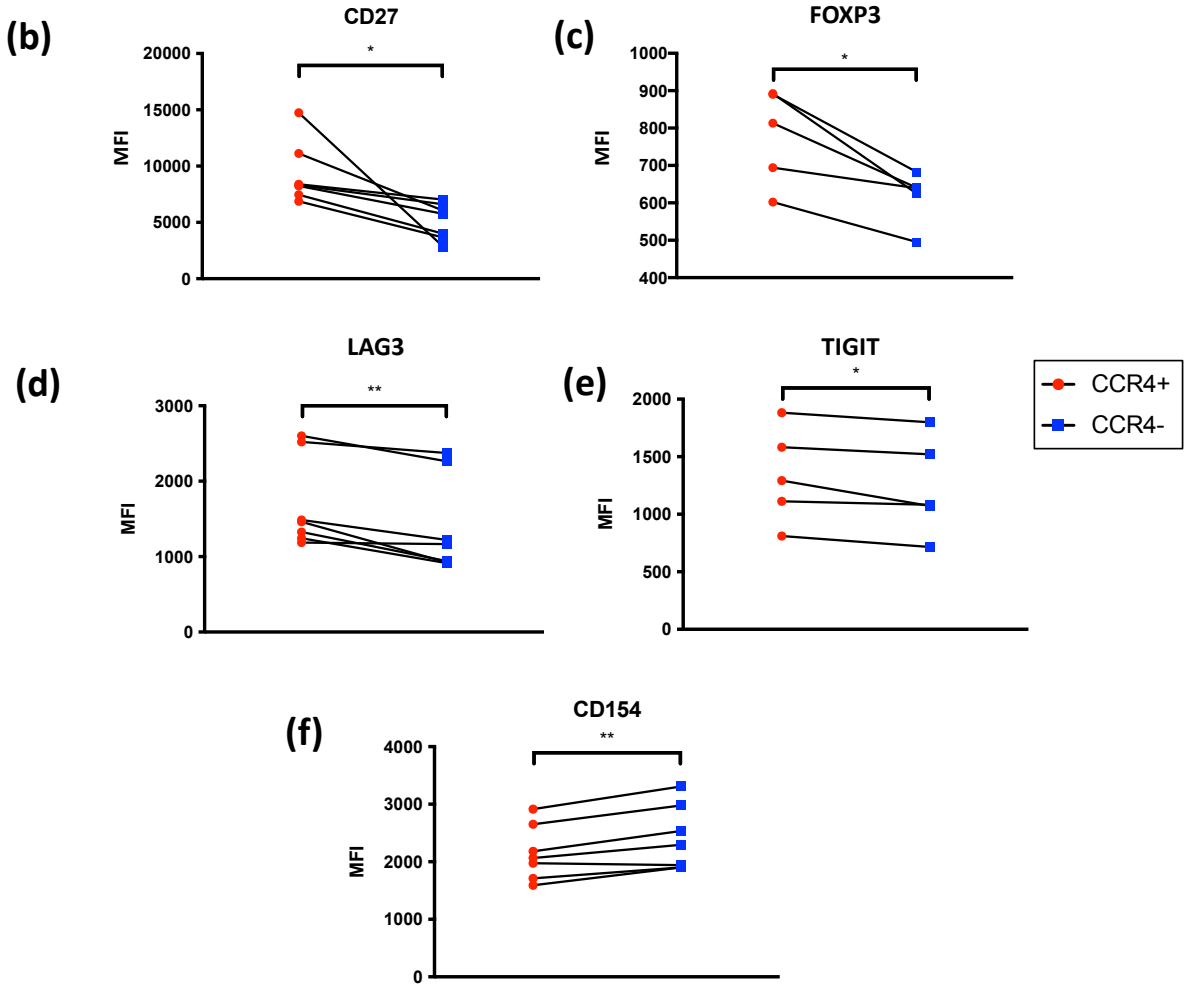

(g) Markers of Treg suppressive capacity

Marker	Function	Reference
FOXP3	• Master regulator of Treg development, differentiation and immunosuppressive function • Confers Treg lineage stability	Li 2015, Cell & Mol Immunol Sakaguchi 2010, Nat Rev Imm
CD27	• CD27 correlates with regulatory activity in Tregs • High expression of CD27 can be used to isolate potent *in vitro*-expanded Tregs	Arroyo Hornero 2020, Comm Bio Coenen 2006, Blood Duggleby 2011, Immunol Imanguli 2014, Leukaemia Nadig 2010, Nat Med
LAG3	• Binds MHCII to interfere with DC maturation and suppress T-cell activation • Prevent cytokine & cytolytic protein release in murine model	Huang 2004, Immunity Do 2015, Mucosal Immunology Thaker 2018, J Immunol.
TIGIT	• Co-inhibitory molecule suppressing pro-inflammatory Th1 & Th17 cell responses • Binds CD155 on DCs, inhibiting IL12 & inducing IL10 production	Joller 2014, Immunity
CD154 (CD40L)	• Co-stimulatory ligand of CD40 • Upon reactivation CD154-negativity identifies epigenetically stable activated Tregs • Marker of Ag-reactive nTregs	Nowak 2018, Front Immunol. Litjens 2012. J. Immunol

Figure 5.2.9 CCR8$^+$ Tregs express markers associated with high regulatory function & Treg stability.

Comparison of functional marker expression on CCR8$^+$ and CCR8$^-$ Tregs.

(a) Thawed, expanded human Tregs were analysed by flow cytometry for expression of markers expressed by highly suppressive Tregs.

Data are represented as (a) a schematic demonstrating the experimental outline, geometric mean fluorescence intensities (MFIs) of (b) CD27, (c) FOXP3, (d) CD154 on CCR8$^+$ (red symbols) and CCR8$^-$ (blue symbols) Tregs; Black lines link samples from the same donor. Statistical significance was assessed using the Paired t test (*, $p<0.05$; **, $p<0.01$).

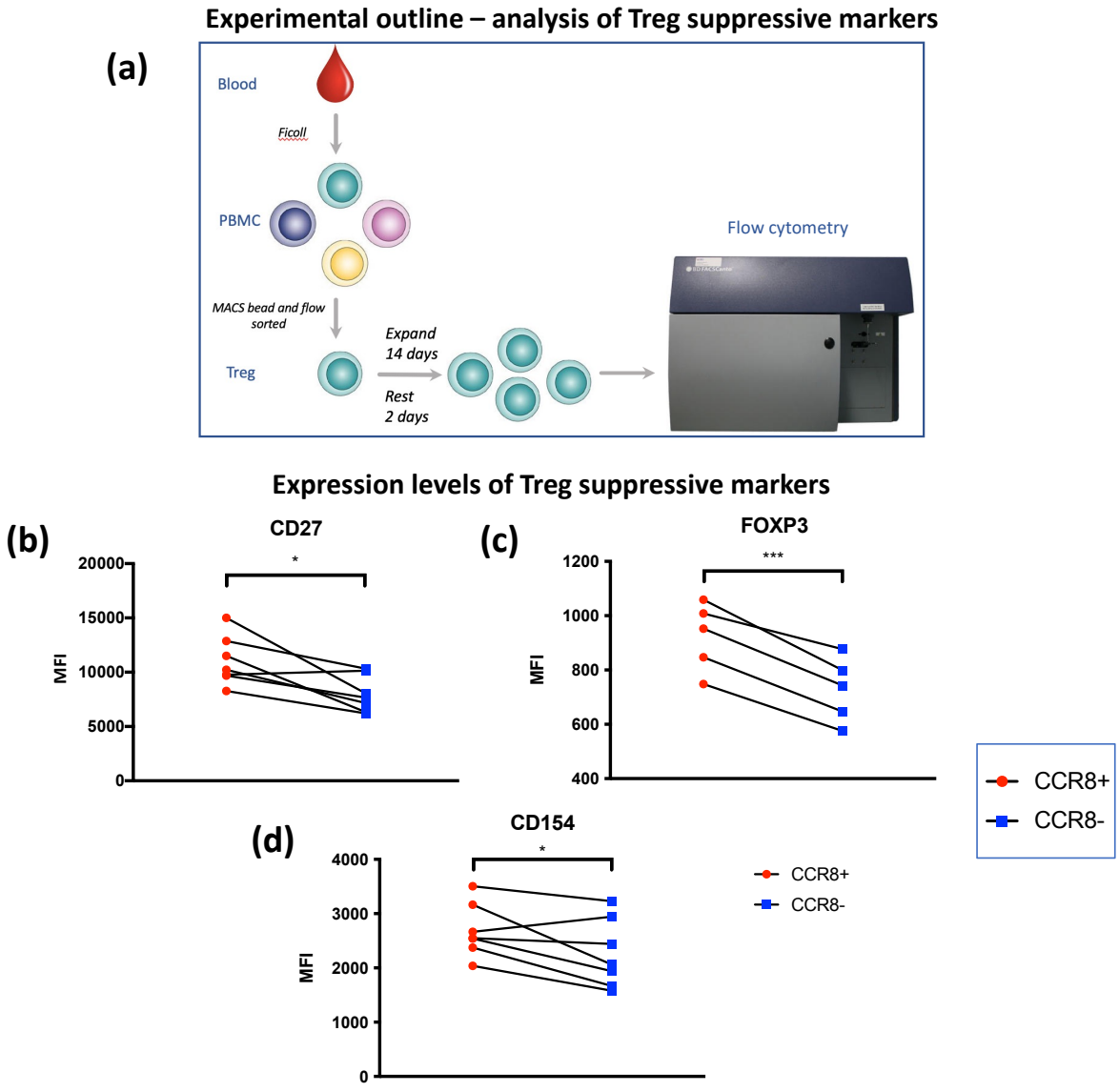
Experimental outline – analysis of Treg suppressive markers
(a)
Blood
Ficoll
PBMC
MACS bead and flow sorted
Treg
Expand 14 days
Rest 2 days
Flow cytometry
Expression levels of Treg suppressive markers
(b)
CD27
*
MFI
20000
15000
10000
5000
0
(c)
FOXP3
***
MFI
1200
1000
800
600
400
(d)
CD154
*
MFI
4000
3000
2000
1000
0
CCR8+
CCR8-

Figure 5.2.9.1 Assessing leucocyte chemotaxis *in vivo*: Model development
Assessment of the ability of chemokine-treated Matrigel to attract leucocytes.
(a) BALB/c-Rag2$^{-/-}$cγ$^{-/-}$ (BRG) mice were injected subcutaneously in the right flank with 200µl Matrigel/RPMI solution and in the left flank with a 200µl solution of Matrigel, RPMI and increasing concentrations of rhCCL17/22. The next day, 2x10^{7} VPD-stained human PBMCs were injected intravenously. 4 days later mice were sacrificed and matrigels harvested. (b) Leucocytes were recovered from matrigels and examined by flow cytometry for the presence of human leucocytes.
Data are represented as (a) a schematic outline of the experiment and (b) FACS plots demonstrating human leukocytes recovered from control and treated matrigels at each concentration of chemokine.

(a)

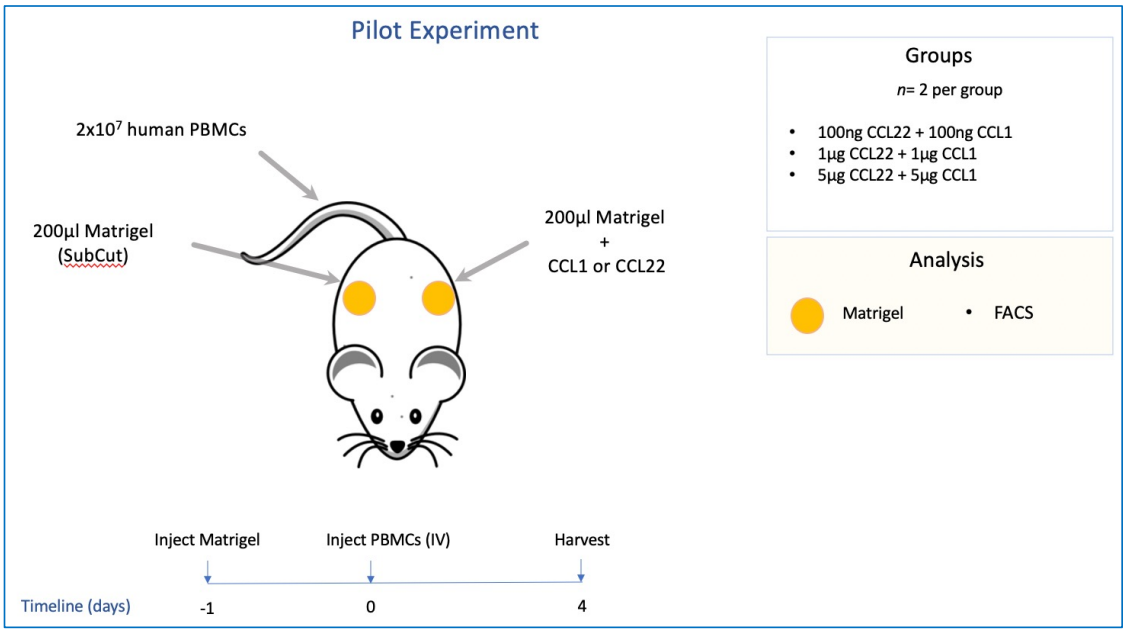
Pilot Experiment
2x10^7 human PBMCs
200µl Matrigel (SubCut)
200µl Matrigel + CCL1 or CCL22
Groups
n= 2 per group
100ng CCL22 + 100ng CCL1
1µg CCL22 + 1µg CCL1
5µg CCL22 + 5µg CCL1
Analysis
Matrigel
FACS
Inject Matrigel
Inject PBMCs (IV)
Harvest
Timeline (days)
-1
0
4

(b)

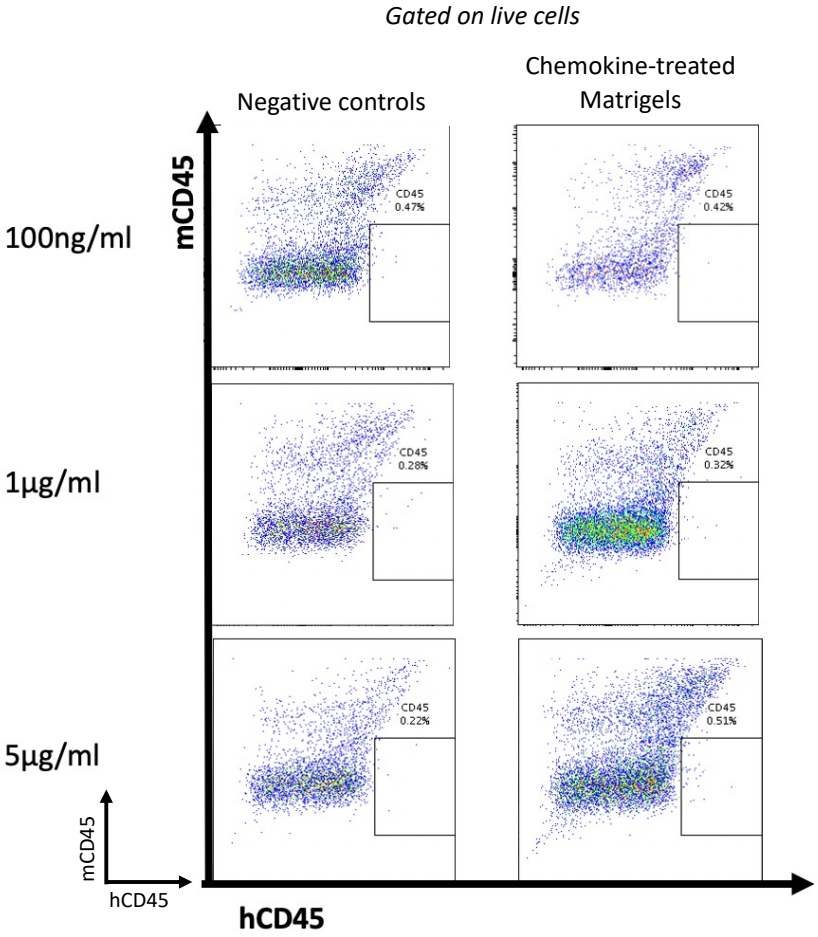
Gated on live cells
Negative controls
Chemokine-treated Matrigels
100ng/ml
1µg/ml
5µg/ml
mCD45
hCD45
CD45 0.47%
CD45 0.42%
CD45 0.28%
CD45 0.32%
CD45 0.22%
CD45 0.51%

Figure 5.2.9.2 Assessing chemotaxis of murine leucocytes to Matrigel treated with murine chemokines +/- murine IFNɣ

Assessment of the ability of chemokine-treated Matrigel to attract murine leucocytes.

(a) Immunocompetent CBA mice were injected subcutaneously in the right flank with 200µl Matrigel/RPMI solution and in the left flank with a 200µl solution of Matrigel, RPMI and recombinant mouse CCL1, CCL22 and MCP-1 ± recombinant mouse IFNɣ. 3 days later mice were sacrificed and matrigels harvested. (b-d) Leucocytes were recovered from matrigels and examined by flow cytometry for the presence of murine $CD3^+$, $CD19^+$, $Gr\text{-}1^+$ and $CD11b^+$ leucocytes.

Data are represented as (a) a schematic outline of the experiment and (b&d) FACS plots demonstrating murine leucocytes recovered from control and treated matrigels and (c) dot plots indicating numbers of migrated leucocytes.

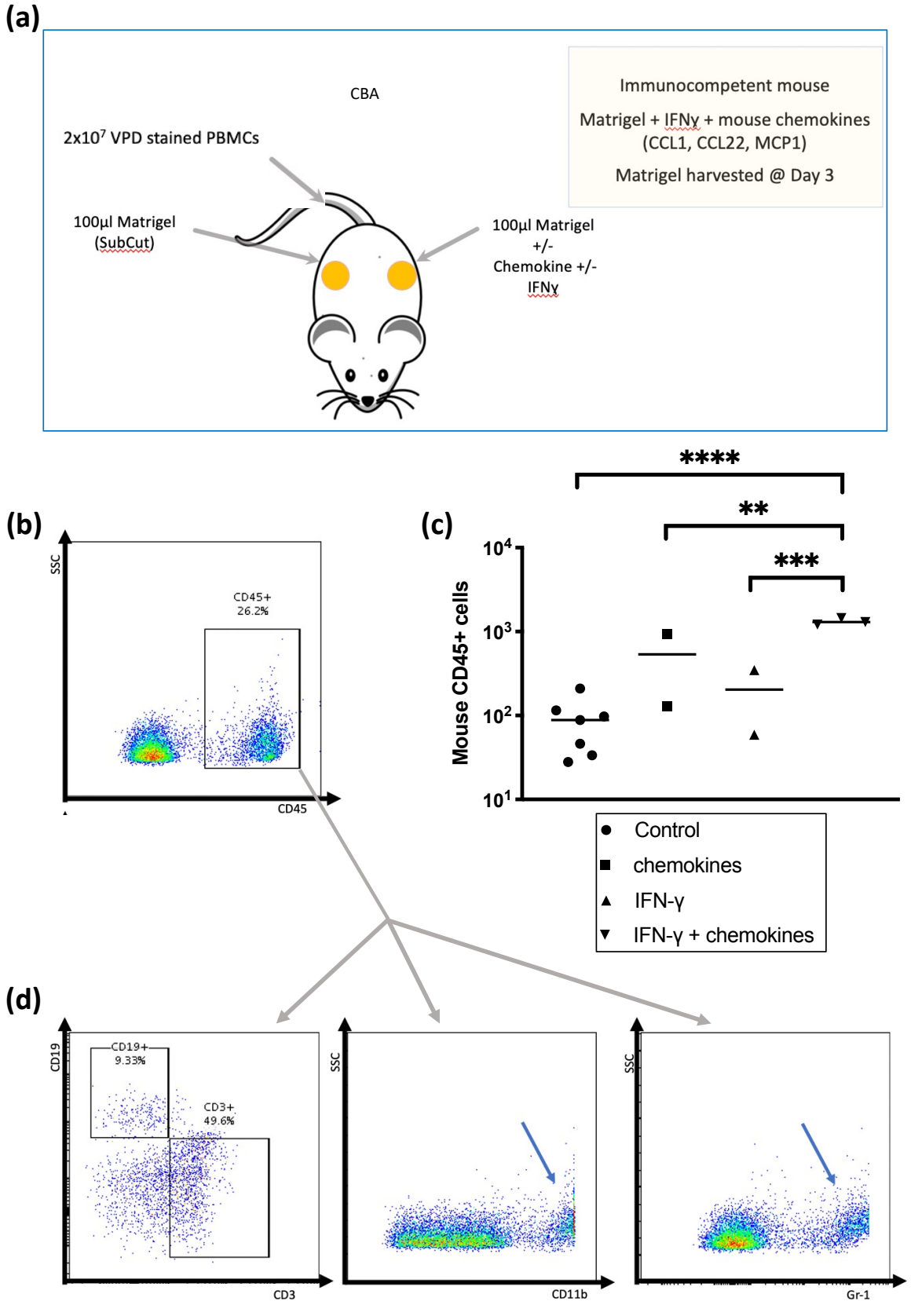
(a)
CBA
Immunocompetent mouse
Matrigel + IFNγ + mouse chemokines (CCL1, CCL22, MCP1)
Matrigel harvested @ Day 3
2x10⁷ VPD stained PBMCs
100µl Matrigel (SubCut)
100µl Matrigel +/- Chemokine +/- IFNγ
(b)
SSC
CD45+ 26.2%
CD45
(c)
****
**
***
Mouse CD45+ cells
10⁴
10³
10²
10¹
Control
chemokines
IFN-γ
IFN-γ + chemokines
(d)
CD19
CD19+ 9.33%
CD3+ 49.6%
CD3
SSC
CD11b
SSC
Gr-1

Figure 5.2.9.3 Treatment of matrigel with human chemokines and IFNɣ increases chemotaxis of human leucocytes

Assessment of the ability of chemokine- and cytokine-treated Matrigel to attract human leucocytes.

(a) BALB/c-Rag2$^{-/-}$cɣ$^{-/-}$ (BRG) mice were humanised with 17x10^{6} human PBMCs. 3 weeks later, mice were injected subcutaneously in the right flank with 200µl Matrigel/RPMI solution and in the left flank with a 200µl solution of Matrigel, RPMI and recombinant human CCL17 and CCL22 ± recombinant human IFNɣ. 3 days later mice were sacrificed and matrigels harvested. (b-c) Leucocytes were recovered from matrigels and examined by flow cytometry for the presence of human (b) CD45+, (c) CD3+ and CD4+ leucocytes.

n=6 in 2 independent experiments. Data are represented as (a) a schematic outline of the experiment and (b) representative FACS plots demonstrating human leucocytes recovered from control (left) and treated (right) matrigels.

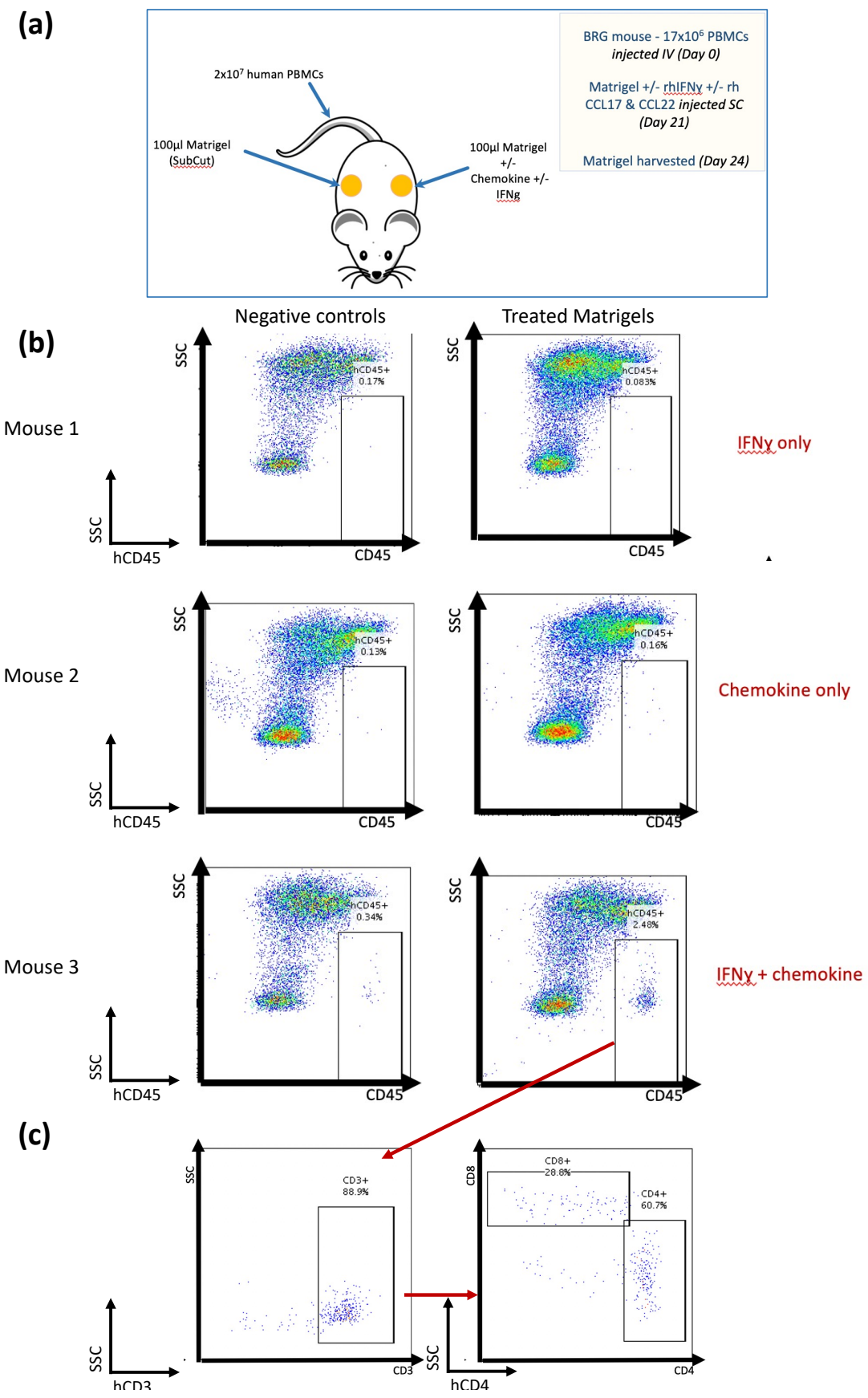
(a)
BRG mouse - 17x10⁶ PBMCs injected IV (Day 0)
Matrigel +/- rhIFNγ +/- rh CCL17 & CCL22 injected SC (Day 21)
Matrigel harvested (Day 24)
2x10⁷ human PBMCs
100µl Matrigel (SubCut)
100µl Matrigel +/- Chemokine +/- IFNg
(b)
Negative controls
Treated Matrigels
Mouse 1
IFNγ only
Mouse 2
Chemokine only
Mouse 3
IFNγ + chemokine
SSC
hCD45
CD45
hCD45+ 0.17%
hCD45+ 0.083%
hCD45+ 0.13%
hCD45+ 0.16%
hCD45+ 0.34%
hCD45+ 2.48%
(c)
CD3+ 88.9%
CD8+ 28.8%
CD4+ 60.7%
CD3
CD8
CD4
hCD3
hCD4

Figure 5.2.9.4 Treatment of Matrigel with chemokines and IL2 increases chemotaxis of human leucocytes, including Tregs.

Assessment of the ability of Matrigel treated with recombinant human (rh) chemokines and rhIL2 to attract human leucocytes.
(a) BALB/c-Rag2$^{-/-}$cγ$^{-/-}$ (BRG) mice were humanised with 17x10^6 human PBMCs and 5x10^6 expanded human Tregs. 3 weeks later, mice were injected subcutaneously in the right flank with 200µl Matrigel/RPMI solution and in the left flank with a 200µl solution of Matrigel, RPMI and recombinant human CCL22 $\pm$ recombinant human IL2. 3 days later mice were sacrificed and Matrigel's harvested. (b-c) Leucocytes were recovered from Matrigel's and examined by flow cytometry for the presence of human (b) CD45+ leucocytes (c) CD3$^+$CD4$^+$ CD25^{hi}CD127 ^{lo} Tregs.

n=3 in a single experiment. Data are represented as (a) a schematic outline of the experiment (b) representative FACS plots demonstrating human leucocytes recovered from IL2-treated (left) and IL2+chemokine-treated (right) Matrigel's; (c) numbers of Tregs recovered from Matrigel's. Statistical significance was assessed using the paired t test.

(a)

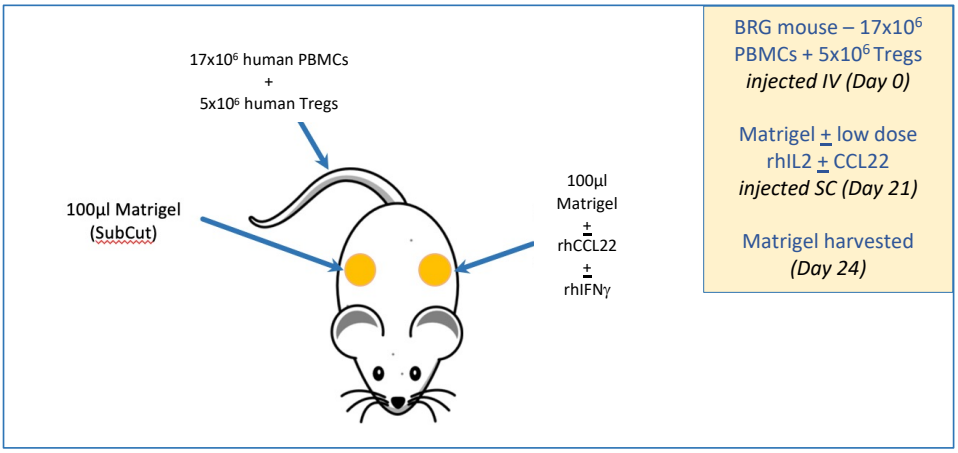
17x10⁶ human PBMCs
+
5x10⁶ human Tregs
100µl Matrigel
(SubCut)
100µl
Matrigel
±
rhCCL22
±
rhIFNγ
BRG mouse – 17x10⁶
PBMCs + 5x10⁶ Tregs
injected IV (Day 0)
Matrigel ± low dose
rhIL2 ± CCL22
injected SC (Day 21)
Matrigel harvested
(Day 24)

(b)

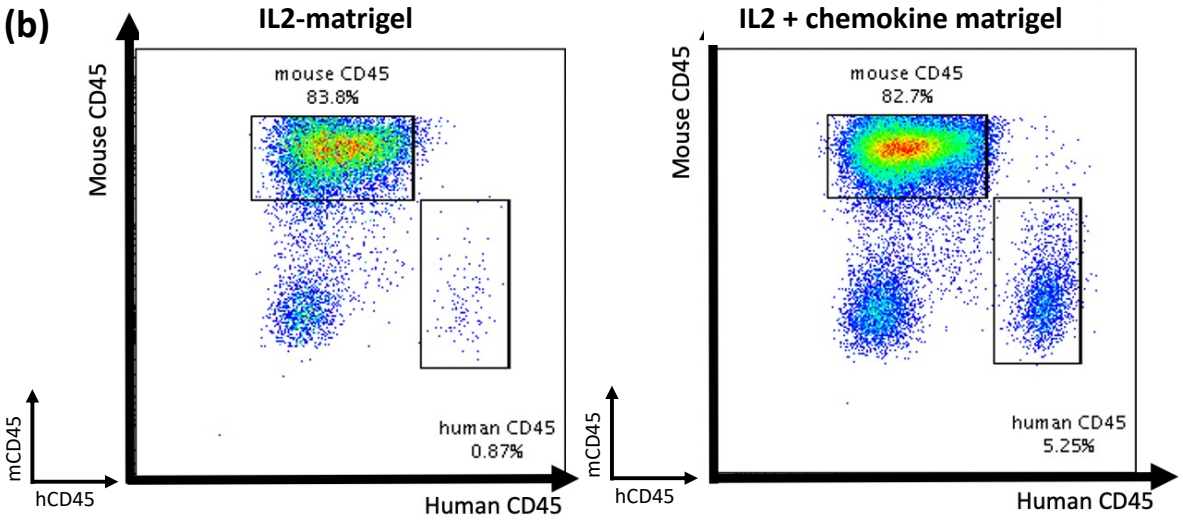
IL2-matrigel
mouse CD45
83.8%
Mouse CD45
human CD45
0.87%
mCD45
hCD45
Human CD45
IL2 + chemokine matrigel
mouse CD45
82.7%
Mouse CD45
human CD45
5.25%
mCD45
hCD45
Human CD45

(c)

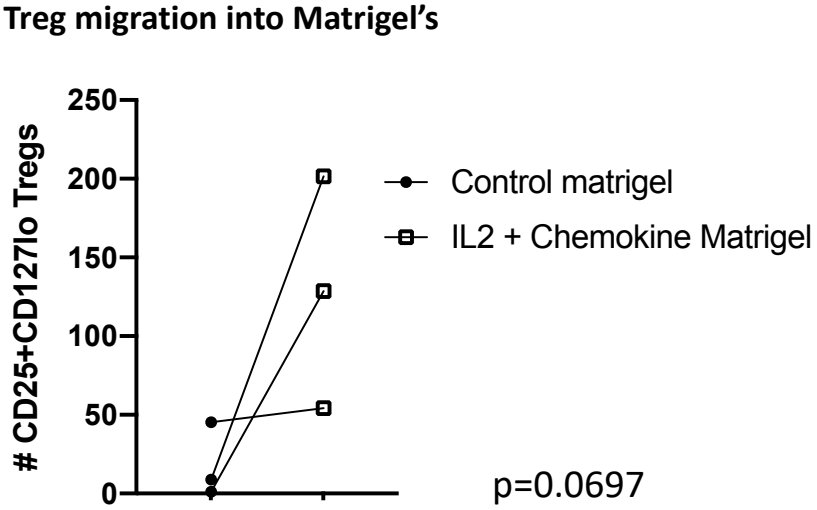
Treg migration into Matrigel's
CD25+CD127lo Tregs
250
200
150
100
50
0
Control matrigel
IL2 + Chemokine Matrigel
p=0.0697

Figure 5.2.10 CCL22-treated Matrigel's prevent human skin allograft rejection to a greater degree than intraperitoneally delivered Tregs alone
Comparison of human skin allograft rejection on BALB/c-Rag2$^{-/-}$cγ$^{-/-}$ (BRG) mice humanised with PBMCs and expanded total Tregs ± local subcutaneous injections of chemokine-treated Matrigel.

(a) BRG mice received 1 cm^2 full-thickness skin grafts procured from excess abdominal free flap tissue from a single donor. After being allowed to heal-in for 5 weeks, 5x10^6 allogeneic human PBMCs and 1x10^6 expanded human Tregs suspended in 200µl RPMI were injected intraperitoneally. (b) & (c) 4 weeks later, 400µl solutions of Matrigel/RPMI, rhCCL22 +/- rhIL2 were injected subcutaneously beneath skin allografts. (d) Grafts were monitored bi-daily and harvested when they had developed features of late rejection or at 100 days (experimental end-point).

2 independent experiments, mice received cells from one of 4 human blood donors. Data are represented as (a) a schematic outline of the experiment, (b) digital photographs demonstrating insertion of matrigels, (c) full-thickness human skin graft with subcutaneous Matrigel (d) macroscopic features of rejection; (e) time-course analysis of allograft survival - survival curves indicating the MST; (f) number of mice per group and the number censored; (g) digital photographs demonstrating matrigels tethered to the underside of skin grafts, and evidence of vessel formation between graft and Matrigel.
Statistical significance was assessed using the Log-rank (Mantel-Cox) test (**, $p<0.01$).

(a)

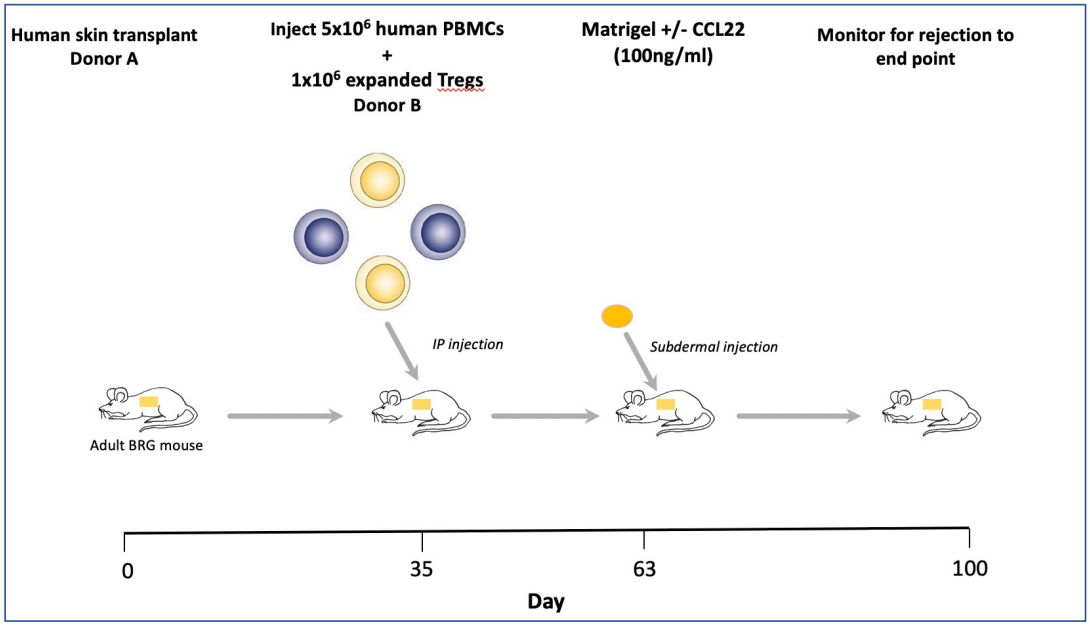
Human skin transplant
Donor A
Inject 5x10⁶ human PBMCs
+
1x10⁶ expanded Tregs
Donor B
Matrigel +/- CCL22
(100ng/ml)
Monitor for rejection to
end point
IP injection
Subdermal injection
Adult BRG mouse
0
35
63
100
Day

(b)


Subcutaneous injection

(c)


Post-injection

(d)

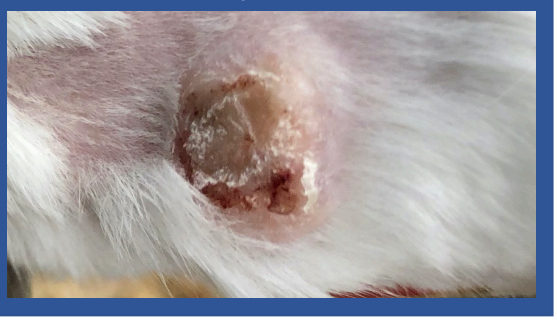
Rejection

(e)

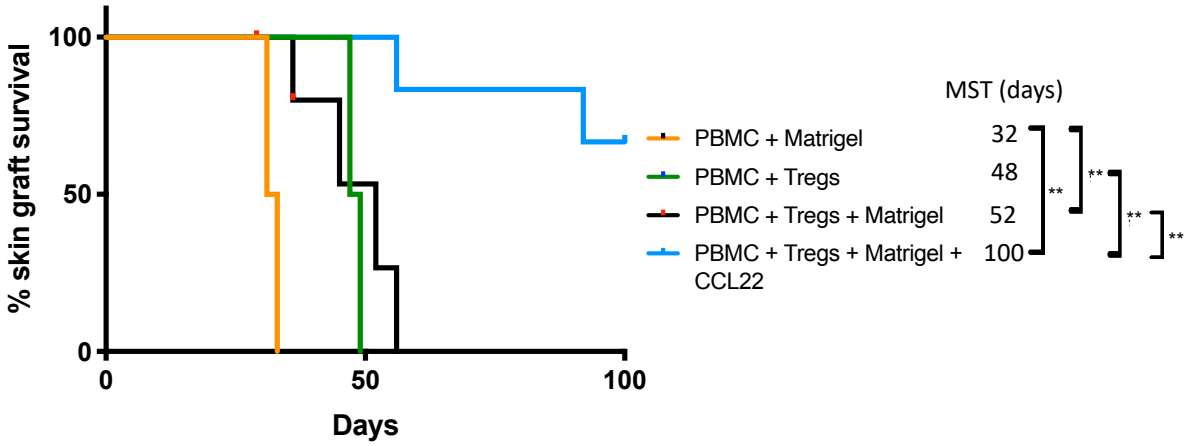

(f)

Group	N	Survival (days)	Censored (day)	MST (days)
PBMC + Matrigel	2	31, 33	0	32
PBMC + Tregs	2	47, 49	0	48
PBMC + Tregs + Matrigel	6	36, 45, 52, 56	2 (29, 36)	52
PBMC + Tregs + Matrigel + CCL22	6	56, 92,100, 100, 100, 100	0	100

(g)

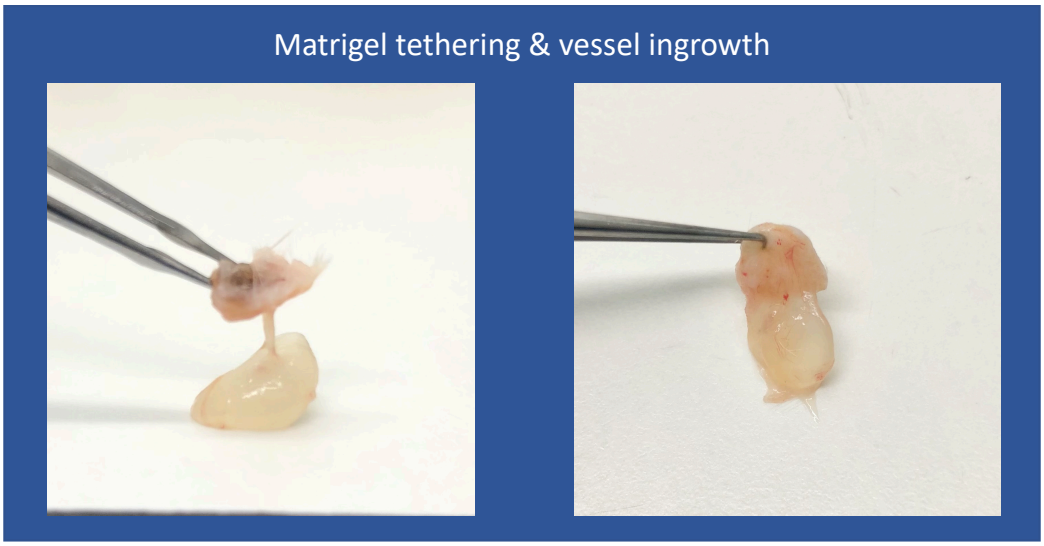

Chapter 6: Discussion

6.1. Introduction

The benefits of regulatory cellular therapies have been well established in the recent literature[404], which describes their potential to reduce the requirement for multi-drug immunosuppression to prevent allograft rejection. Many experimental studies that preceded clinical trials in cellular therapies benefited from the ability to model human allo-transplantation *in vivo* in humanised mice. In this thesis, we have 1) developed a novel multilineage humanised immune system mouse model capable of modelling functional human skin transplant rejection and 2) demonstrated the potential to prevent skin allograft rejection more effectively *in vivo* by administering chemokines near allografted skin. The findings presented indicate that 1) elucidating the processes involved in skin allograft rejection within a more haematopoietically replete model of human immunity may expand the value of preclinical research and the development of preventive therapies, and 2) manipulation of the CCR4-CCL17/22 chemokine axis to may—possibly through a concentration of effect—increase the potency of Treg therapy by guiding cells to transplanted allografts.

6.2. Summary of experimental results

6.2.1. Chapter 3

The aim of chapter 3 was to develop a humanised immune system mouse model capable of long-term multilineage haematopoeitic reconstitution, without requiring irradiative myeloablation. As such, we employed the stemness qualities of hUCB HSPCs selected

according to expression of the primitive marker CD133, which we isolated with high purity (***Figure 3.1.1)***. Following cryopreservation, as few as $1x10^3$ HSPCs robustly reconstituted the bone marrow, spleen and blood of non-irradiated NBSGW mice with $hCD45^+$ leucocytes, which persisted for longer than 20 weeks. In the blood, these comprised lymphocytes (B, T and NK cells), myeloid cells and small numbers of erythrocytes and platelets (***Figure 3.1.2***). Next, to evaluate whether after humanisation the HSPC-NBSGW model can support continuous human immune cell development and functional maturation, we assessed cellular compositions within primary and secondary lymphoid organs. B cells in the bone marrow were phenotypically immature (small and $CD10^+$) (***Figure 3.1.3 (b-c)***), naïve (***Figure 3.1.3 (e-f)***) and antigen-inexperienced, whereas in the spleen and blood we identified more mature and memory B cells. Importantly, these included class-switched memory B cells ($CD27^+IgD^-$), frequencies of which were higher following antigenic challenge with allogeneic skin grafts (***Figure 3.1.3 (g-h)***). The surprisingly robust populations of mature B cells we identified may relate to the production of hBAFF by reconstituting cells and expression of its receptors on human B cells, which has yet to be demonstrated in HIS models lacking specific BAFF knock-in[282] (***Figure 3.1.3 (i, k & l)***).

Naïve and mature $CD8^+$ and $CD4^+$ T cells predominantly reconstituted the spleen and blood in proportions representative of human immunity. Furthermore, these frequencies resembled human peripheral blood more closely than commonly used PBMC-humanised mice which do not support naïve T cell reconstitution (***Figure 3.1.4 (h-k)***). In addition to peripherally developing T cells, we found HSPC-NBSGW thymi to be humanised with $hCD45^+$ cells—predominantly $CD4^+CD8^+$ double-positive thymocytes (***Figure 3.1.5 (d-e)***) —as well as $hCD3^-$ cells expressing human MHC class I and class II (***Figure 3.1.5 (i-l)***). This suggests that *de novo*

development of T cells, which undergo thymic selection against human MHC molecules may precede peripheral maturation and support long-term lymphopoiesis.

The functional potential of HSPC-NBSGW $CD8^+$ T cells was indicated by expression of cytotoxic granzymes and perforin at levels comparable with healthy adults (***Figure 3.1.4 (l-n)***).

In HSPC-NBSGW mice we also identified developing myeloid cells of the innate immune system, which were most populous within the bone marrow (***Figure 3.1.2 (b)***. Importantly, these included phenotypically characteristic monocytes/macrophages and dendritic cells, which expressed pattern recognition receptors (CD14) and antigen presentation (HLA) molecules ***(Figure 3.1.6)***.

Having determined the capacity for robust reconstitution of adaptive and innate immune cells, we investigated the completeness of HSPC-NBSGW human haematopoiesis through evaluation of erythropoiesis and platelet reconstitution. Human erythroid precursors at recognised stages of development repopulated the bone marrow in a dose-dependent manner, however the peripheral blood was largely devoid of mature erythrocytes (***Figure 3.1.7 (a-d)***). We determined this to result at least in part from erythrocyte phagocytosis, as intravenous administration of clodronate liposomes—which depleted murine phagocytes—significantly increased peripheral blood erythrocytes (***Figure 3.1.7 (l-s)***). To determine whether aberrant inhibitory signalling to phagocytes may be a factor influencing erythrocyte phagocytosis, we evaluated CD47 ("don't eat me") expression and identified that erythrocytes express less surface CD47 than leucocytes in bone marrow, spleen, and blood (***Figure 3.1.7 (t-w)***). Following clodronate treatment, there were no changes in phagocyte frequencies or human erythrocyte CD47 expression however surprisingly, splenic phagocyte frequencies increased (***Figure 3.1.7 (l)***), and this was associated with a significant rise in CD47 expression on erythrocytes (***Figure 3.1.7 (y)***). This could indicate the influence of a selection

pressure applied to human erythrocytes based on CD47 expression level, however analysis of peripheral blood erythrocytes will be required to delineate this relationship further.

Next, to establish the capacity for long-term reconstitution we assessed engraftment of Lin^-CD34^+ and $Lin^-CD34^+CD38^{lo/-}$ self-renewing pluripotent stem cells and found these to be maintained in the bone marrow for at least 20 weeks (***Figure 3.1.9***). Secondary transplantation of these cells into NBSGW mice led to successful engraftment, evidencing long-term repopulating capability. Finally, to increase the utility of stem cells harvested from cord blood, we assessed the potential to expand $CD133^+$ UCB-HSPCs using a novel bromodomain and extra-terminal motif (BET) domain inhibitor "CPI203". HSPCs expanded in this manner retained bone marrow HSC repopulating ability (***Figure 3.1.10 (a-d)***) and reliably engrafted NBSGW mice after secondary transplantation (***Figure 3.1.11 (e-f)***).

Taken together, data in chapter 3 demonstrates a novel robust, multilineage humanised mouse model, which demonstrates long-term repopulating ability and is technically uncomplicated. The HSPC-NBSGW model supports development and maturation of human haematopoeitic cells, providing a useful platform for the study of human haematological and immunological processes and pathologies.

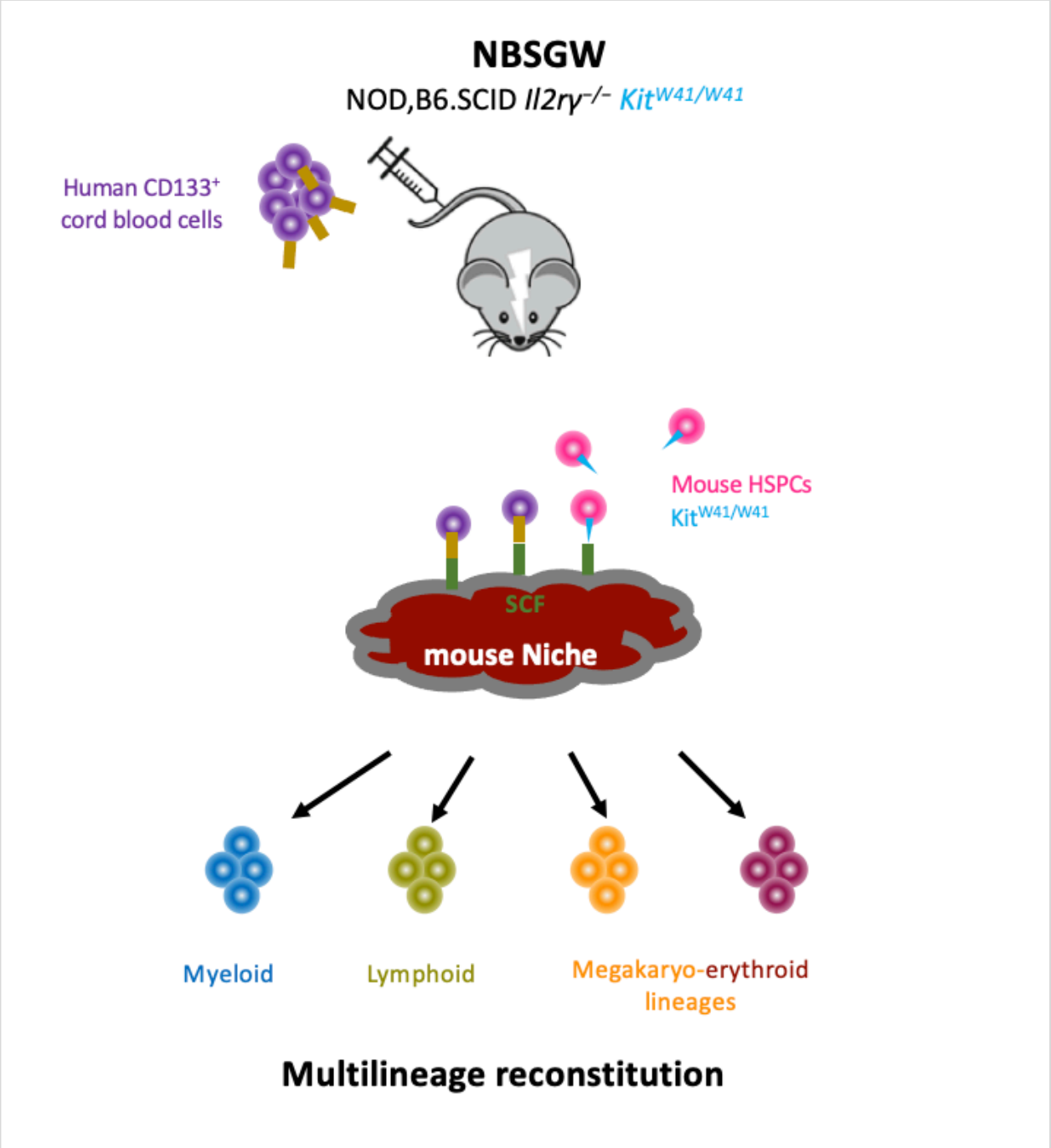

Figure 6.2. Summary schematic representing major findings from chapter 3
Engraftment of hUCB CD133+ HSPCs within permissive murine bone marrow niche precedes reconstitution of multilineage human hematopoiesis.

6.2.2. Chapter 4

Having established reliable haematopoiesis in HSPC-NBSGW mice—including human innate and adaptive immune cells—we aimed to assess both cell functionality and capacity to reproduce human allogeneic immune responses. Our first step was to assess whether NBSGW mice could engraft human split skin xenografts. Skins completely healed by 35 days and persisted for 100 days without features of clinical rejection or recipient mouse illness **(*Figure 4.1.1*)**. Healed grafts demonstrated clinical features healthy skin, together with vascular ingrowth and characteristic histologic architecture. With confirmation of healthy engraftment of human skin, we investigated the functional integrity of HSPC-NBSGW immune cells by assessing their *in vivo* responses to allografted skins **(*Figure 4.1.2.1*)**. 10/14 mice receiving skin transplants demonstrated macroscopic features of allo-rejection and the median survival time was 70 days. 4 mice were censored. Microscopically, rejection was associated with interstitial, perifollicular and perivascular inflammatory cell infiltrates and marked microarchitectural damage **(*Figure 4.1.2.2*)**. Skins transplanted onto HSPC-NBSGW mice, which didn't reject demonstrated inflammatory cell infiltrates that were less dense and showed less marked microarchitectural disruptions. Skins transplanted onto unhumanised NBSGW mice maintained appearances of healthy skin. To explore the mechanisms underlying rejection, we assessed the immune cell profiles in lymphoid organs and the peripheral blood of rejecters and non-rejecters **(*Figure 4.1.3.1*)**. T cells were significantly more populous in the spleens of rejecters and were predominantly effector memory type **(*Figure 4.1.3.2 (c) & (d)*)**. By contrast, spleens of rejecters had substantially lower frequencies of B cells, whereas non-rejecters had frequencies similar to un-transplanted HSPC-NBSGW mice **(*Figure 4.1.3.3*).**

Myeloid cells were found in similar proportions in the blood of rejecters and non-rejecters, however within the bone marrow, cDCs were more populous in rejecters **(*Figure 4.1.3.4 (b)*)**. After observing dynamic changes in immune cell compositions following allotransplantation, we sought to definitively test cell functionality *in vitro*. We stimulated T cells harvested from rejecters and observed robust proliferation following αCD3/αCD28 stimulation and following re-exposure to APCs from the original skin donors (second-set allo-proliferation) **(*Figure 4.1.4.1*)**. This was associated with the release of Th1, Th2 and Th17 cytokines **(*Figure 4.1.4.1 (e)*)**. B cell effector function was indicated by surface expression of IgA & IgG on mature ($CD10^-$) cells, and by higher expression of secreted IgM and IgG in the plasma of rejecters compared with non-rejecters, which by contrast expressed higher IgD **(*Figure 4.1.4.2*)**. We evaluated the function of HSPC-NBSGW myeloid cells through their capacity to be stimulated, to present antigen and to stimulate T cells **(*Figure 4.1.4.3*).** Following co-culture with allogeneic human T cells, we observed increased expression of the stimulatory markers CD80 and CD86 and of protein and lipid antigen presentation molecules HLA-DR and CD1a. Furthermore, we demonstrated the capacity of HSPC-NBSGW myeloid cells to trigger proliferation of both human peripheral blood T cells and HSPC-NBSGW T cells.

Next, we investigated the molecular mechanisms involved in rejection by evaluating RNA expression in skin and spleen biopsies. Genes representative of pathways of cytotoxicity and antigen processing were most significantly upregulated in rejecters compared with non-rejecters **(*Figure 4.1.4.4*)**. Overall, gene expression patterns were similar between non-rejecters and un-transplanted mice but differed substantially from expression patterns seen in rejecters.

Considering murine innate cells are present in NBSGW mice, we assessed whether these cells mount detectable responses to transplanted human UCB HSPCs or skin grafts. In addition to

an absence of murine cells infiltrating skin grafts **(*Figure 4.1.1 (h)*)**, we noted only small increases in frequencies of splenic macrophages and myeloid DCs and no increases in activation marker expression **(*Figure 4.1.5).***

Having demonstrated the capacity to model human skin allograft rejection in HSPC-NBSGW mice, we compared the dynamics of rejection in this model, with both the PBMC-humanised NBSGW model and the established PBMC-humanised BRG model **(*Figure 4.1.6*)**. PBMC-humanised NBSGW mice demonstrated the capacity for complete skin allograft rejection. Rejection on both humanised NBSGW models took longer than on BRG mice. MSTs were longest for HSPC-NBSGW mice **(*Figure 4.1.6 (c)*).** On analysis of human leucocyte composition, we found the highest chimerism in HSPC-NBSGW mice, which maintained a multilineage immune cell repertoire, unlike PBMC-humanised mice which almost exclusively consisted of T cells **(*Figure 4.1.6.1*)**.

To investigate whether we could increase the speed and frequency of skin allograft rejection in HSPC-NBSGW mice without compromising multilineage reconstitution, we co-transplanted $CD45^{+}CD34^{-}$ mononuclear cells (MNCs) into HSPC-NBSGW mice 2 weeks after human skin transplantation **(*Figure 4.1.7*)**. These mice rejected allografts substantially faster than HSPC-NBSGW mice (39 vs 94 days) **(*Figure 4.1.7 (b & c*)** and this was associated with higher T cell (particularly $CD7^{-}CD45RA^{-}$ Tem) and lower B cell frequencies and numbers **(*Figure 4.1.7.2 (a)&(b)*) & (*Figure 4.1.7.1 (f)-(h)*).** There was no effect on overall leucocyte or myeloid reconstitution.

Taken together, Chapter 4 demonstrates that HSPC-NBSGW successfully supports the modelling of human skin allograft rejection. Furthermore, it builds on established humanised mouse models as the first to incorporate the activity of functional adaptive and innate human immune cells in this setting.

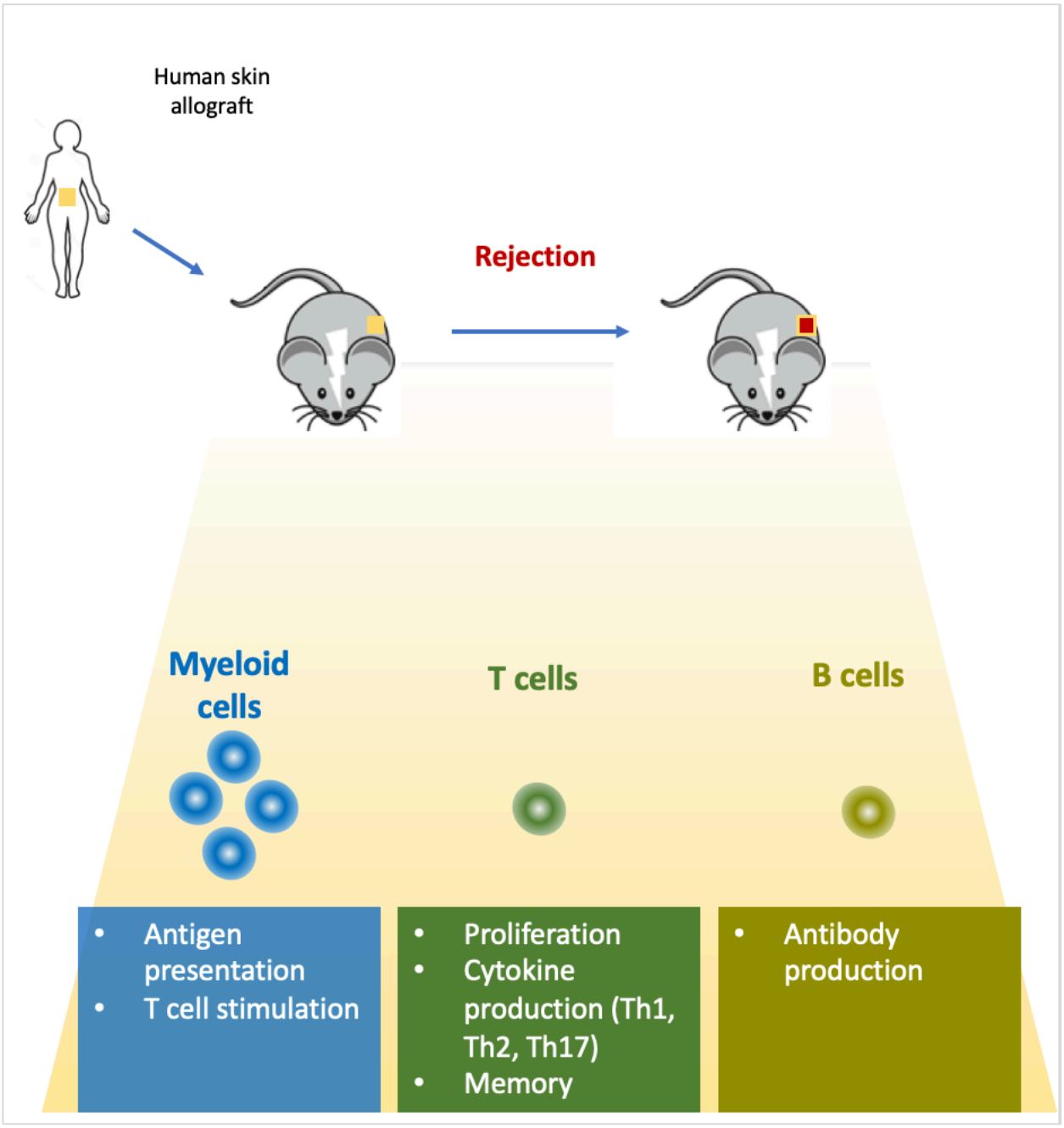

Figure 6.3. Summary schematic representing the major findings from chapter 4
Functional human adaptive and innate immune cells cause rejection of human skin allografts in HSPC-NBSGW mice

6.2.3. Chapter 5

In chapter 5 we investigated the surface expression of the skin-homing chemokine receptors CCR4 and CCR8 on human Tregs, which we hypothesised may identify highly suppressive subpopulations that could enhance Treg cellular therapy. To this end, we first assessed surface CCR4 and CCR8 expression on peripheral blood Tregs and Tconvs **(*Figure 5.2.1)***. We identified higher expression of both receptors on Tregs than Tconvs. Expression was primarily seen on $CD45RA^-$ memory Tregs and co-expression was exclusive to Tregs. To evaluate whether the reportedly high suppressive capabilities of $CCR4^+$ [167] and $CCR8^+$- [183] expressing Tregs were solely a reflection of high chemotactic trafficking potential, we assessed the regulatory capacity of expanded, sorted Tregs in *in vitro* suppression assays (***Figure 5.2.2 & 5.2.3)***. Following expansion, the majority of Tregs expressed CCR4 (60-70%) (***Figure 5.2.2 (a-c)***, however CCR8 expression increased only modestly **(*Figure 5.2.3 (a-c)*).** Receptor-expressing Tregs suppressed T cell proliferation more potently than non-receptor-expressing Tregs **(*Figure 5.2.2 (f) – (i)*)** and **(*Figure 5.2.3 (e) – (h)*)**, suggesting mechanisms other than chemotactic recruitment relate to their superior suppressive capacity.

Having identified superior regulatory capacity *in vitro*, we assessed whether adoptive transfer of sorted-expanded receptor-expressing Tregs may prevent *in vivo* human skin allograft rejection within the PBMC-humanised BRG mouse model. Our results demonstrated that $CCR4^+$ Tregs prevent human skin allograft rejection more effectively than $CCR4^-$ Tregs **(*Figure 5.2.4 (c-d)*),** however Treg CCR8 expression did not relate to significant differences in allograft rejection **(*Figure 5.2.5 (b-d)*)**.

To attain a more granular understanding of Treg CCR4/8 expression patterns, we performed a time course analysis of expression following αCD3/αCD28 bead stimulation. Non-CCR4-

expressing (naïve) Tregs showed transitory expression of CCR4, and with high-dose stimulation, expression could be restored into the long-term by re-stimulation **(*Figure 5.2.6*)**. CCR4-expressing memory Tregs given low dose stimulation maintained high levels of CCR4 expression even in the absence of re-stimulation. CCR8 expression did not increase following low dose stimulation of Tregs, however high dose stimulation transiently increased expression. Unlike CCR4, increased expression following repeat stimulation was not maintained long-term **(*Figure 5.2.7*)**.

Next, we profiled $CCR4^+/8^+$ Tregs by flow cytometry to identify whether other markers of highly suppressive Tregs were co-expressed. FOXP3, CD27, LAG3 and TIGIT were expressed more abundantly and CD154 less abundantly on expanded $CCR4^+$ vs $CCR4^-$ Tregs, consistent with a profile of Tregs of high regulatory capacity and lineage stability **(*Figure 5.2.8*)**. $CCR8^+$ Tregs expressed FOXP3, CD27 and CD154 more abundantly than $CCR8^-$ Tregs **(*Figure 5.2.9 (e)*)**.

Having identified the high suppressive potency of $CCR4^+$ Tregs both *in vitro* and *in vivo*, we sought to identify whether we could recruit these cells by CCL22-mediated chemotaxis, and if so, whether this might affect skin allograft survival **(*Figure 5.2.9.2.*)**. To achieve this, we developed an experimental model in immunocompetent mice, using recombinant murine chemokine-impregnated Matrigels. We found that with the re-creation of an inflammatory microenvironment (co-impregnation with cytokines) leucocytes could be recruited to Matrigels *in vivo*. We then translated this method into a humanised model and demonstrated the ability to recruit human leucocytes (including Tregs) into Matrigels **(*Figure 5.2.9.4. (c)*)**. Finally, we employed the humanised mouse skin transplantation model to assess whether injecting chemokine-impregnated Matrigels beneath allografts influences survival **(*Figure***

5.2.10.). We demonstrated that treatment with CCL22-impregnated Matrigels significantly prolongs allograft survival, enabling the majority of allografts to survive long-term.

Taken together, chapter 5 demonstrates both the inherent suppressive potency of Tregs expressing CCR4 and the potential to recruit these Tregs by chemotaxis toward skin allografts to prevent rejection.

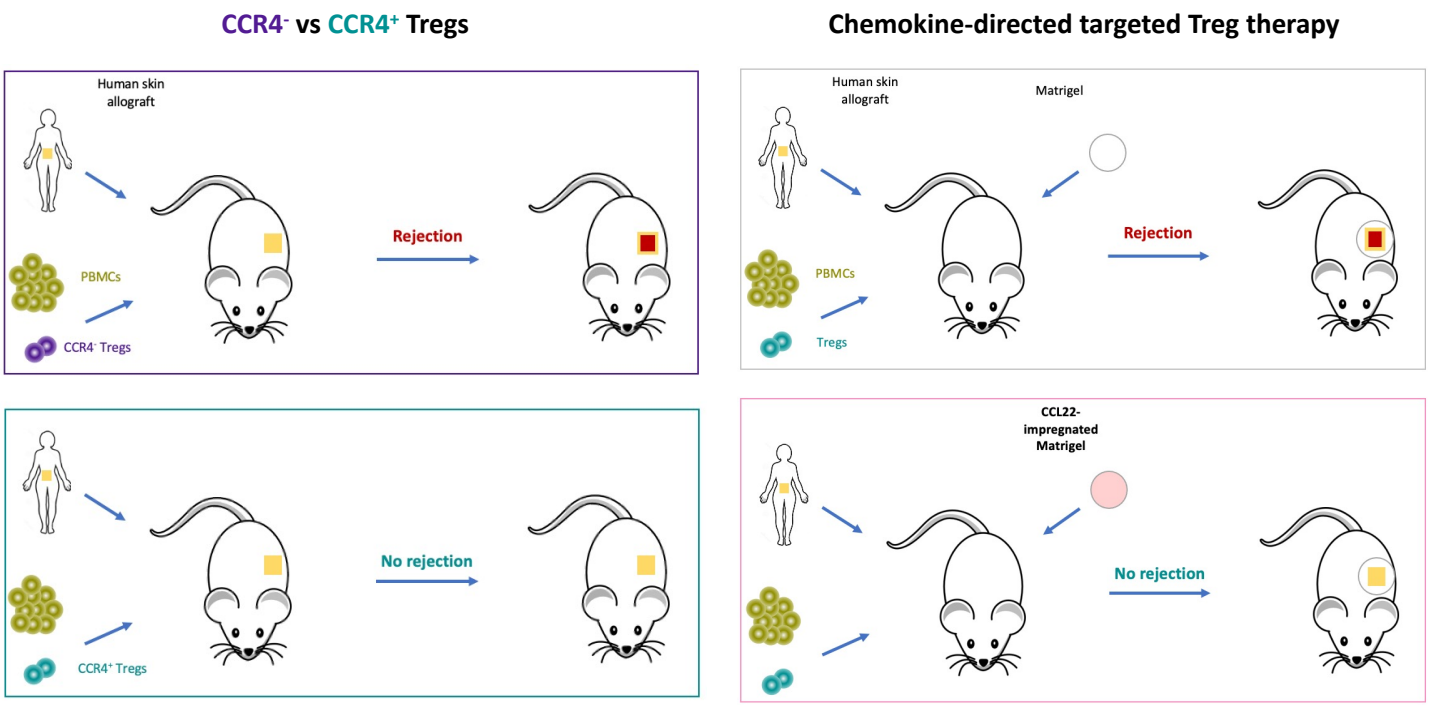

Figure 6.4. Summary schematic representing the major findings from chapter 5
CCR4⁺ Tregs are more potent suppressors of skin allograft rejection than CCR4⁻ Tregs (left). Local injection of CCL22-impregnated Matrigels prevents skin allograft rejection (right).

6.3. General discussion

The development of humanised animal models has enabled preclinical research to overcome biological differences that exist between humans and other species, and study human immunity more accurately *in vivo*. Transplantation research modelled in humanised mice has provided evidence of the therapeutic potential of Tregs, paving the way for Phase I/II clinical trials of Treg ACTs[405]. However, whereas initial trials assessing the feasibility of Treg therapies demonstrate promise, further research and modifications that may limit potential risks—including risks of off-target effects—should be pursued. The data presented in this thesis contribute to the advancement of immunology and transplant research in three principal ways. Firstly, the development of a technically undemanding mouse model of functional human adaptive and innate immunity, which supports long running *in vivo* investigations of human tissue transplantation presents opportunities to expand research in the field. Secondly, by demonstrating the ability to exploit chemokine signaling and direct cell recruitment *in vivo*, our results indicate a simple mechanism by which we may be able to target cellular therapies.

6.3.1. Deeper insights into HIS mouse models in research

In this thesis, we have developed a highly efficient HIS model capable of producing robust long-term multilineage reconstitution of human hematopoiesis. In addition to robust human leucopoiesis, it supports erythropoiesis and thrombopoiesis which features terminal maturation within the bone marrow and circulating erythrocytes and platelets upon

depletion of host phagocytes. This technically uncomplicated model stands to enhance the capacity to study disorders of human erythropoiesis in the context of complete human lymphoid development.

Optimal human HSC engraftment requires a permissive bone marrow niche that is favourable for human hematopoiesis. This has been achieved through 1) mutation of critical murine growth factor receptors such as the c-kit receptor (W41/Wv alleles) in NSGW41, NSGWv/+, NSGWv, NBSGW, SRG-W41 and BRgWv mice, 2) direct treatment with an anti-c-Kit receptor antibody, 3) provision of exogenous human cytokines, 4) knock-in of human cytokine genes (e.g. SCF, TPO, GM-CSF, M-CSF, IL-3 in NSG-SGM3/NSGS, MSTRG and MISTRG mice) [195,196,198,201,208,211,273-276], and 5) transplant of hematopoietic niches (e.g. human mesenchymal stromal cells, or thymus) with or without expression of human cytokine transgenes (e.g. NSG-SGM3-BLT mice [406]). NSGW41, BRgWv, NBSGW and SRG-W41 mice are reported to show robust human HSPC engraftment in the absence of irradiation and this is coupled with improved human bone marrow erythropoiesis compared to irradiated NSG mice [195,196,198,273,274,276,406,407]. Our results extend these and other findings of our own[272] by demonstrating consistent engraftment and human leucocyte reconstitution following intravenous transplantation of as few as $1x10^3$ $CD133^+$ HSPCs in adult nonirradiated NBSGW recipients over the extended period of 20-22 weeks, regardless of sex and without the requirement to co-transplant other human hematopoietic niche tissues. To our knowledge this is the lowest hUCB HSPC dose reported to achieve such high bone marrow (75.5%), splenic (73.5%) and peripheral blood (29%) engraftment at this late a time point. It is also notable, that in this model, leucocyte subset reconstitution approximates more closely to human peripheral blood populations[408] than previously described in humanised NBSGW

mice[208]. The capacity to achieve robust reconstitution in adult mice is particularly attractive due to the ease of intravenous injection compared with neonates and the potential simplicity of injecting fresh cells, with the flexibility of not requiring timed breeding.

Importantly, we have also demonstrated that development and maturation of human lymphocytes and myeloid cells occurs within this model, producing humanised mice that more completely represent human immunity. Reconstitution of both T and B lymphocytes in this model is important for studies of vaccination and infection immunity, enabling incorporation of humoral and cellular components of the human immune system. Additionally, as effective antibody class switching is dependent on T cell help, humanised mice supporting robust T and B cell reconstitution can allow studies on the development of protective humoral immunity in various infectious diseases.

hUCB HSPC-humanised mice typically support engraftment of human B cells at high frequencies[277]. In several models, these develop quite normally in the bone marrow yet demonstrate features of developmental block[255], manifesting defective peripheral maturation and humoral responses[193,278]. We have demonstrated development of a large population of mature B cells in the spleens and peripheral blood of HSPC-NBSGW mice. Since only mature B cells can carry out effective antigen presentation and effector function, this is likely to be a distinguishing feature of this model. We further demonstrate frequencies of class-switched memory B cells to increase following exposure to allogeneic human skin transplants. This feature suggests the functional capacity for HSPC-NBSGW B cells to respond to immune challenge and may represent an important step in fields such as transplantation research, where enhanced human T- and B cell function may enable more accurate reflections

of human allo-responses to be realised. As the detrimental effects of donor-specific antibodies and the tolerogenic effects of regulatory B cells are increasingly becoming focal points of attention in transplantation, models such as this may incorporate functional humoral immune responses into the predominantly T cell biased PBMC-based humanised models.

The re-creation of cellular immune responses is a fundamental requirement of HIS mice. Following humanisation with $CD133^+$ hUCB HSPCs, we demonstrate peripheral reconstitution of the T cell subsets in proportions that more accurately reflect human blood profiles than have previously been achieved following humanisation with PBMCs. It should be noted that while PBMC-driven HIS models have been very useful in studying T cell-driven immune responses[361], cellular therapies[409] and biologics[410], disproportionately large T cell reconstitution in humanised mice generated using PBMCs (particularly Tem cells) risks the development of xenogeneic GvHD and underrepresentation of the global immunological complexity.

Within the thymus we identified a humanised thymic cell microenvironment with a sizeable fraction of $CD4^+CD8^+$ double positive human thymocytes, similar to that seen in thymus biopsies from human infants[198] and $CD3^-$ leucocytes expressing human MHC class I and II. Identification of T cells in the peripheral blood only after 12 weeks in the earliest instances, suggests *de novo* T cell development is occurring rather than proliferation of transplanted mature hUCB MNCs.

Crucially, both *in vitro* and *in vivo* we have demonstrated functional capability of the reconstituting humanised immune system. In the context of APC activation and antigen presentation, effector cell proliferation, maturation and production of class-switched antibodies, cytokines and cytolytic proteins, the evidence presented is in keeping with accepted immunological principles.

From our experience, humanisation using $50x10^3$ human HSPCs produces rapid, robust, and reliable reconstitution, supporting the use of this dose for a broad range of *in vivo* experiments. A recognised shortcoming of the use of human cord blood in mouse experiments—which we also experienced—is the limited number of mice that can be engrafted from a single UCB unit when high numbers of HSPCs are used per mouse. It is our view that experimental biases resulting from low numbers of donor replicates may be overcome if more mice can be robustly engrafted (i.e. >20% peripheral blood chimerism) using smaller UCB fractions (i.e. $<50x10^3$ HSPCs). We show that this is possible and feel that where investigators may find benefit in expanding the utility of a single UCB unit, a longer period of engraftment may be an acceptable compromise, particularly considering the reported longevity of humanised NBSGW mice (survival $\geq$ 36 weeks post-humanisation[209]).

As efforts continue to broaden the use of humanised small animal models for the *in vivo* study of human haematopoiesis, immunology, cancer and infection, technically uncomplicated models achieving ever-closer functional human haematopoiesis such as the HSPC-NBSGW reported here represent an important practical next step.

6.3.2. Manipulation of chemokine signalling to improve Treg therapy

This thesis demonstrates in an *in vivo* humanised model, the potential to refine Treg cell therapies through the manipulation of molecular pathways such as chemotaxis. This technique may facilitate the development of targeted cellular therapies and help to address concerns held about current treatment strategies.

Both in transplantation and in autoimmune diseases[411,412], Treg therapy typically involves intravenous infusion of large cell numbers (e.g. 1–10 million cells/kg[413]). Systemic administration in this manner results in broad distribution of Tregs throughout the circulation and tissues, which can cause loss of substantial numbers of infused cells[414], dilution of the suppressive effect and increased risk of off-target effects, such as phenotype destabilisation (e.g. in inflammatory environments), immunocompromise and toxicity[415]. In addition, our increasing understanding of Treg heterogeneity highlights the need to be able to differentiate between Treg subsets with varying properties, lineage stabilities and efficacies in order to enable production of therapies that are optimised for safety and effectiveness. In this thesis, we show $CCR4^+$ and $CCR8^+$ Tregs to be potently suppressive. Whereas the role of CCR8 is newly emerging, CCR4 is well established as a key component of immune regulation—capable of recruiting a subset of Tregs that suppress anti-tumour immune responses, allergic airway and inflammatory skin reactions and autoimmune diseases.

Chemotaxis is an essential property of Tregs in health and disease. Tissue homeostasis[416] and recruitment to inflammatory tissues for containment[417] are processes that are under the influence of distinct chemokine axes. In cutaneous malignancies such as melanoma[418] and cutaneous T cell lymphoma (CTCL), Treg recruitment to tumour-induced skin sites has been shown to be governed by CCR4-cognate chemokine expression. In CTCL, treatment with an anti-CCR4 monoclonal antibody (Mogamulizumab)—which reduces Treg numbers and CCR4

expression by antibody-dependent cellular cytotoxicity[419]—has been shown to increase progression-free survival in a phase 3 clinical trial[420]. Similarly in canine bladder cancer, Mogamulizumab reduces CCR4$^+$ Tregs and improves survival[421].

In a variety of other tumours, immune checkpoint inhibitors have been shown to increase CCL17 and CCL22 expression, which in turn increases migration of Tregs into the tumour microenvironment. Concomitant CCR4 antagonism effectively inhibits Treg recruitment and enhances antitumor efficacy[422].

CCR8 has been identified as a marker specific for tumour-infiltrating Tregs[183,368] and an IRF4-dependent "effector" Treg gene[423]. Anti–CCR8-mediated Treg depletion has been shown in murine tumour models to enable potent antitumor responses[185]. Other chemokine axes have also been identified as therapeutic targets in immuno-oncology. For example, manipulation of CCL5/CCR5 and CXCL12/CXCR4 signalling has shown promise in shifting TIL:Treg ratios in favour of anti-tumour immunity in pancreatic ductal adenocarcinoma[424].

Realising the critical value of leucocyte migration for successful ACT, studies into receptors including CCR2, CCR4, CXCR2, CXCR3, CXCR4 and CX3CR1 have been conducted to enhance T cell trafficking[387,425]. Owing to its potency, engineered expression of CCR4 on CD30 CAR-T cells represents one of only two chemokines currently under investigation in a clinical trial (NCT03602157).

In addition to chemotactic function, CCR4 has recently been postulated to alternatively influence Treg suppressive function[426,427]. In elegant imaging experiments, CCR4 and CCL22 have been shown to form cell-cell interactions between Tregs and DCs, enabling Tregs to outcompete Tconvs[428]- a crucial aspect of suppressive function[429]. These features at least partly explain the severe autoimmunity seen in selective absence of CCR4 from Tregs[169] and diminished Treg function caused by CCR4 antagonists[430,431].

We hypothesised that guiding injected Tregs to allografts by exploiting the CCL22-CCR4 chemotactic axis may enhance the efficacy of anti-rejection adoptive cell therapy. This strategy is particularly attractive for skin allotransplantation owing to the high suppressive potency and skin-homing capacity of $CCR4^+$ Tregs. The promising results we demonstrated are supported by recent work showing efficient inhibition of skin inflammation following local (intradermal) injections of low numbers of Tregs[432]. Direct injection may permit easy administration into highly accessible allografts. Potential advantages of chemokine-mediated targeted ACT include recruitment of Tregs to less easily accessible areas and targeted recruitment of highly potent Tregs expressing chemokine receptors such as CCR4 & CCR8. In addition, direct immunomodulatory properties exerted by CCL22 include reduction of DC CD80 and MHC class I and II expression, which affects antigen presentation capacity and ability to activate T cells[433]. CCL22 administration itself may therefore confer additional localised immune suppression.

6.4. Future directions

The findings in this thesis contribute to the development of advanced preclinical models for human immunology research and broaden the use prospects of ACTs for the prevention of SOT and VCA rejection. In the short term, further evaluation of HSPC-NBSGW haematopoiesis to identify the full array of engrafting cells may help to optimise its use in more advanced investigations of human transplantation and testing of regulatory therapies. In the longer term, to build on the promise of chemokine-directed targeted Treg therapy, optimisation of

the construct for compatible use in humans will be an essential antecedent to a phase 0 clinical trial.

To provide greater confidence to the experimental use of the HSPC-NBSGW model it will be important to confirm the nature of certain features we identified.

For example, although we identified RNA expression of HLA class II, humanised thymic environment expressing HLA class I and II molecules, robust reconstitution of human T and B cells, and demonstrated T cell responsiveness to human αCD3/αCD28 stimulation, allogeneic memory responses against human (and not mouse) antigen and development of class-switched immunoglobulin producing B cells, attainment of fully functional adaptive immunity must be indicated by the capacity to elicit specific IgG responses upon vaccination. Definitive demonstration of the capacity for long-term self-sustaining T cell lymphopoiesis from thymocytes can be achieved through analysis of T Reg Excision Cycles by PCR +/- CD31/CD27+CD45RA expression, which can indicate whether peripheral T cells develop from thymic emigrants.

For B cells, despite identifying surface and serum IgG expression, additional evidence to prove isotype class switching occurs in developing B cells may be demonstrated through analysis of activation-induced cytidine deaminase (AID) expression in germinal centre structures or by assessment of surface antibody expression following *in vitro* stimulation of CFSE/VPD labelled splenic B cells.

Regarding HSPC-NBSGW myeloid cells, although we demonstrated successful APC stimulation and presentation through the direct pathway, the likely long-term dominance of indirect allorecognition in transplant rejection suggests the importance of determining the capacity of the model to replicate it. This could be assessed by measuring the proliferation of T cells

co-cultured with autologous irradiated APCs in the absence or presence of sonicates derived from allogeneic cells.

Experiments to delineate the mechanisms of rejection involved in the HSPC-NBSGW skin transplantation model may reveal its comparability to established models and clinical rejection. At the tissue level, this can be achieved by immunohistochemistry analysis of skins, which may identify features of cellular and humoral rejection.

Treg ACTs currently being trialled in SOT and autoimmune diseases are being modified in myriad ways to functionalise their actions for specific purposes. The reliable chemotactic capacity of CCR4, suppressive potency of $CCR4^+$ Tregs and regulatory capability of CCL22 give unique promise to anti-rejection therapies for skin-containing allografts. The promise demonstrated in clinical trials of CCR4-targeting ACTs adds to this and supports an endeavour to pursue clinical trials in CCR4-axis-based Treg therapies, which could provide a valuable reconstructive option for patients with severe and complex injuries. Before this, the immunological features associated with the allograft preservation demonstrated must be elucidated, as described above. Interesting considerations in this regard would be to compare whole Tregs vs $CCR4^+$ Tregs and to evaluate the minimum effective Treg dose required to prevent rejection with local chemokine administration. It will also be important to determine chemokine concentrations maintained within the functionalised Matrigels post-insertion. If as we suspect, a chemokine gradient is established, which attracts Tregs toward allografted skin, the same would need to be achievable in biological matrices safe for use in humans (e.g. hydrogels and existing dermal matrices).

6.5 Concluding remarks

In this thesis we have presented an advanced HIS mouse model that is technically uncomplicated and bridges the mechanistic gap in preclinical research. We have also demonstrated a translational ACT with the potential to enhance regulatory therapy in transplantation. Further work to evaluate the translatability of this model to real human immunity more granularly may herald new prospects for the application of humanised models, approximating their use more closely with clinical studies in transplantation. Finally, this thesis provides a pre-clinical evidence base for a chemokine-directed targeted Treg therapy in skin or VCA transplantation.

Publications

Publications

Adigbli G, Issa F. Preserving Treg Function: Beyond mTOR Inhibitors. *Transplantation*. 2018;102(2):179-82

Adigbli G, Ménoret S, Cross AR, Hester J, Issa F, Anegon I. Humanization of Immunodeficient Animals for the Modeling of Transplantation, Graft Versus Host Disease and Regenerative Medicine. *Transplantation*. 2020 **

Hua P*, Hester J*, Adigbli G*, Li R, Psaila B, Roy A, et al. The BET inhibitor CPI203 promotes ex vivo expansion of cord blood long-term repopulating HSCs and megakaryocytes. *Blood*. 2020;136(21):2410-5 **

Adigbli G*, Hua P*, Uchiyama M, Roberts I, Hester J, Watt SM, et al. Development of LT-HSC-Reconstituted Non-Irradiated NBSGW Mice for the Study of Human Hematopoiesis In Vivo. *Frontiers in Immunology*. 2021;12(836) **

Mohseni YR, Saleem A, Tung SL, Dudreuilh C, Lang C, Peng Q, et al. Chimeric antigen receptor-modified human regulatory T cells that constitutively express IL-10 maintain their phenotype and are potently suppressive. *European journal of immunology*. 2021;51(10):2522-30

Adigbli G, Berlin C, Issa F. Research Highlights. *Transplantation*. 2021;105(10):2128-9.

Abstracts

European Haematology Association, Congress, July 2020 Poster: CPI203 promotes ex-vivo expansion of cord blood long-term repopulating HSCs and megakaryocytes. (G.Adigbli et al).

European Haematology Association conference abstract: EP1469 The BET inhibitor CPI203 promotes ex vivo expansion of cord blood longterm repopulating HSCs and megakaryocytes. G. Adigbli, June 2020.

European Congress of Immunology. Amsterdam, Netherlands. September 2018. Poster: Investigating the role of CCR4 and CCR8 on human regulatory T cell function in transplantation. (G.Adigbli et al).

CCR4 and CCR8 chemokine receptor expression on highly suppressive regulatory T cells. P.C3.04.01. G. Adigbli, 2018. European Congress of Immunology abstract.

NDS Research Day, Oxford University, 2019. Oral: “A novel humanised mouse model of

human skin transplantation". (G.Adigbli et al).

British Society of Immunology Symposium, Oxford, 2019. Oral: "Multilineage human haematopoietic reconstitution in NBSGW mice". (G.Adigbli et al).

The Transplantation Society annual international conference abstract: Repopulation of functional multilineage human haematopoietic cells in nonirradiated NBSGW mice. Transplantation, Sep 2020. (G.Adigbli et al).

* These authors contributed equally to this publication (acknowledged in print)
** Published material from these articles is included in this thesis with the permission of co-authors and supervisors

References

1. Jay, V. This month in history: Jacques Louis Reverdin. *J R Soc Med* **92**, 548 (1999).
2. Zirm, E. Eine erfolgreiche totale Keratoplastik. *Albrecht von Graefes Archiv für Ophthalmologie* **64**, 580-593 (1906).
3. Armitage, W.J., Tullo, A.B. & Larkin, D.F.P. The first successful full-thickness corneal transplant: a commentary on Eduard Zirm's landmark paper of 1906. *Br J Ophthalmol* **90**, 1222-1223 (2006).
4. Armitage, W.J*., et al.* High-risk Corneal Transplantation: Recent Developments and Future Possibilities. *Transplantation* **103**, 2468-2478 (2019).
5. Ellis, H. Two pioneers of plastic surgery: Sir Harold Delf Gillies and Sir Archibald McIndoe. *Br J Hosp Med (Lond)* **71**, 698 (2010).
6. SKIN homografts in clinical practice. *Br Med J* **2**, 1073-1074 (1951).
7. Gibson, T. & Medawar, P.B. The fate of skin homografts in man. *J Anat* **77**, 299-310.294 (1943).
8. Medawar, P.B. The behaviour and fate of skin autografts and skin homografts in rabbits: A report to the War Wounds Committee of the Medical Research Council. *J Anat* **78**, 176-199 (1944).
9. Medawar, P.B. A second study of the behaviour and fate of skin homografts in rabbits: A Report to the War Wounds Committee of the Medical Research Council. *J Anat* **79**, 157-176.154 (1945).
10. Sade, R.M. Transplantation at 100 years: Alexis Carrel, pioneer surgeon. *Ann Thorac Surg* **80**, 2415-2418 (2005).
11. The Production of Antibodies (2nd Edition). *The Journal of Immunology* **66**, 485 (1951).
12. Billingham, R.E., Brent, L. & Medawar, P.B. 'Actively Acquired Tolerance' of Foreign Cells. *Nature* **172**, 603-606 (1953).
13. Guild, W.R., Harrison, J.H., Merrill, J.P. & Murray, J. Successful homotransplantation of the kidney in an identical twin. *Trans Am Clin Climatol Assoc* **67**, 167-173 (1955).
14. Murray, J.E*., et al.* Study on transplantation immunity after total body irradiation: clinical and experimental investigation. *Surgery* **48**, 272-284 (1960).
15. Calne, R.Y. Inhibition of the rejection of renal homografts in dogs by purine analogues. *Plast Reconstr Surg* **28**, 65-81 (1961).
16. Murray, J.E., Merrill, J.P., Harrison, J.H., Wilson, R.E. & Dammin, G.J. Prolonged survival of human-kidney homografts by immunosuppressive drug therapy. *The New England journal of medicine* **268**, 1315-1323 (1963).
17. Gilbert, R. Transplant is successful with a cadaver forearm. *Med Trib Med News* **5**, 20-21 (1964).
18. Gilbert, R. Hand transplanted from cadaver is reamputated. *Med Trib Med News* **5**(1964).
19. MURRAY, J.E. ORGAN TRANSPLANTATION (SKIN, KIDNEY, HEART) AND THE PLASTIC SURGEON. *Plastic and Reconstructive Surgery* **47**, 425-431 (1971).
20. Dubernard, J.-M*., et al.* Human hand allograft: report on first 6 months. *The Lancet* **353**, 1315-1320 (1999).
21. Devauchelle, B*., et al.* First human face allograft: early report. *Lancet* **368**, 203-209 (2006).

22. Dubernard, J.-M.*, et al.* Outcomes 18 Months after the First Human Partial Face Transplantation. *New England Journal of Medicine* **357**, 2451-2460 (2007).
23. Mendenhall, S.D.*, et al.* Prevalence and Distribution of Potential Vascularized Composite Allotransplant Donors, Implications for Optimizing the Donor-recipient Match. *Plast Reconstr Surg Glob Open* **6**, e1833-e1833 (2018).
24. Choo, S.Y. The HLA system: genetics, immunology, clinical testing, and clinical implications. *Yonsei medical journal* **48**, 11-23 (2007).
25. Wood, K.J. & Goto, R. Mechanisms of Rejection: Current Perspectives. *Transplantation* **93**, 1-10 (2012).
26. LaRosa, D.F., Rahman, A.H. & Turka, L.A. The innate immune system in allograft rejection and tolerance. *Journal of immunology (Baltimore, Md. : 1950)* **178**, 7503-7509 (2007).
27. Dai, H.*, et al.* PIRs mediate innate myeloid cell memory to nonself MHC molecules. *Science* **368**, 1122 (2020).
28. He, H., Stone, J.R. & Perkins, D.L. Analysis of differential immune responses induced by innate and adaptive immunity following transplantation. *Immunology* **109**, 185-196 (2003).
29. Nelson, P.J. & Krensky, A.M. Chemokines, chemokine receptors, and allograft rejection. *Immunity* **14**, 377-386 (2001).
30. Lu, C.Y., Penfield, J.G., Kielar, M.L., Vazquez, M.A. & Jeyarajah, D.R. Hypothesis: is renal allograft rejection initiated by the response to injury sustained during the transplant process? *Kidney Int* **55**, 2157-2168 (1999).
31. Bharat, A.*, et al.* Early posttransplant inflammation promotes the development of alloimmunity and chronic human lung allograft rejection. *Transplantation* **83**, 150-158 (2007).
32. Kawashima, M. & Juvet, S.C. The role of innate immunity in the long-term outcome of lung transplantation. *Ann Transl Med* **8**, 412 (2020).
33. Floerchinger, B., Oberhuber, R. & Tullius, S.G. Effects of brain death on organ quality and transplant outcome. *Transplant Rev (Orlando)* **26**, 54-59 (2012).
34. Koudstaal, L.G.*, et al.* Brain death induces inflammation in the donor intestine. *Transplantation* **86**, 148-154 (2008).
35. Hancock, W.W., Gao, W., Faia, K.L. & Csizmadia, V. Chemokines and their receptors in allograft rejection. *Current opinion in immunology* **12**, 511-516 (2000).
36. El-Sawy, T., Fahmy, N.M. & Fairchild, R.L. Chemokines: directing leukocyte infiltration into allografts. *Current opinion in immunology* **14**, 562-568 (2002).
37. Carvalho-Gaspar, M., Billing, J.S., Spriewald, B.M. & Wood, K.J. Chemokine gene expression during allograft rejection: Comparison of two quantitative PCR techniques. *Journal of immunological methods* **301**, 41-52 (2005).
38. Alegre, M.-L., Lakkis, F.G. & Morelli, A.E. Antigen Presentation in Transplantation. *Trends in immunology* **37**, 831-843 (2016).
39. Larsen, C.P., Morris, P.J. & Austyn, J.M. Migration of dendritic leukocytes from cardiac allografts into host spleens. A novel pathway for initiation of rejection. *The Journal of experimental medicine* **171**, 307-314 (1990).
40. Lakkis, F.G., Arakelov, A., Konieczny, B.T. & Inoue, Y. Immunologic 'ignorance' of vascularized organ transplants in the absence of secondary lymphoid tissue. *Nature Medicine* **6**, 686-688 (2000).

41. Lechler, R., Ng, W.F. & Steinman, R.M. Dendritic cells in transplantation--friend or foe? *Immunity* **14**, 357-368 (2001).
42. Talmage, D.W., Dart, G., Radovich, J. & Lafferty, K.J. Activation of transplant immunity: effect of donor leukocytes on thyroid allograft rejection. *Science* **191**, 385-388 (1976).
43. Larsen, C.P.*, et al.* Migration and maturation of Langerhans cells in skin transplants and explants. *The Journal of experimental medicine* **172**, 1483-1493 (1990).
44. Hancock, W.W., Thomson, N.M. & Atkins, R.C. Composition of interstitial cellular infiltrate identified by monoclonal antibodies in renal biopsies of rejecting human renal allografts. *Transplantation* **35**, 458-463 (1983).
45. Jose, M.D., Ikezumi, Y., van Rooijen, N., Atkins, R.C. & Chadban, S.J. Macrophages act as effectors of tissue damage in acute renal allograft rejection. *Transplantation* **76**, 1015-1022 (2003).
46. Chadban, S.J., Wu, H. & Hughes, J. Macrophages and kidney transplantation. *Semin Nephrol* **30**, 278-289 (2010).
47. Wyburn, K.R., Jose, M.D., Wu, H., Atkins, R.C. & Chadban, S.J. The role of macrophages in allograft rejection. *Transplantation* **80**, 1641-1647 (2005).
48. Jaeschke, H., Farhood, A. & Smith, C.W. Neutrophils contribute to ischemia/reperfusion injury in rat liver in vivo. *Faseb j* **4**, 3355-3359 (1990).
49. Morita, K.*, et al.* Early chemokine cascades in murine cardiac grafts regulate T cell recruitment and progression of acute allograft rejection. *Journal of immunology (Baltimore, Md. : 1950)* **167**, 2979-2984 (2001).
50. El-Sawy, T., Belperio, J.A., Strieter, R.M., Remick, D.G. & Fairchild, R.L. Inhibition of polymorphonuclear leukocyte-mediated graft damage synergizes with short-term costimulatory blockade to prevent cardiac allograft rejection. *Circulation* **112**, 320-331 (2005).
51. Kitchens, W.H.*, et al.* The changing role of natural killer cells in solid organ rejection and tolerance. *Transplantation* **81**, 811-817 (2006).
52. Bingaman, A.W.*, et al.* Vigorous allograft rejection in the absence of danger. *Journal of immunology (Baltimore, Md. : 1950)* **164**, 3065-3071 (2000).
53. Kroemer, A.*, et al.* The innate NK cells, allograft rejection, and a key role for IL-15. *Journal of immunology (Baltimore, Md. : 1950)* **180**, 7818-7826 (2008).
54. Koenig, A.*, et al.* Missing self triggers NK cell-mediated chronic vascular rejection of solid organ transplants. *Nat Commun* **10**, 5350 (2019).
55. Beilke, J.N., Kuhl, N.R., Van Kaer, L. & Gill, R.G. NK cells promote islet allograft tolerance via a perforin-dependent mechanism. *Nat Med* **11**, 1059-1065 (2005).
56. Yu, G., Xu, X., Vu, M.D., Kilpatrick, E.D. & Li, X.C. NK cells promote transplant tolerance by killing donor antigen-presenting cells. *The Journal of experimental medicine* **203**, 1851-1858 (2006).
57. Grafals, M. & Thurman, J.M. The Role of Complement in Organ Transplantation. *Frontiers in immunology* **10**, 2380-2380 (2019).
58. Hajishengallis, G., Reis, E.S., Mastellos, D.C., Ricklin, D. & Lambris, J.D. Novel mechanisms and functions of complement. *Nat Immunol* **18**, 1288-1298 (2017).
59. Morgan, B.P., Walters, D., Serna, M. & Bubeck, D. Terminal complexes of the complement system: new structural insights and their relevance to function. *Immunol Rev* **274**, 141-151 (2016).

60. Li, X.C. The significance of non-T-cell pathways in graft rejection: implications for transplant tolerance. *Transplantation* **90**, 1043-1047 (2010).
61. Bergler, T*., et al.* Infiltration of Macrophages Correlates with Severity of Allograft Rejection and Outcome in Human Kidney Transplantation. *PLoS One* **11**, e0156900 (2016).
62. Wang, G., Kong, G. & Li, X.C. Adaptive features of innate immune cells and their relevance to graft rejection. *Current opinion in organ transplantation* **24**, 664-669 (2019).
63. Kim, E.J*., et al.* Costimulation blockade alters germinal center responses and prevents antibody-mediated rejection. *Am J Transplant* **14**, 59-69 (2014).
64. Marino, J., Paster, J. & Benichou, G. Allorecognition by T Lymphocytes and Allograft Rejection. *Frontiers in Immunology* **7**(2016).
65. Goulmy, E. Human minor histocompatibility antigens. *Current opinion in immunology* **8**, 75-81 (1996).
66. Peugh, W.N., Superina, R.A., Wood, K.J. & Morris, P.J. The role of H-2 and non-H-2 antigens and genes in the rejection of murine cardiac allografts. *Immunogenetics* **23**, 30-37 (1986).
67. Pilat, N., Sayegh, M.H. & Wekerle, T. Costimulatory pathways in transplantation. *Semin Immunol* **23**, 293-303 (2011).
68. Goral, S. The three-signal hypothesis of lymphocyte activation/targets for immunosuppression. *Dialysis & Transplantation* **40**, 14-16 (2011).
69. Barker, C.F. & Billingham, R. The role of afferent lymphatics in the rejection of skin homografts. *The Journal of experimental medicine* **128**, 197-221 (1968).
70. Steinmuller, D. Passenger leukocytes and the immunogenicity of skin allografts. *Journal of Investigative Dermatology* **75**, 107-115 (1980).
71. Billingham, R.E. The passenger cell concept in transplantation immunology. *Cellular immunology* **2**, 1 (1971).
72. Lindahl, K.F. & Wilson, D.B. Histocompatibility antigen-activated cytotoxic T lymphocytes. II. Estimates of the frequency and specificity of precursors. *The Journal of experimental medicine* **145**, 508-522 (1977).
73. Ashwell, J., Chen, C. & Schwartz, R. High frequency and nonrandom distribution of alloreactivity in T cell clones selected for recognition of foreign antigen in association with self class II molecules. *The Journal of Immunology* **136**, 389-395 (1986).
74. Suchin, E.J*., et al.* Quantifying the frequency of alloreactive T cells in vivo: new answers to an old question. *The Journal of Immunology* **166**, 973-981 (2001).
75. Benichou, G., Valujskikh, A. & Heeger, P.S. Contributions of direct and indirect T cell alloreactivity during allograft rejection in mice. *The Journal of Immunology* **162**, 352-358 (1999).
76. Bevan, M.J. High determinant density may explain the phenomenon of alloreactivity. *Immunology Today* **5**, 128-130 (1984).
77. Portoles, P., Rojo, J.M. & Janeway, C.A., Jr. Asymmetry in the recognition of antigen: self class II MHC and non-self class II MHC molecules by the same T-cell receptor. *J Mol Cell Immunol* **4**, 129-137 (1989).
78. Benichou, G*., et al.* Limited T cell response to donor MHC peptides during allograft rejection. Implications for selective immune therapy in transplantation. *The Journal of Immunology* **153**, 938-945 (1994).

79. Boisgérault, F.*, et al.* Induction of T-cell response to cryptic MHC determinants during allograft rejection. *Human immunology* **61**, 1352-1362 (2000).
80. E E Sercarz*, et al.* Dominance and Crypticity of T Cell Antigenic Determinants. *Annual review of immunology* **11**, 729-766 (1993).
81. Suciu-Foca, N., Harris, P.E. & Cortesini, R. Intramolecular and intermolecular spreading during the course of organ allograft rejection. *Immunological reviews* **164**, 241-246 (1998).
82. Smyth, L.A., Herrera, O.B., Golshayan, D., Lombardi, G. & Lechler, R.I. A novel pathway of antigen presentation by dendritic and endothelial cells: Implications for allorecognition and infectious diseases. *Transplantation* **82**, S15-S18 (2006).
83. Marino, J.*, et al.* Donor exosomes rather than passenger leukocytes initiate alloreactive T cell responses after transplantation. *Science immunology* **1**, aaf8759 (2016).
84. Liu, Q.*, et al.* Donor dendritic cell-derived exosomes promote allograft-targeting immune response. *The Journal of clinical investigation* **126**, 2805-2820 (2016).
85. Hughes, A.D.*, et al.* Cross-dressed dendritic cells sustain effector T cell responses in islet and kidney allografts. *The Journal of clinical investigation* **130**, 287-294 (2020).
86. Hwang, J.-R., Byeon, Y., Kim, D. & Park, S.-G. Recent insights of T cell receptor-mediated signaling pathways for T cell activation and development. *Experimental & Molecular Medicine* **52**, 750-761 (2020).
87. Chen, L. & Flies, D.B. Molecular mechanisms of T cell co-stimulation and co-inhibition. *Nature Reviews Immunology* **13**, 227-242 (2013).
88. Boomer, J.S. & Green, J.M. An enigmatic tail of CD28 signaling. *Cold Spring Harbor perspectives in biology* **2**, a002436 (2010).
89. Janardhan, S.V., Praveen, K., Marks, R. & Gajewski, T.F. Evidence implicating the Ras pathway in multiple CD28 costimulatory functions in CD4+ T cells. *PLoS One* **6**, e24931 (2011).
90. Walker, L.S. & Sansom, D.M. Confusing signals: recent progress in CTLA-4 biology. *Trends Immunol* **36**, 63-70 (2015).
91. Qureshi, O.S.*, et al.* Trans-endocytosis of CD80 and CD86: a molecular basis for the cell-extrinsic function of CTLA-4. *Science* **332**, 600-603 (2011).
92. Wu, H., Gong, J. & Liu, Y. Indoleamine 2, 3-dioxygenase regulation of immune response (Review). *Mol Med Rep* **17**, 4867-4873 (2018).
93. Rudd, C.E., Taylor, A. & Schneider, H. CD28 and CTLA-4 coreceptor expression and signal transduction. *Immunological reviews* **229**, 12-26 (2009).
94. Colvin, R.B. & Smith, R.N. Antibody-mediated organ-allograft rejection. *Nature reviews. Immunology* **5**, 807-817 (2005).
95. Terasaki, P.I. & Cai, J. Humoral theory of transplantation: further evidence. *Current opinion in immunology* **17**, 541-545 (2005).
96. Russell, P.S., Chase, C.M. & Colvin, R.B. Alloantibody- and T cell-mediated immunity in the pathogenesis of transplant arteriosclerosis: lack of progression to sclerotic lesions in B cell-deficient mice. *Transplantation* **64**, 1531-1536 (1997).
97. Dalloul, A. B-Cell-Mediated Strategies to Fight Chronic Allograft Rejection. *Frontiers in Immunology* **4**(2013).
98. Moreau, A., Varey, E., Anegon, I. & Cuturi, M.-C. Effector mechanisms of rejection. *Cold Spring Harb Perspect Med* **3**, a015461 (2013).

99. Crome, S., Wang, A. & Levings, M. Translational mini-review series on Th17 cells: function and regulation of human T helper 17 cells in health and disease. *Clinical & Experimental Immunology* **159**, 109-119 (2010).
100. van Besouw, N.M.*, et al.* Interleukin-17–producing CD4+ cells home to the graft early after human heart transplantation. *The Journal of Heart and Lung Transplantation* **34**, 933-940 (2015).
101. Sullivan, J.A., Adams, A.B. & Burlingham, W.J. The Emerging Role of TH17 Cells in Organ Transplantation. *Transplantation* **97**, 483-489 (2014).
102. Abadja, F., Sarraj, B. & Ansari, M.J. Significance of T helper 17 immunity in transplantation. *Current opinion in organ transplantation* **17**, 8-14 (2012).
103. Brady, J., Hayakawa, Y., Smyth, M.J. & Nutt, S.L. IL-21 induces the functional maturation of murine NK cells. *The Journal of Immunology* **172**, 2048-2058 (2004).
104. van Besouw, N.M.*, et al.* The Number of Donor-Specific IL-21 Producing Cells Before and After Transplantation Predicts Kidney Graft Rejection. *Frontiers in Immunology* **10**(2019).
105. Heeger, P.S.*, et al.* Pretransplant frequency of donor-specific, IFN-gamma-producing lymphocytes is a manifestation of immunologic memory and correlates with the risk of posttransplant rejection episodes. *Journal of immunology (Baltimore, Md. : 1950)* **163**, 2267-2275 (1999).
106. Gill, R.G. & Burrack, A.L. Diverse Routes of Allograft Tolerance Disruption by Memory T Cells. *Frontiers in Immunology* **11**, 2671 (2020).
107. Tanaka, K.*, et al.* Classification of human liver transplant recipients by their preoperative CD8+ T cell subpopulation and its relation to outcome. *Liver Transplantation* **12**, 792-800 (2006).
108. Nadazdin, O.*, et al.* Host alloreactive memory T cells influence tolerance to kidney allografts in nonhuman primates. *Science translational medicine* **3**, 86ra51-86ra51 (2011).
109. Sallusto, F., Lenig, D., Förster, R., Lipp, M. & Lanzavecchia, A. Two subsets of memory T lymphocytes with distinct homing potentials and effector functions. *Nature* **401**, 708-712 (1999).
110. Zhang, Q. & Lakkis, F.G. Memory T Cell Migration. *Frontiers in Immunology* **6**(2015).
111. Mueller, S.N., Zaid, A. & Carbone, F.R. Tissue-resident T cells: dynamic players in skin immunity. *Frontiers in immunology* **5**, 332-332 (2014).
112. Watanabe, R.*, et al.* Human skin is protected by four functionally and phenotypically discrete populations of resident and recirculating memory T cells. *Sci Transl Med* **7**, 279ra239 (2015).
113. Fujimoto, S.*, et al.* CCR4 and CCR10 are expressed on epidermal keratinocytes and are involved in cutaneous immune reaction. *Cytokine* **44**, 172-178 (2008).
114. Josefowicz, S.Z., Lu, L.-F. & Rudensky, A.Y. Regulatory T cells: mechanisms of differentiation and function. *Annual review of immunology* **30**, 531-564 (2012).
115. Sawitzki, B.*, et al.* Regulatory cell therapy in kidney transplantation (The ONE Study): a harmonised design and analysis of seven non-randomised, single-arm, phase 1/2A trials. *The Lancet* **395**, 1627-1639 (2020).
116. Miska, J.*, et al.* Real-time immune cell interactions in target tissue during autoimmune-induced damage and graft tolerance. *The Journal of experimental medicine* **211**, 441-456 (2014).

117. Tang, Q.*, et al.* Visualizing regulatory T cell control of autoimmune responses in nonobese diabetic mice. *Nat Immunol* **7**, 83-92 (2006).
118. Thauland, T.J., Koguchi, Y., Dustin, M.L. & Parker, D.C. CD28-CD80 interactions control regulatory T cell motility and immunological synapse formation. *Journal of immunology (Baltimore, Md. : 1950)* **193**, 5894-5903 (2014).
119. Luster, A.D., Alon, R. & von Andrian, U.H. Immune cell migration in inflammation: present and future therapeutic targets. *Nature Immunology* **6**, 1182-1190 (2005).
120. von Andrian, U.H. & Mempel, T.R. Homing and cellular traffic in lymph nodes. *Nature Reviews Immunology* **3**, 867-878 (2003).
121. Zlotnik, A. & Yoshie, O. Chemokines: a new classification system and their role in immunity. *Immunity* **12**, 121-127 (2000).
122. Murdoch, C. & Finn, A. Chemokine receptors and their role in inflammation and infectious diseases. *Blood* **95**, 3032-3043 (2000).
123. Campbell, J.J.*, et al.* Chemokines and the arrest of lymphocytes rolling under flow conditions. *Science* **279**, 381-384 (1998).
124. Lloyd, A.R., Oppenheim, J.J., Kelvin, D.J. & Taub, D.D. Chemokines regulate T cell adherence to recombinant adhesion molecules and extracellular matrix proteins. *Journal of immunology (Baltimore, Md. : 1950)* **156**, 932-938 (1996).
125. Melter, M., McMahon, G., Fang, J., Ganz, P. & Briscoe, D.M. Current understanding of chemokine involvement in allograft transplantation. *Pediatr Transplant* **3**, 10-21 (1999).
126. Hancock, W.W.*, et al.* Donor-derived IP-10 initiates development of acute allograft rejection. *The Journal of experimental medicine* **193**, 975-980 (2001).
127. Hancock, W.W.*, et al.* Requirement of the chemokine receptor CXCR3 for acute allograft rejection. *The Journal of experimental medicine* **192**, 1515-1520 (2000).
128. Miura, M.*, et al.* Monokine induced by IFN-gamma is a dominant factor directing T cells into murine cardiac allografts during acute rejection. *Journal of immunology (Baltimore, Md. : 1950)* **167**, 3494-3504 (2001).
129. Kapoor, A.*, et al.* Early expression of interferon-gamma inducible protein 10 and monokine induced by interferon-gamma in cardiac allografts is mediated by CD8+ T cells. *Transplantation* **69**, 1147-1155 (2000).
130. Kapoor, A.*, et al.* Intragraft expression of chemokine gene occurs early during acute rejection of allogeneic cardiac grafts. *Transplantation proceedings* **32**, 793-795 (2000).
131. Watarai, Y.*, et al.* Intraallograft chemokine RNA and protein during rejection of MHC-matched/multiple minor histocompatibility-disparate skin grafts. *Journal of immunology (Baltimore, Md. : 1950)* **164**, 6027-6033 (2000).
132. Gao, W.*, et al.* Targeting of the chemokine receptor CCR1 suppresses development of acute and chronic cardiac allograft rejection. *The Journal of clinical investigation* **105**, 35-44 (2000).
133. Pattison, J.*, et al.* RANTES chemokine expression in cell-mediated transplant rejection of the kidney. *Lancet* **343**, 209-211 (1994).
134. Belperio, J.A. & Ardehali, A. Chemokines and transplant vasculopathy. *Circ Res* **103**, 454-466 (2008).
135. Takada, M., Nadeau, K.C., Shaw, G.D., Marquette, K.A. & Tilney, N.L. The cytokine-adhesion molecule cascade in ischemia/reperfusion injury of the rat kidney.

Inhibition by a soluble P-selectin ligand. *The Journal of clinical investigation* **99**, 2682-2690 (1997).
136. Wang, C.Y.*, et al.* Cardiac graft intercellular adhesion molecule-1 (ICAM-1) and interleukin-1 expression mediate primary isograft failure and induction of ICAM-1 in organs remote from the site of transplantation. *Circ Res* **82**, 762-772 (1998).
137. Sosa, R.A.*, et al.* Early cytokine signatures of ischemia/reperfusion injury in human orthotopic liver transplantation. *JCI insight* **1**, e89679-e89679 (2016).
138. Takada, M., Chandraker, A., Nadeau, K.C., Sayegh, M.H. & Tilney, N.L. The role of the B7 costimulatory pathway in experimental cold ischemia/reperfusion injury. *The Journal of clinical investigation* **100**, 1199-1203 (1997).
139. Schadde, E. & Knechtle, S.J. chemokines in transplantation. *Transplantation Reviews* **21**, 107-118 (2007).
140. Hauser, I.A.*, et al.* Prediction of Acute Renal Allograft Rejection by Urinary Monokine Induced by IFN-γ (MIG). *Journal of the American Society of Nephrology* **16**, 1849 (2005).
141. Segerer, S., Nelson, P.J. & SCHLÖNDORFF, D. Chemokines, chemokine receptors, and renal disease: from basic science to pathophysiologic and therapeutic studies. *Journal of the American Society of Nephrology* **11**, 152-176 (2000).
142. Fischereder, M.*, et al.* CC chemokine receptor 5 and renal-transplant survival. *The Lancet* **357**, 1758-1761 (2001).
143. Scurci, I., Martins, E. & Hartley, O. CCR5: Established paradigms and new frontiers for a 'celebrity' chemokine receptor. *Cytokine* **109**, 81-93 (2018).
144. Kohlmeier, J.E.*, et al.* Inflammatory chemokine receptors regulate CD8+ T cell contraction and memory generation following infection. *Journal of Experimental Medicine* **208**, 1621-1634 (2011).
145. Reshef, R.*, et al.* Blockade of Lymphocyte Chemotaxis in Visceral Graft-versus-Host Disease. *New England Journal of Medicine* **367**, 135-145 (2012).
146. Khandelwal, P.*, et al.* CCR5 inhibitor as novel acute graft versus host disease prophylaxis in children and young adults undergoing allogeneic stem cell transplant: results of the phase II study. *Bone marrow transplantation* **55**, 1552-1559 (2020).
147. Bräsen, J.H.*, et al.* Macrophage density in early surveillance biopsies predicts future renal transplant function. *Kidney international* **92**, 479-489 (2017).
148. Singh, R., Kapoor, R., Srivastava, A. & Mittal, R. Impact of chemokine receptor CCR2 and CCR5 gene polymorphism on allograft outcome in North Indian renal transplant recipients. *Scandinavian journal of immunology* **69**, 51-56 (2009).
149. Abdi, R.*, et al.* Chemokine receptor polymorphism and risk of acute rejection in human renal transplantation. *Journal of the American Society of Nephrology* **13**, 754-758 (2002).
150. Abdi, R.*, et al.* Differential role of CCR2 in islet and heart allograft rejection: tissue specificity of chemokine/chemokine receptor function in vivo. *The Journal of Immunology* **172**, 767-775 (2004).
151. Gerlach, C.*, et al.* The Chemokine Receptor CX3CR1 Defines Three Antigen-Experienced CD8 T Cell Subsets with Distinct Roles in Immune Surveillance and Homeostasis. *Immunity* **45**, 1270-1284 (2016).
152. Chen, L. & Shen, Z. Tissue-resident memory T cells and their biological characteristics in the recurrence of inflammatory skin disorders. *Cellular & Molecular Immunology* **17**, 64-75 (2020).

153. Lian, C.G.*, et al.* Biomarker evaluation of face transplant rejection: association of donor T cells with target cell injury. *Modern Pathology* **27**, 788-799 (2014).
154. Sasson, S.C., Gordon, C.L., Christo, S.N., Klenerman, P. & Mackay, L.K. Local heroes or villains: tissue-resident memory T cells in human health and disease. *Cellular & Molecular Immunology* **17**, 113-122 (2020).
155. Beura, L.K., Rosato, P.C. & Masopust, D. Implications of Resident Memory T Cells for Transplantation. *American Journal of Transplantation* **17**, 1167-1175 (2017).
156. Su, C.A. & Fairchild, R.L. Memory T Cells in Transplantation. *Current Transplantation Reports* **1**, 137-146 (2014).
157. Zhang, Q., Chen, Y., Fairchild, R.L., Heeger, P.S. & Valujskikh, A. Lymphoid Sequestration of Alloreactive Memory CD4 T Cells Promotes Cardiac Allograft Survival. *The Journal of Immunology* **176**, 770 (2006).
158. Vincenti, F.*, et al.* A phase I/II randomized open-label multicenter trial of efalizumab, a humanized anti-CD11a, anti-LFA-1 in renal transplantation. *Am J Transplant* **7**, 1770-1777 (2007).
159. Kim, J.M., Rasmussen, J.P. & Rudensky, A.Y. Regulatory T cells prevent catastrophic autoimmunity throughout the lifespan of mice. *Nat Immunol* **8**, 191-197 (2007).
160. Yano, H., Andrews, L.P., Workman, C.J. & Vignali, D.A.A. Intratumoral regulatory T cells: markers, subsets and their impact on anti-tumor immunity. *Immunology* **157**, 232-247 (2019).
161. Ding, Y., Xu, J. & Bromberg, J.S. Regulatory T cell migration during an immune response. *Trends Immunol* **33**, 174-180 (2012).
162. Huehn, J. & Hamann, A. Homing to suppress: address codes for Treg migration. *Trends Immunol* **26**, 632-636 (2005).
163. MacDonald, K.G., Orban, P.C. & Levings, M.K. T regulatory cell therapy in transplantation: stability, localization and functional specialization. *Curr Opin Organ Transplant* **17**, 343-348 (2012).
164. Wei, S., Kryczek, I. & Zou, W. Regulatory T-cell compartmentalization and trafficking. *Blood* **108**, 426-431 (2006).
165. Ermann, J.*, et al.* Only the CD62L+ subpopulation of CD4+CD25+ regulatory T cells protects from lethal acute GVHD. *Blood* **105**, 2220-2226 (2005).
166. Smigiel, K.S.*, et al.* CCR7 provides localized access to IL-2 and defines homeostatically distinct regulatory T cell subsets. *The Journal of experimental medicine* **211**, 121-136 (2014).
167. Sugiyama, D.*, et al.* Anti-CCR4 mAb selectively depletes effector-type FoxP3+ CD4+ regulatory T cells, evoking antitumor immune responses in humans. *Proceedings of the National Academy of Sciences* **110**, 17945-17950 (2013).
168. Pere, H.*, et al.* A CCR4 antagonist combined with vaccines induces antigen-specific CD8+ T cells and tumor immunity against self antigens. *Blood* **118**, 4853-4862 (2011).
169. Sather, B.D.*, et al.* Altering the distribution of Foxp3(+) regulatory T cells results in tissue-specific inflammatory disease. *The Journal of experimental medicine* **204**, 1335-1347 (2007).
170. Zhang, N.*, et al.* Regulatory T cells sequentially migrate from inflamed tissues to draining lymph nodes to suppress the alloimmune response. *Immunity* **30**, 458-469 (2009).
171. Curiel, T.J.*, et al.* Specific recruitment of regulatory T cells in ovarian carcinoma fosters immune privilege and predicts reduced survival. *Nat Med* **10**, 942-949 (2004).

172. Duvic, M.*, et al.* Phase 1/2 study of mogamulizumab, a defucosylated anti-CCR4 antibody, in previously treated patients with cutaneous T-cell lymphoma. *Blood*, blood-2014-2009-600924 (2015).
173. Gobert, M.*, et al.* Regulatory T cells recruited through CCL22/CCR4 are selectively activated in lymphoid infiltrates surrounding primary breast tumors and lead to an adverse clinical outcome. *Cancer research* **69**, 2000-2009 (2009).
174. Yang, Z.-Z., Novak, A.J., Stenson, M.J., Witzig, T.E. & Ansell, S.M. Intratumoral CD4+ CD25+ regulatory T-cell-mediated suppression of infiltrating CD4+ T cells in B-cell non-Hodgkin lymphoma. *Blood* **107**, 3639-3646 (2006).
175. Sun, W.*, et al.* Blockade of MCP-1/CCR4 signaling-induced recruitment of activated regulatory cells evokes an antitumor immune response in head and neck squamous cell carcinoma. *Oncotarget* **7**, 37714-37727 (2016).
176. Matsuo, K.*, et al.* CCR4 is critically involved in effective antitumor immunity in mice bearing intradermal B16 melanoma. *Cancer Letters* **378**, 16-22 (2016).
177. Afshar, R.*, et al.* Compartmentalized chemokine-dependent regulatory T-cell inhibition of allergic pulmonary inflammation. *The Journal of allergy and clinical immunology* **131**, 1644-1652 (2013).
178. Curiel, T.J.*, et al.* Specific recruitment of regulatory T cells in ovarian carcinoma fosters immune privilege and predicts reduced survival. *Nature Medicine* **10**, 942-949 (2004).
179. Bayry, J.*, et al.* In silico identified CCR4 antagonists target regulatory T cells and exert adjuvant activity in vaccination. *Proceedings of the National Academy of Sciences of the United States of America* **105**, 10221-10226 (2008).
180. Ishida, T.*, et al.* Defucosylated Anti-CCR4 Monoclonal Antibody (KW-0761) for Relapsed Adult T-Cell Leukemia-Lymphoma: A Multicenter Phase II Study. *Journal of Clinical Oncology* **30**, 837-842 (2012).
181. Iellem, A.*, et al.* Unique chemotactic response profile and specific expression of chemokine receptors CCR4 and CCR8 by CD4(+)CD25(+) regulatory T cells. *The Journal of experimental medicine* **194**, 847-853 (2001).
182. Coghill, J.M.*, et al.* CC chemokine receptor 8 potentiates donor Treg survival and is critical for the prevention of murine graft-versus-host disease. *Blood* **122**, 825-836 (2013).
183. Plitas, G.*, et al.* Regulatory T cells exhibit distinct features in human breast cancer. *Immunity* **45**, 1122-1134 (2016).
184. Wang, T.*, et al.* CCR8 blockade primes anti-tumor immunity through intratumoral regulatory T cells destabilization in muscle-invasive bladder cancer. *Cancer Immunology, Immunotherapy* **69**, 1855-1867 (2020).
185. Campbell, J.R.*, et al.* Fc-optimized Anti-CCR8 Antibody Depletes Regulatory T Cells in Human Tumor Models. *Cancer Research*, canres.3585.2020 (2021).
186. Van Damme, H.*, et al.* Therapeutic depletion of CCR8⁺ tumor-infiltrating regulatory T cells elicits antitumor immunity and synergizes with anti-PD-1 therapy. *Journal for ImmunoTherapy of Cancer* **9**, e001749 (2021).
187. Barsheshet, Y.*, et al.* CCR8+ FOXp3+ Treg cells as master drivers of immune regulation. *Proceedings of the National Academy of Sciences* **114**, 6086-6091 (2017).
188. Vila-Caballer, M.*, et al.* Disruption of the CCL1-CCR8 axis inhibits vascular Treg recruitment and function and promotes atherosclerosis in mice. *Journal of Molecular and Cellular Cardiology* **132**, 154-163 (2019).

189. Himmel, M.E*., et al.* Human CD4+ FOXP3+ regulatory T cells produce CXCL8 and recruit neutrophils. *European journal of immunology* **41**, 306-312 (2011).
190. Nguyen, K.D*., et al.* XCL1 enhances regulatory activities of CD4+ CD25(high) CD127(low/-) T cells in human allergic asthma. *Journal of immunology (Baltimore, Md. : 1950)* **181**, 5386-5395 (2008).
191. Patterson, S.J*., et al.* T regulatory cell chemokine production mediates pathogenic T cell attraction and suppression. *The Journal of clinical investigation* **126**, 1039-1051 (2016).
192. Viola, A. & Luster, A.D. Chemokines and their receptors: drug targets in immunity and inflammation. *Annu Rev Pharmacol Toxicol* **48**, 171-197 (2008).
193. Shultz, L.D., Ishikawa, F. & Greiner, D.L. Humanized mice in translational biomedical research. *Nature reviews. Immunology* **7**, 118-130 (2007).
194. Qing, Y., Lin, Y. & Gerson, S.L. An intrinsic BM hematopoietic niche occupancy defect of HSC in scid mice facilitates exogenous HSC engraftment. *Blood* **119**, 1768-1771 (2012).
195. McDermott, S.P., Eppert, K., Lechman, E.R., Doedens, M. & Dick, J.E. Comparison of human cord blood engraftment between immunocompromised mouse strains. *Blood* **116**, 193-200 (2010).
196. Brehm, M.A*., et al.* Parameters for establishing humanized mouse models to study human immunity: analysis of human hematopoietic stem cell engraftment in three immunodeficient strains of mice bearing the IL2rgamma(null) mutation. *Clinical immunology (Orlando, Fla.)* **135**, 84-98 (2010).
197. Adigbli, G*., et al.* Humanization of Immunodeficient Animals for the Modeling of Transplantation, Graft Versus Host Disease and Regenerative Medicine. *Transplantation* (2020).
198. Cosgun, K.N*., et al.* Kit regulates HSC engraftment across the human-mouse species barrier. *Cell Stem Cell* **15**, 227-238 (2014).
199. Labarthe, L*., et al.* Frontline Science: Exhaustion and senescence marker profiles on human T cells in BRGSF-A2 humanized mice resemble those in human samples. *Journal of leukocyte biology* (2019).
200. Gonzalez, L., Strbo, N. & Podack, E.R. Humanized mice: novel model for studying mechanisms of human immune-based therapies. *Immunol Res* **57**, 326-334 (2013).
201. Schmidt, M.R*., et al.* Human BLyS facilitates engraftment of human PBL derived B cells in immunodeficient mice. *PLoS One* **3**, e3192 (2008).
202. Shultz, L.D*., et al.* Human lymphoid and myeloid cell development in NOD/LtSz-scid IL2R gamma null mice engrafted with mobilized human hemopoietic stem cells. *Journal of immunology (Baltimore, Md. : 1950)* **174**, 6477-6489 (2005).
203. Billerbeck, E*., et al.* Development of human CD4+FoxP3+ regulatory T cells in human stem cell factor-, granulocyte-macrophage colony-stimulating factor-, and interleukin-3-expressing NOD-SCID IL2Rgamma(null) humanized mice. *Blood* **117**, 3076-3086 (2011).
204. Rongvaux, A*., et al.* Development and function of human innate immune cells in a humanized mouse model. *Nat Biotechnol* **32**, 364-372 (2014).
205. Herndler-Brandstetter, D*., et al.* Humanized mouse model supports development, function, and tissue residency of human natural killer cells. *Proceedings of the National Academy of Sciences of the United States of America* **114**, E9626-e9634 (2017).

206. Ono, R.*, et al.* Co-activation of macrophages and T cells contribute to chronic GVHD in human IL-6 transgenic humanised mouse model. *EBioMedicine* **41**, 584-596 (2019).
207. Shultz, L.D.*, et al.* Human lymphoid and myeloid cell development in NOD/LtSz-scid IL2Rγnull mice engrafted with mobilized human hemopoietic stem cells. *The Journal of Immunology* **174**, 6477-6489 (2005).
208. McIntosh, B.E.*, et al.* Nonirradiated NOD,B6.SCID Il2rgamma-/- Kit(W41/W41) (NBSGW) mice support multilineage engraftment of human hematopoietic cells. *Stem Cell Reports* **4**, 171-180 (2015).
209. Hess, N.J.*, et al.* Different Human Immune Lineage Compositions Are Generated in Non-Conditioned NBSGW Mice Depending on HSPC Source. *Frontiers in Immunology* **11**, 1-11 (2020).
210. Dessels, C., Alessandrini, M. & Pepper, M.S. Factors Influencing the Umbilical Cord Blood Stem Cell Industry: An Evolving Treatment Landscape. *Stem cells translational medicine* **7**, 643-650 (2018).
211. Fiorini, C.*, et al.* Developmentally-faithful and effective human erythropoiesis in immunodeficient and Kit mutant mice. *American journal of hematology* **92**, E513-e519 (2017).
212. McGuckin, C.P.*, et al.* Multiparametric analysis of immature cell populations in umbilical cord blood and bone marrow. *Eur J Haematol* **71**, 341-350 (2003).
213. Miraglia, S.*, et al.* A novel five-transmembrane hematopoietic stem cell antigen: isolation, characterization, and molecular cloning. *Blood* **90**, 5013-5021 (1997).
214. Yin, A.H.*, et al.* AC133, a novel marker for human hematopoietic stem and progenitor cells. *Blood* **90**, 5002-5012 (1997).
215. Gallacher, L.*, et al.* Isolation and characterization of human CD34(-)Lin(-) and CD34(+)Lin(-) hematopoietic stem cells using cell surface markers AC133 and CD7. *Blood* **95**, 2813-2820 (2000).
216. Sumide, K.*, et al.* A revised road map for the commitment of human cord blood CD34-negative hematopoietic stem cells. *Nature Communications* **9**, 2202 (2018).
217. Matsuoka, Y.*, et al.* The number of CD34(+)CD133(+) hematopoietic stem cells residing in umbilical cord blood (UCB) units is not correlated with the numbers of total nucleated cells and CD34(+) cells: a possible new indicator for quality evaluation of UCB units. *Int J Hematol* **108**, 571-579 (2018).
218. Takahashi, M.*, et al.* CD133 is a positive marker for a distinct class of primitive human cord blood-derived CD34-negative hematopoietic stem cells. *Leukemia* **28**, 1308-1315 (2014).
219. Issa, F.*, et al.* Ex vivo-expanded human regulatory T cells prevent the rejection of skin allografts in a humanized mouse model. *Transplantation* **90**, 1321-1327 (2010).
220. Vuyyuru, R., Patton, J. & Manser, T. Human immune system mice: current potential and limitations for translational research on human antibody responses. *Immunol Res* **51**, 257-266 (2011).
221. Manz, M.G. Human-hemato-lymphoid-system mice: opportunities and challenges. *Immunity* **26**, 537-541 (2007).
222. Gimeno, R.*, et al.* Monitoring the effect of gene silencing by RNA interference in human CD34+ cells injected into newborn RAG2-/-γc-/-mice: functional inactivation of p53 in developing T cells. *Blood* **104**, 3886-3893 (2004).

223. Ishikawa, F*., et al.* Development of functional human blood and immune systems in NOD/SCID/IL2 receptor {gamma} chain(null) mice. *Blood* **106**, 1565-1573 (2005).
224. Traggiai, E*., et al.* Development of a human adaptive immune system in cord blood cell-transplanted mice. *Science* **304**, 104-107 (2004).
225. Bosma, G.C., Custer, R.P. & Bosma, M.J. A severe combined immunodeficiency mutation in the mouse. *Nature* **301**, 527-530 (1983).
226. Serreze, D.V. & Leiter, E.H. Defective activation of T suppressor cell function in nonobese diabetic mice. Potential relation to cytokine deficiencies. *Journal of immunology (Baltimore, Md. : 1950)* **140**, 3801-3807 (1988).
227. Ito, M*., et al.* NOD/SCID/gamma(c)(null) mouse: an excellent recipient mouse model for engraftment of human cells. *Blood* **100**, 3175-3182 (2002).
228. King, M.A*., et al.* Human peripheral blood leucocyte non-obese diabetic-severe combined immunodeficiency interleukin-2 receptor gamma chain gene mouse model of xenogeneic graft-versus-host-like disease and the role of host major histocompatibility complex. *Clinical and experimental immunology* **157**, 104-118 (2009).
229. Shultz, L.D*., et al.* Generation of functional human T-cell subsets with HLA-restricted immune responses in HLA class I expressing NOD/SCID/IL2rγ^{null} humanized mice. *Proceedings of the National Academy of Sciences* **107**, 13022 (2010).
230. Suzuki, M*., et al.* Induction of human humoral immune responses in a novel HLA-DR-expressing transgenic NOD/Shi-scid/γcnull mouse. *International immunology* **24**, 243-252 (2012).
231. Rahmig, S*., et al.* Improved Human Erythropoiesis and Platelet Formation in Humanized NSGW41 Mice. *Stem cell reports* **7**, 591-601 (2016).
232. Katano, I*., et al.* Long-term maintenance of peripheral blood derived human NK cells in a novel human IL-15-transgenic NOG mouse. *Scientific reports* **7**, 17230 (2017).
233. Ito, R*., et al.* Establishment of a human allergy model using human IL-3/GM-CSF-transgenic NOG mice. *Journal of immunology (Baltimore, Md. : 1950)* **191**, 2890-2899 (2013).
234. Katano, I*., et al.* Predominant development of mature and functional human NK cells in a novel human IL-2-producing transgenic NOG mouse. *Journal of immunology (Baltimore, Md. : 1950)* **194**, 3513-3525 (2015).
235. Danner, R*., et al.* Expression of HLA class II molecules in humanized NOD.Rag1KO.IL2RgcKO mice is critical for development and function of human T and B cells. *PLoS One* **6**, e19826 (2011).
236. Harris, D.T., Badowski, M., Balamurugan, A. & Yang, O.O. Long-term human immune system reconstitution in non-obese diabetic (NOD)-Rag (-)-gamma chain (-) (NRG) mice is similar but not identical to the original stem cell donor. *Clinical and experimental immunology* **174**, 402-413 (2013).
237. Strowig, T*., et al.* Transgenic expression of human signal regulatory protein alpha in Rag2-/-gamma(c)-/- mice improves engraftment of human hematopoietic cells in humanized mice. *Proceedings of the National Academy of Sciences of the United States of America* **108**, 13218-13223 (2011).
238. Miller, P.H*., et al.* Analysis of parameters that affect human hematopoietic cell outputs in mutant c-kit-immunodeficient mice. *Experimental hematology* **48**, 41-49 (2017).

239. Rich, B.S.*, et al.* Endogenous antibodies for tumor detection. *Scientific reports* **4**, 5088-5088 (2014).
240. Legrand, N.*, et al.* Functional CD47/signal regulatory protein alpha (SIRPα) interaction is required for optimal human T- and natural killer- (NK) cell homeostasis in vivo. *Proceedings of the National Academy of Sciences* **108**, 13224 (2011).
241. Traggiai, E.*, et al.* Development of a human adaptive immune system in cord blood cell-transplanted mice. *Science (New York, N.Y.)* **304**, 104-107 (2004).
242. Willinger, T.*, et al.* Human IL-3/GM-CSF knock-in mice support human alveolar macrophage development and human immune responses in the lung. *Proceedings of the National Academy of Sciences* **108**, 2390 (2011).
243. Yamauchi, T.*, et al.* Polymorphic Sirpa is the genetic determinant for NOD-based mouse lines to achieve efficient human cell engraftment. *Blood* **121**, 1316-1325 (2013).
244. Li, Y.*, et al.* A novel Flt3-deficient HIS mouse model with selective enhancement of human DC development. *European journal of immunology* **46**, 1291-1299 (2016).
245. Zeng, Y.*, et al.* Creation of an immunodeficient HLA-transgenic mouse (HUMAMICE) and functional validation of human immunity after transfer of HLA-matched human cells. *PLoS One* **12**, e0173754 (2017).
246. Pantelouris, E.M. Absence of thymus in a mouse mutant. *Nature* **217**, 370-371 (1968).
247. Adigbli, G.*, et al.* Humanization of Immunodeficient Animals for the Modeling of Transplantation, Graft Versus Host Disease, and Regenerative Medicine. *Transplantation* **104**, 2290-2306 (2020).
248. Tarunina, M.*, et al.* A Novel High-Throughput Screening Platform Reveals an Optimized Cytokine Formulation for Human Hematopoietic Progenitor Cell Expansion. *Stem cells and development* **25**, 1709-1720 (2016).
249. Hu, Z., Van Rooijen, N. & Yang, Y.-G. Macrophages prevent human red blood cell reconstitution in immunodeficient mice. *Blood* **118**, 5938-5946 (2011).
250. Roederer, M. Interpretation of cellular proliferation data: avoid the panglossian. *Cytometry A* **79**, 95-101 (2011).
251. Kenter, M.J. & Cohen, A.F. Establishing risk of human experimentation with drugs: lessons from TGN1412. *Lancet* **368**, 1387-1391 (2006).
252. Suntharalingam, G.*, et al.* Cytokine storm in a phase 1 trial of the anti-CD28 monoclonal antibody TGN1412. *N Engl J Med* **355**, 1018-1028 (2006).
253. Mestas, J. & Hughes, C.C. Of mice and not men: differences between mouse and human immunology. *Journal of immunology (Baltimore, Md. : 1950)* **172**, 2731-2738 (2004).
254. Wunderlich, M.*, et al.* Improved multilineage human hematopoietic reconstitution and function in NSGS mice. *PloS one* **13**, e0209034-e0209034 (2018).
255. Watanabe, Y.*, et al.* The analysis of the functions of human B and T cells in humanized NOD/shi-scid/gammac(null) (NOG) mice (hu-HSC NOG mice). *International immunology* **21**, 843-858 (2009).
256. Lang, J.*, et al.* Studies of Lymphocyte Reconstitution in a Humanized Mouse Model Reveal a Requirement of T Cells for Human B Cell Maturation. *The Journal of Immunology* **190**, 2090 (2013).

257. Biswas, S.*, et al.* Humoral immune responses in humanized BLT mice immunized with West Nile virus and HIV-1 envelope proteins are largely mediated via human CD5+ B cells. *Immunology* **134**, 419-433 (2011).
258. Matsumura, T.*, et al.* Functional CD5+ B cells develop predominantly in the spleen of NOD/SCID/gammac(null) (NOG) mice transplanted either with human umbilical cord blood, bone marrow, or mobilized peripheral blood CD34+ cells. *Experimental hematology* **31**, 789-797 (2003).
259. Ichii, M.*, et al.* The density of CD10 corresponds to commitment and progression in the human B lymphoid lineage. *PLoS One* **5**, e12954 (2010).
260. Agematsu, K.*, et al.* B cell subpopulations separated by CD27 and crucial collaboration of CD27+ B cells and helper T cells in immunoglobulin production. *European journal of immunology* **27**, 2073-2079 (1997).
261. Loder, F.*, et al.* B cell development in the spleen takes place in discrete steps and is determined by the quality of B cell receptor-derived signals. *The Journal of experimental medicine* **190**, 75-89 (1999).
262. Sanz, I.*, et al.* Challenges and Opportunities for Consistent Classification of Human B Cell and Plasma Cell Populations. *Frontiers in Immunology* **10**, 1-17 (2019).
263. Wu, Y.-C.B., Kipling, D. & Dunn-Walters, D.K. The relationship between CD27 negative and positive B cell populations in human peripheral blood. *Frontiers in immunology* **2**, 81-81 (2011).
264. Stavnezer, J., Guikema, J.E.J. & Schrader, C.E. Mechanism and regulation of class switch recombination. *Annual review of immunology* **26**, 261-292 (2008).
265. Kreuzaler, M.*, et al.* Soluble BAFF levels inversely correlate with peripheral B cell numbers and the expression of BAFF receptors. *The Journal of Immunology* **188**, 497-503 (2012).
266. Smulski, C.R. & Eibel, H. BAFF and BAFF-receptor in B cell selection and survival. *Frontiers in immunology* **9**, 2285 (2018).
267. Zhang, J.*, et al.* Bone marrow dendritic cells regulate hematopoietic stem/progenitor cell trafficking. *The Journal of clinical investigation* **129**, 2920-2931 (2019).
268. Sade-Feldman, M.*, et al.* Clinical Significance of Circulating CD33+CD11b+HLA-DR- Myeloid Cells in Patients with Stage IV Melanoma Treated with Ipilimumab. *Clinical cancer research : an official journal of the American Association for Cancer Research* **22**, 5661-5672 (2016).
269. Zhang, W.*, et al.* Myeloid-derived suppressor cells in transplantation: the dawn of cell therapy. *J Transl Med* **16**, 19-19 (2018).
270. Bronte, V.*, et al.* Identification of a CD11b(+)/Gr-1(+)/CD31(+) myeloid progenitor capable of activating or suppressing CD8(+) T cells. *Blood* **96**, 3838-3846 (2000).
271. Qiu, L.B., Dickson, H., Hajibagheri, N. & Crocker, P.R. Extruded erythroblast nuclei are bound and phagocytosed by a novel macrophage receptor. *Blood* **85**, 1630-1639 (1995).
272. Hua, P.*, et al.* The BET inhibitor CPI203 promotes ex vivo expansion of cord blood long-term repopulating HSCs and megakaryocytes. *Blood* (2020).
273. Theocharides, A.P.A., Rongvaux, A., Fritsch, K., Flavell, R.A. & Manz, M.G. Humanized hemato-lymphoid system mice. *Haematologica* **101**, 5-19 (2016).
274. Chen, B.*, et al.* Complement Depletion Improves Human Red Blood Cell Reconstitution in Immunodeficient Mice. *Stem cell reports* **9**, 1034-1042 (2017).

275. Rahmig, S.*, et al.* Improved Human Erythropoiesis and Platelet Formation in Humanized NSGW41 Mice. *Stem Cell Reports* **7**, 591-601 (2016).
276. Miller, P.H.*, et al.* Analysis of parameters that affect human hematopoietic cell outputs in mutant c-kit-immunodeficient mice. *Experimental hematology* **48**, 41-49 (2017).
277. Brehm, M.A., Shultz, L.D. & Greiner, D.L. Humanized mouse models to study human diseases. *Curr Opin Endocrinol Diabetes Obes* **17**, 120-125 (2010).
278. Lang, J.*, et al.* Receptor editing and genetic variability in human autoreactive B cells. *Journal of Experimental Medicine* **213**, 93-108 (2016).
279. Mackay, F. & Schneider, P. Cracking the BAFF code. *Nature reviews. Immunology* **9**, 491-502 (2009).
280. Treml, J.F., Hao, Y., Stadanlick, J.E. & Cancro, M.P. The BLyS family: toward a molecular understanding of B cell homeostasis. *Cell biochemistry and biophysics* **53**, 1-16 (2009).
281. Mackay, F. & Schneider, P. TACI, an enigmatic BAFF/APRIL receptor, with new unappreciated biochemical and biological properties. *Cytokine & growth factor reviews* **19**, 263-276 (2008).
282. Lang, J.*, et al.* Replacing mouse BAFF with human BAFF does not improve B-cell maturation in hematopoietic humanized mice. *Blood advances* **1**, 2729-2741 (2017).
283. Ferrer, G., Moreno, C. & Montserrat, E. Comment on "Soluble BAFF levels inversely correlate with peripheral B cell numbers and the expression of BAFF receptors". *The Journal of Immunology* **188**, 2930-2931 (2012).
284. Vallerskog, T.*, et al.* Differential effects on BAFF and APRIL levels in rituximab-treated patients with systemic lupus erythematosus and rheumatoid arthritis. *Arthritis Res Ther* **8**, R167 (2006).
285. Mosier, D.E., Gulizia, R.J., Baird, S.M. & Wilson, D.B. Transfer of a functional human immune system to mice with severe combined immunodeficiency. *Nature* **335**, 256-259 (1988).
286. Takata, H. & Takiguchi, M. Three memory subsets of human CD8+ T cells differently expressing three cytolytic effector molecules. *Journal of immunology (Baltimore, Md. : 1950)* **177**, 4330-4340 (2006).
287. Liu, W. & Li, X.C. An overview on non-T cell pathways in transplant rejection and tolerance. *Curr Opin Organ Transplant* **15**, 422-426 (2010).
288. Kirk, A.D.*, et al.* Results from a human renal allograft tolerance trial evaluating the humanized CD52-specific monoclonal antibody alemtuzumab (CAMPATH-1H). *Transplantation* **76**, 120-129 (2003).
289. Wu, T.*, et al.* Histopathologic characteristics of human intestine allograft acute rejection in patients pretreated with thymoglobulin or alemtuzumab. *The American journal of gastroenterology* **101**, 1617-1624 (2006).
290. He, H., Stone, J.R. & Perkins, D.L. Analysis of robust innate immune response after transplantation in the absence of adaptive immunity. *Transplantation* **73**, 853-861 (2002).
291. Morelli, A.E. & Thomson, A.W. Tolerogenic dendritic cells and the quest for transplant tolerance. *Nature reviews. Immunology* **7**, 610-621 (2007).
292. Gill, R.G. NK cells: elusive participants in transplantation immunity and tolerance. *Current opinion in immunology* **22**, 649-654 (2010).

293. de Vries, V.C. & Noelle, R.J. Mast cell mediators in tolerance. *Current opinion in immunology* **22**, 643-648 (2010).
294. Fraser, C.C., Chen, B.P., Webb, S., van Rooijen, N. & Kraal, G. Circulation of human hematopoietic cells in severe combined immunodeficient mice after Cl2MDP-liposome-mediated macrophage depletion. *Blood* **86**, 183-192 (1995).
295. Cancello, R.*, et al.* Reduction of macrophage infiltration and chemoattractant gene expression changes in white adipose tissue of morbidly obese subjects after surgery-induced weight loss. *Diabetes* **54**, 2277-2286 (2005).
296. Wellen, K.E. & Hotamisligil, G.S. Obesity-induced inflammatory changes in adipose tissue. *The Journal of clinical investigation* **112**, 1785-1788 (2003).
297. Bu, L., Gao, M., Qu, S. & Liu, D. Intraperitoneal injection of clodronate liposomes eliminates visceral adipose macrophages and blocks high-fat diet-induced weight gain and development of insulin resistance. *AAPS J* **15**, 1001-1011 (2013).
298. Takenaka, K.*, et al.* Polymorphism in Sirpa modulates engraftment of human hematopoietic stem cells. *Nat Immunol* **8**, 1313-1323 (2007).
299. Barclay, A.N. & Van den Berg, T.K. The interaction between signal regulatory protein alpha (SIRPalpha) and CD47: structure, function, and therapeutic target. *Annual review of immunology* **32**, 25-50 (2014).
300. Legrand, N.*, et al.* Functional CD47/signal regulatory protein alpha (SIRP(alpha)) interaction is required for optimal human T- and natural killer- (NK) cell homeostasis in vivo. *Proceedings of the National Academy of Sciences of the United States of America* **108**, 13224-13229 (2011).
301. Yamauchi, T.*, et al.* Polymorphic Sirpa is the genetic determinant for NOD-based mouse lines to achieve efficient human cell engraftment. *Blood* **121**, 1316-1325 (2013).
302. Anniss, A.M. & Sparrow, R.L. Expression of CD47 (integrin-associated protein) decreases on red blood cells during storage. *Transfusion and apheresis science : official journal of the World Apheresis Association : official journal of the European Society for Haemapheresis* **27**, 233-238 (2002).
303. Stewart, A., Urbaniak, S., Turner, M. & Bessos, H. The application of a new quantitative assay for the monitoring of integrin-associated protein CD47 on red blood cells during storage and comparison with the expression of CD47 and phosphatidylserine with flow cytometry. *Transfusion* **45**, 1496-1503 (2005).
304. Oldenborg, P.A., Gresham, H.D. & Lindberg, F.P. CD47-signal regulatory protein alpha (SIRPalpha) regulates Fcgamma and complement receptor-mediated phagocytosis. *The Journal of experimental medicine* **193**, 855-862 (2001).
305. Brittain, J.E., Mlinar, K.J., Anderson, C.S., Orringer, E.P. & Parise, L.V. Integrin-associated protein is an adhesion receptor on sickle red blood cells for immobilized thrombospondin. *Blood* **97**, 2159-2164 (2001).
306. Jaiswal, S.*, et al.* CD47 is upregulated on circulating hematopoietic stem cells and leukemia cells to avoid phagocytosis. *Cell* **138**, 271-285 (2009).
307. Wan, X.*, et al.* Red blood cell-derived nanovesicles for safe and efficient macrophage-targeted drug delivery in vivo. *Biomaterials science* **7**, 187-195 (2019).
308. Burger, P., Hilarius-Stokman, P., de Korte, D., van den Berg, T.K. & van Bruggen, R. CD47 functions as a molecular switch for erythrocyte phagocytosis. *Blood* **119**, 5512-5521 (2012).

309. Isenberg, J.S.*, et al.* Differential interactions of thrombospondin-1, -2, and -4 with CD47 and effects on cGMP signaling and ischemic injury responses. *The Journal of biological chemistry* **284**, 1116-1125 (2009).
310. Oldenborg, P.A., Gresham, H.D., Chen, Y., Izui, S. & Lindberg, F.P. Lethal autoimmune hemolytic anemia in CD47-deficient nonobese diabetic (NOD) mice. *Blood* **99**, 3500-3504 (2002).
311. Nagahara, M.*, et al.* Correlated expression of CD47 and SIRPA in bone marrow and in peripheral blood predicts recurrence in breast cancer patients. *Clinical Cancer Research* **16**, 4625-4635 (2010).
312. de Back, D.Z., Kostova, E.B., van Kraaij, M., van den Berg, T.K. & van Bruggen, R. Of macrophages and red blood cells; a complex love story. *Front Physiol* **5**, 9-9 (2014).
313. Bessis, M.C. & Breton-Gorius, J. Iron metabolism in the bone marrow as seen by electron microscopy: a critical review. *Blood* **19**, 635-663 (1962).
314. Bessis, M. [Erythroblastic island, functional unity of bone marrow]. *Rev Hematol* **13**, 8-11 (1958).
315. Klei, T.R.L., Meinderts, S.M., van den Berg, T.K. & van Bruggen, R. From the Cradle to the Grave: The Role of Macrophages in Erythropoiesis and Erythrophagocytosis. *Frontiers in Immunology* **8**(2017).
316. Milhem, M.*, et al.* Modification of hematopoietic stem cell fate by 5aza 2'deoxycytidine and trichostatin A. *Blood* **103**, 4102-4110 (2004).
317. Chaurasia, P., Gajzer, D.C., Schaniel, C., D'Souza, S. & Hoffman, R. Epigenetic reprogramming induces the expansion of cord blood stem cells. *The Journal of clinical investigation* **124**, 2378-2395 (2014).
318. Hua, P.*, et al.* Single-cell assessment of transcriptome alterations induced by Scriptaid in early differentiated human haematopoietic progenitors during ex vivo expansion. *Scientific reports* **9**, 1-9 (2019).
319. Knudsen, K.J.*, et al.* ERG promotes the maintenance of hematopoietic stem cells by restricting their differentiation. *Genes Dev* **29**, 1915-1929 (2015).
320. Wilson, A.*, et al.* c-Myc controls the balance between hematopoietic stem cell self-renewal and differentiation. *Genes Dev* **18**, 2747-2763 (2004).
321. Blome-Eberwein, S.*, et al.* Clinical practice of glycerol preserved allograft skin coverage. *Burns* **28**, 10-12 (2002).
322. Zhou, J., He, W., Luo, G. & Wu, J. Fundamental Immunology of Skin Transplantation and Key Strategies for Tolerance Induction. *Archivum Immunologiae et Therapiae Experimentalis* **61**, 397-405 (2013).
323. Sinha, I. & Pomahac, B. Split rejection in vascularized composite allotransplantation. *Eplasty* **13**, e53-e53 (2013).
324. Petruzzo, P.*, et al.* The International Registry on Hand and Composite Tissue Transplantation. *Transplantation* **90**, 1590-1594 (2010).
325. Suematsu, S.*, et al.* IgG1 plasmacytosis in interleukin 6 transgenic mice. *Proceedings of the National Academy of Sciences of the United States of America* **86**, 7547-7551 (1989).
326. Kanitakis, J.*, et al.* Clinicopathologic features of graft rejection of the first human hand allograft. *Transplantation* **76**, 688-693 (2003).
327. Kanitakis, J.*, et al.* Clinicopathologic monitoring of the skin and oral mucosa of the first human face allograft: Report on the first eight months. *Transplantation* **82**, 1610-1615 (2006).

328. Zdichavsky, M.*, et al.* Scoring of skin rejection in a swine composite tissue allograft model. *Journal of Surgical Research* **85**, 1-8 (1999).
329. Muñoz-Espín, D. & Serrano, M. Cellular senescence: from physiology to pathology. *Nature reviews Molecular cell biology* **15**, 482-496 (2014).
330. Racki, W.J.*, et al.* NOD-scid IL2rgamma(null) mouse model of human skin transplantation and allograft rejection. *Transplantation* **89**, 527-536 (2010).
331. Van Laethem, F., Tikhonova, A.N. & Singer, A. MHC restriction is imposed on a diverse T cell receptor repertoire by CD4 and CD8 co-receptors during thymic selection. *Trends in immunology* **33**, 437-441 (2012).
332. Merkenschlager, M.*, et al.* How many thymocytes audition for selection? *The Journal of experimental medicine* **186**, 1149-1158 (1997).
333. Tikhonova, A.N.*, et al.* αβ T cell receptors that do not undergo major histocompatibility complex-specific thymic selection possess antibody-like recognition specificities. *Immunity* **36**, 79-91 (2012).
334. Zerrahn, J., Held, W. & Raulet, D.H. The MHC reactivity of the T cell repertoire prior to positive and negative selection. *Cell* **88**, 627-636 (1997).
335. Krovi, S.H., Kappler, J.W., Marrack, P. & Gapin, L. Inherent reactivity of unselected TCR repertoires to peptide-MHC molecules. *Proceedings of the National Academy of Sciences* **116**, 22252-22261 (2019).
336. Strom, T.B., Tilney, N.L., Carpenter, C.B. & Busch, G.J. Identity and cytotoxic capacity of cells infiltrating renal allografts. *The New England journal of medicine* **292**, 1257-1263 (1975).
337. Rosenberg, A.S., Mizuochi, T., Sharrow, S.O. & Singer, A. Phenotype, specificity, and function of T cell subsets and T cell interactions involved in skin allograft rejection. *The Journal of experimental medicine* **165**, 1296-1315 (1987).
338. Shiao, S.L., McNiff, J.M. & Pober, J.S. Memory T cells and their costimulators in human allograft injury. *Journal of immunology (Baltimore, Md. : 1950)* **175**, 4886-4896 (2005).
339. Russell, J.H. & Ley, T.J. Lymphocyte-mediated cytotoxicity. *Annual review of immunology* **20**, 323-370 (2002).
340. Sutton, V.R.*, et al.* Initiation of apoptosis by granzyme B requires direct cleavage of bid, but not direct granzyme B-mediated caspase activation. *The Journal of experimental medicine* **192**, 1403-1414 (2000).
341. Narula, J.*, et al.* Annexin-V imaging for noninvasive detection of cardiac allograft rejection. *Nat Med* **7**, 1347-1352 (2001).
342. Ogura, Y.*, et al.* Apoptosis and allograft rejection in the absence of CD8+ T cells. *Transplantation* **71**, 1827-1834 (2001).
343. Ruggeri, L.*, et al.* Effectiveness of donor natural killer cell alloreactivity in mismatched hematopoietic transplants. *Science* **295**, 2097-2100 (2002).
344. Kroemer, A., Edtinger, K. & Li, X.C. The innate natural killer cells in transplant rejection and tolerance induction. *Curr Opin Organ Transplant* **13**, 339-343 (2008).
345. Villard, J. The role of natural killer cells in human solid organ and tissue transplantation. *J Innate Immun* **3**, 395-402 (2011).
346. Rocha, P.N., Plumb, T.J., Crowley, S.D. & Coffman, T.M. Effector mechanisms in transplant rejection. *Immunol Rev* **196**, 51-64 (2003).
347. Dalloul, A.H., Chmouzis, E., Ngo, K. & Fung-Leung, W.P. Adoptively transferred CD4+ lymphocytes from CD8 -/- mice are sufficient to mediate the rejection of MHC class II

or class I disparate skin grafts. *Journal of immunology (Baltimore, Md. : 1950)* **156**, 4114-4119 (1996).
348. Valujskikh, A.*, et al.* T cells reactive to a single immunodominant self-restricted allopeptide induce skin graft rejection in mice. *The Journal of clinical investigation* **101**, 1398-1407 (1998).
349. Brennan, T.V.*, et al.* Preferential priming of alloreactive T cells with indirect reactivity. *Am J Transplant* **9**, 709-718 (2009).
350. Xiao, F.*, et al.* Ex vivo expanded human regulatory T cells delay islet allograft rejection via inhibiting islet-derived monocyte chemoattractant protein-1 production in CD34+ stem cells-reconstituted NOD-scid IL2rgammanull mice. *PLoS One* **9**, e90387 (2014).
351. Le Moine, A., Goldman, M. & Abramowicz, D. Multiple pathways to allograft rejection. *Transplantation* **73**, 1373-1381 (2002).
352. Goldman, M., Le Moine, A., Braun, M., Flamand, V. & Abramowicz, D. A role for eosinophils in transplant rejection. *Trends Immunol* **22**, 247-251 (2001).
353. Le Moine, A.*, et al.* IL-5 mediates eosinophilic rejection of MHC class II-disparate skin allografts in mice. *Journal of immunology (Baltimore, Md. : 1950)* **163**, 3778-3784 (1999).
354. Crespo, M.*, et al.* Acute humoral rejection in renal allograft recipients: I. Incidence, serology and clinical characteristics. *Transplantation* **71**, 652-658 (2001).
355. Müller, A.M.S., Linderman, J.A., Florek, M., Miklos, D. & Shizuru, J.A. Allogeneic T cells impair engraftment and hematopoiesis after stem cell transplantation. *Proceedings of the National Academy of Sciences* **107**, 14721 (2010).
356. Maeda, K.*, et al.* IL-6 blocks a discrete early step in lymphopoiesis. *Blood* **106**, 879-885 (2005).
357. Sitnicka, E., Ruscetti, F., Priestley, G., Wolf, N. & Bartelmez, S. Transforming growth factor beta 1 directly and reversibly inhibits the initial cell divisions of long-term repopulating hematopoietic stem cells. (1996).
358. Selleri, C., Sato, T., Anderson, S., Young, N.S. & Maciejewski, J.P. Interferon-γ and tumor necrosis factor-α suppress both early and late stages of hematopoiesis and induce programmed cell death. *Journal of cellular physiology* **165**, 538-546 (1995).
359. Shono, Y.*, et al.* Bone marrow graft-versus-host disease: early destruction of hematopoietic niche after MHC-mismatched hematopoietic stem cell transplantation. *Blood, The Journal of the American Society of Hematology* **115**, 5401-5411 (2010).
360. Martin, P.*, et al.* Graft failure in patients receiving T cell-depleted HLA-identical allogeneic marrow transplants. *Bone marrow transplantation* **3**, 445 (1988).
361. Nadig, S.N.*, et al.* In vivo prevention of transplant arteriosclerosis by ex vivo-expanded human regulatory T cells. *Nature medicine* **16**, 809-813 (2010).
362. Wood, K.J., Bushell, A. & Jones, N.D. Immunologic unresponsiveness to alloantigen in vivo: a role for regulatory T cells. *Immunological reviews* **241**, 119-132 (2011).
363. Sagoo, P., Lombardi, G. & Lechler, R.I. Regulatory T cells as therapeutic cells. *Curr Opin Organ Transplant* **13**, 645-653 (2008).
364. Boardman, D.A.*, et al.* Expression of a chimeric antigen receptor specific for donor HLA class I enhances the potency of human regulatory T cells in preventing human skin transplant rejection. *American Journal of Transplantation* (2016).

365. Issa, F., Hester, J., Milward, K. & Wood, K.J. Homing of regulatory T cells to human skin is important for the prevention of alloimmune-mediated pathology in an in vivo cellular therapy model. *PloS one* **7**, e53331 (2012).
366. Plitas, G. & Rudensky, A.Y. Regulatory T Cells in Cancer. *Annual Review of Cancer Biology* **4**, 459-477 (2020).
367. Ollila, T.A., Sahin, I. & Olszewski, A.J. Mogamulizumab: a new tool for management of cutaneous T-cell lymphoma. *Onco Targets Ther* **12**, 1085-1094 (2019).
368. De Simone, M.*, et al.* Transcriptional Landscape of Human Tissue Lymphocytes Unveils Uniqueness of Tumor-Infiltrating T Regulatory Cells. *Immunity* **45**, 1135-1147 (2016).
369. Anderson, C.A.*, et al.* A degradatory fate for CCR4 suggests a primary role in Th2 inflammation. *Journal of leukocyte biology* **107**, 455-466 (2020).
370. Taub, D.D., Turcovski-Corrales, S.M., Key, M.L., Longo, D.L. & Murphy, W.J. Chemokines and T lymphocyte activation: I. Beta chemokines costimulate human T lymphocyte activation in vitro. *The Journal of Immunology* **156**, 2095-2103 (1996).
371. Hori, S., Nomura, T. & Sakaguchi, S. Control of regulatory T cell development by the transcription factor Foxp3. *Science* **299**, 1057-1061 (2003).
372. Oldenhove, G.*, et al.* Decrease of Foxp3+ Treg cell number and acquisition of effector cell phenotype during lethal infection. *Immunity* **31**, 772-786 (2009).
373. Yang, X.O.*, et al.* Molecular antagonism and plasticity of regulatory and inflammatory T cell programs. *Immunity* **29**, 44-56 (2008).
374. Arroyo Hornero, R.*, et al.* CD70 expression determines the therapeutic efficacy of expanded human regulatory T cells. *Communications Biology* **3**, 375 (2020).
375. Huang, C.-T.*, et al.* Role of LAG-3 in regulatory T cells. *Immunity* **21**, 503-513 (2004).
376. Do, J.s.*, et al.* An IL-27/Lag3 axis enhances Foxp3+ regulatory T cell–suppressive function and therapeutic efficacy. *Mucosal Immunology* **9**, 137-145 (2016).
377. Joller, N.*, et al.* Treg cells expressing the coinhibitory molecule TIGIT selectively inhibit proinflammatory Th1 and Th17 cell responses. *Immunity* **40**, 569-581 (2014).
378. Nowak, A.*, et al.* CD137+CD154- Expression As a Regulatory T Cell (Treg)-Specific Activation Signature for Identification and Sorting of Stable Human Tregs from In Vitro Expansion Cultures. *Frontiers in immunology* **9**, 199-199 (2018).
379. Sugiyama, D.*, et al.* Anti-CCR4 mAb selectively depletes effector-type FoxP3⁺CD4⁺ regulatory T cells, evoking antitumor immune responses in humans. *Proceedings of the National Academy of Sciences* **110**, 17945 (2013).
380. Duvic, M.*, et al.* Phase 1/2 study of mogamulizumab, a defucosylated anti-CCR4 antibody, in previously treated patients with cutaneous T-cell lymphoma. *Blood* **125**, 1883-1889 (2015).
381. Gobert, M.*, et al.* Regulatory T cells recruited through CCL22/CCR4 are selectively activated in lymphoid infiltrates surrounding primary breast tumors and lead to an adverse clinical outcome. *Cancer Res* **69**, 2000-2009 (2009).
382. Yang, Z.Z., Novak, A.J., Stenson, M.J., Witzig, T.E. & Ansell, S.M. Intratumoral CD4+CD25+ regulatory T-cell-mediated suppression of infiltrating CD4+ T cells in B-cell non-Hodgkin lymphoma. *Blood* **107**, 3639-3646 (2006).
383. Matsuo, K.*, et al.* CCR4 is critically involved in effective antitumor immunity in mice bearing intradermal B16 melanoma. *Cancer Lett* **378**, 16-22 (2016).

384. Shevyrev, D. & Tereshchenko, V. Treg Heterogeneity, Function, and Homeostasis. *Frontiers in Immunology* **10**(2020).
385. Kawai, K., Uchiyama, M., Hester, J. & Issa, F. IL-33 drives the production of mouse regulatory T cells with enhanced in vivo suppressive activity in skin transplantation. *American Journal of Transplantation* **n/a**.
386. Di Stasi, A*., et al.* T lymphocytes coexpressing CCR4 and a chimeric antigen receptor targeting CD30 have improved homing and antitumor activity in a Hodgkin tumor model. *Blood* **113**, 6392-6402 (2009).
387. Rapp, M*., et al.* C-C chemokine receptor type-4 transduction of T cells enhances interaction with dendritic cells, tumor infiltration and therapeutic efficacy of adoptive T cell transfer. *Oncoimmunology* **5**, e1105428 (2016).
388. Zou, Y*., et al.* Application of the chemokine-chemokine receptor axis increases the tumor-targeted migration ability of cytokine-induced killer cells in patients with colorectal cancer. *Oncol Lett* **20**, 123-134 (2020).
389. Mollica Poeta, V., Massara, M., Capucetti, A. & Bonecchi, R. Chemokines and Chemokine Receptors: New Targets for Cancer Immunotherapy. *Front Immunol* **10**, 379 (2019).
390. Heath, W.R. & Carbone, F.R. The skin-resident and migratory immune system in steady state and memory: innate lymphocytes, dendritic cells and T cells. *Nature immunology* **14**, 978 (2013).
391. Ho, A.W. & Kupper, T.S. T cells and the skin: from protective immunity to inflammatory skin disorders. *Nature Reviews Immunology* **19**, 490-502 (2019).
392. Clark, R.A*., et al.* The vast majority of CLA+ T cells are resident in normal skin. *The Journal of Immunology* **176**, 4431-4439 (2006).
393. D'Ambrosio, D*., et al.* Cutting Edge: Selective Up-Regulation of Chemokine Receptors CCR4 and CCR8 upon Activation of Polarized Human Type 2 Th Cells. *The Journal of Immunology* **161**, 5111 (1998).
394. Aisenbrey, E.A. & Murphy, W.L. Synthetic alternatives to Matrigel. *Nature Reviews Materials* **5**, 539-551 (2020).
395. Morein, D., Erlichman, N. & Ben-Baruch, A. Beyond Cell Motility: The Expanding Roles of Chemokines and Their Receptors in Malignancy. *Frontiers in Immunology* **11**(2020).
396. Roy, I*., et al.* CXCL12 Chemokine Expression Suppresses Human Pancreatic Cancer Growth and Metastasis. *PLOS ONE* **9**, e90400 (2014).
397. Duarte, J.H., Zelenay, S., Bergman, M.L., Martins, A.C. & Demengeot, J. Natural Treg cells spontaneously differentiate into pathogenic helper cells in lymphopenic conditions. *European journal of immunology* **39**, 948-955 (2009).
398. Zhou, X*., et al.* Instability of the transcription factor Foxp3 leads to the generation of pathogenic memory T cells in vivo. *Nature immunology* **10**, 1000-1007 (2009).
399. Duggleby, R.C., Shaw, T.N., Jarvis, L.B., Kaur, G. & Hill Gaston, J. CD27 expression discriminates between regulatory and non-regulatory cells after expansion of human peripheral blood CD4+ CD25+ cells. *Immunology* **121**, 129-139 (2007).
400. Nadig, S.N*., et al.* In vivo prevention of transplant arteriosclerosis by ex vivo-expanded human regulatory T cells. *Nat Med* **16**, 809-813 (2010).
401. Litjens, N.H.R., Boer, K. & Betjes, M.G.H. Identification of Circulating Human Antigen-Reactive CD4⁺FOXP3⁺ Natural Regulatory T Cells. *The Journal of Immunology* **188**, 1083 (2012).

402. Workman, C.J. & Vignali, D.A. Negative regulation of T cell homeostasis by lymphocyte activation gene-3 (CD223). *The Journal of Immunology* **174**, 688-695 (2005).
403. Anderson, Ana C., Joller, N. & Kuchroo, Vijay K. Lag-3, Tim-3, and TIGIT: Co-inhibitory Receptors with Specialized Functions in Immune Regulation. *Immunity* **44**, 989-1004 (2016).
404. Fortunato, M., Morali, K., Passeri, L. & Gregori, S. Regulatory Cell Therapy in Organ Transplantation: Achievements and Open Questions. *Front Immunol* **12**, 641596 (2021).
405. Kawai, K., Uchiyama, M., Hester, J., Wood, K. & Issa, F. Regulatory T cells for tolerance. *Human Immunology* **79**, 294-303 (2018).
406. Jangalwe, S., Shultz, L.D., Mathew, A. & Brehm, M.A. Improved B cell development in humanized NOD-scid IL2Rγ(null) mice transgenically expressing human stem cell factor, granulocyte-macrophage colony-stimulating factor and interleukin-3. *Immun Inflamm Dis* **4**, 427-440 (2016).
407. Lan, P., Tonomura, N., Shimizu, A., Wang, S. & Yang, Y.G. Reconstitution of a functional human immune system in immunodeficient mice through combined human fetal thymus/liver and CD34+ cell transplantation. *Blood* **108**, 487-492 (2006).
408. Rongvaux, A.*, et al.* Human hemato-lymphoid system mice: current use and future potential for medicine. *Annual review of immunology* **31**, 635-674 (2013).
409. Issa, F.*, et al.* Transiently Activated Human Regulatory T Cells Upregulate BCL-XL Expression and Acquire a Functional Advantage in vivo. *Front Immunol* **10**, 889 (2019).
410. Zaitsu, M., Issa, F., Hester, J., Vanhove, B. & Wood, K.J. Selective blockade of CD28 on human T cells facilitates regulation of alloimmune responses. *JCI Insight* **2**, 1-13 (2017).
411. Bluestone, J.A., Trotta, E. & Xu, D. The therapeutic potential of regulatory T cells for the treatment of autoimmune disease. *Expert Opinion on Therapeutic Targets* **19**, 1091-1103 (2015).
412. Issa, F., Chandrasekharan, D. & Wood, K.J. Regulatory T cells as modulators of chronic allograft dysfunction. *Current opinion in immunology* **23**, 648-654 (2011).
413. McMurchy, A.N., Bushell, A., Levings, M.K. & Wood, K.J. Moving to tolerance: Clinical application of T regulatory cells. *Semin Immunol* **23**, 304-313 (2011).
414. Sharif-Paghaleh, E.*, et al.* In vivo SPECT reporter gene imaging of regulatory T cells. *PloS one* **6**, e25857 (2011).
415. Tang, Q. & Vincenti, F. Transplant trials with Tregs: perils and promises. *The Journal of clinical investigation* **127**, 2505-2512 (2017).
416. Ebert, L.M., Schaerli, P. & Moser, B. Chemokine-mediated control of T cell traffic in lymphoid and peripheral tissues. *Mol Immunol* **42**, 799-809 (2005).
417. Kang, S.G.*, et al.* Identification of a chemokine network that recruits FoxP3(+) regulatory T cells into chronically inflamed intestine. *Gastroenterology* **132**, 966-981 (2007).
418. Shabaneh, T.B.*, et al.* Oncogenic BRAFV600E governs regulatory T-cell recruitment during melanoma tumorigenesis. *Cancer research* **78**, 5038-5049 (2018).
419. Ni, X.*, et al.* Reduction of Regulatory T Cells by Mogamulizumab, a Defucosylated Anti-CC Chemokine Receptor 4 Antibody, in Patients with Aggressive/Refractory Mycosis Fungoides and Sézary Syndrome. *Clinical Cancer Research* **21**, 274 (2015).

420. Cowan, R.A.*, et al.* Efficacy and safety of mogamulizumab by patient baseline blood tumour burden: a post hoc analysis of the MAVORIC trial. *J. Eur. Acad. Dermatol. Venereol.* **n/a**.
421. Maeda, S., Murakami, K., Inoue, A., Yonezawa, T. & Matsuki, N. CCR4 Blockade Depletes Regulatory T Cells and Prolongs Survival in a Canine Model of Bladder Cancer. *Cancer Immunology Research* **7**, 1175 (2019).
422. Marshall, L.A.*, et al.* Tumors establish resistance to immunotherapy by regulating T_{reg} recruitment via CCR4. *Journal for ImmunoTherapy of Cancer* **8**, e000764 (2020).
423. Alvisi, G.*, et al.* IRF4 instructs effector Treg differentiation and immune suppression in human cancer. *The Journal of clinical investigation* **130**, 3137-3150 (2020).
424. Gong, R. & Ren, H. Targeting chemokines/chemokine receptors: a promising strategy for enhancing the immunotherapy of pancreatic ductal adenocarcinoma. *Signal Transduction and Targeted Therapy* **5**, 149 (2020).
425. Garetto, S.*, et al.* Tailored chemokine receptor modification improves homing of adoptive therapy T cells in a spontaneous tumor model. *Oncotarget* **7**, 43010 (2016).
426. Vignali, D.A., Collison, L.W. & Workman, C.J. How regulatory T cells work. *Nature reviews immunology* **8**, 523-532 (2008).
427. Molinaro, R.*, et al.* CCR4 controls the suppressive effects of regulatory T cells on early and late events during severe sepsis. *PLoS One* **10**, e0133227 (2015).
428. Rapp, M.*, et al.* CCL22 controls immunity by promoting regulatory T cell communication with dendritic cells in lymph nodes. *Journal of Experimental Medicine* **216**, 1170-1181 (2019).
429. Sakaguchi, S., Wing, K., Onishi, Y., Prieto-Martin, P. & Yamaguchi, T. Regulatory T cells: how do they suppress immune responses? *International immunology* **21**, 1105-1111 (2009).
430. Pere, H.*, et al.* A CCR4 antagonist combined with vaccines induces antigen-specific CD8+ T cells and tumor immunity against self antigens. *Blood, The Journal of the American Society of Hematology* **118**, 4853-4862 (2011).
431. Bayry, J.*, et al.* In silico identified CCR4 antagonists target regulatory T cells and exert adjuvant activity in vaccination. *Proceedings of the National Academy of Sciences* **105**, 10221-10226 (2008).
432. Landman, S.*, et al.* Intradermal injection of low dose human regulatory T cells inhibits skin inflammation in a humanized mouse model. *Scientific reports* **8**, 1-10 (2018).
433. Kühnemuth, B.*, et al.* CCL22 impedes T cell activation capacities of dendritic cells by reducing membrane expression of MHC molecules and CD80. *The Journal of Immunology* **198**, 133.133 (2017).